NEW INFLOW PEFORMANCE RELATIONSHIPS

FOR GAS CONDENSATE RESERVOIRS

A Thesis

by

YANIL DEL CASTILLO MARAVI

Submitted to the Office of Graduate Studies of
Texas A&M University
in partial fulfillment of the requirements for the degree of

MASTER OF SCIENCE

August 2003

Major Subject: Petroleum Engineering

NEW INFLOW PEFORMANCE RELATIONSHIPS

FOR GAS CONDENSATE RESERVOIRS

A Thesis

by

YANIL DEL CASTILLO MARAVI

Submitted to the Office of Graduate Studies of
Texas A&M University
in partial fulfillment of the requirements for the degree of

MASTER OF SCIENCE

Approved as to style and content by:

Rosalind A. Archer (Co-Chair of Committee)	Thomas A. Blasingame (Co-Chair of Committee)
Maria A. Barrufet (Member)	Mark E. Everett (Member)
	Hans C. Juvkam-Wold (Interim Head of Department)

August 2003

Major Subject: Petroleum Engineering

ABSTRACT

New Inflow Performance Relationships for Gas Condensate Reservoirs. (August 2003)

Yanil Del Castillo Maravi, B.S., Universidad Nacional de Ingenieria

Co-Chairs of Advisory Committee: Dr. Rosalind A. Archer
Dr. Thomas A. Blasingame

In this work we propose two new Vogel-type Inflow Performance Relations (or *IPR*) correlations for gas-condensate reservoir systems. One correlation predicts dry gas production the other predicts condensate (liquid) production. These correlations provide a linkage between reservoir rock and fluid properties (dewpoint, temperature, and endpoint relative permeabilities, composition, etc.) to the flowrate-pressure performance for the reservoir system.

The proposed *IPR* relationships for compositional reservoir systems are based on data from over 3000 compositional reservoir simulation cases developed using various fluid properties and relative permeability curves. The resulting *IPR* curves for gas condensate systems are *quadratic* in behavior — similar to the Vogel *IPR* trends (the Vogel (quadratic) rate-pressure profile is generally presumed for the case of a solution gas-drive reservoir system). However, in the case of a gas-condensate reservoir system, the coefficients in the quadratic relationship vary significantly depending on the richness of the gas condensate fluid (*i.e.*, the composition) as well as the relative permeability-saturation behavior. Using an *alternating conditional expectation* approach (*i.e.*, non-parametric regression), an approximate model was developed to estimate these coefficients.

This work also includes a discussion of the Vogel *IPR* for solution gas-drive systems. The original work proposed by Vogel is based on an empirical correlation of numerical simulations for a solution-gas-drive system. Our work provides a critical validation and extension of the Vogel work by establishing a simple, yet rigorous formulation for flowrate-pressure performance in terms of effective permeabilities and pressure-dependent fluid properties.

The direct application of this work is to predict the *IPR* for a given reservoir system directly from rock-fluid properties and fluid properties. This formulation provides a new mechanism that can be used to couple the flowrate and pressure behavior for solution gas-drive systems and we believe that it *may be possible* to extend the proposed semi-analytical concept to gas-condensate reservoir systems. However, for this work we have only considered a semi-empirical *IPR* approach (*i.e.*, a data-derived correlation) for the case of gas-condensate reservoir systems. We recognize that further work should be performed in this area, and we encourage future research on the topic of semi-analytical modeling of *IPR* behavior for gas-condensate reservoir systems.

DEDICATION

This thesis is dedicated to almighty God;
To my mother Elsa and my daughter Alessandra for all of your support, encouragement, your unconditional love, your patience and prayers, I love you all.

ACKNOWLEDGEMENTS

I would like to express my personal appreciation to the following people and organizations for their support and assistance during my graduate studies:

Dr. Rosalind A. Archer, co-chair of my advisory committee, for her valuable guidance, intellectual contributions, and her continued assistance and motivation to conclude this research.

Dr. Thomas A. Blasingame, co-chair of my advisory committee, for his direct contributions, insightful suggestions, and his patience throughout my research.

Dr. Maria A. Barrufet for serving as a member of my advisory committee, for permitting me access to a series of condensate fluid studies used in this research — and in particular, for her valuable advice and suggestions.

Dr. Mark E. Everett for serving as a member of my advisory committee.

Dr. Peter Valko, for his assistance with the *GRACE* algorithm used in this research (*i.e.*, the non-parametric regression code).

Dr. Stephen Holditch, for his financial support and his motivation for me to continue this research.

The Fulbright Commission and the Peruvian Ministry of Energy and Mines (CAREC), for sponsorship of my graduate studies, and the opportunity to pursue graduate studies in Petroleum Engineering.

TABLE OF CONTENTS

Page

LIST OF TABLES

LIST OF FIGURES

FIGURE Page

CHAPTER I

INTRODUCTION AND LITERATURE REVIEW

1.1 Introduction

Predicting the relationship between the flowrate and the pressure drop performance in the reservoir is very important for continuous production optimization in the field. An inflow performance relationship (*IPR*) model is typically used for this task. *IPR* models allow us to consider various operating conditions; determine the optimum production scheme, and design production equipment and artificial lift systems. *IPR* modeling (inflow) can be combined with tubing analysis (outflow) using "nodal analysis" techniques which allow us to monitor well productivity and to choose the proper remedial treatment options (acidizing, fracturing, workover, etc) to restore optimum well performance.

Typically, gas condensate reservoirs are discovered as single-phase gas reservoirs. As the reservoir pressure drops below the dewpoint pressure, isothermal condensation occurs and produces a "ring" of liquid condensate, which is mainly composed of intermediate and heavier components. The "buildup" of the condensate ring generates a reduction in gas deliverability, due mainly to the reduction in gas relative permeability. This condition leaves a substantial portion of the condensed liquid in the reservoir due to the high liquid-to-gas viscosity ratio (and relative permeability effects). Ultimately, the buildup of condensate in the reservoir affects the economic value of the project.

Characterization of gas condensate reservoirs is often a difficult task because multiphase flow exists in the reservoir — and during production the fluid changes its overall composition in both time and space. This situation complicates well deliverability analysis, well testing, evaluation of productivity and/or the sizing of surface facilities.

For gas condensate wells, standard dry-gas deliverability equations based on deliverability or isochronal testing have traditionally been used as *IPR* models. The severe deliverability reduction caused by condensate blockage makes this approach inadequate.

The generation of proper *IPR* curves for a gas condensate reservoir system will allow for the identification and quantification of well productivity losses in addition to estimating the correct surface control parameters required to achieve optimum production. The consideration of *IPR* curves can also reduce uncertainties in missing reservoir parameters such as reservoir pressure and skin factor.

The primary objective of this research is to determine a simple method to calculate the deliverability of a gas condensate system based on simple reservoir and fluid properties. To study this phenomenon, we use

---

This thesis follows the style of *SPE Reservoir Evaluation and Engineering*.

a homogeneous and isotropic single-well radial model in order to simulate the gas condensate and dry gas deliverability of various gas condensate reservoir systems.

Chapter I of this thesis presents a comprehensive review of the theory regarding *IPR* models for single-phase oil, solution gas-drive reservoirs and gas-condensate systems. Chapter II presents the inventory of fluids and relative permeability curves used for simulation as well as the *IPR* profiles obtained for the 64 condensate-systems (*i.e.,* the gas condensate and dry gas performance profiles).

Chapter III details the methodology we used to develop the dimensionless gas condensate and dry gas *IPR* profiles. The model proposed for gas condensate systems is a modified version of the Vogel *IPR* model, where the "Vogel" model is commonly used for solution gas-drive reservoirs. We note that for gas condensate reservoir systems, the quadratic shape of the *IPR* curve (*i.e.*, the "Vogel" model) is variable and depends on the rock and fluid properties of the reservoir system. Chapter IV addresses the correlation approach we used to predict the coefficients in the Vogel model for quadratic *IPR* behavior. Finally, conclusions and recommendations are presented in Chapter V. In addition to the main body of the thesis text, we also utilize a series of Appendices where we provide supporting data, analyses, and methodologies. The Appendices are given as follows:

- Appendix A — Inventory of Gas Condensate Simulation Cases
- Appendix B — Simulation Cases used for Validation (Gas Condensate Systems
- Appendix C — *IPR* Model — Wiggins, *et al.* Approach for Solution Gas-Drive Systems
- Appendix D — *IPR* Model — New Approach for Solution Gas-Drive Systems
- Appendix E — Eclipse Data File (Sample)

1.2 Literature Review

1.2.1 Oil *IPR* (Slightly Compressible Liquid) and Solution-Gas-drive (Compressible Liquid) *IPR*

For the case of "liquid" flow (*i.e.*, for a well producing a black oil) we can derive a linear relation for the flowrate as a function of the pressure drop using material balance and the diffusivity equation for a slightly compressible liquid. This is the so-called "pseudosteady-state" flow equation, and is given as:

$$\overline{p} = p_{wf} + 141.2\frac{q_o B_o \mu_o}{kh}\left[\frac{1}{2}\ln\left[\frac{4}{e^{\gamma}}\frac{A}{r_w^2}\frac{1}{C_A}\right]+s\right] \quad \text{.....(1.1)}$$

Eq. 1.1 can be written more compactly as:

$$\overline{p} = p_{wf} + q_o b_{pss} \quad \text{.....(1.2)}$$

where:

$$b_{pss} = 141.2\frac{B_o \mu_o}{kh}\left[\frac{1}{2}\ln\left[\frac{4}{e^{\gamma}}\frac{A}{r_w^2}\frac{1}{C_A}\right]+s\right] \quad \text{.....(1.3)}$$

We can also use the compact form of the pseudosteady-state flow equation to define the "productivity index," which is a convenient reference for flow behavior. The productivity index, J, is defined as:

$$J = \frac{q_o}{\overline{p} - p_{wf}} = \frac{1}{b_{pss}} \quad \text{.....(1.4)}$$

It is important to note that for a single–phase liquid flow, the productivity index is a constant. As Muskat[1] demonstrated, a straight-line relationship between the flowrate and the pressure drop does not exist and there is no single, unique productivity index that exists when two phases (oil and gas) are flowing in a reservoir (*i.e.,* the case of a solution gas-drive reservoir system). Muskat based his conclusions on theoretical calculations using material balance for the steady-state flow of two mobile phases (oil and gas) in combination with experimental data (relative permeability, oil viscosity, gas solubility, oil formation volume factor and pre-established values for the gas-oil ratio). Muskat presented graphs of producing oil rates versus differential pressures for two-phase flow in the reservoir, which resulted in curved (*i.e.*, nonlinear) relationships — demonstrating that the productivity index will vary depending on the characteristics of the fluid, rock and also on parameters such as gas-oil ratio, pressure differential and reservoir pressure.

The prediction of the "inflow relationship" (*i.e.*, the relationship between the bottomhole pressure and the flowrate) is important as this helps us to analyze and predict individual well performance. This relationship is called the "inflow performance relationship" (or *IPR*). The first presentation of an inflow performance relationship (or *IPR*) concept was made by Rawlins and Schellhardt[2] in 1935. In **Fig. 1.1** we provide a reproduction of this figure — where Rawlins and Schellhardt used this plot to illustrate the effect of liquid loading on gas production performance.

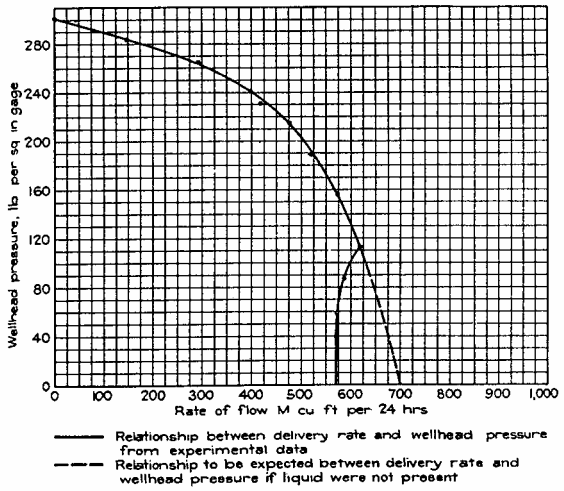

Fig. 1.1 — Primitive IPR plot for a gas well experiencing liquid loading (circa 1935) (after Rawlins and Schellhardt[2]).

In 1954 Gilbert[3] introduced the concept of an "inflow performance relationship" (or *IPR*) for the purpose of optimizing producing rates and flowing bottomhole pressures. In **Fig. 1.2** we reproduce Gilbert's *IPR* diagram for orientation.

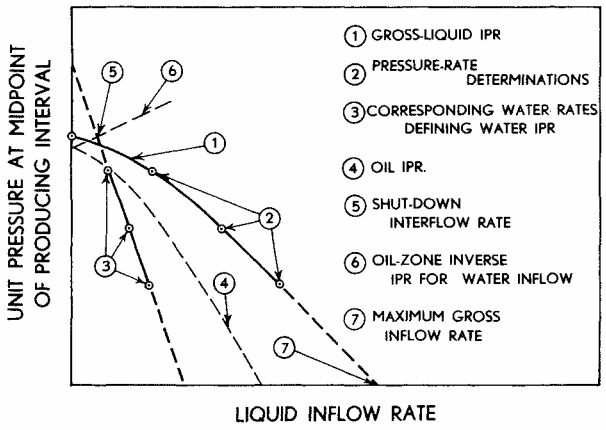

Fig. 1.2 — Primitive IPR plot for a gas well experiencing liquid loading (circa 1935) (after Gilbert[3]).

Using the pseudosteady-state flow equation (Eq. 1.2) or the productivity index form (Eq. 1.4), we can define the "inflow performance relation" (or *IPR*) for the liquid case in terms of the rate normalized by the maximum rate (*i.e.*, the rate for the case where p_{wf}=0). Mathematically, we can express the maximum oil rate using Eq. 1.2 as:

$$q_{o,\max} = \frac{\bar{p}}{b_{pss}} \quad (\text{where } p_{wf} = 0) \qquad \text{.....(1.5)}$$

Similarly, using Eq. 1.2 or Eq. 1.4 to solve for the rate at any time, we have:

$$q_o = \frac{1}{b_{pss}}(\bar{p} - p_{wf}) \qquad \text{.....(1.6)}$$

Dividing Eq. 1.6 by Eq. 1.5 we obtain the "*IPR* form," which is given as:

$$\frac{q_o}{q_{o,\max}} = 1 - \frac{p_{wf}}{\bar{p}} \qquad \text{.....(1.7)}$$

Raghavan[4] provides a general treatment of the inflow performance for the solution gas-drive case, and has chosen as the fundamental flow relation (for pseudosteady-state conditions), the following result:

$$q_o = J \int_{p_{wf}}^{\bar{p}} \frac{k_{ro}(S_o)}{\mu_o B_o} dp \qquad \text{.....(1.8)}$$

Where the J is the "*modified* productivity index" for this case, and is defined by:

$$J = \frac{1}{141.2}\frac{kh}{\left[\ln(r_e / r_w) - \frac{3}{4} + s\right]} \quad \text{.....(1.9)}$$

For the solution gas-drive case the *IPR* result is obtained directly from Eq. 1.8 (solved at any condition and at "open flow" conditions (*i.e.*, where p_{wf}=0)). These conditions yield the following result

$$\frac{q_o}{q_{o,\max}} = \frac{\int_{p_{wf}}^{\bar{p}} \frac{k_{ro}(S_o)}{\mu_o B_o} dp}{\int_0^{\bar{p}} \frac{k_{ro}(S_o)}{\mu_o B_o} dp} \quad \text{.....(1.10)}$$

We note (as did Raghavan), that the form given by Eq. 1.10 is not useful in a practical sense — we must reduce the integrals to simple functions of pressure.

One approach, suggested by Fetkovich[5] in the pursuit of another form of an *IPR* result, is that we could assume that the mobility function $k_{ro}(S_o)/(\mu_o B_o)$ is a "simple" function of pressure. For example, Fetkovich proposed the following:

$$\frac{k_{ro}(S_o)}{\mu_o B_o} = ap \text{ (where } a \text{ is simply a constant)} \quad \text{.....(1.11)}$$

Substituting Eq. 1.11 into Eq. 1.10, we obtain the following result:

$$\frac{q_o}{q_{o,\max}} = 1 - \frac{p_{wf}^2}{\bar{p}^2} \quad \text{.....(1.12)}$$

One could argue that Eq. 1.12 (and the assumption that lead to it (*i.e.*, Eq. 1.11)) is too simplistic to model all of the changes of the pressure and saturation-dependent properties during depletion. This would be true — but, as a practical result, Eq. 1.12 seems viable. Fetkovich[5] chose the "backpressure equation" as his fundamental relation in an effort to derive an alternate *IPR* model. For reference, the backpressure equation is given as:

$$q_o = J'(\bar{p}^2 - p_{wf}^2)^n \quad \text{.....(1.13)}$$

Finally, the "Fetkovich form" of the *IPR* equation is given as the "backpressure" modification of Eq. 1.12, which is written as:

$$\frac{q_o}{q_{o,\max}} = \left[1 - \frac{p_{wf}^2}{\bar{p}^2}\right]^n \quad \text{.....(1.14)}$$

For reference, the base assumption provided by Fetkovich form (i.e., $k_{ro}(S_o)/(\mu_o B_o)=ap$) is illustrated in schematic form in **Fig. 1.3**.

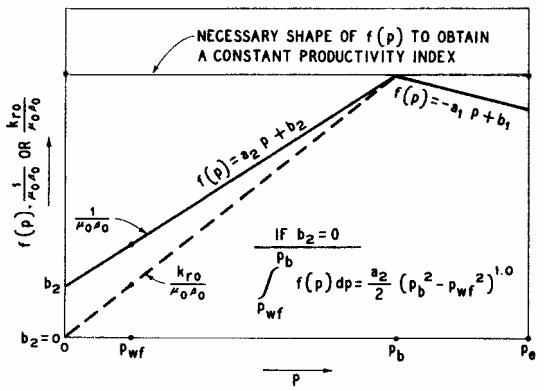

Fig. 1.3 — Mobility-pressure behavior for a solution gas-drive reservoir[5].

In 1968 Vogel[6] established an empirical relationship based on reservoir simulation results for a solution gas-drive reservoir. Vogel used twenty-one reservoir data sets to generate a broad suite of cases. In this work Vogel noted that the *shape* of the pressure (p_{wf}) versus production (q_o) curves were very similar at various values of cumulative oil production. As such, Vogel defined the dimensionless inflow performance curve by dividing the pressures and flowrates at each point by the intercepts on the respective *x* and *y*-axes (*i.e.*, the average reservoir pressure on the *y*-axis and the maximum oil flowrate on the *x*-axis).

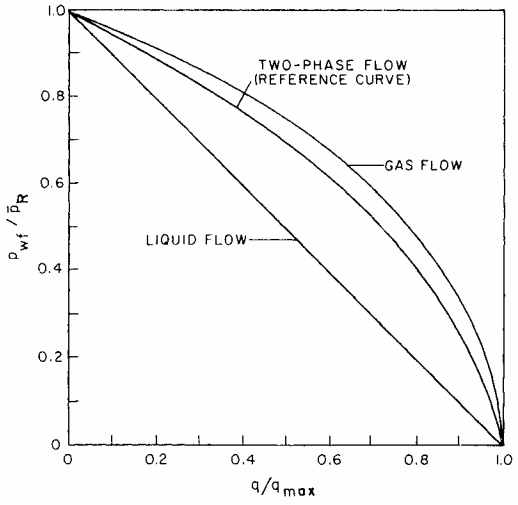

Fig. 1.4 — IPR schematic plot for single-phase oil, single-phase gas; and solution gas-drive systems (after Vogel[6]).

In performing this work, Vogel elected to produce a "reference curve" where this result is an average of the various depletion cases for a given reservoir scenario. Vogel recognized that the liquid (oil), gas (dry gas), and solution gas-drive cases have distinct behavior trends and was simply trying to produce a

mechanism for predicting production performance with a relatively simple result. In **Fig. 1.4** we present the Vogel plot illustrating the liquid (oil), gas (dry gas), and solution gas-drive cases.

The "Vogel correlation" for *IPR* behavior in a solution gas-drive system is given by:

$$\frac{q_o}{q_{o,\max}} = 1 - 0.2\left[\frac{p_{wf}}{\overline{p}}\right] - 0.8\left[\frac{p_{wf}}{\overline{p}}\right]^2 \quad \text{.....(1.15)}$$

In **Fig. 1.5** we reproduce the Vogel plot illustrating the *IPR* behavior for solution gas-drive systems at various stages of depletion — the "reference curve" is the Vogel correlation.

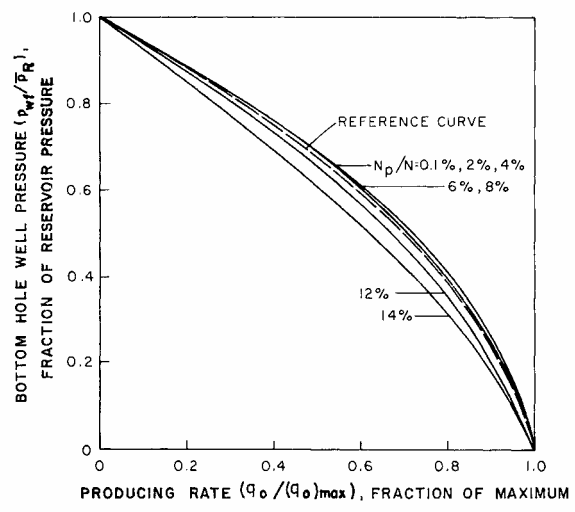

Fig. 1.5 — IPR behavior for solution gas-drive systems at various stages of depletion — the "reference curve" is the correlation presented by Vogel (after Vogel[6]).

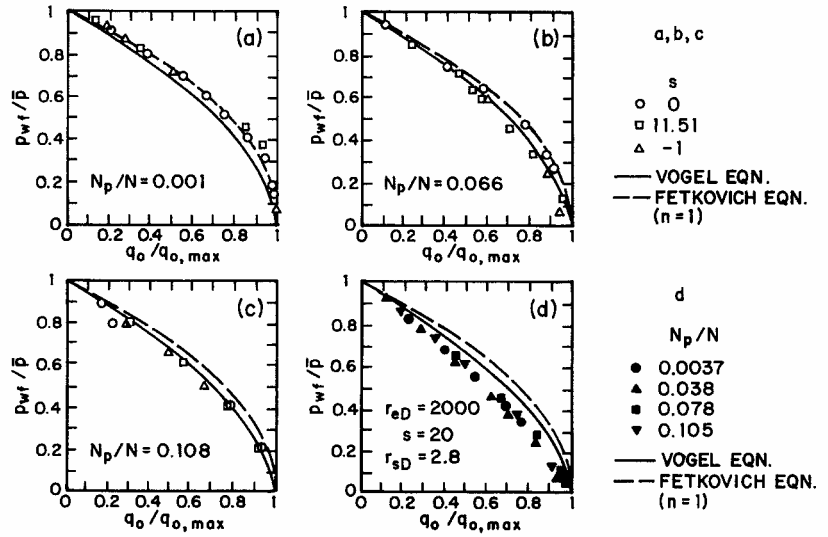

Fig. 1.6 — IPR behavior for a solution gas-drive reservoir (after Camacho and Raghavan[4]).

Recently, Camacho and Raghavan[4] showed that Vogel's result (Eq. 1.15) is directionally correct, while Fetkovich's result (Eq. 1.14) is less consistent with regard to matching the reservoir performance data compared to Vogel's result — except at early times (see **Fig. 1.6**)

In continuing our discussion of empirical approaches, Richardson and Shaw[7] presented a generalized inflow performance relationship (*IPR*) for solution gas-drive reservoirs as a function of the parameter, v:

$$\frac{q_o}{q_{o,\max}} = 1 - v\left[\frac{p_{wf}}{\bar{p}}\right] - (1-v)\left[\frac{p_{wf}}{\bar{p}}\right]^2 \quad \text{.....(1.16)}$$

The motivation for this "generalization" is most likely the desire to add "flexibility" to the Vogel form — to permit the relation to be "calibrated" to a particular data set, and perhaps even to establish a general formulation for the *IPR* concept. As comment, we note that using v=0.2 in Eq. 1.16 yields the Vogel case, and using v=1 in Eq. 1.16 yields the "black oil" result (Eq. 1.7) — similarly, the substitution of v=0 in Eq. 1.16 yields the modified Fetkovich *IPR* result (Eq. 1.12)

Richardson and Shaw provide a schematic plot to illustrate the behavior of the *IPR* function above and below the bubblepoint pressure (see **Fig. 1.7** for a reproduction of this schematic plot).

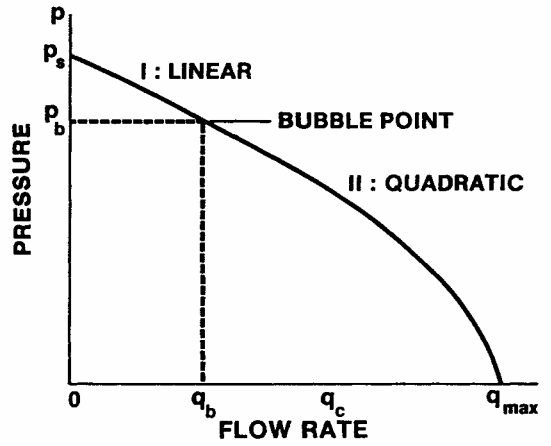

Fig. 1.7 — Schematic IPR behavior for a solution gas-drive reservoir — note the "linear" and "quadratic" characteristic regions (for $p>p_b$ and $p<p_b$, respectively) (after Richardson and Shaw[7]).

Particular to this work, Richardson and Shaw discuss procedures for testing wells where the objective is to use production data to solve for the v-parameter directly (where the v-parameter is optimized for a given case) — for example, using a two or three-rate test. We note in advance that we will use the formulation given by Eq. 1.16 to derive our new *IPR* models for gas and condensate behavior in gas condensate reservoir systems. It is interesting to note also that the modified Vogel relationship (Eq. 1.16) was previously used by Seidle and Erickson[8] for a different fluid system (*i.e.,* gas and water flow in coalbed gas wells).

Another attempt to quantify the *IPR* behavior for solution gas-drive systems was presented by Wiggins, *et. al.*[9] — where the result of this work is a polynomial series given in terms of $q_o/q_{o,\max}$ and $p_{wf}/\overline{p}$. The Wiggins, *et. al.* result is given by:

$$\frac{q_o}{q_{o,\max}} = 1 + a_1\left[\frac{p_{wf}}{\overline{p}}\right] + a_2\left[\frac{p_{wf}}{\overline{p}}\right]^2 + a_3\left[\frac{p_{wf}}{\overline{p}}\right]^3 + \ldots \quad (1.17)$$

Where the a_1, a_2, a_3, ... a_n coefficients are determined based on the mobility function and its derivatives taken at the average reservoir pressure ($\overline{p}$). This is a relatively impractical approach because of the derivatives involved. However, we must recognize that the *IPR* behavior can be related to fundamental flow theories. In **Appendix C** we reproduce the detailed theoretical approach presented by Wiggins, *et. al.*[9]

As an aside, Wiggins, *et al.* (ref. 6) also presents plots of oil mobility as functions of pressure (taken at various flowrates) as a means of calibrating their proposed *IPR* model (*i.e.*, Eq. 1.17). The purpose of presenting these mobility-pressure profiles was to establish the "stability" of the mobility profile for a given depletion level — which would confirm the use of an *IPR* model based on a "snapshot" of reservoir performance. An example mobility-pressure profile taken from the Wiggins, *et* al. reference is shown in **Fig. 1.8**.

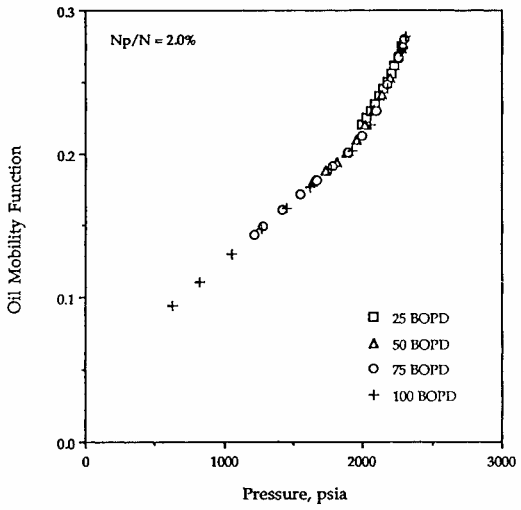

Fig. 1.8 — Oil mobility profiles as a function of pressure — various flowrates ("Case 2") (after Wiggins, *et al.*[9])

We will comment that the "double-linear" trend illustrated in **Fig. 1.8** is consistent with other work produced for solution gas-drive systems, and is somewhat in dispute with the model proposed by Fetkovich (see **Fig. 1.3**).

Another theoretical attempt to relate the *IPR* behavior with fundamental flow theories is developed in **Appendix D** — where this result is a second degree polynomial with a variable coefficient (v) that may in fact be a fairly strong function of pressure (and saturation). The starting point for this development is the pseudopressure formulation for the oil phase, which is given as:

$$p_{po}(p) = \left[\frac{\mu_o B_o}{k_o}\right]_{p_n} \int_{p_{base}}^{p} \left[\frac{k_o}{\mu_o B_o}\right] dp \quad \text{.....(1.18)}$$

In this work we presume that the oil mobility function has a linear relationship with average reservoir pressure. This may seem to be an intuitive (or even convenient assumption) — however, others (Fetkovich, in particular) have made this assumption and found it to be reasonable for many field applications. Specifically, the presumed behavior of the oil mobility function is given as:

$$\left[\frac{k_o}{\mu_o B_o}\right]_{\bar{p}} = f(\bar{p}) = a + 2b\bar{p} \quad \text{.....(1.19)}$$

Where a and b are constants established from the presumed behavior of the mobility profile.

Substituting Eq. 1.19 in Eq. 1.18 and manipulating (the details are provided in **Appendix D**), we have:

$$\frac{q_o}{q_{o,\max}} = 1 - v\left[\frac{p_{wf}}{\bar{p}}\right] - (1-v)\left[\frac{p_{wf}}{\bar{p}}\right]^2 \quad \text{.....(1.20)}$$

Where we immediately recognize that Eq. 1.20 has exactly the same form as the relation given by Richardson and Shaw (Eq. 1.16). The advantage of the new formation is that we have determined the relationship of the v-parameter and the pressure and saturation functions (*i.e.,* k_o, B_o, and μ_o). Specifically, the v-parameter is given as:

$$v = \frac{1}{\left(1 + \frac{b}{a}\bar{p}\right)} \quad \text{.....(1.21)}$$

For $\bar{p}$ =0, Eq. 1.19 reduces to:

$$\left[\frac{k_o}{\mu_o B_o}\right]_{\bar{p}=0} = a \quad \text{.....(1.22)}$$

Substituting Eqs. 1.19 and 1.22 into Eq. 1.21, we have

$$\nu = \frac{2\left[\frac{k_o}{\mu_o B_o}\right]_{\bar{p}=0}}{\left[\left[\frac{k_o}{\mu_o B_o}\right]_{\bar{p}=0} + \left[\frac{k_o}{\mu_o B_o}\right]_{\bar{p}}\right]} \quad \text{.....(1.23)}$$

Where Eq. 1.23 illustrates the unique dependence of the ν-parameter on the pressure and saturation dependent properties (k_o, B_o, and μ_o). We refer the reader to **Fig. 1.3** for the physical interpretation of Eq. 1.19. Another, perhaps more useful form of the ν-parameter defined by a new "β" parameter is given by:

$$\nu = \frac{2}{\beta + 1} \quad \text{.....(1.24)}$$

$$1 - \nu = \frac{\beta - 1}{\beta + 1} \quad \text{.....(1.25)}$$

where:

$$\beta = \frac{\left[\frac{k_o}{\mu_o B_o}\right]_{\bar{p}}}{\left[\frac{k_o}{\mu_o B_o}\right]_{\bar{p}=0}} \quad \text{.....(1.26)}$$

Substituting Eqs. 1.24 and 1.25 into Eq. 1.20 gives

$$\frac{q_o}{q_{o,\max}} = 1 - \frac{2}{\beta + 1}\left[\frac{p_{wf}}{\bar{p}}\right] - \frac{\beta - 1}{\beta + 1}\left[\frac{p_{wf}}{\bar{p}}\right]^2 \quad \text{.....(1.27)}$$

While we do not advocate Eq. 1.27 as a "new" form (we recommend the "Vogel" form (*i.e.*, Eq. 1.20)), we do recognize Eq. 1.27 as an "alternate" formulation — one with a direct analytical basis.

The most important results given by Wiggins, *et al.*[9].and our own work in **Appendix D** confirm the generalized quadratic rate-pressure model (*i.e.*, the model given by Richardson and Shaw[7] (Eq. 1.16)). While the relationship of the ν-parameter and the rock-fluid and fluid properties is achieved in the proposals given by Wiggins, *et al.*, as well as our own work (**Appendix D**), these relationships can only be applied indirectly or inferred. We continue to recommend the technique proposed by Richardson and Shaw to establish estimates of the ν-parameter.

1.2.2 *IPR* for Gas-Condensate Systems

In this section we discuss methods to represent *IPR* behavior for gas-condensate reservoir systems. Analogs and references to the solution gas-drive system are common for the case of a gas-condensate

system. However, our goal is to isolate the important factors/elements that must be addressed in order to correlate *IPR* behavior for gas-condensate reservoir systems.

Inflow performance relationships have been considered for gas-condensate reservoir systems by several authors — where virtually all of these studies have involved the use of compositional numerical simulation and (in most cases) a statistical correlation of the simulation results. This approach is necessary because the case of a gas-condensate reservoir is more complex due to the evolution of the condensate bank and multiphase flow, as well as the continuous changes in gas and liquid composition as fluid flow towards the well.

Fussell[10] addressed the case of production performance from gas condensate reservoir systems using a 1-D radial compositional simulator. O'Dell and Miller[11] introduced a gas-rate equation based on a pseudopressure function— where this formulation addresses the effect of condensate blockage. Their results show that even a minor region of condensate blockage/banking can substantially reduce the deliverability of the well.

Fevang and Whitson[12] present a gas-rate flow equation for gas-condensate systems, which employs a pseudopressure function (expressed in terms of conventional formation volume factors and gas-oil-ratios) as a mechanism to account for the effect of condensate banking. Their result is given by:

$$q_g = \frac{1}{141.2}\frac{kh}{\left[\ln(r_e/r_w)-3/4+s\right]}\int_{p_{wf}}^{\bar{p}}\left[\frac{k_{rg}}{\mu_g B_g}+R_s\frac{k_{ro}}{\mu_o B_o}\right]dp \quad \text{.....(1.28)}$$

Fevang and Whitson suggested that the pseudopressure integral could be evaluated by expanding the integral into three regions: (taken from ref. 12). We note that the effect of condensate blockage is implicitly incorporated in the method by which the pseudopressure integral is calculated.

- Region 1: An inner, near-wellbore region considered the main cause of productivity loss; where both gas and oil flow simultaneously (at different velocities).
- Region 2: A region of condensate "buildup" where two phases co-exist but only gas is mobile.
- Region 3: A region containing single-phase (original) reservoir gas.

For a given producing condition in a gas-condensate well under depletion, one, two or three flow regions may exist (**Fig. 1.9**). If the flowing bottomhole pressure is above the initial dewpoint pressure, then the fluid in the reservoir exists as a single phase gas. If the flowing bottomhole pressure is below the dew-point, the reservoir may contain three flow regions — where the size of these regions will change with time as the reservoir is depleted. Rousennac[13] has provided a schematic cartoon and example saturation-radius plot in **Fig. 1.9**.

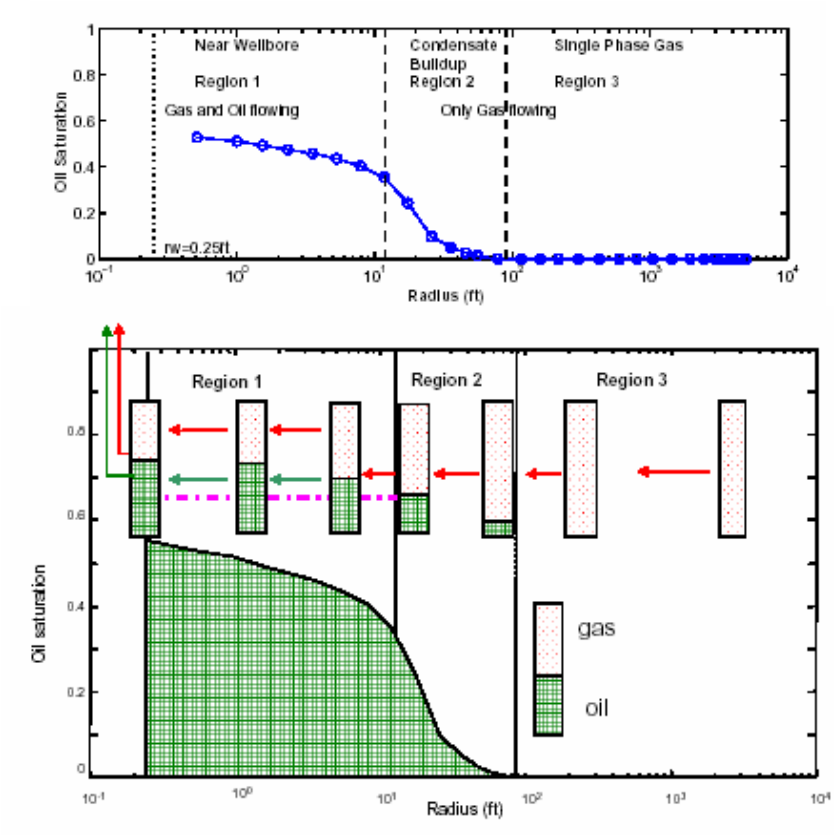

Fig. 1.9 — Schematic gas-condensate flow behavior during a drawdown (after Roussennac[13])

Fevang and Whitson[12] characterized the "flow regions" in **Fig. 1.9** as follows.

- Region 1 has a constant composition (*i.e.*, GOR) where the dewpoint of the producing mixture is equal to the reservoir pressure at the outer boundary of Region 1.
- Region 2 has a variable gas composition, which becomes leaner as we approach the well.
- Region 3 — the composition is constant and equal to that of the original reservoir gas.

The producing GOR, PVT properties, and gas-oil relative permeabilities are required in order to calculate the pseudopressure function given by Fevang and Whitson[12] (Eq. 1.28). While Eq. 1.28 is straightforward — *i.e.*, an integral in terms of pressure and saturation-dependent functions, these functions can not be known accurately in advance — which renders Eq. 1.28 as a possible analysis relation, *but not a predictive* (*or modelling*) *relation*.

It is worthwhile to note that Fevang and Whitson comment that *critical oil saturation* (S_{oc}) *has no effect on gas- condensate well deliverability*. While it is not our intention to dispute this comment, we will note that our work has addressed the influence of the following parameters on gas-condensate well deliverability: relative permeability, fluid composition, dewpoint pressure, reservoir temperature, S_{oc}, and S_{gr}.

In this work, we provide a simple methodology to estimate *IPR* functions for wells in gas-condensate reservoir systems — without the requirement of gas-to-oil ratio and saturation profiles in the reservoir as a function of pressure. The new *IPR* approach is developed using a large database of compositional reservoir simulation cases. We use the form of the Richardson and Shaw[7] model, but the ν-parameter will vary depending on the properties of a given reservoir fluid (as noted by the group of parameters we have identified as influential in the case of gas-condensate reservoir systems (see above)).

1.3 Research Objectives

1. To develop a simple and consistent method to correlate *IPR* trends for gas condensate reservoir systems — without direct knowledge of the distributions of GOR and the saturation profiles. Such functions vary continuously with time and space according to changes in fluid composition and pressure. A Vogel-type approach (q/q_{max} and $p_{wf}/\overline{p}$) will be used.

2. To prove that a modified Vogel correlation can be used to predict the *IPR* for gas condensate reservoir systems.

3. To develop functional correlations for the parameters ν_o and ν_g for the case of gas condensate reservoirs (*i.e.*, the Richardson and Shaw model (ref. 7) (the generalized Vogel-type model)). These correlations will be developed in terms of simple functions of fluid and reservoir properties.

1.4 Outline of the Thesis

The outline of the thesis is as follows:

- Chapter I — Literature Review
  - Introduction
  - Literature Review
  - Research Objectives
  - Outline of the Thesis
- Chapter II — Simulated Performance of Gas-Condensate Reservoirs
  - Modeling Issues
  - Fluids Inventory
  - Relative Permeability Curves Inventory
  - Performance Simulations
- Chapter III — *IPR* Behavior of Gas-Condensate Reservoirs
  - Model and Methodology
  - Plots and Discussion
- Chapter IV — Correlation of *IPR* Behavior
  - Rationale
  - Approach
  - Correlation
  - Validation — Examples of Application
  - Calibration

- Conclusions and Recommendations
  - Conclusions
  - Recommendations
- Appendix A — Inventory of Gas Condensate Simulation Cases
- Appendix B — Simulation Cases used for Validation (Gas Condensate Systems
- Appendix C — *IPR* Model — Wiggins, *et al.* Approach for Solution Gas-Drive Systems
- Appendix D — *IPR* Model — New Approach for Solution Gas-Drive Systems
- Appendix E — Eclipse Data File (Sample)

CHAPTER II

SIMULATED PERFORMANCE OF GAS-CONDENSATE RESERVOIRS

2.1 Modeling Issues

2.1.1 Reservoir Fluid Model

The depletion of a gas-condensate reservoir involves continuous composition changes of the reservoir fluid. The gas will become leaner close to the well due to condensate "drop out," and the condensate will eventually flow when the critical condensate saturation is exceeded. Fevang, *et al*.[14] analyzed production performance results using black-oil and compositional reservoir simulation models with a variety of fluids (ranging from medium-rich gas-condensates to fluids near the critical point) and they also considered various production schemes (natural depletion and injection). Fevang, *et al*. concluded that a black-oil model *could* accurately represent all such depletion cases whenever the proper PVT data are considered. However, compositional models are strongly recommended for gas injection studies for pressures below the dewpoint. Nevertheless Fevang, *et al*. also pointed out that there are significant differences in well deliverability depending on the $C7^+$ fraction split. Since we are interested in well deliverability/ performance, we have used a fully compositional model for our present work.

2.1.2 Grid and Reservoir Characteristics

We used a 1-D radial grid for our simulation model since the main purpose of this study is to evaluate the productivity of a single well in a gas condensate reservoir system. Many authors[5,10,11] have studied well productivity losses due to condensate blockage. In addition, Malachowski[15] concluded that when coarse grids are used in the simulation of gas-condensate reservoir systems, then the condensate saturation near the wellbore is underestimated. In wells constrained to a constant bottomhole pressure this course grid scenario provides an overestimate of the production rate and well productivity. Zapata[16] also demonstrated the effect of coarse grid simulation on cumulative condensate production.

Bottomhole pressure and production rates are required for *IPR* calculations — and, as such, we use fine grid cells near the wellbore to properly model the well productivity losses due to the build-up of condensate near the wellbore. We do maintain the use of coarser grids for the remainder of the reservoir. Most radial grid cell sizes are generated using a logarithmic distribution with the ratio between two consecutive cell sizes usually being 1.47. The maximum radial cell length was 500 ft.

All simulation cases were generated under the constraint of a constant bottomhole pressure. A small time step was selected in the beginning to model the initial stages of condensate banking, which, as previously stated, is an important issue for our analysis. Individual simulations were run for approximately 120 years to generate a complete *IPR* trend, an to assess the effect of condensate banking on ultimate recovery.

All cells in this study have a uniform thickness of 30 ft. The reservoir model is homogeneous and isotropic, with an absolute permeability of 5 md and a porosity of 0.20 (fraction). The simulation cases were generated from an initial pressure equal to the dewpoint pressure of the selected fluid, which means that, initially, the only fluid in the reservoir was gas (no water saturation was considered for any case in this study).

2.1.3 Assumptions in the Simulation

- Interfacial tension effects and non-Darcy flow effects are not considered.
- Capillary pressure is not considered.
- Near wellbore effects are accurately represented by a refined grid.
- Phase equilibrium is accurately calculated by the equation of state (EOS).
- A reduced permeability zone (skin) is not considered.
- Gravitational segregation of the condensate is not considered.
- No compositional gradient is considered.

2.2 Fluids Inventory

In order to develop an *IPR* model that could be applicable to lean and rich gas-condensate systems, 6 different fluids were selected for simulation. The first 4 fluids were synthetic — these include a light, a medium and a heavy component. **Table 2.1**summarizes their compositions[13].

Table 2.1 — Synthetic fluids.

Fluid	1	2	3	4
C1, mole fraction	0.8963	0.8700	0.9561	0.8700
C4, mole fraction	0.0300	0.0300	0.0150	0.0150
C10, mole fraction	0.0737	0.1000	0.0289	0.1150
$M_{mixture}$ (lb_m/lb-mole)	26.0027	29.1026	20.0832	30.2393

Additionally two real gas-condensate fluid samples from Colombia were selected. **Table 2.2** shows the detailed molar composition of the first sample "Cusiana" (Fluid 5).

Table 2.2 — Fluid 5 – Molar composition.

Components	Mole fraction z_i	Molecular weight M_i	$M_i z_i$
N2	0.0052	28.0130	0.1457
C1	0.6897	16.0430	11.0649
CO2	0.0457	44.0100	2.0113
C2	0.0889	30.0700	2.6732
C3	0.0418	44.0970	1.8433
IC4	0.0099	58.1240	0.5754
NC4	0.0140	58.1240	0.8137
IC5	0.0071	72.1510	0.5123
NC5	0.0060	72.1510	0.4329
Benzene	0.0000	78.1140	0.0000
C6	0.0099	86.1780	0.8532
Toluene	0.0000	92.1410	0.0000
C7	0.0102	96.0000	0.9792
C8	0.0128	107.0000	1.3696
C9	0.0097	121.0000	1.1737
C10	0.0073	134.0000	0.9782
C11	0.0053	147.0000	0.7791
C12	0.0044	161.0000	0.7084
C13	0.0048	175.0000	0.8400
C14	0.0041	190.0000	0.7790
C15	0.0036	206.0000	0.7416
C16	0.0028	222.0000	0.6216
C17	0.0026	237.0000	0.6162
C18	0.0024	251.0000	0.6024
C19	0.0019	263.0000	0.4997
C20	0.0016	275.0000	0.4400
C21	0.0013	291.0000	0.3783
C22	0.0011	300.0000	0.3300
C23	0.0010	312.0000	0.3120
C24	0.0008	324.0000	0.2592
C25	0.0007	337.0000	0.2359
C26	0.0006	349.0000	0.2094
C27	0.0006	360.0000	0.2160
C28	0.0005	372.0000	0.1860
C29	0.0004	382.0000	0.1528
$C30^+$	0.0013	394.0000	0.5122
		$M_{mixture}$ (lb_m/lb-mole)	34.8463

Tables 2.3 and 2.4 provide the separator test and the constant composition expansion (CCE) data at 254 ^oF as reported by Jaramillo[17].

Table 2.3 — Fluid 5 – Separator test at 254 deg F.

Pressure (psig)	Temperature (deg F)	GOR (scf/STB)	Gas specific gravity γ_g
500	180	6696.5	0.7728
30	150	208.2	1.205
15	80	68.07	2.078

Table 2.4 — Fluid 5 – Constant composition expansion at 254 deg F.

Pressure (psig)	Relative volume (fraction)	Liquid Saturation (fraction)	Gas density (lb_m/ft^3)
6358.1	0.9612	-	26.0075
6255.3	0.9665	-	25.8639
6157.4	0.9716	-	25.7266
6054.5	0.9773	-	25.5767
5958.7	0.9830	-	25.4269
5891.8	0.9869	-	25.3270
5841.8	0.9898	-	25.2584
5793.9	0.9927	-	25.1772
5744.0	0.9958	-	25.1023
5695.0	0.9990	-	25.0211
5680.0	1.0000	-	24.9962
5644.1	1.0030	0.017	-
5545.3	1.0100	0.059	-
5446.4	1.0190	0.091	-
5346.5	1.0280	0.117	-
5253.7	1.0370	0.138	-
5055.9	1.0570	0.168	-
4740.4	1.0930	0.205	-
4436.8	1.1360	0.212	-
4144.2	1.1870	0.214	-
3846.6	1.2490	0.212	-
3544.1	1.3280	0.205	-
3240.5	1.4260	0.194	-
2936.9	1.5500	0.180	-
2660.3	1.6940	0.164	
2350.7	1.9010	0.144	-
2044.1	2.1790	0.124	-
1737.6	2.5680	0.103	-
1435.0	3.1240	0.082	-
1133.4	4.0040	0.062	-

Fluid 5 contains too many individual components for reservoir simulation purposes, so lumping components is necessary. The selection of "pseudo-component" groups is based on differences in molecular weight and thermodynamic behavior as described by Whitson.[16] Once the "lumping" of components was

completed, the Peng-Robinson EOS (with the shifting for volume correction) was selected as the EOS and the associated tuning was achieved by performing regression on parameters such as the binary interaction coefficients (BIC) (between the heaviest and lightest pseudo-components), critical properties, shift parameters, and the acentric factors as detailed in Jaramillo[17] and Zapata.[16] The final pseudo-component groups and their properties are shown in **Table 2.5**. **Figures 2.1 and 2.2** present the tuned EOS using only 6 pseudo-components and 1 pure component (CO_2). The viscosity data were modeled based on the composition of the mixture using the Lohrenz method.[18]

Table 2.5 — Fluid 5 – Pseudo-components.

Pseudo-component	Components	Mole fraction	Molecular weight	Critical pressure (psig)	Critical temperature (deg F)	Critical volume (ft^3/lb_m)	Critical compressibility factor
	CO2	0.0457	44.0100	1056.60	88.79	1.51	0.27
GRP1	N2-C1	0.6949	16.1330	651.77	-117.46	1.57	0.28
GRP2	C2-C3	0.1307	34.5560	664.04	127.16	2.64	0.28
GRP3	IC4 to C6	0.0469	67.9640	490.47	350.28	4.68	0.27
GRP4	Toluene to C10	0.0400	112.5200	384.19	591.91	7.26	0.26
GRP5	C11 to C16	0.0250	178.7900	269.52	781.91	11.10	0.24
GRP6	C17 to $C30^+$	0.0168	303.6400	180.20	1001.10	17.67	0.22

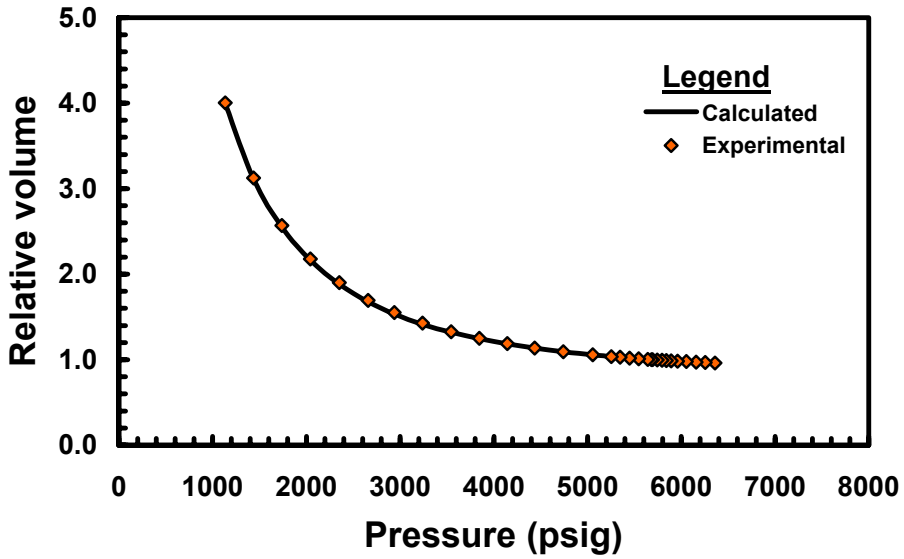

Fig. 2.1 — Comparison of experimental (CCE) and calculated EOS relative volume – .Cusiana.

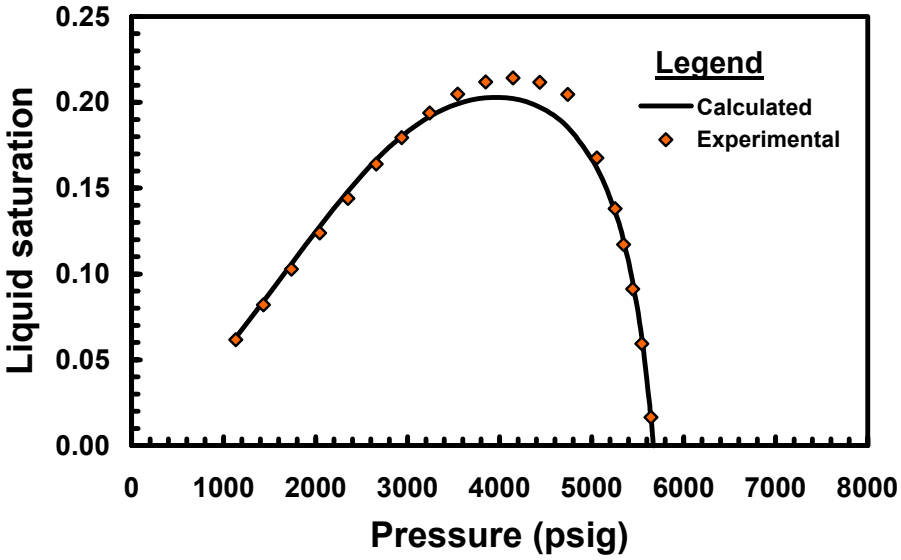

Fig. 2.2 — Comparison of experimental (CCE) and calculated EOS liquid saturation – Cusiana.

The last fluid selected for simulation corresponds to a Cupiagua sample[19]. **Table 2.6** shows its molar composition. **Table 2.7** shows the experimental results of a constant composition expansion (CCE) test at 285 °F as reported by Guerra[19].

Table 2.6 — Fluid 6 – Molar composition.

Components	Mole fraction ($\check{z}_i$)	Molecular weight (M_i)	M_i x $\check{z}_i$
N2	0.0025	28.0130	0.0692
C1	0.6171	16.0430	9.8998
CO2	0.0461	44.0100	2.0288
C2	0.0944	30.0700	2.8382
C3	0.0514	44.0970	2.2678
IC4	0.0136	58.1240	0.7934
NC4	0.0180	58.1240	1.0456
IC5	0.0098	72.1510	0.7085
NC5	0.0074	72.1510	0.5361
Benzene	0.0014	78.1140	0.1063
C6	0.0127	86.1780	1.0987
Toluene	0.0042	92.1410	0.3874
C7	0.0150	96.0000	1.4414
C8	0.0160	107.0000	1.7147
C9	0.0135	121.0000	1.6371
C10	0.0100	134.0000	1.3400
C11	0.0071	147.0000	1.0393
C12	0.0058	161.0000	0.9322

Table 2.6 — (Continued).

Components	Mole fraction ($\check{z}_i$)	Molecular weight (M_i)	M_i x $\check{z}_i$
C13	0.0066	175.0000	1.1515
C14	0.0057	190.0000	1.0754
C15	0.0049	206.0000	1.0011
C16	0.0038	222.0000	0.8547
C17	0.0035	237.0000	0.8247
C18	0.0035	251.0000	0.8709
C19	0.0029	263.0000	0.7600
C20	0.0025	275.0000	0.6875
C21	0.0021	291.0000	0.6198
C22	0.0020	300.0000	0.5910
C23	0.0018	312.0000	0.5522
C24	0.0016	324.0000	0.5184
C25	0.0015	337.0000	0.4954
C26	0.0013	349.0000	0.4676
C27	0.0012	360.0000	0.4464
C28	0.0011	372.0000	0.4055
C29	0.0010	382.0000	0.3782
$C30^+$	0.0070	394.0000	2.7658
		$M_{mixture}$ (lb_m/lb-mole)	44.3503

Table 2.7 — Fluid 6 – Constant composition expansion at 285 deg F.

Pressure (psia)	Relative volume (fraction)	Liquid Saturation (fraction)
8000.0	0.9060	-
7000.0	0.9350	-
6500.0	0.9540	-
6300.0	0.9630	-
6171.0	0.9680	-
6000.0	0.9760	-
5800.0	0.9860	-
5600.0	0.9980	-
5330.0	1.0000	0.001
5322.0	1.0170	0.007
5316.0	1.0180	0.039
5306.0	1.0180	0.112
5289.0	1.0190	0.172
5260.0	1.0210	0.231
5200.0	1.0260	0.285
5100.0	1.0350	0.324
4962.0	1.0480	0.347
4710.0	1.0730	0.360
4274.0	1.1300	0.353
3684.0	1.2370	0.323
3114.0	1.3990	0.288
2493.0	1.6750	0.233
1930.0	2.1240	0.180

Fluid 6 also contains too many individual components for reservoir simulation — as in the previous case, pseudo-component lumping was necessary. The grouping was done following similar criteria, establishing pseudo-components of similar physical properties, chemical properties, and molecular weights. The Whitson criteria (ref. 16) were again used to split the plus fraction as explained by Guerra.[19] Unlike Fluid 5, the CO_2 component was included as part of the one of the pseudo-component groups.

After the pseudo-component grouping was completed the Peng-Robinson EOS (with shifting for volume correction) was selected as the EOS. This volume correction was important to minimize erroneous predictions of gas *z*-factors and fluid densities. The parameters selected for tuning the EOS were the binary interaction coefficients (BIC) between the heaviest and lightest pseudo-components, critical properties, shift parameters, and acentric factors as explained by Guerra.[19] The final pseudo-component groups and their properties are shown in **Table 2.8**. **Figures 2.3 and 2.4** show that the tuned EOS using 7 pseudo-components matches the laboratory data quite well. The fluid viscosities were modeled using the Pedersen correlation.[20]

Table 2.8 — Fluid 6 – Pseudo-components.

Pseudo-component	Components	Mole fraction	Molecular weight	Critical pressure (psia)	Critical temperature (deg F)	Critical volume (ft^3/lb_m)	Critical compressibility factor
GRP1	N2 - C1	0.6195	16.0880	725.83	-87.18	1.59	0.29
GRP2	CO2 - C2	0.1405	34.6440	865.67	34.65	2.09	0.29
GRP3	C3 to NC4	0.0831	49.4400	615.11	169.27	3.60	0.28
GRP4	IC5 to Toluene	0.0356	84.4250	557.89	399.51	5.62	0.27
GRP5	C7 to C10	0.0546	125.3100	464.37	574.61	7.81	0.26
GRP6	C11 to C17	0.0373	212.3600	300.86	771.16	12.80	0.23
GRP7	C18 to $C30^+$	0.0295	394.4800	196.00	995.39	21.14	0.21

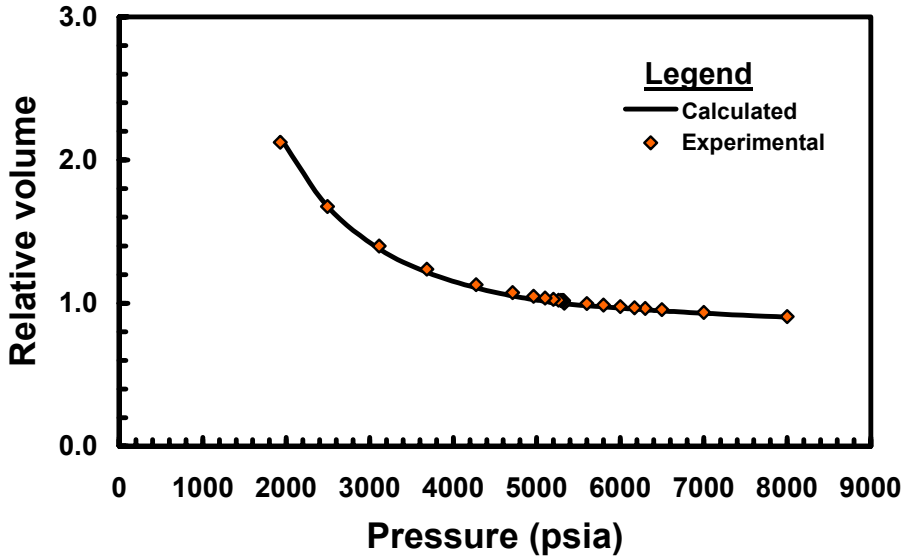

Fig. 2.3 — Comparison of experimental (CCE) and calculated EOS relative volume – Cupiagua.

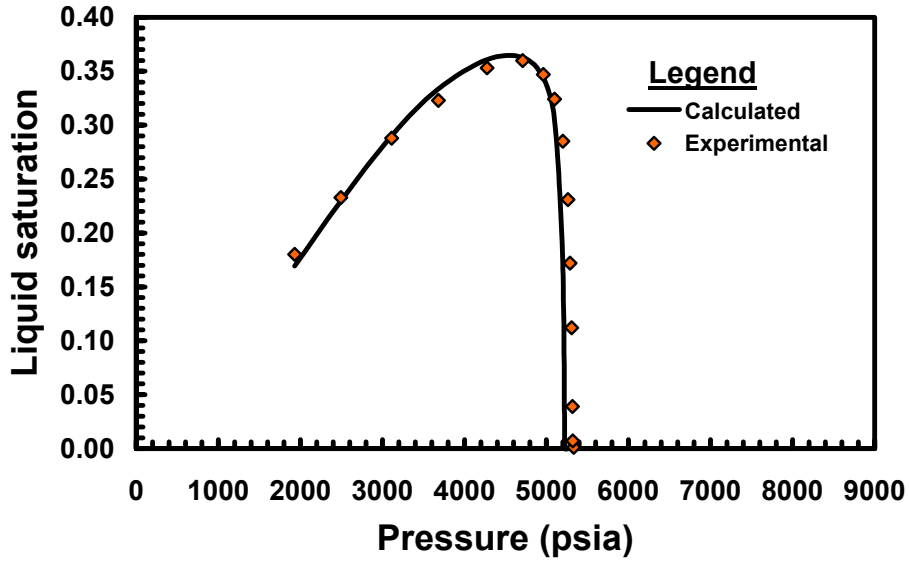

Fig. 2.4 — Comparison of experimental (CCE) and calculated EOS liquid saturation – Cupiagua.

It is important to note that once the EOS is properly tuned for each of the two last fluids using laboratory data, none of the fluid properties (including the BIC[21]) were modified — even when the fluid was used in simulations at different reservoir temperatures.

2.3 Relative Permeability Curves Inventory

There is no definitive relative permeability model to represent fluid flow in gas-condensate reservoirs due to the complexity of the laboratory measurements required and the dependency on interfacial tension, capillary forces, flowrate and other parameters. In an effort to cover a wide range of possibilities, seven different sets of relative permeability curves were used as a database to form a general *IPR*. Two groups of curves were considered as shown in **Table 2.9**. The first group included sets 1, 2, 3, 6, 7 — *i.e.*, the "Corey" relative permeability curves, which are defined by the following equations:

$$k_{ro} = k_{ro}(S_{wi})(S_o{}^*)^2\left[\frac{S_o}{1-S_{wi}}\right]^{(2+\lambda)/\lambda} \quad \text{.....(2.1)}$$

$$k_{rg} = k_{rg}(S_{wi})(S_g{}^*)^2\left[1-\left[1-S_g{}^*\right]^{(2+\lambda)/\lambda}\right] \quad \text{.....(2.2)}$$

Where: $S_o{}^* = \dfrac{S_o - S_{oc}}{1-S_{wi}-S_{oc}}$ $\qquad$ $S_g{}^* = \dfrac{S_g - S_{gr}}{1-S_{wi}-S_{gr}}$

Table 2.9 — Summary of parameters used in each set.

	set 1	set 2	set 3	set 4	set 5	set 6	set 7
S_{wi}	0	0	0	0	0	0	0
$k_{ro}(S_{wi})$	1	1	1	1	1	1	1
$k_{rg}(S_{wi})$	1	1	1	1	1	1	1
λ_1	2	2	2			2	2
λ_2	2	30	0.1			2	2
S_{oc}	0.1	0.1	0.1	0.1	0	0.3	0.3
S_{gr}	0	0	0	0.5	0	0	0.15
Model	Corey	Corey	Corey	not Corey	not Corey	Corey	Corey

λ_1 = Parameter to generate the oil relative permeability curve

λ_2 = Parameter to generate the gas relative permeability curve

The second group of curves was composed of sets 4, 5 where non-Corey curves were included in the analysis. Sets 1, 2 and 3 have the same relative oil permeability (k_{ro}). The relative permeability to gas is less favorable in set 2 but is more favorable in set 3. Sets 6 and 7 were considered to address the importance of different saturation endpoints. As **Fig. 2.5** shows, all the curves present a reduction of relative gas permeability (or mobility) when condensate saturation increases.

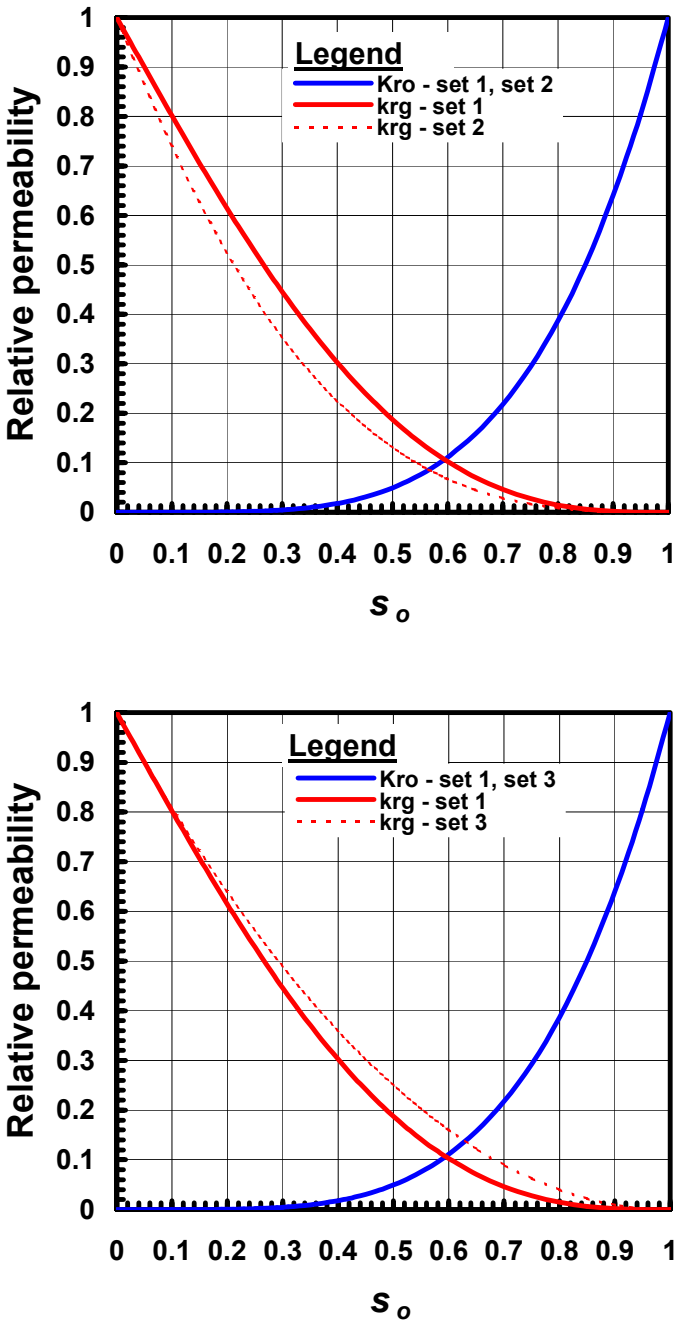

Fig. 2.5 — Relative permeability sets.

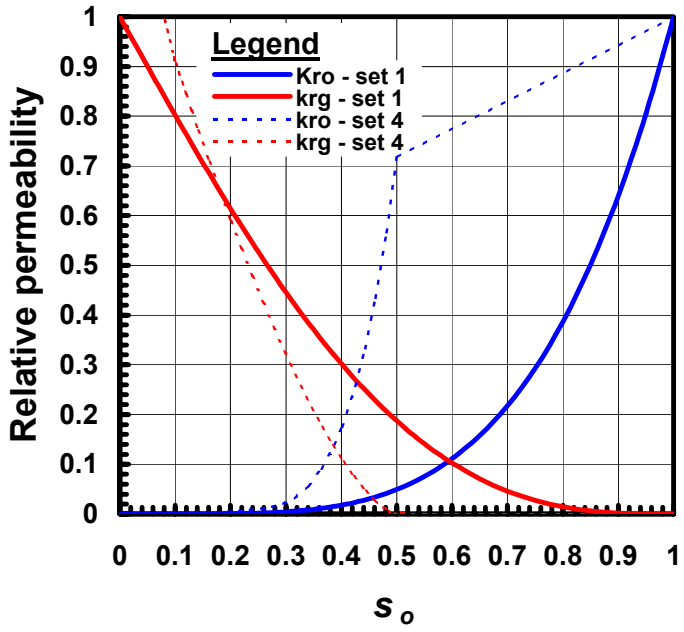

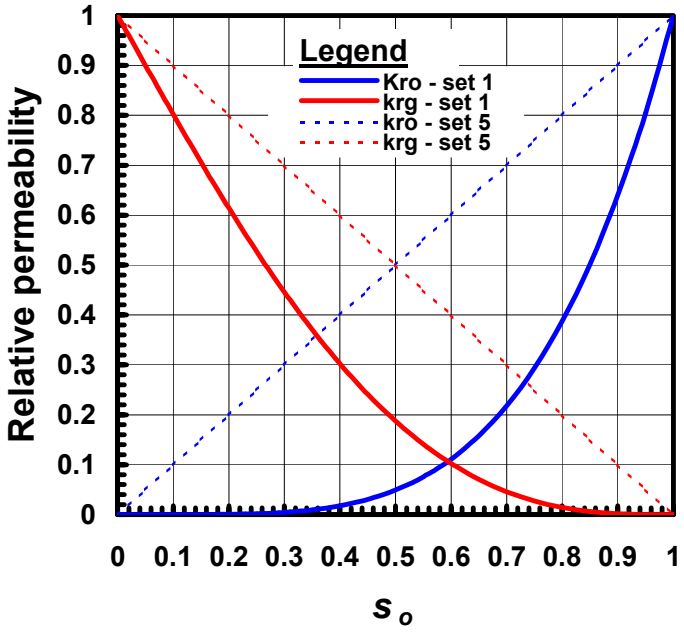

Fig. 2.5 — (Continued).

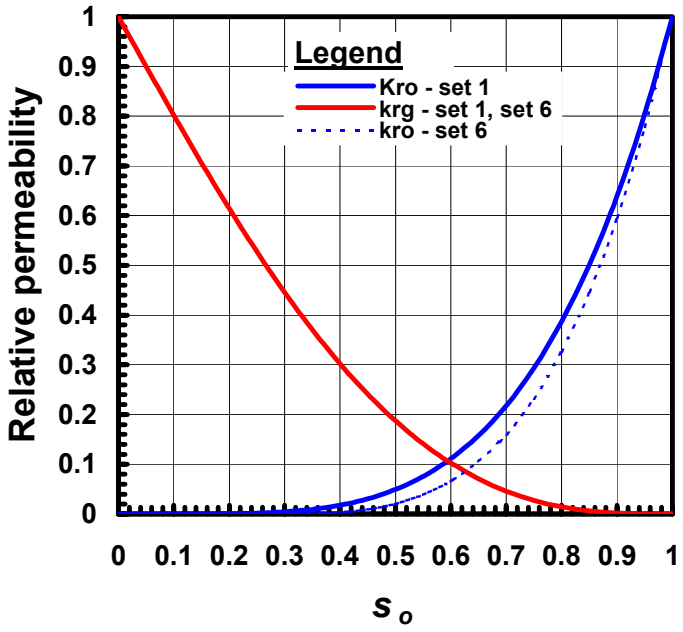

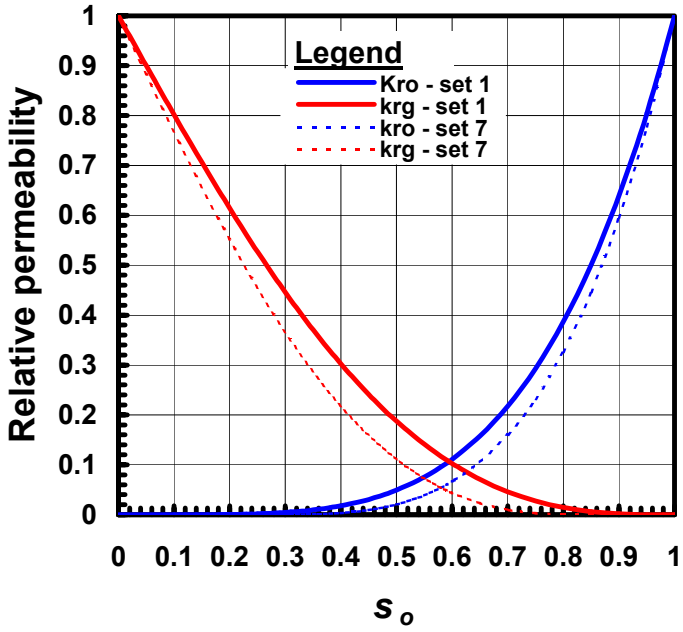

Fig. 2.5 — (Continued).

2.4 Performance Simulations

Once the simulation model was defined, it was run at three different temperatures (230, 260, 300 ^{o}F) considering various combinations of the seven relative permeability sets and the six fluids previously selected. **Table 2.10** shows the 62 cases simulated.

Table 2.10 — Simulated cases (62 cases).

Case	k_r set	Fluid set	S_{oc} (frac)	S_{gr} (frac)	p_{dew} (psia)	T (deg F)	N/G (STB/ MSCF)	Mole Fraction C1 (frac)	C2-C3 (frac)	C4-C6 (frac)	$C7^{+}$ (frac)	ρ_{mit} (lb_m/ft^3)	$M_{mixture}$ (lb_m/ lb-mole)
1	1	1	0.10	0.00	4278	260	0.1094	0.896	0.000	0.030	0.074	15.431	26.00
2	2	1	0.10	0.00	4278	260	0.1094	0.896	0.000	0.030	0.074	15.431	26.00
3	3	1	0.10	0.00	4278	260	0.1094	0.896	0.000	0.030	0.074	15.431	26.00
4	4	1	0.10	0.50	4278	260	0.1094	0.896	0.000	0.030	0.074	15.431	26.00
5	5	1	0.00	0.00	4278	260	0.1094	0.896	0.000	0.030	0.074	15.431	26.00
6	1	2	0.10	0.00	4575	260	0.1541	0.870	0.000	0.030	0.100	18.705	29.10
7	1	3	0.10	0.00	2845	260	0.0388	0.956	0.000	0.015	0.029	12.551	20.08
8	1	4	0.10	0.00	4814	260	0.1800	0.870	0.000	0.015	0.115	19.833	30.23
9	1	5	0.10	0.00	5015	260	0.1578	0.690	0.131	0.047	0.082	24.352	34.85
10	4	5	0.10	0.50	5015	260	0.1578	0.690	0.131	0.047	0.082	24.352	34.85
11	5	5	0.00	0.00	5015	260	0.1578	0.690	0.131	0.047	0.082	24.352	34.85
12	4	5	0.10	0.50	5040	230	0.1578	0.690	0.131	0.047	0.082	25.791	34.85
13	4	5	0.10	0.50	4925	300	0.1578	0.690	0.131	0.047	0.082	22.570	34.85
14	4	6	0.10	0.50	5113	260	0.2655	0.617	0.146	0.067	0.121	30.635	44.35
15	4	6	0.10	0.50	5084	230	0.2655	0.617	0.146	0.067	0.121	33.289	44.35
16	4	6	0.10	0.50	5117	300	0.2655	0.617	0.146	0.067	0.121	36.078	44.35
17	1	5	0.10	0.00	5040	230	0.1578	0.690	0.131	0.047	0.082	25.791	34.85
18	2	5	0.10	0.00	5015	260	0.1578	0.690	0.131	0.047	0.082	24.352	34.85
19	3	5	0.10	0.00	5015	260	0.1578	0.690	0.131	0.047	0.082	24.352	34.85
20	2	5	0.10	0.00	5040	230	0.1578	0.690	0.131	0.047	0.082	25.791	34.85
21	3	5	0.10	0.00	5040	230	0.1578	0.690	0.131	0.047	0.082	25.791	34.85
22	1	5	0.10	0.00	4925	300	0.1578	0.690	0.131	0.047	0.082	22.570	34.85
23	2	5	0.10	0.00	4925	300	0.1578	0.690	0.131	0.047	0.082	22.570	34.85
24	3	5	0.10	0.00	4925	300	0.1578	0.690	0.131	0.047	0.082	22.570	34.85
25	5	5	0.00	0.00	4925	300	0.1578	0.690	0.131	0.047	0.082	22.570	34.85
26	1	6	0.10	0.00	5113	260	0.2655	0.617	0.146	0.067	0.121	30.635	44.35
27	5	6	0.00	0.00	5113	260	0.2655	0.617	0.146	0.067	0.121	30.635	44.35
28	1	6	0.10	0.00	5084	230	0.2655	0.617	0.146	0.067	0.121	33.289	44.35
29	5	6	0.00	0.00	5084	230	0.2655	0.617	0.146	0.067	0.121	33.289	44.35
30	1	6	0.10	0.00	5117	300	0.2655	0.617	0.146	0.067	0.121	36.078	44.35
31	5	6	0.00	0.00	5117	300	0.2655	0.617	0.146	0.067	0.121	36.078	44.35
32	4	2	0.10	0.50	4575	260	0.1541	0.870	0.000	0.030	0.100	18.705	29.10
33	5	2	0.00	0.00	4575	260	0.1541	0.870	0.000	0.030	0.100	18.705	29.10
34	5	3	0.00	0.00	2845	260	0.0388	0.956	0.000	0.015	0.029	12.551	20.08
35	4	4	0.10	0.50	4814	260	0.1800	0.870	0.000	0.015	0.115	19.833	30.23
36	5	4	0.00	0.00	4814	260	0.1800	0.870	0.000	0.015	0.115	19.833	30.23
37	1	1	0.10	0.00	4512	230	0.1094	0.896	0.000	0.030	0.074	17.613	26.00
38	4	1	0.10	0.50	4512	230	0.1094	0.896	0.000	0.030	0.074	17.613	26.00
39	5	1	0.00	0.00	4512	230	0.1094	0.896	0.000	0.030	0.074	17.613	26.00
40	1	1	0.10	0.00	3864	300	0.1094	0.896	0.000	0.030	0.074	15.469	26.00
41	4	1	0.10	0.50	3864	300	0.1094	0.896	0.000	0.030	0.074	15.469	26.00
42	5	1	0.00	0.00	3864	300	0.1094	0.896	0.000	0.030	0.074	15.469	26.00
43	1	2	0.10	0.00	4755	230	0.1541	0.870	0.000	0.030	0.100	19.778	29.10
44	4	2	0.10	0.50	4755	230	0.1541	0.870	0.000	0.030	0.100	19.778	29.10
45	5	2	0.00	0.00	4755	230	0.1541	0.870	0.000	0.030	0.100	19.778	29.10
46	1	2	0.10	0.00	4249	300	0.1541	0.870	0.000	0.030	0.100	17.428	29.10
47	4	2	0.10	0.50	4249	300	0.1541	0.870	0.000	0.030	0.100	17.428	29.10
48	5	2	0.00	0.00	4249	300	0.1541	0.870	0.000	0.030	0.100	17.428	29.10
49	6	1	0.30	0.00	4278	260	0.1094	0.896	0.000	0.030	0.074	15.431	26.00
50	6	2	0.30	0.00	4575	260	0.1541	0.870	0.000	0.030	0.100	18.705	29.10

Table 2.10 — (Continued).

Case	k_r set	Fluid set	S_{wc} (frac)	S_{gr} (frac)	p_{dew} (psia)	T (deg F)	N/G (STB/ MSCF)	Mole Fraction C1 (frac)	C2-C3 (frac)	C4-C6 (frac)	$C7^+$ (frac)	ρ_{mix} (lb_m/ft^3)	$M_{mixture}$ (lb_m/ lb-mole)
51	6	5	0.30	0.00	5015	260	0.1578	0.690	0.131	0.047	0.082	24.352	34.85
52	6	6	0.30	0.00	5113	260	0.2655	0.617	0.146	0.067	0.121	30.635	44.35
53	6	6	0.30	0.00	5084	230	0.2655	0.617	0.146	0.067	0.121	33.289	44.35
54	6	6	0.30	0.00	5117	300	0.2655	0.617	0.146	0.067	0.121	36.078	44.35
55	6	1	0.30	0.00	3864	300	0.1094	0.896	0.000	0.030	0.074	15.469	26.00
56	6	5	0.30	0.00	4925	300	0.1578	0.690	0.131	0.047	0.082	22.570	34.85
57	7	1	0.30	0.15	4278	260	0.1094	0.896	0.000	0.030	0.074	15.431	26.00
58	7	1	0.30	0.15	3864	300	0.1094	0.896	0.000	0.030	0.074	15.469	26.00
59	7	5	0.30	0.15	5015	260	0.1578	0.690	0.131	0.047	0.082	24.352	34.85
60	7	5	0.30	0.15	4925	300	0.1578	0.690	0.131	0.047	0.082	22.570	34.85
61	7	6	0.30	0.15	5100	260	0.2655	0.617	0.146	0.067	0.121	30.635	44.35
62	7	6	0.30	0.15	5117	300	0.2655	0.617	0.146	0.067	0.121	36.078	44.35

For each case considered, 30 to 45 simulations with constant but different bottomhole pressures were run. Each of the simulations was begun at the dew point pressure of the fluid at the conditions selected; with the purpose being to evaluate only the phase behavior of the condensate in the two-phase region, where condensate and gas coexist together and go through significant composition changes. Maximum surface gas (G) and surface condensate (N) volumes with respect to the separator were determined for each simulated case to evaluate the recovery of these fluids. The pressure of the separator was set to 14.7 psia and its temperature to 60 deg F.

Condensate and gas production rates at eight selected values of both condensate and gas production were tabulated as a function of bottomhole flowing pressure. The deliverability curves for condensate and dry gas were constructed as follows: p_{wf} versus q_o or p_{wf} versus q_g for a specific cumulative oil production (N_p) or cumulative gas production (G_p) respectively. The resulting condensate and gas *IPR* curves are shown in detail in **Appendix A**.

When analyzing the results shown in **Appendix A**, all the condensate and dry gas *IPR* curves display some curvature when producing below the dew point pressure. A similar curvature in the *IPR* curves was reported by Xiong[22] for the dry gas phase in a gas-condensate reservoir. It is important to notice that there is a remarkable difference in shape between the condensate *IPR* curves for a very rich condensate system such as Fluid 6 (Cupiagua), which has the greatest liquid drop up (35%) and the greatest N values, and the other fluids. The *IPR* curves of the rich gas-condensate will become closer to each other when fluid becomes richer (compare **Figs. 2.6 and 2.7**).

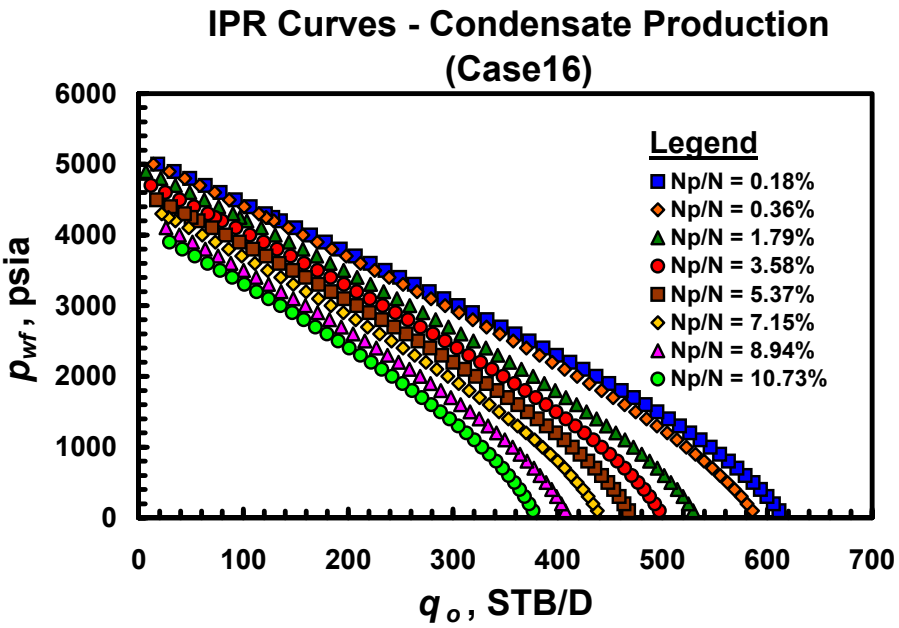

Fig. 2.6 — Dimensional IPR trends for Case 16 — Very rich gas condensate performance trends (Cupiagua).

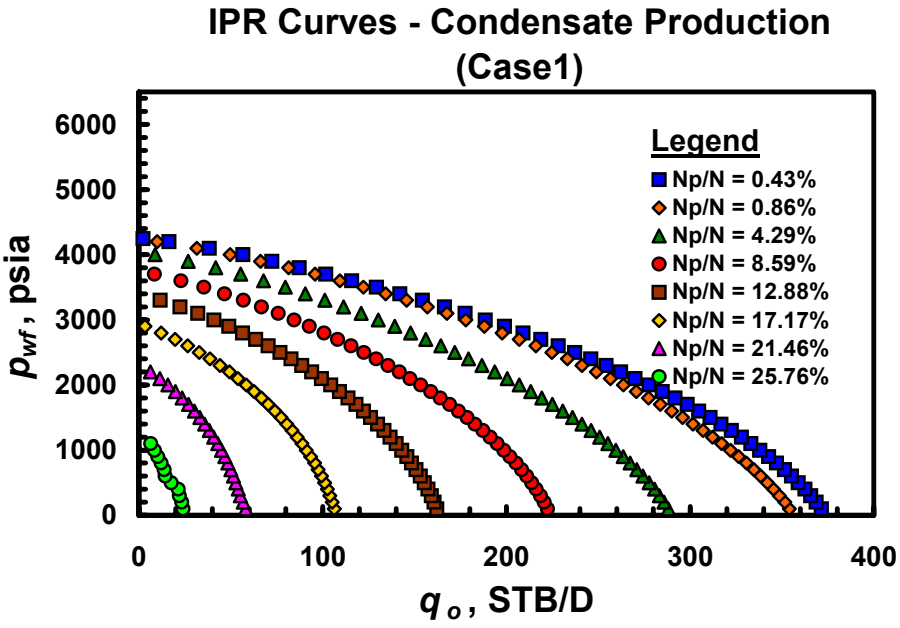

Fig. 2.7 — Dimensional IPR trends for Case 1 — Lean gas condensate performance trends.

Comparing the dimensional *IPR* curves of both condensate and dry gas, we found that the shape of the dry gas *IPR* curves changes more significantly with the stage of depletion than the condensate curves. There was also a more pronounced overlap in the dry gas *IPR* curves, which means that these cases reach very similar values at different stages of depletion on both axes x and y (q_o and p_{wf}). Finally we can conclude that in spite of some initial differences, both the condensate and the dry gas *IPR* curves somewhat resemble the *IPR* curves presented by Vogel[6] for solution gas-drive reservoirs. This led us to attempt to fit a quadratic model to both sets of curves.

CHAPTER III

IPR BEHAVIOR OF GAS CONDENSATE RESERVOIRS

3.1 Model and Methodology

As discussed in Chapter II, the dimensional *IPR* curves for gas-condensate reservoirs were generated using the same procedure that Vogel[6] proposed for solution gas-drive reservoirs. Since the traditional "*IPR* curvature" was observed in all 62 simulated cases, quadratic polynomials were fitted to each curve (condensate liquid and dry gas) and extrapolated to determine the appropriate intercepts on the x and y axes ($q_{o,max}$ and $\bar{p}$ respectively).

The dimensional *IPR* curves were used as the basis for dimensionless *IPR* curves in the form of a modified Vogel relationship. For the condensate (or "oil" phase) we have:

$$\frac{q_o}{q_{o,\max}} = 1 - v_o \left[\frac{p_{wf}}{\bar{p}}\right] - (1 - v_o)\left[\frac{p_{wf}}{\bar{p}}\right]^2 \quad \text{.....(3.1)}$$

The parameter v_o is determined using a non-linear optimization routine, specifically the "Solver" module as implemented in Microsoft Excel.[23] During this calculation estimates of the intercept values on each curve (*i.e.*, the. $q_{o,max}$ and $\bar{p}$ values) are also simultaneously refined.

We will provide an orientation to the optimization process as implemented in MS Excel — specifically, our process for optimizing the $q_{o,max}$ and $\bar{p}$ values (and the v_o parameter) for a particular depletion ratio, N_p/N. We first consider the "y-axis"— $q_o/q_{o,max}$ for a given N_p/N trend, given as:

$$y_{i,j} = \frac{(q_o)_{i,j}}{(q_{o,max})_j} \quad \text{.....(3.2)}$$

$$x_{i,j} = \frac{(p_{wf})_i}{(\bar{p})_j} \ (p_{wf} \text{ is constant for a given simulation case}) \quad \text{.....(3.3)}$$

We cast the optimization problem into the following double summation form, where Solver is used to minimize the "residual function" for the condensate case, J_o:

$$J_o = \sum_{j=1}^{(m)_{N_p}} \sum_{i=1}^{(n)_{p_{wf}}} \left| \left[y_{i,j} - \left[1 - v_o x_{i,j} - (1 - v_o) x_{i,j}^2 \right] \right] \right| \quad \text{.....(3.4)}$$

We note that we have cast this problem into an *absolute error form* as opposed to the typical "least squares" formulation. This is relevant — the Solver algorithm is completely general, and we believe that

this formulation (in terms of absolute error) yields better results than the least squares formulation for this problem. For the gas case we use the same procedures as given above in order to estimate the v_g parameter as well as the optimized values of $q_{g,max}$ and $\bar{p}$.

The relevant governing equations include the "gas form" of the *IPR* equation

$$\frac{q_g}{q_{g,\max}} = 1 - v_g \left[\frac{p_{wf}}{\bar{p}}\right] - (1 - v_g)\left[\frac{p_{wf}}{\bar{p}}\right]^2 \quad \text{.....(3.5)}$$

and the "residual function" for the dry gas case, J_g:

$$J_g = \sum_{j=1}^{(m)_{G_p}} \sum_{i=1}^{(n)_{p_{wf}}} \left| \left[y_{i,j} - \left[1 - v_g x_{i,j} - (1 - v_g) x_{i,j}^2 \right] \right] \right| \quad \text{..... (3.6)}$$

An example of the resulting dimensionless *IPR* curves is shown in **Fig. 3.1** where wee illustrate that, when using the appropriate values of v_o and v_g, the eight-inflow performance curves can be collapsed into a single dimensionless curve (this confirms the Vogel (in principle) approach for applications to gas condensate reservoir performance).

In spite of the differences between the dimensional ***IPR*** curves for condensate and dry gas (as previously explained in Chapter II) and the ones generated by Vogel[6], it was possible to non-dimensionalize both sets of curves using a modified Vogel *IPR*. In **Appendix A** we present the dimensionless *IPR* curves for each of the 62 simulated cases.

To test the accuracy of the dimensionless *IPR* for reproducing the dimensional (or field) behavior, the rates that were initially obtained from simulation at constant bottomhole pressure were compared to those calculated using the modified Vogel correlation (Eq. 3.1 or Eq. 3.5). Knowing the v_o and v_g parameters from the dimensionless *IPR* formulation and also the intercepts in the *x* and *y* directions ($q_{o,g,max}$ and $\bar{p}$ respectively) for each stage of depletion (N_p/N or G_p/G), the dimensional *IPR* curves for condensate and dry gas were satisfactorily reconstructed (see **Figs. 3.2 and 3.3**). It is important to notice that even at late depletion stages (or low reservoir pressures) the modified Vogel correlation[7] seems to accurately represent the "real" performance obtained from simulation.

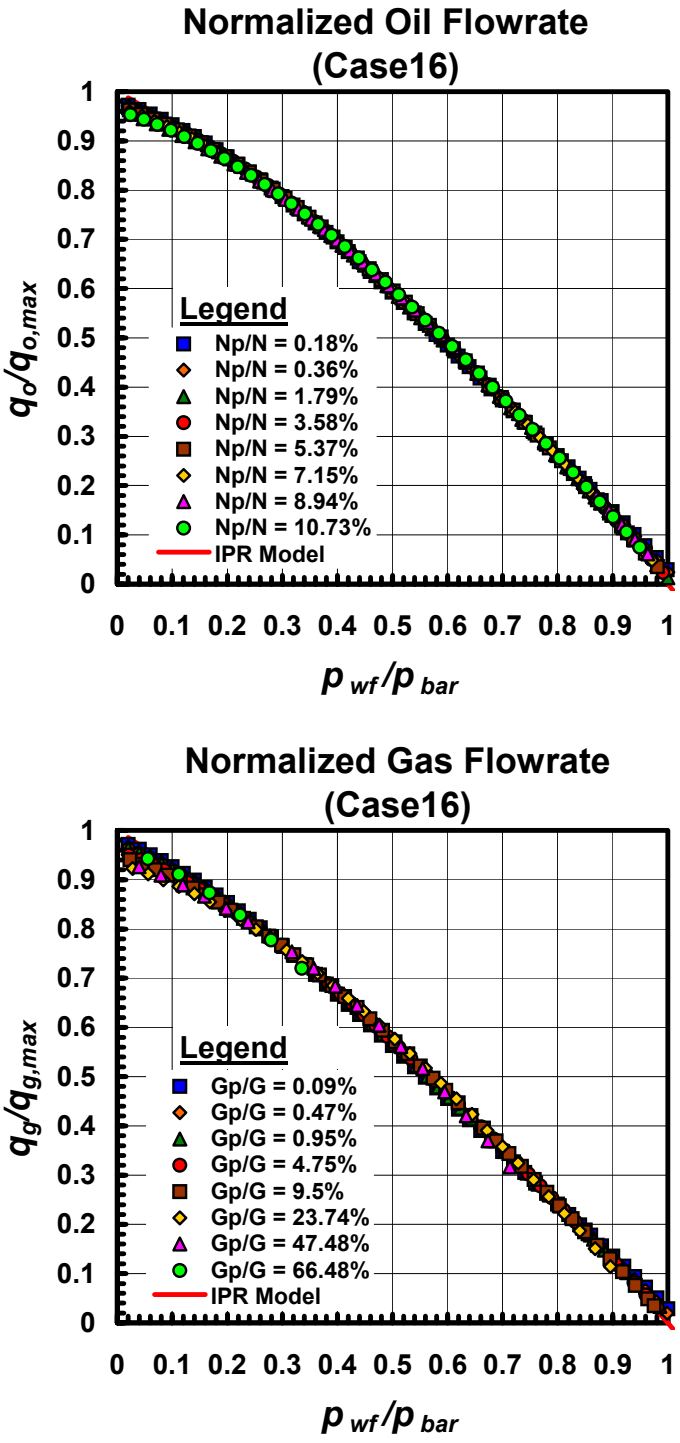

Fig. 3.1 — Dimensionless IPR trends for Case 16 — gas condensate and dry gas performance trends.

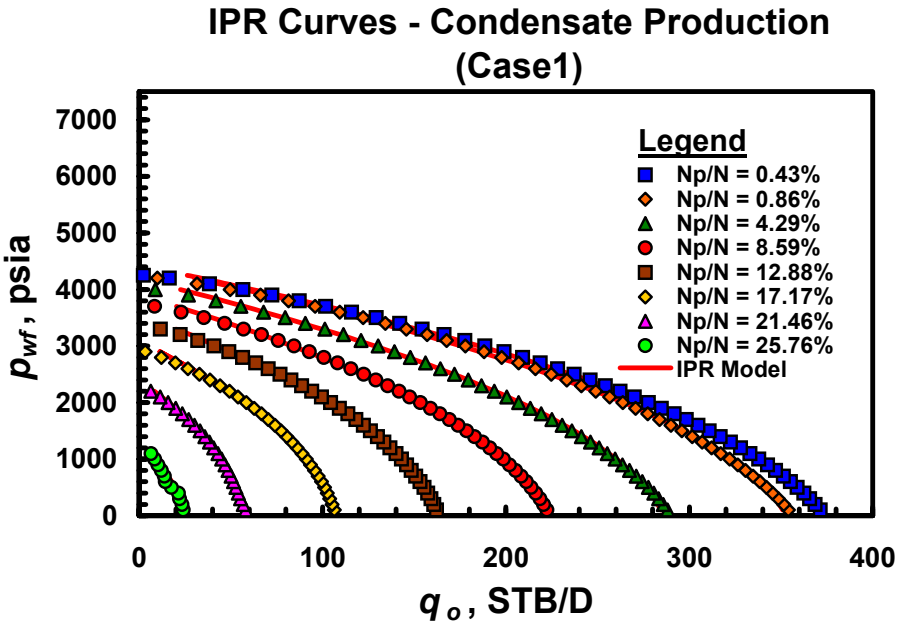

Fig. 3.2 — Dimensional IPR trends for Case 1 — calculated versus simulated gas condensate production.

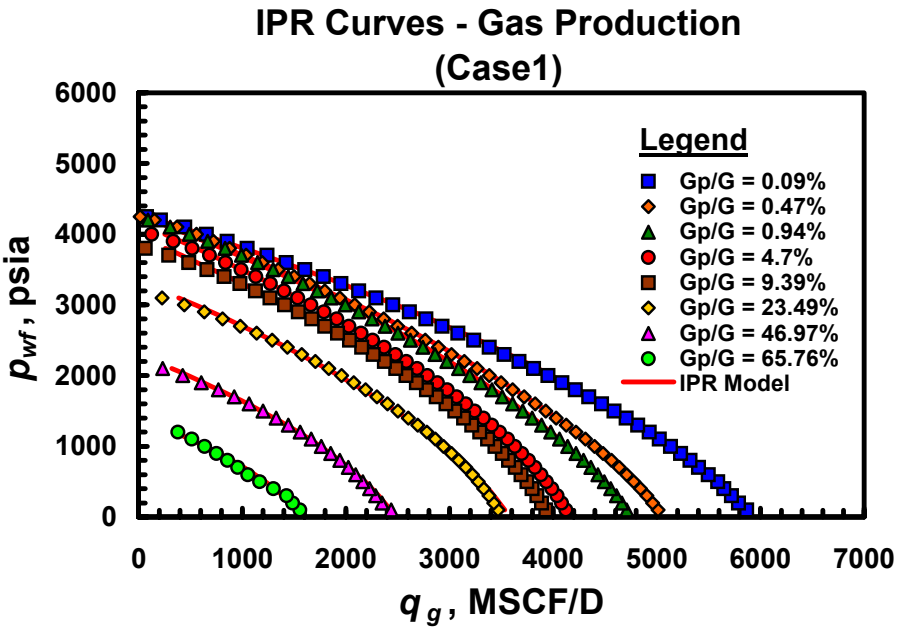

Fig. 3.3 — Dimensional IPR trends for Case 1 — calculated versus simulated dry gas production.

Analysis of the results shown in **Appendix A** in detail at very late stages of depletion, the dimensionless *IPR* curves for dry gas or condensate do not accurately predict the well performance for a gas-condensate reservoir. In the case of dry gas we propose that the *IPR* concept can only be applied below a value of 40 percent for the dry gas depletion ratio (G_p/G), and in the case of condensate, we propose a maximum value of 20 percent for the condensate depletion ratio (N_p/N). Nevertheless, these maximum percentages for applicability are not fixed for all cases considered — we do note exceptional case for both the condensate as well as in the dry gas cases (dimensionless *IPR* results). Additionally, in all the cases involving the richest condensate fluid (Cupiagua) the maximum condensate depletion ratio (N_p/N) was approximately 10 percent — however, this value was achieved due to maximum cumulative production at the end of almost 120 years.

The Vogel[6] correlation for solution gas-drive reservoirs showed that after 12 percent of recovery (*i.e.*, N_p/N) the dimensionless *IPR* curve is no longer very accurate. Our study has determined that, for the case of gas condensate reservoir systems, the modified Vogel correlation can be applied up to a dry gas depletion ratio (G_p/G) of 40 percent and a condensate depletion ratio (N_p/N) of 20 percent. These values cover the normal range of recovery factors encountered for gas-condensate reservoirs under natural depletion — therefore, the application of the dimensionless model is feasible. **Table 3.1** shows the ν_o and ν_g parameters for each of the 62 simulated cases.

Table 3.1 — ν_o and ν_g parameters (62 cases).

Case	k_r set	Fluid set	S_{wc} (frac)	S_{gr} (frac)	p_{dew} (psia)	T (deg F)	N/G (STB/ MSCF)	Mole Fraction C1 (frac)	C2-C3 (frac)	C4-C6 (frac)	$C7^+$ (frac)	ρ_{init} (lb_m/ft^3)	$M_{mixture}$ (lb_m/ lb-mole)	ν_o (dim-less)	ν_g (dim-less)
1	1	1	0.10	0.00	4278	260	0.1094	0.896	0.000	0.030	0.074	15.431	26.00	0.18	0.42
2	2	1	0.10	0.00	4278	260	0.1094	0.896	0.000	0.030	0.074	15.431	26.00	0.19	0.42
3	3	1	0.10	0.00	4278	260	0.1094	0.896	0.000	0.030	0.074	15.431	26.00	0.15	0.43
4	4	1	0.10	0.50	4278	260	0.1094	0.896	0.000	0.030	0.074	15.431	26.00	0.19	0.25
5	5	1	0.00	0.00	4278	260	0.1094	0.896	0.000	0.030	0.074	15.431	26.00	0.27	0.45
6	1	2	0.10	0.00	4575	260	0.1541	0.870	0.000	0.030	0.100	18.705	29.10	0.19	0.49
7	1	3	0.10	0.00	2845	260	0.0388	0.956	0.000	0.015	0.029	12.551	20.08	0.20	0.28
8	1	4	0.10	0.00	4814	260	0.1800	0.870	0.000	0.015	0.115	19.833	30.23	0.21	0.51
9	1	5	0.10	0.00	5015	260	0.1578	0.690	0.131	0.047	0.082	24.352	34.85	0.25	0.50
10	4	5	0.10	0.50	5015	260	0.1578	0.690	0.131	0.047	0.082	24.352	34.85	0.29	0.48
11	5	5	0.00	0.00	5015	260	0.1578	0.690	0.131	0.047	0.082	24.352	34.85	0.34	0.56
12	4	5	0.10	0.50	5040	230	0.1578	0.690	0.131	0.047	0.082	25.791	34.85	0.31	0.49
13	4	5	0.10	0.50	4925	300	0.1578	0.690	0.131	0.047	0.082	22.570	34.85	0.26	0.45
14	4	6	0.10	0.50	5113	260	0.2655	0.617	0.146	0.067	0.121	30.635	44.35	0.64	0.75
15	4	6	0.10	0.50	5084	230	0.2655	0.617	0.146	0.067	0.121	33.289	44.35	0.65	0.73
16	4	6	0.10	0.50	5117	300	0.2655	0.617	0.146	0.067	0.121	36.078	44.35	0.61	0.72
17	1	5	0.10	0.00	5040	230	0.1578	0.690	0.131	0.047	0.082	25.791	34.85	0.26	0.52
18	2	5	0.10	0.00	5015	260	0.1578	0.690	0.131	0.047	0.082	24.352	34.85	0.25	0.49
19	3	5	0.10	0.00	5015	260	0.1578	0.690	0.131	0.047	0.082	24.352	34.85	0.26	0.51
20	2	5	0.10	0.00	5040	230	0.1578	0.690	0.131	0.047	0.082	25.791	34.85	0.26	0.51
21	3	5	0.10	0.00	5040	230	0.1578	0.690	0.131	0.047	0.082	25.791	34.85	0.25	0.52
22	1	5	0.10	0.00	4925	300	0.1578	0.690	0.131	0.047	0.082	22.570	34.85	0.24	0.48
23	2	5	0.10	0.00	4925	300	0.1578	0.690	0.131	0.047	0.082	22.570	34.85	0.24	0.47
24	3	5	0.10	0.00	4925	300	0.1578	0.690	0.131	0.047	0.082	22.570	34.85	0.24	0.47
25	5	5	0.00	0.00	4925	300	0.1578	0.690	0.131	0.047	0.082	22.570	34.85	0.34	0.53
26	1	6	0.10	0.00	5113	260	0.2655	0.617	0.146	0.067	0.121	30.635	44.35	0.55	0.77
27	5	6	0.00	0.00	5113	260	0.2655	0.617	0.146	0.067	0.121	30.635	44.35	0.66	0.80
28	1	6	0.10	0.00	5084	230	0.2655	0.617	0.146	0.067	0.121	33.289	44.35	0.58	0.81
29	5	6	0.00	0.00	5084	230	0.2655	0.617	0.146	0.067	0.121	33.289	44.35	0.68	0.83
30	1	6	0.10	0.00	5117	300	0.2655	0.617	0.146	0.067	0.121	36.078	44.35	0.52	0.73
31	5	6	0.00	0.00	5117	300	0.2655	0.617	0.146	0.067	0.121	36.078	44.35	0.62	0.74
32	4	2	0.10	0.50	4575	260	0.1541	0.870	0.000	0.030	0.100	18.705	29.10	0.23	0.45
33	5	2	0.00	0.00	4575	260	0.1541	0.870	0.000	0.030	0.100	18.705	29.10	0.33	0.51
34	5	3	0.00	0.00	2845	260	0.0388	0.956	0.000	0.015	0.029	12.551	20.08	0.16	0.39
35	4	4	0.10	0.50	4814	260	0.1800	0.870	0.000	0.015	0.115	19.833	30.23	0.27	0.48
36	5	4	0.00	0.00	4814	260	0.1800	0.870	0.000	0.015	0.115	19.833	30.23	0.35	0.53
37	1	1	0.10	0.00	4512	230	0.1094	0.896	0.000	0.030	0.074	17.613	26.00	0.14	0.44
38	4	1	0.10	0.50	4512	230	0.1094	0.896	0.000	0.030	0.074	17.613	26.00	0.18	0.43
39	5	1	0.00	0.00	4512	230	0.1094	0.896	0.000	0.030	0.074	17.613	26.00	0.28	0.49
40	1	1	0.10	0.00	3864	300	0.1094	0.896	0.000	0.030	0.074	15.469	26.00	0.22	0.40
41	4	1	0.10	0.50	3864	300	0.1094	0.896	0.000	0.030	0.074	15.469	26.00	0.22	0.29
42	5	1	0.00	0.00	3864	300	0.1094	0.896	0.000	0.030	0.074	15.469	26.00	0.26	0.39
43	1	2	0.10	0.00	4755	230	0.1541	0.870	0.000	0.030	0.100	19.778	29.10	0.17	0.52
44	4	2	0.10	0.50	4755	230	0.1541	0.870	0.000	0.030	0.100	19.778	29.10	0.25	0.47
45	5	2	0.00	0.00	4755	230	0.1541	0.870	0.000	0.030	0.100	19.778	29.10	0.34	0.55
46	1	2	0.10	0.00	4249	300	0.1541	0.870	0.000	0.030	0.100	17.428	29.10	0.26	0.45
47	4	2	0.10	0.50	4249	300	0.1541	0.870	0.000	0.030	0.100	17.428	29.10	0.24	0.43
48	5	2	0.00	0.00	4249	300	0.1541	0.870	0.000	0.030	0.100	17.428	29.10	0.31	0.45
49	6	1	0.30	0.00	4278	260	0.1094	0.896	0.000	0.030	0.074	15.431	26.00	0.19	0.41
50	6	2	0.30	0.00	4575	260	0.1541	0.870	0.000	0.030	0.100	18.705	29.10	0.18	0.49

Table 3.1 — (Continued).

Case	k_r set	Fluid set	S_{wc} (frac)	S_{gr} (frac)	p_{dew} (psia)	T (deg F)	N/G (STB/ MSCF)	Mole Fraction C1 (frac)	C2-C3 (frac)	C4-C6 (frac)	$C7^+$ (frac)	ρ_{init} (lb_m/ft^3)	$M_{mixture}$ (lb_m/ lb-mole)	v_o (dim-less)	v_g (dim-less)
51	6	5	0.30	0.00	5015	260	0.1578	0.690	0.131	0.047	0.082	24.352	34.85	0.26	0.52
52	6	6	0.30	0.00	5113	260	0.2655	0.617	0.146	0.067	0.121	30.635	44.35	0.52	0.76
53	6	6	0.30	0.00	5084	230	0.2655	0.617	0.146	0.067	0.121	33.289	44.35	0.57	0.82
54	6	6	0.30	0.00	5117	300	0.2655	0.617	0.146	0.067	0.121	36.078	44.35	0.50	0.72
55	6	1	0.30	0.00	3864	300	0.1094	0.896	0.000	0.030	0.074	15.469	26.00	0.24	0.41
56	6	5	0.30	0.00	4925	300	0.1578	0.690	0.131	0.047	0.082	22.570	34.85	0.26	0.45
57	7	1	0.30	0.15	4278	260	0.1094	0.896	0.000	0.030	0.074	15.431	26.00	0.26	0.39
58	7	1	0.30	0.15	3864	300	0.1094	0.896	0.000	0.030	0.074	15.469	26.00	0.26	0.42
59	7	5	0.30	0.15	5015	260	0.1578	0.690	0.131	0.047	0.082	24.352	34.85	0.25	0.46
60	7	5	0.30	0.15	4925	300	0.1578	0.690	0.131	0.047	0.082	22.570	34.85	0.28	0.41
61	7	6	0.30	0.15	5100	260	0.2655	0.617	0.146	0.067	0.121	30.635	44.35	0.57	0.79
62	7	6	0.30	0.15	5117	300	0.2655	0.617	0.146	0.067	0.121	36.078	44.35	0.52	0.74

3.2 Plots and Discussion

In **Table 3.1** we present the results of the 62 cases considered — these data include PVT data, fluid type, residual saturations and the v_o and v_g parameter results. Specifically, different mixture compositions, condensate fluid richness, dewpoint pressures, reservoir temperatures, relative permeability models, and relative permeability end points were considered to evaluate the effect of these variables on the v_o and v_g parameters.

Unlike the standard Vogel case, the values of the v_o and v_g parameters are not unique for different gas condensate reservoirs and vary depending on the fluid and reservoir properties. In spite of this variance, the values of the v_o and v_g parameters are constant for a given condensate system — which means that these properties will not vary significantly with the depletion stage. This makes it possible to use the modified Vogel correlation not only to calculate the a "current" *IPR* curve, but also to predict future *IPR* behavior. Once v_o and v_g are determined for a particular condensate system, we can use the same v_o and v_g parameters to calculate future *IPR* trends for condensate and/or dry gas — changing only the intercepts according to the stage of depletion (*i.e.*, the $q_{o,g,max}$ and $\overline{p}$ values).

Analyzing the results obtained in **Table 3.1** in more detail we believe that the value of v_g is always higher than the corresponding v_o value for the same case — see **Fig. 3.4**.

In an attempt to establish a general variable that could represent the richness of the condensate fluid, the ratio of *N*/*G* was selected as well as the initial molecular weight of the mixture. These are "univariate" relations and are presented in **Figs. 3.5 and 3.6** where we noted that both cases seem comparable in illustrating the fluid richness and both plots seem to indicate a direct relation between the v_o and v_g parameters.

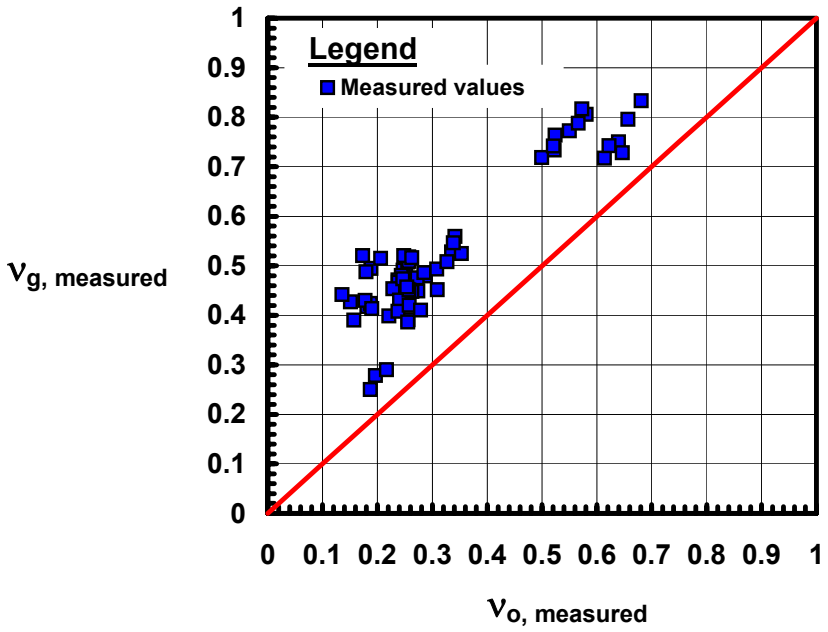

Fig. 3.4 — Comparison of the ν_o and ν_g parameters.

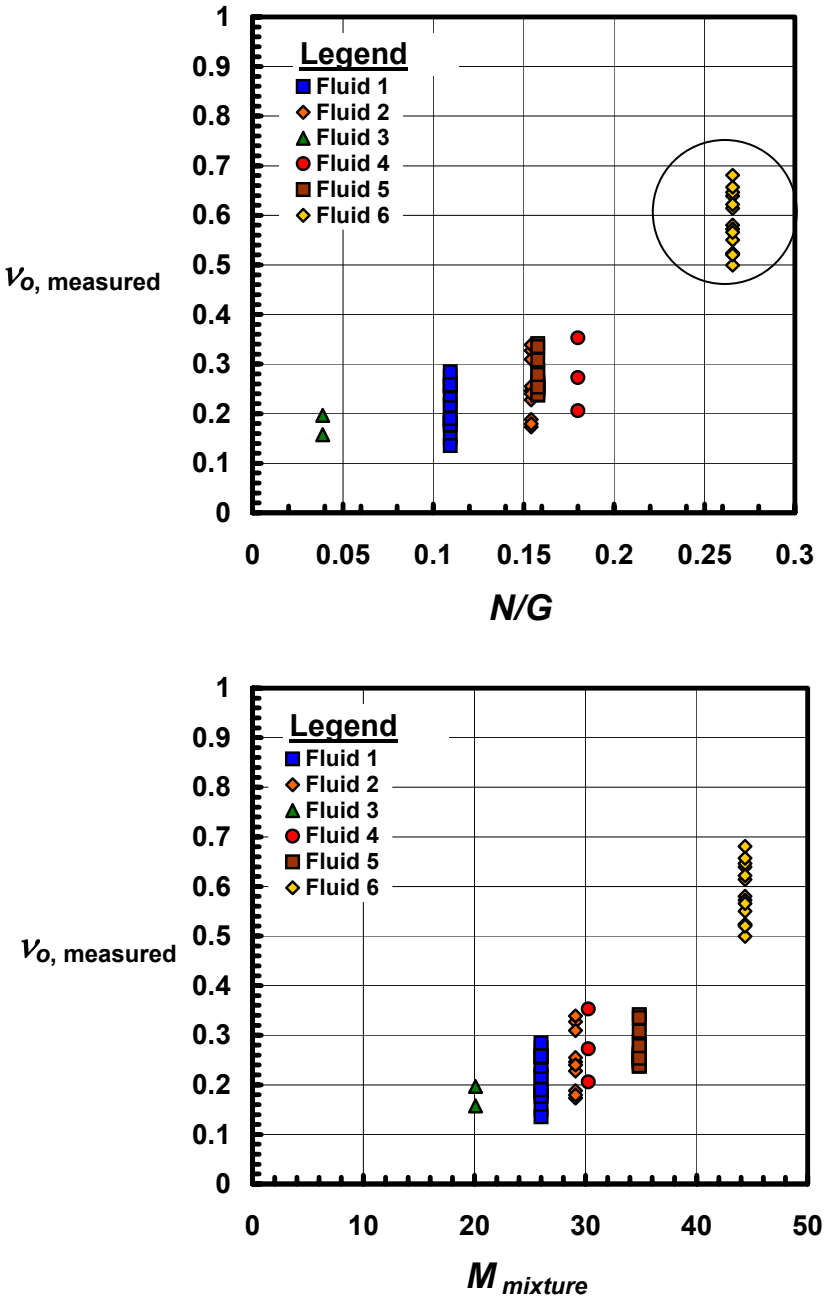

Fig. 3.5 — ν_o versus N/G and molecular weight of the mixture ($M_{mixture}$).

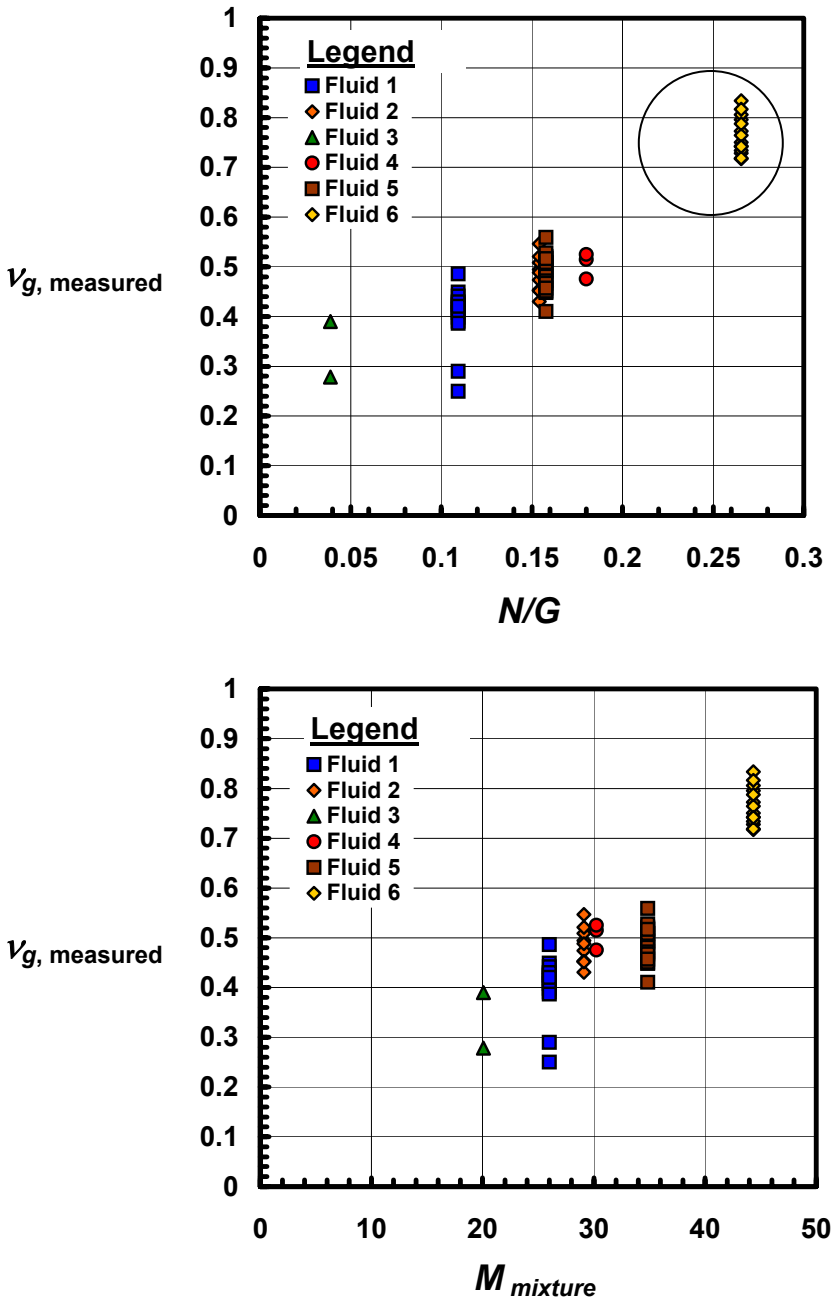

Fig. 3.6 — ν_g versus N/G and molecular weight of the mixture ($M_{mixture}$).

Figures 3.5 and 3.6 also show that there is a clear, well separated group of points with the highest ν_o and ν_g values when compared with the other fluids. This group corresponds to the richest condensate fluid (Cupiagua — Fluid 6).

Now that we have established the variation of the ν_o and ν_g parameters with the fluid properties, we will also evaluate how the change in values of the ν_o and/or ν_g parameters affect the shape of the dimensionless *IPR* and how accurately these need to be predicted in order to get an accurate dimensionless and dimensional *IPR*. In **Fig. 3.7** we show that, for gas condensate reservoirs, as the values of ν_o and/or ν_g are reduced, the curvature is increased. We note that Richardson and Shaw[7] first recorded this phenomenon for solution gas-drive reservoir cases.

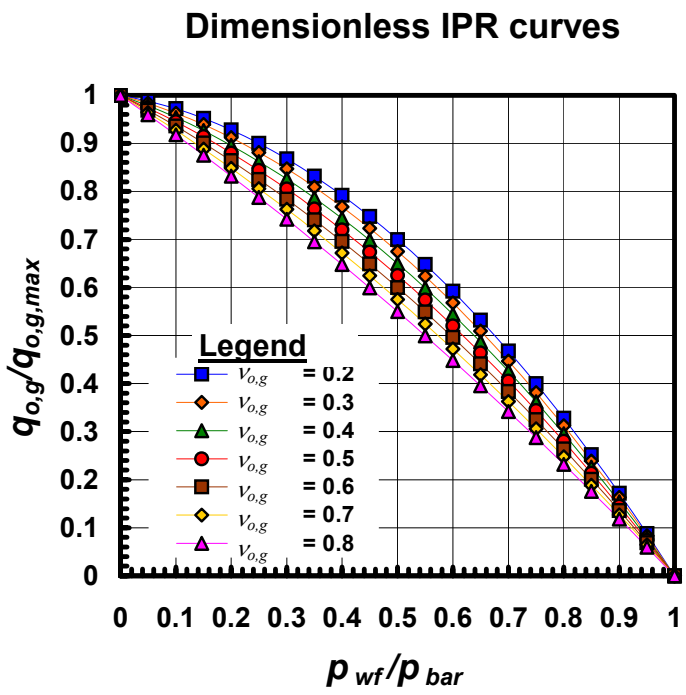

Fig. 3.7 — Variation of dimensionless IPR shape with ν_o and ν_g parameters.

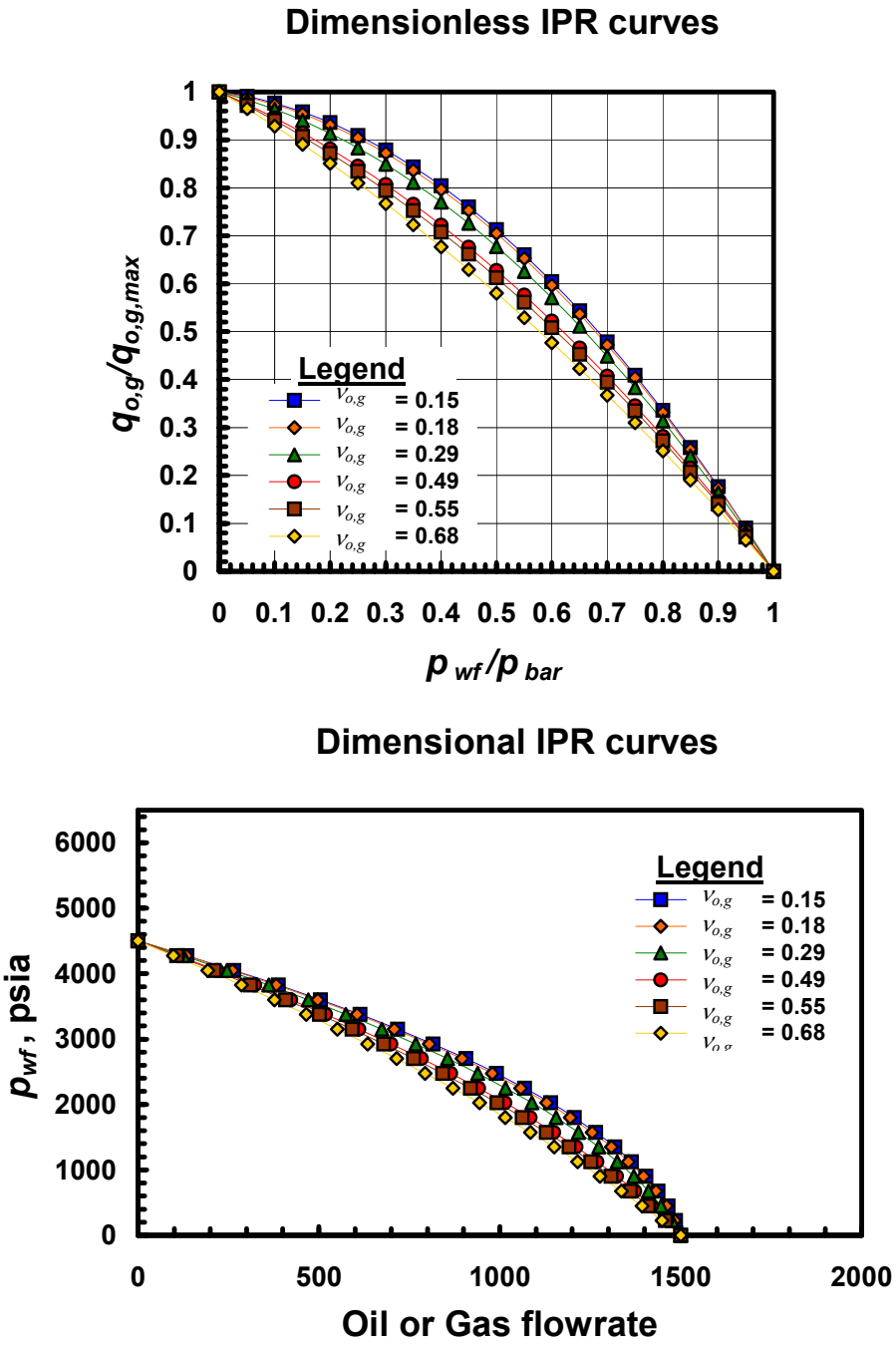

Fig. 3.8 — Sensitivity analysis on the v_o and v_g parameters.

Figure 3.8 shows a sensitivity analysis for the ν_o and ν_g parameters. We note that similar curve shapes result for different values of the parameters as observed in the dimensionless *IPR*. In order to evaluate the impact of changes in the value in the ν_o and/or ν_g parameters in the dimensional *IPR* form we selected the intercepts in *x* and *y* (*i.e.*, the $q_{o,g,max}$ and $\bar{p}$ values for a particular depletion stage (*e.g.*, $\bar{p}$ = 4500 psia and $q_{o,,max}$ = 1500 STB/D or $q_{g,max}$= 1500 MSCF/D)). For a given flowrate the maximum pressure difference between the *IPR* curves generated with values of 0.15 or 0.29 (ν_o or ν_g) was 150 psi. We note that this maximum pressure difference was also observed when we compared the *IPR* curves generated with values of ν_o or ν_g of 0.49 and 0.68.

Finally, we can conclude from our comparison that the determination of the exact value of the ν_o or ν_g parameters is not crucial. There is a margin of error that can be accepted without significantly changing the gas or condensate well deliverability. The characteristic behavior of the ν_o and ν_g parameters observed in this chapter will help us define the variables needed to correlate and predict ν_o and ν_g.

CHAPTER IV

CORRELATION OF *IPR* BEHAVIOR

4.1 Rationale

As established in Chapter III, the calculation of the dimensional *IPR* curves either for condensate and/or dry gas using the modified Vogel relationship (Eq. 3.1 (condensate) or Eq. 3.5 (gas)) requires prior knowledge of the ν_o and ν_g parameters for the particular condensate system. If these parameters are defined or correlated in some convenient fashion, then only the proper intercepts (*i.e.*, the $q_{o,max,}$ $q_{g,max}$ and $\bar{p}$ values) for the depletion stage are required to completely define the "dimensional" (or field) *IPR* curves. The "y" intercept (*i.e.*, the reservoir pressure) can be taken from a pressure transient test ($\bar{p}$) and the "x" intercept (*i.e.*, $q_{o,max}$ or $q_{g,max}$) can be estimated using production test data (*i.e.*, $q_{o,g}$ and p_{wf}).

In order to establish the primary variables for the correlation of the ν_o and ν_g parameters, the effect of changes in fluid and reservoir properties was investigated. We found that the ν_o and ν_g parameters vary with the fluid richness (that can be represented by the ratio of *N* over *G* or by the molecular weight of the mixture), fluid composition, temperature, dewpoint pressure, initial gas density, and relative permeability end points as shown in **Table 3.1**.

Based on this initial analysis, 11 independent variables were selected: the ratio of *N* over *G*, molecular weight of the mixture ($M_{mixture}$), the C1 mole fraction (C1), the C2 to C3 mole fraction (C2-C3), the C4 to C6 mole fraction (C4-C6), the C7 plus mole fraction ($C7^+$), reservoir temperature (T), dewpoint pressure (p_{dew}), initial gas density(ρ) and relative permeability end points (S_{oc}, S_{gr}). It is important to mention that impurities such as N_2 and CO_2 were not considered as part of the molar compositions used in this Chapter.

After selecting an the initial set of 11 independent variables, we examined **Table 3.1** which lists all the variables associated with a particular ν_o and ν_g value. A subset of this table is shown in **Table 4.1** — where this table illustrates cases which have similar ν_o and ν_g values, but different shapes of the relative permeability curves. We will note that the endpoint relative permeability values appear to have an independent relationship with the ν_o and ν_g values.

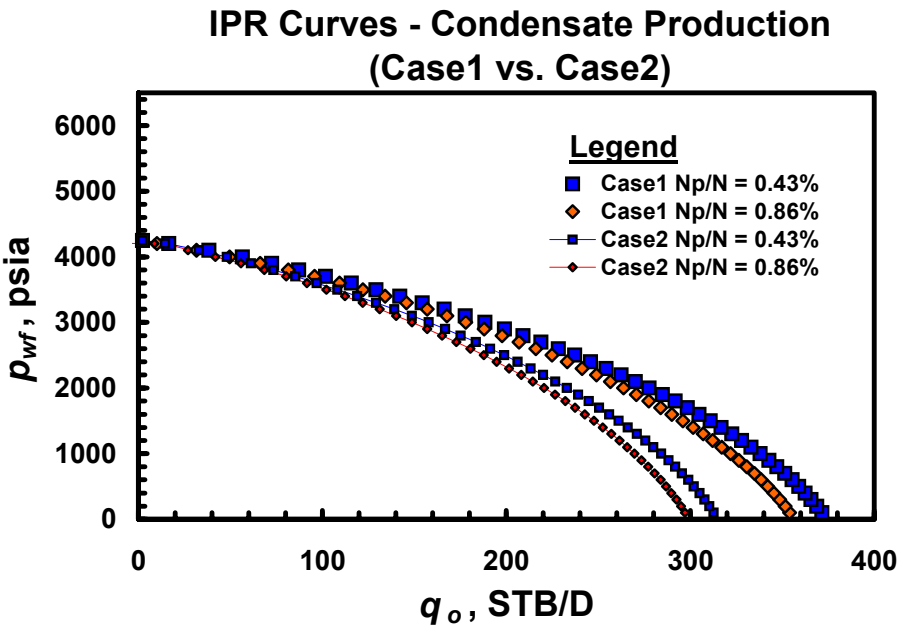

Fig. 4.1 — Effect on gas condensate production — k_{rg} less favorable (Case 2).

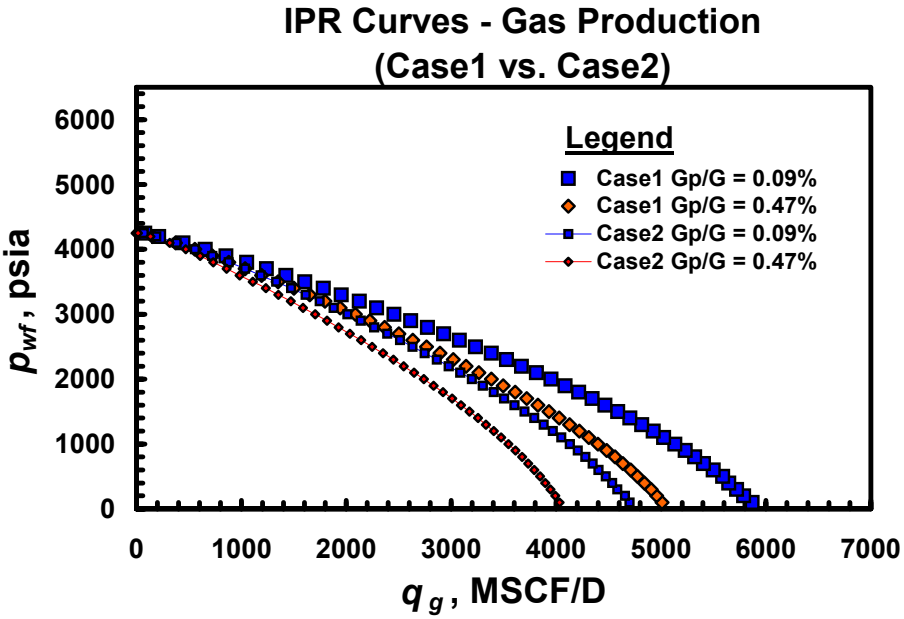

Fig. 4.2 — Effect on dry gas production — k_{rg} less favorable (Case 2).

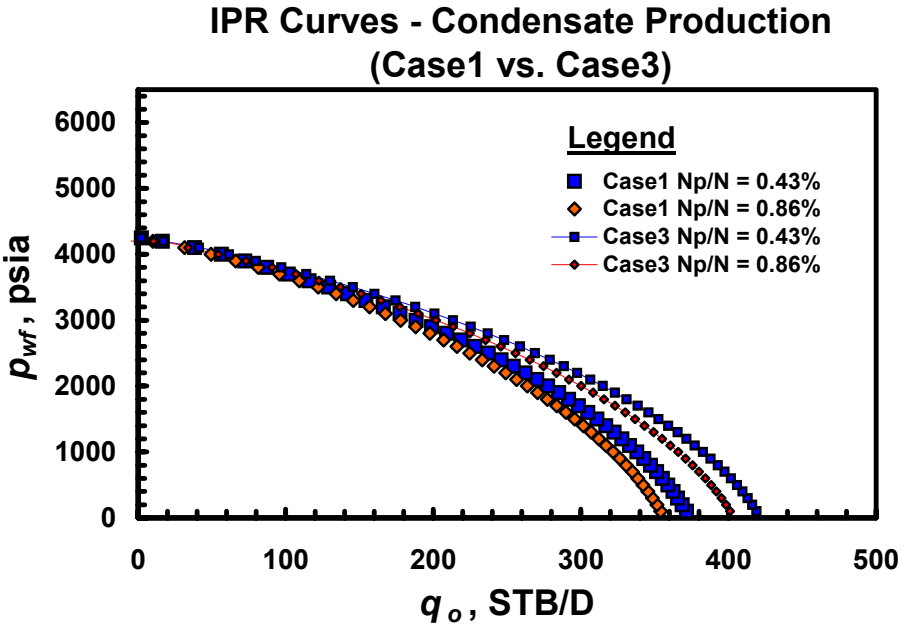

Fig. 4.3 — Effect on gas condensate production — k_{rg} more favorable (Case 3).

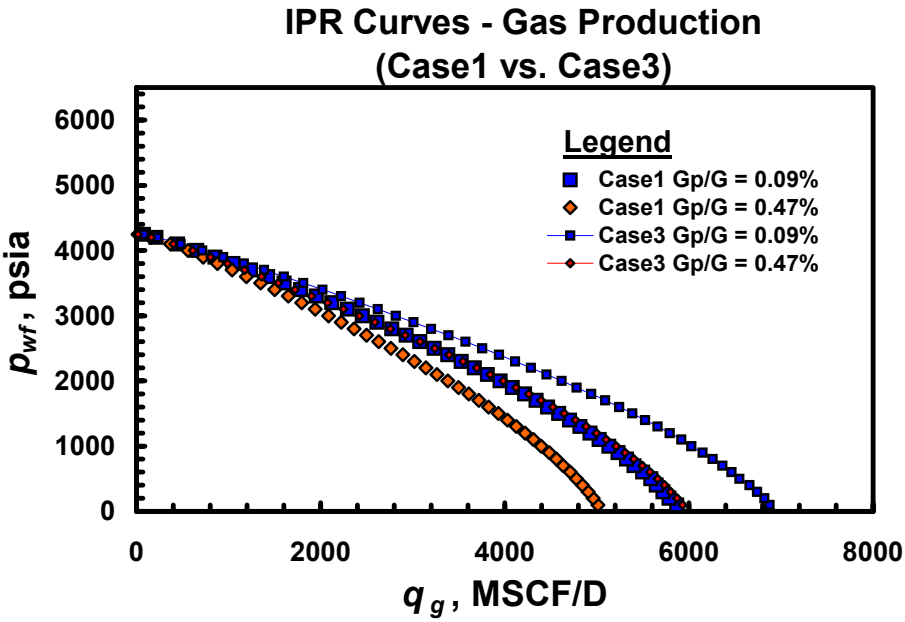

Fig. 4.4 — Effect on dry gas production — k_{rg} more favorable (Case 3).

Table 4.1 — Subset of IPR variables — v_o and v_g values are similar despite differences in relative permeabilty (shape).

Case	k_r set	Fluid set	S_{oc} (frac)	S_{gr} (frac)	p_{dew} (psia)	T (deg F)	N/G (STB/ MSCF)	Mole Fraction C1 (frac)	C2-C3 (frac)	C4-C6 (frac)	$C7^+$ (frac)	ρ_{init} (lb_m/ft^3)	$M_{mixture}$ (lb_m/ lb-mole)	v_o (dim-less)	v_g (dim-less)
1	1	1	0.10	0.00	4278	260	0.1094	0.896	0.000	0.030	0.074	15.431	26.00	0.18	0.42
2	2	1	0.10	0.00	4278	260	0.1094	0.896	0.000	0.030	0.074	15.431	26.00	0.19	0.42
3	3	1	0.10	0.00	4278	260	0.1094	0.896	0.000	0.030	0.074	15.431	26.00	0.15	0.43
9	1	5	0.10	0.00	5015	260	0.1578	0.690	0.131	0.047	0.082	24.352	34.85	0.25	0.50
18	2	5	0.10	0.00	5015	260	0.1578	0.690	0.131	0.047	0.082	24.352	34.85	0.25	0.49
19	3	5	0.10	0.00	5015	260	0.1578	0.690	0.131	0.047	0.082	24.352	34.85	0.26	0.51
17	1	5	0.10	0.00	5040	230	0.1578	0.690	0.131	0.047	0.082	25.791	34.85	0.26	0.52
20	2	5	0.10	0.00	5040	230	0.1578	0.690	0.131	0.047	0.082	25.791	34.85	0.26	0.51
21	3	5	0.10	0.00	5040	230	0.1578	0.690	0.131	0.047	0.082	25.791	34.85	0.25	0.52
22	1	5	0.10	0.00	4925	300	0.1578	0.690	0.131	0.047	0.082	22.570	34.85	0.24	0.48
23	2	5	0.10	0.00	4925	300	0.1578	0.690	0.131	0.047	0.082	22.570	34.85	0.24	0.47
24	3	5	0.10	0.00	4925	300	0.1578	0.690	0.131	0.047	0.082	22.570	34.85	0.24	0.47

The data in **Table 4.1** show that the values of the v_o and v_g can be quite insensitive to the shape of the relative permeability curves. If the relative permeability to gas is less favorable, there is a reduction in condensate and dry gas production rate as shown in **Figs. 4.1 and 4.2**. On the contrary, if the relative permeability to gas is more favorable, both the condensate and dry gas production rates are increased for a fixed bottomhole pressure as shown in **Figs. 4.3 and 4.4**.

Figure 4.5 shows that we can generate different dimensional *IPR* curves from very similar estimates of the v_g parameters when different intercepts are taken.

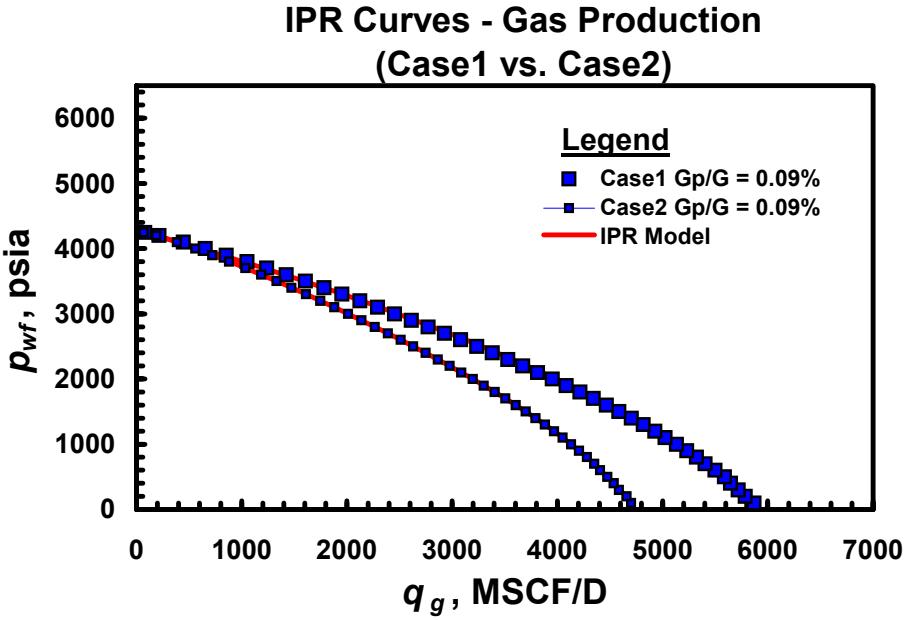

Fig. 4.5 — Comparison of IPR curves using the same v_g parameter.

Based on our observations, we can conclude that there are significant differences between the dimensional *IPR* curves when the shape of the relative permeability curve is altered. Moreover, a unique dimensionless *IPR* curve (*i.e.*, fixed values for the v_o and v_g parameters) can represent different dimensional *IPR* curves for different intercepts (although somewhat obvious comment, it warrants not that the dimensional *IPR* trends are defined by the $q_{o,max}$ (or $q_{g,max}$) and $\bar{p}$ values intercepts).

4.2 Approach

In order to establish a relationship between the dependent variable ν_o (or ν_g) and the multiple independent variables (as stated earlier), a non-parametric regression software was used (GRACE[24]). In the general "GRACE" formulation no functional form is assumed to relate the dependent and multiple independent variables.

"The GRACE algorithm[24] is based on the concept of developing non-parametric transformations of the dependent and independent variables. *Moreover, the transformations are contructed pointwise based only on the data.* The final result is a maximum, optimal correlation between the dependent and multiple independent variables with a minimum error. However, the GRACE method does not provide a functional form for the individual transformations nor does it provide a predictive equation. In order to generate numerical correlations it is necessary to assume functional fomrs for the transform function — in our work we used simple polynomials to fit the optimal data transformations and generate a predictive equation from which we can estimate ν_o (or ν_g).

Since the shape of the relative permeability curves does not have any significant impact on the ν_o and ν_g parameters (as discussed in the previous section), we decided not to consider all the cases shown in **Table 4.1**. Only a single representative case from each of the four groups (*i.e.*, the similar ν_o and ν_g parameter cases) was selected since the other cases can be reproduced considering different intercepts. **Table 4.2** shows that 54 cases remain in our correlation inventory for ν_o and ν_g.

Table 4.2 — Data considered for GRACE correlation (54 cases).

Case	k_r set	Fluid set	S_{oc} (frac)	S_{gr} (frac)	p_{dew} (psia)	T (deg F)	N/G (STB/ MSCF)	Mole Fraction C1 (frac)	Mole Fraction C2-C3 (frac)	Mole Fraction C4-C6 (frac)	Mole Fraction $C7^+$ (frac)	ρ_{init} (lb_m/ft^3)	$M_{mixture}$ (lb_m/ lb-mole)	v_o (dim-less)	v_g (dim-less)
1	1	1	0.10	0.00	4278	260	0.1094	0.896	0.000	0.030	0.074	15.431	26.00	0.18	0.42
4	4	1	0.10	0.50	4278	260	0.1094	0.896	0.000	0.030	0.074	15.431	26.00	0.19	0.25
5	5	1	0.00	0.00	4278	260	0.1094	0.896	0.000	0.030	0.074	15.431	26.00	0.27	0.45
6	1	2	0.10	0.00	4575	260	0.1541	0.870	0.000	0.030	0.100	18.705	29.10	0.19	0.49
7	1	3	0.10	0.00	2845	260	0.0388	0.956	0.000	0.015	0.029	12.551	20.08	0.20	0.28
8	1	4	0.10	0.00	4814	260	0.1800	0.870	0.000	0.015	0.115	19.833	30.23	0.21	0.51
9	1	5	0.10	0.00	5015	260	0.1578	0.690	0.131	0.047	0.082	24.352	34.85	0.25	0.50
10	4	5	0.10	0.50	5015	260	0.1578	0.690	0.131	0.047	0.082	24.352	34.85	0.29	0.48
11	5	5	0.00	0.00	5015	260	0.1578	0.690	0.131	0.047	0.082	24.352	34.85	0.34	0.56
12	4	5	0.10	0.50	5040	230	0.1578	0.690	0.131	0.047	0.082	25.791	34.85	0.31	0.49
13	4	5	0.10	0.50	4925	300	0.1578	0.690	0.131	0.047	0.082	22.570	34.85	0.26	0.45
14	4	6	0.10	0.50	5113	260	0.2655	0.617	0.146	0.067	0.121	30.635	44.35	0.64	0.75
15	4	6	0.10	0.50	5084	230	0.2655	0.617	0.146	0.067	0.121	33.289	44.35	0.65	0.73
16	4	6	0.10	0.50	5117	300	0.2655	0.617	0.146	0.067	0.121	36.078	44.35	0.61	0.72
17	1	5	0.10	0.00	5040	230	0.1578	0.690	0.131	0.047	0.082	25.791	34.85	0.26	0.52
22	1	5	0.10	0.00	4925	300	0.1578	0.690	0.131	0.047	0.082	22.570	34.85	0.24	0.48
25	5	5	0.00	0.00	4925	300	0.1578	0.690	0.131	0.047	0.082	22.570	34.85	0.34	0.53
26	1	6	0.10	0.00	5113	260	0.2655	0.617	0.146	0.067	0.121	30.635	44.35	0.55	0.77
27	5	6	0.00	0.00	5113	260	0.2655	0.617	0.146	0.067	0.121	30.635	44.35	0.66	0.80
28	1	6	0.10	0.00	5084	230	0.2655	0.617	0.146	0.067	0.121	33.289	44.35	0.58	0.81
29	5	6	0.00	0.00	5084	230	0.2655	0.617	0.146	0.067	0.121	33.289	44.35	0.68	0.83
30	1	6	0.10	0.00	5117	300	0.2655	0.617	0.146	0.067	0.121	36.078	44.35	0.52	0.73
31	5	6	0.00	0.00	5117	300	0.2655	0.617	0.146	0.067	0.121	36.078	44.35	0.62	0.74
32	4	2	0.10	0.50	4575	260	0.1541	0.870	0.000	0.030	0.100	18.705	29.10	0.23	0.45
33	5	2	0.00	0.00	4575	260	0.1541	0.870	0.000	0.030	0.100	18.705	29.10	0.33	0.51
34	5	3	0.00	0.00	2845	260	0.0388	0.956	0.000	0.015	0.029	12.551	20.08	0.16	0.39
35	4	4	0.10	0.50	4814	260	0.1800	0.870	0.000	0.015	0.115	19.833	30.23	0.27	0.48
36	5	4	0.00	0.00	4814	260	0.1800	0.870	0.000	0.015	0.115	19.833	30.23	0.35	0.53
37	1	1	0.10	0.00	4512	230	0.1094	0.896	0.000	0.030	0.074	17.613	26.00	0.14	0.44
38	4	1	0.10	0.50	4512	230	0.1094	0.896	0.000	0.030	0.074	17.613	26.00	0.18	0.43
39	5	1	0.00	0.00	4512	230	0.1094	0.896	0.000	0.030	0.074	17.613	26.00	0.28	0.49
40	1	1	0.10	0.00	3864	300	0.1094	0.896	0.000	0.030	0.074	15.469	26.00	0.22	0.40
41	4	1	0.10	0.50	3864	300	0.1094	0.896	0.000	0.030	0.074	15.469	26.00	0.22	0.29
42	5	1	0.00	0.00	3864	300	0.1094	0.896	0.000	0.030	0.074	15.469	26.00	0.26	0.39
43	1	2	0.10	0.00	4755	230	0.1541	0.870	0.000	0.030	0.100	19.778	29.10	0.17	0.52
44	4	2	0.10	0.50	4755	230	0.1541	0.870	0.000	0.030	0.100	19.778	29.10	0.25	0.47
45	5	2	0.00	0.00	4755	230	0.1541	0.870	0.000	0.030	0.100	19.778	29.10	0.34	0.55
46	1	2	0.10	0.00	4249	300	0.1541	0.870	0.000	0.030	0.100	17.428	29.10	0.26	0.45
47	4	2	0.10	0.50	4249	300	0.1541	0.870	0.000	0.030	0.100	17.428	29.10	0.24	0.43
48	5	2	0.00	0.00	4249	300	0.1541	0.870	0.000	0.030	0.100	17.428	29.10	0.31	0.45
49	6	1	0.30	0.00	4278	260	0.1094	0.896	0.000	0.030	0.074	15.431	26.00	0.19	0.41
50	6	2	0.30	0.00	4575	260	0.1541	0.870	0.000	0.030	0.100	18.705	29.10	0.18	0.49
51	6	5	0.30	0.00	5015	260	0.1578	0.690	0.131	0.047	0.082	24.352	34.85	0.26	0.52
52	6	6	0.30	0.00	5113	260	0.2655	0.617	0.146	0.067	0.121	30.635	44.35	0.52	0.76
53	6	6	0.30	0.00	5084	230	0.2655	0.617	0.146	0.067	0.121	33.289	44.35	0.57	0.82
54	6	6	0.30	0.00	5117	300	0.2655	0.617	0.146	0.067	0.121	36.078	44.35	0.50	0.72
55	6	1	0.30	0.00	3864	300	0.1094	0.896	0.000	0.030	0.074	15.469	26.00	0.24	0.41
56	6	5	0.30	0.00	4925	300	0.1578	0.690	0.131	0.047	0.082	22.570	34.85	0.26	0.45
57	7	1	0.30	0.15	4278	260	0.1094	0.896	0.000	0.030	0.074	15.431	26.00	0.26	0.39
58	7	1	0.30	0.15	3864	300	0.1094	0.896	0.000	0.030	0.074	15.469	26.00	0.26	0.42
59	7	5	0.30	0.15	5015	260	0.1578	0.690	0.131	0.047	0.082	24.352	34.85	0.25	0.46
60	7	5	0.30	0.15	4925	300	0.1578	0.690	0.131	0.047	0.082	22.570	34.85	0.28	0.41
61	7	6	0.30	0.15	5100	260	0.2655	0.617	0.146	0.067	0.121	30.635	44.35	0.57	0.79
62	7	6	0.30	0.15	5117	300	0.2655	0.617	0.146	0.067	0.121	36.078	44.35	0.52	0.74

4.3 Correlation

In order to establish the best correlations for the ν_o and ν_g parameters, GRACE analyses were performed using 10 different *combinations* of the 11 independent variables. The predicted ν_o and ν_g values were compared to the actual values in a crossplot to establish validity of a particular regression. To measure how widely the predicted values were dispersed from the actual values, the standard deviation of the errors was calculated as well as the average absolute error for each of the 10 correlation cases.

Table 4.3 shows the GRACE results obtained for the condensate production cases. Case 9 considered the fewest number of variables while still maintaining a low standard deviation and a low average absolute error. For this case, **Fig. 4.6** illustrates that a good correlation exists between the calculated and measured ν_o values.

Table 4.3 — Results: GRACE correlation — gas condensate.

	Independent variables											Error	
	Mole fraction												
Case	C1	C2-C3	C4-C6	$C7^+$	p_{dew} (psia)	T (deg F)	S_{oc} (frac)	S_{gr} (frac)	ρ_{init} (lb_m/ft^3)	$M_{mixture}$ (lb_m/lb-mole)	N/G (STB/MSCF)	Std. Dev.	Avg. Error (%)
1	X	X	X	X	X	X	X	X	X			0.0349	9.73
2	X	X	X	X	X	X	X	X	X	X		0.0333	9.64
3	X			X	X	X	X	X	X			0.0322	9.19
4	X			X	X	X	X	X	X	X		0.0333	9.48
5	X			X	X	X	X	X	X	X	X	0.0328	9.12
6	X				X	X	X	X	X	X	X	0.0325	8.97
7	X				X	X	X	X	X	X		0.0338	9.62
8	X				X	X	X	X		X	X	0.0355	9.39
9	X				X	X	X	X		X		0.0354	9.23
10					X	X	X	X	X	X	X	0.0348	10.09

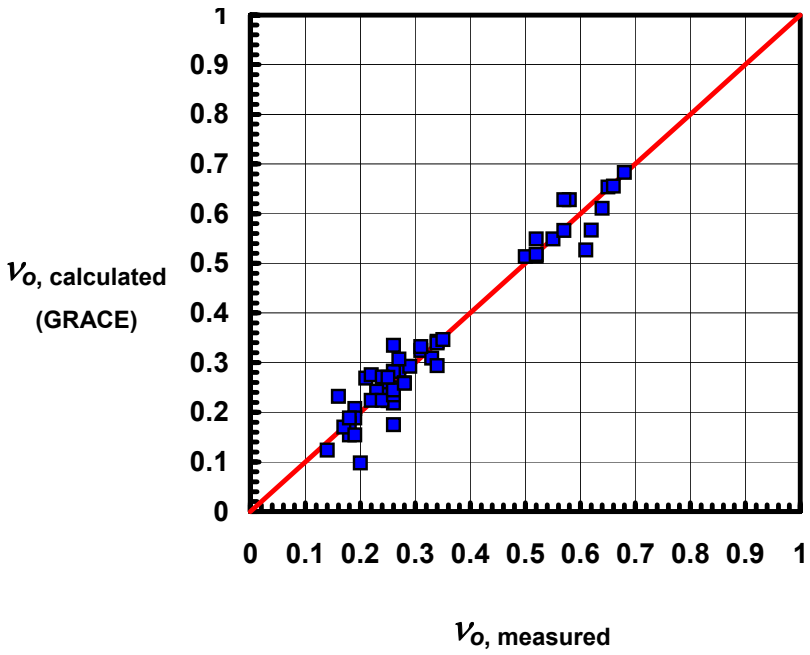

Fig. 4.6 — GRACE correlation (Case 9) — gas condensate.

At this point, using only the GRACE algorithm we cannot establish a predictive model for the ν_o parameter. To do so, it is necessary to assume a function form for the transformation functions — in our work we selected quadratic polynomials. **Table 4.4** shows the results of the fitting of the dependent and independent variables (using quadratic polynomials for the transformation functions). In all the cases, only a "moderate" fit of the dependent variable (*i.e.*, ν_o) was achieved at best. For Case 9 we obtained the best fit for the independent variables (see **Fig. 4.7**). Regardless of the case or approach, we note that when an explicit correlation is found for the ν_o parameter a significant deterioration of the prediction at the higher ν_o values is observed — as shown in **Fig. 4.8**.

Table 4.4 — Results: GRACE + polynomial regression — gas condensate.

	Variables													
	Independent											Dependent	Error	
	Mole fraction													
Case	C1	C2-C3	C4-C6	$C7^+$	p_{dew} (psia)	T (deg F)	S_{oc} (frac)	S_{gr} (frac)	ρ_{init} (lb_m/ft^3)	$M_{mixture}$ (lb_m/lb-mole)	N/G (STB/MSCF)	v_o	Std. Dev.	Avg. Error (%)
1	ok	ok	ok	ok	R	ok	ok	ok	ok			R	0.0500	14.45
2	ok	ok	B	ok	ok	ok	ok	ok	R	ok		R	0.042	11.75
3	B			ok	ok	ok	ok	ok	B			R	0.0560	17.60
4	ok			B	ok	ok	ok	ok	R	ok		R	0.0448	12.54
5	ok			B	ok	ok	ok	ok	R	ok	B	R	0.0436	12.05
6	ok				ok	ok	ok	ok	R	ok	ok	R	0.0437	12.15
7	ok				ok	ok	ok	ok	R	ok		R	0.0452	12.57
8	ok				ok	ok	ok	ok		ok	R	R	0.0448	12.24
9	ok				ok	ok	ok	ok		ok		R	0.0449	12.40
10					ok	ok	ok	ok	R	ok	R	R	0.0443	11.42

OK = There is a good correlation between the transformations and the polynomial regression

R = There is a moderate difference between the transformations and polynomial regression

B = There is a big difference between the transformations and polynomial regression

VB = There is a major difference between the transformations and polynomial regression

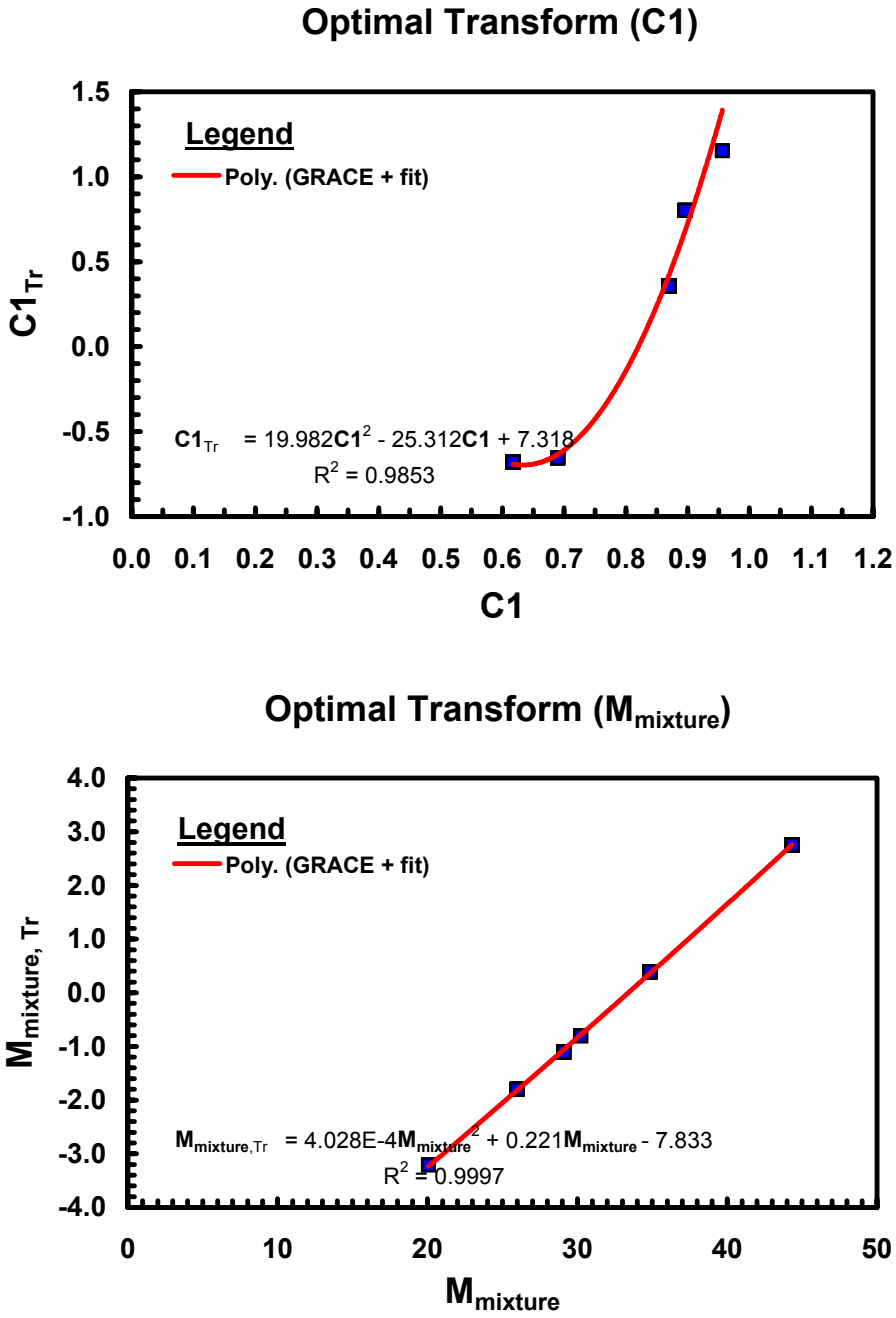

Fig. 4.7 — Transformations of independent variables (Case 9) — gas condensate.

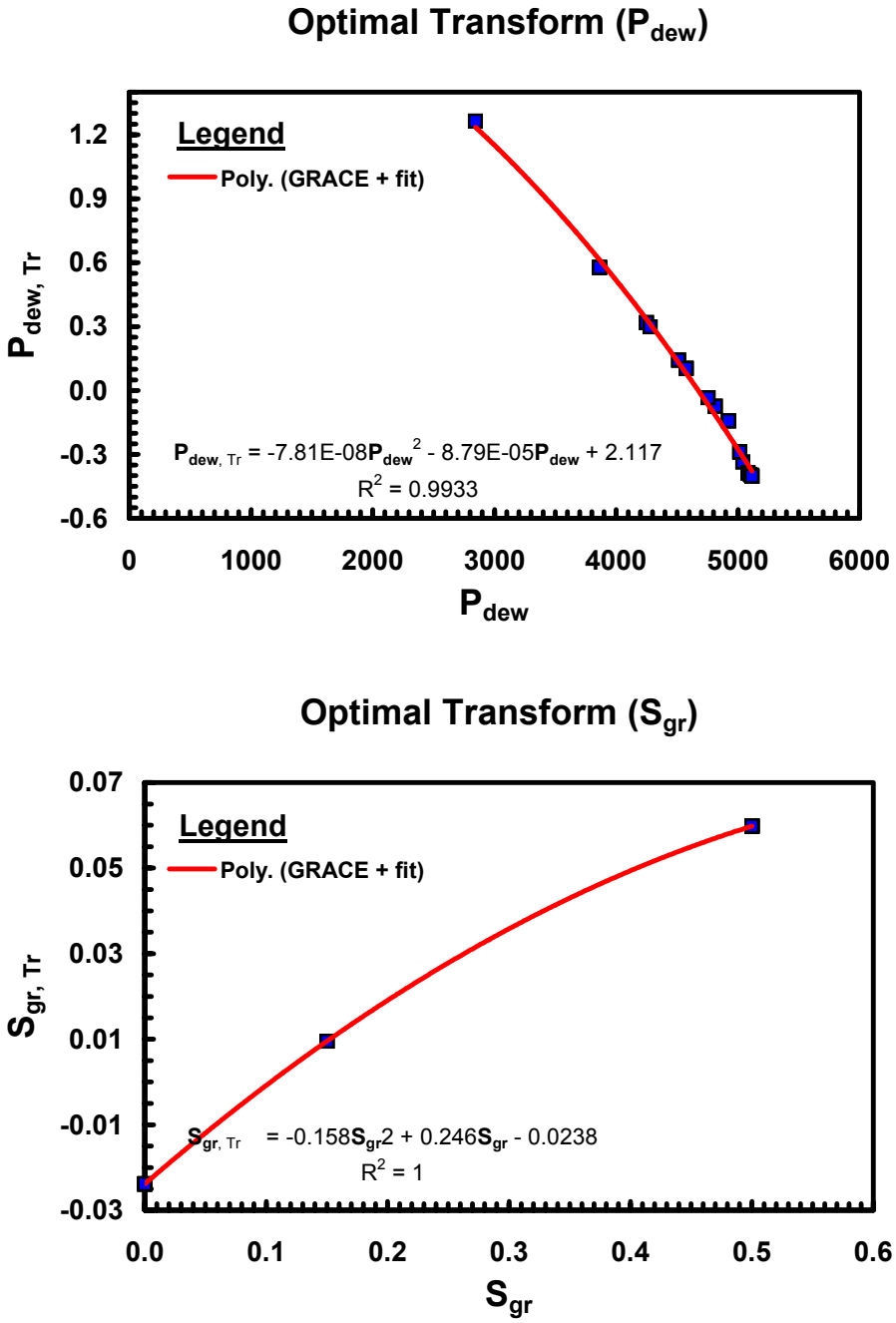

Fig. 4.7 — (Continued).

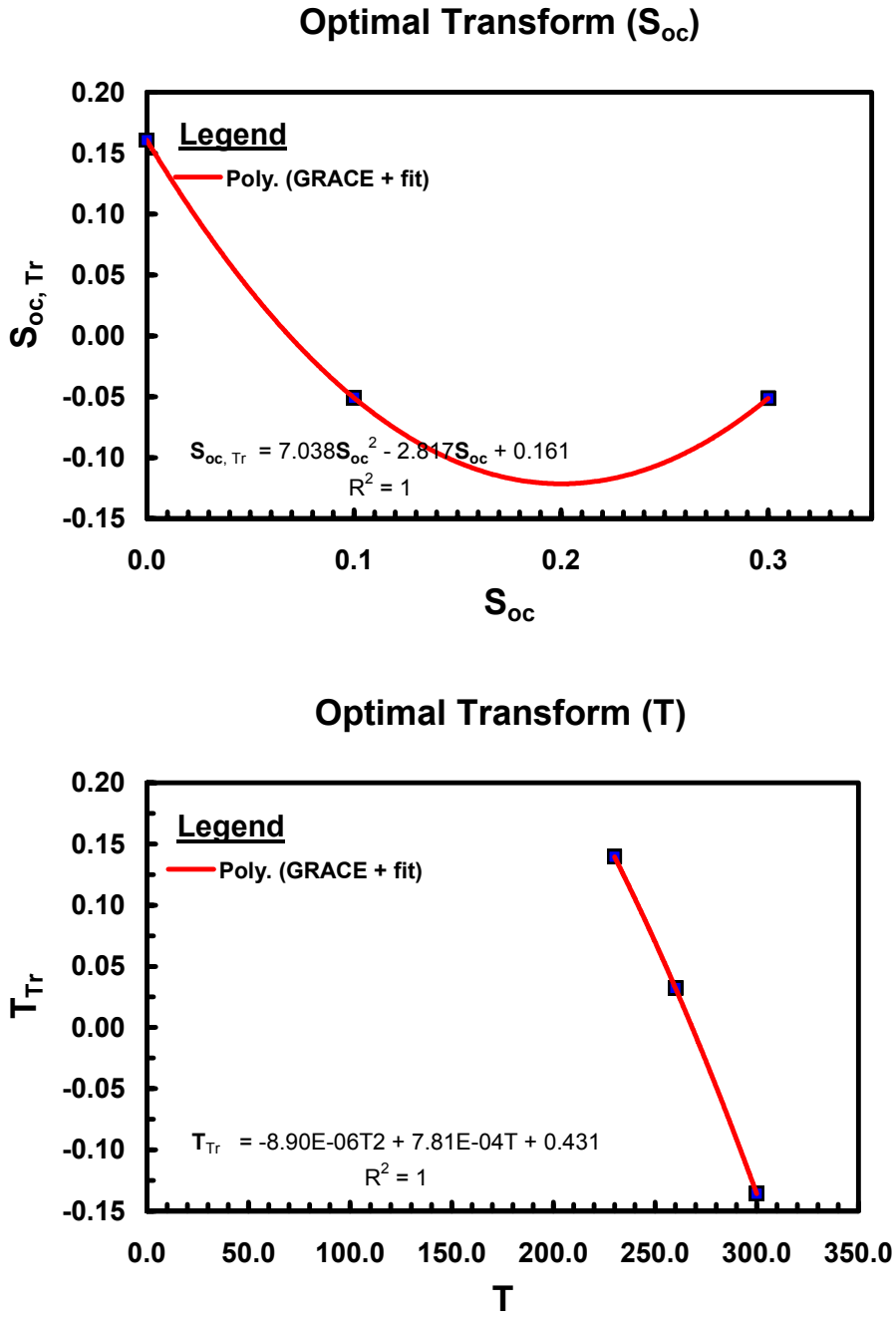

Fig. 4.7 — (Continued).

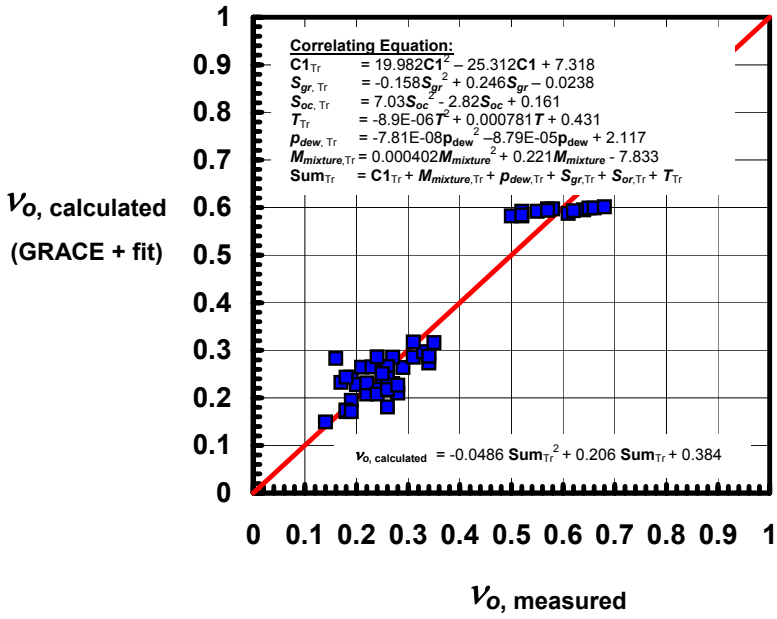

Fig. 4.8 — GRACE + polynomial regression (Case 9) — gas condensate.

Comparing **Tables 4.3 and 4.4** we observe an increase in the standard deviation as well as in the average absolute error when assuming functional approximations for the transformations. **Figure 4.9** also shows that significant differences occur from GRACE (non-parameteric regression) to the GRACE algorithm plus polynomial regression. This is particularly true for the top group of points (in **Fig. 4.9**), where these data correspond to the richest condensate fluid (Cupiagua — Fluid 6).

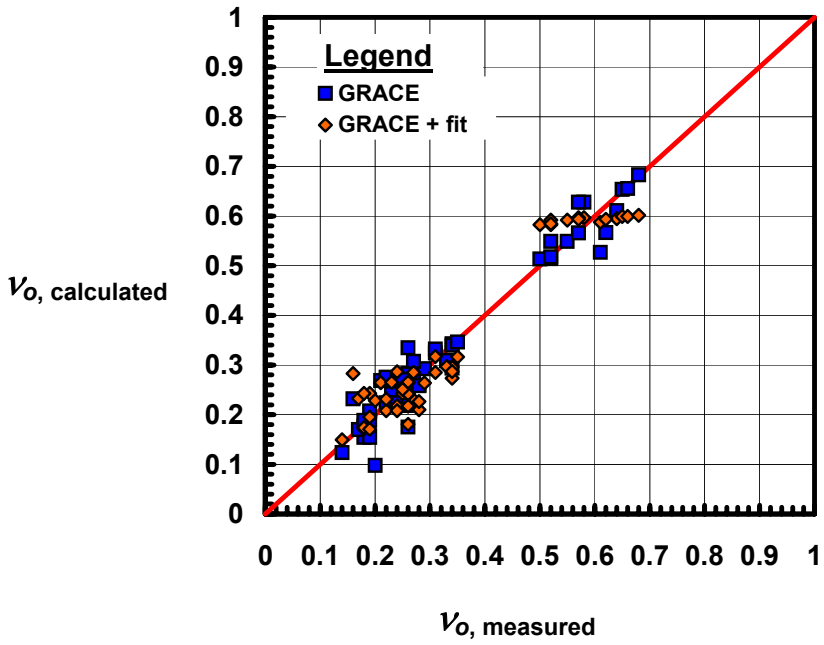

Fig. 4.9 — GRACE versus GRACE + polynomial regression (Case 9) — gas condensate.

Following the same procedure outlined for the condensate, we attempted to develop an explicit correlation for the ν_g parameter. **Table 4.5** shows the GRACE (non-parametric regression) results for the dry gas cases. It appears that only 6 variables (Case 9) are required to accurately predict the ν_g parameter. **Figure 4.10** shows that there is a strong correlation between the predicted and the actual ν_g values.

Table 4.5 — Results: GRACE correlation — dry gas.

	Independent variables										Error	
	Mole fraction											
Case	C1	C2-C3	C4-C6	$C7^+$	p_{dew} (psia)	T (deg F)	S_{oc} (frac)	S_{gr} (frac)	ρ_{init} (lb_m/ft^3)	$M_{mixture}$ (lb_m/lb-mole)	Std. Dev.	Avg. Error (%)
1	X	X	X	X	X	X	X	X			0.0217	3.35
2	X	X	X	X	X	X	X	X	X		0.0227	3.45
3	X	X	X	X	X	X	X	X		X	0.0254	3.92
4					X	X	X	X		X	0.0257	3.91
5	X			X	X	X	X	X		X	0.0246	3.81
6				X	X	X	X	X		X	0.0243	3.70
7	X			X	X	X	X	X			0.0219	3.41
8	X			X	X	X	X	X	X		0.0216	3.42
9	X				X	X	X	X		X	0.0249	3.87
10	X				X	X	X	X	X	X	0.0229	3.59

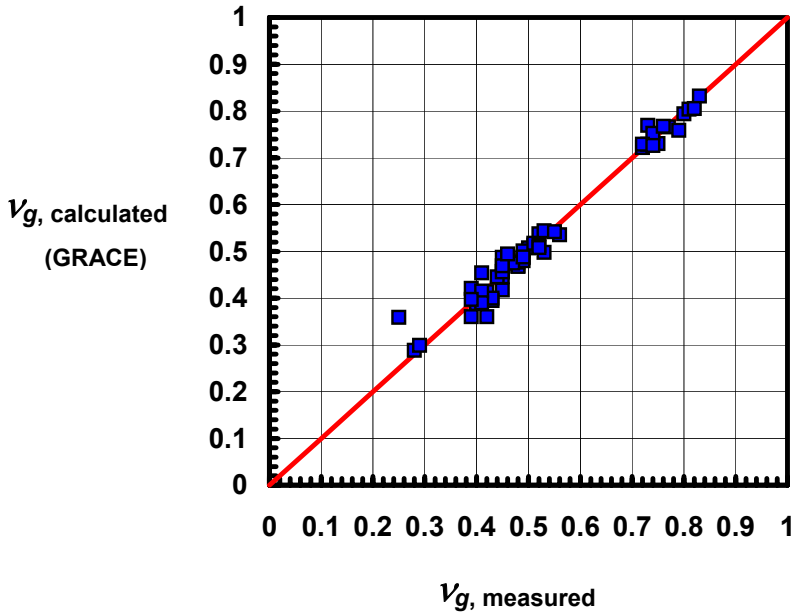

Fig. 4.10 — GRACE correlation (Case 9) — dry gas.

Analyzing the regression results obtained using second-degree polynomial functions (**Table 4.6**), it appears that Case 9 achieves the best fit for both the dependent (measured v_g) and independent variables as shown in **Fig. 4.11.** We also note that this correlation does not present significant deterioratons at high v_g values as shown in **Fig. 4.12**.

Table 4.6 — Results: GRACE + polynomial regression — dry gas.

	Variables												
	Independent										Dependent	Error	
	Mole fraction												
Case	C1	C2-C3	C4-C6	C7+	p_{dew} (psia)	T (deg F)	S_{oc} (frac)	S_{gr} (frac)	(init (lbm/ft3)	Mmixture (lbm/lb-mole)	v_g	Std. Dev.	Avg. Error (%)
1	ok	ok	R	ok	ok	ok	ok	ok			R	0.0303	5.11
2	ok	ok	R	R	ok	ok	ok	ok	ok		R	0.0293	5.16
3	ok	ok	VB	ok	R	ok	ok	ok		ok	ok	0.0275	4.56
4					R	ok	ok	ok		VB	ok	0.0438	7.81
5	ok			VB	ok	ok	ok	ok		ok	R	0.0281	4.70
6				ok	R	ok	ok	ok		ok	R	0.0287	4.95
7	ok			ok	ok	ok	ok	ok			R	0.0328	5.83
8	R			ok	VB	ok	ok	ok	R		R	0.0364	6.21
9	ok				ok	ok	ok	ok		ok	ok	0.0271	4.51
10	ok				R	ok	ok	ok	R	ok	R	0.0277	4.67

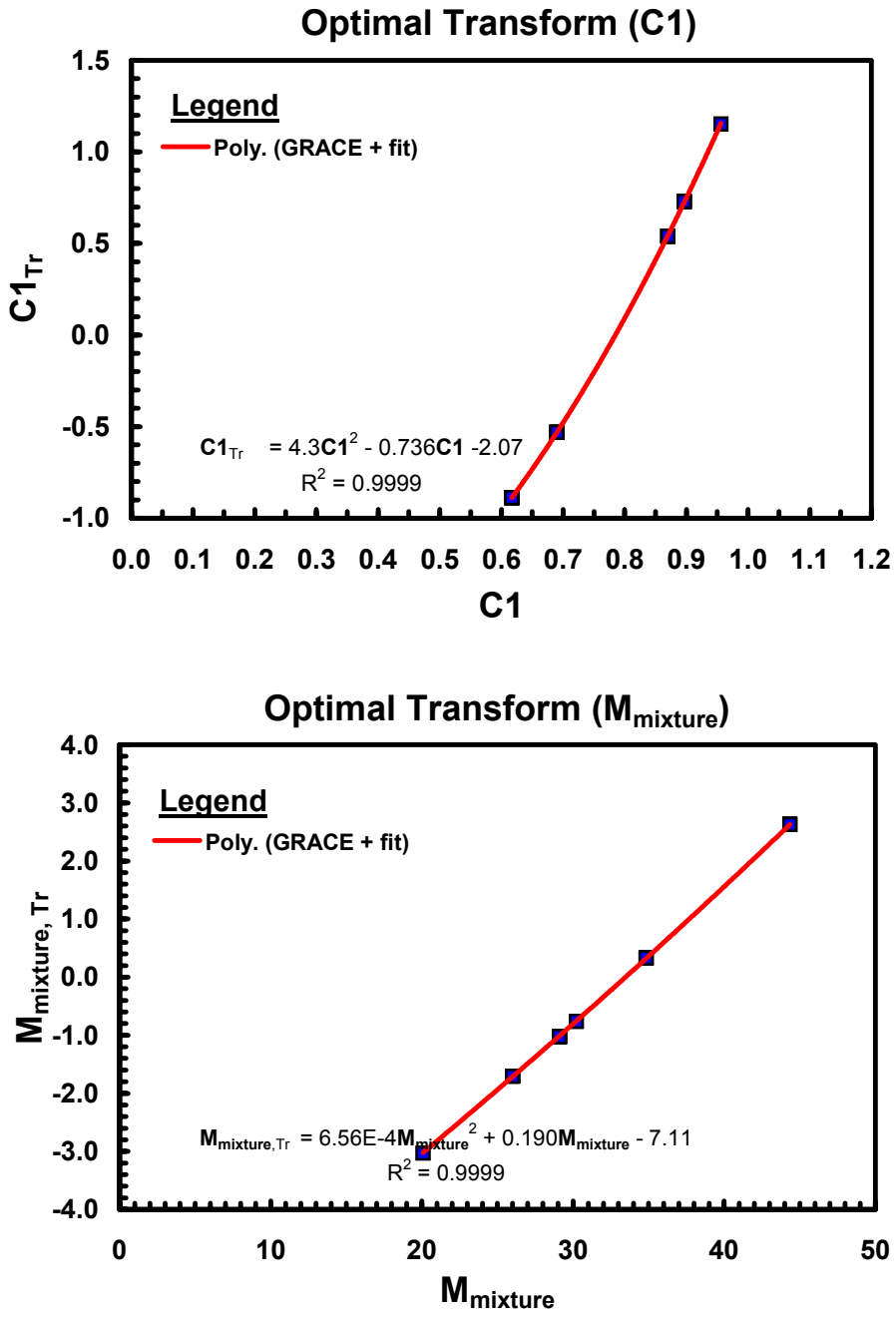

Fig. 4.11 — Transformations of independent variables (Case 9) — dry gas.

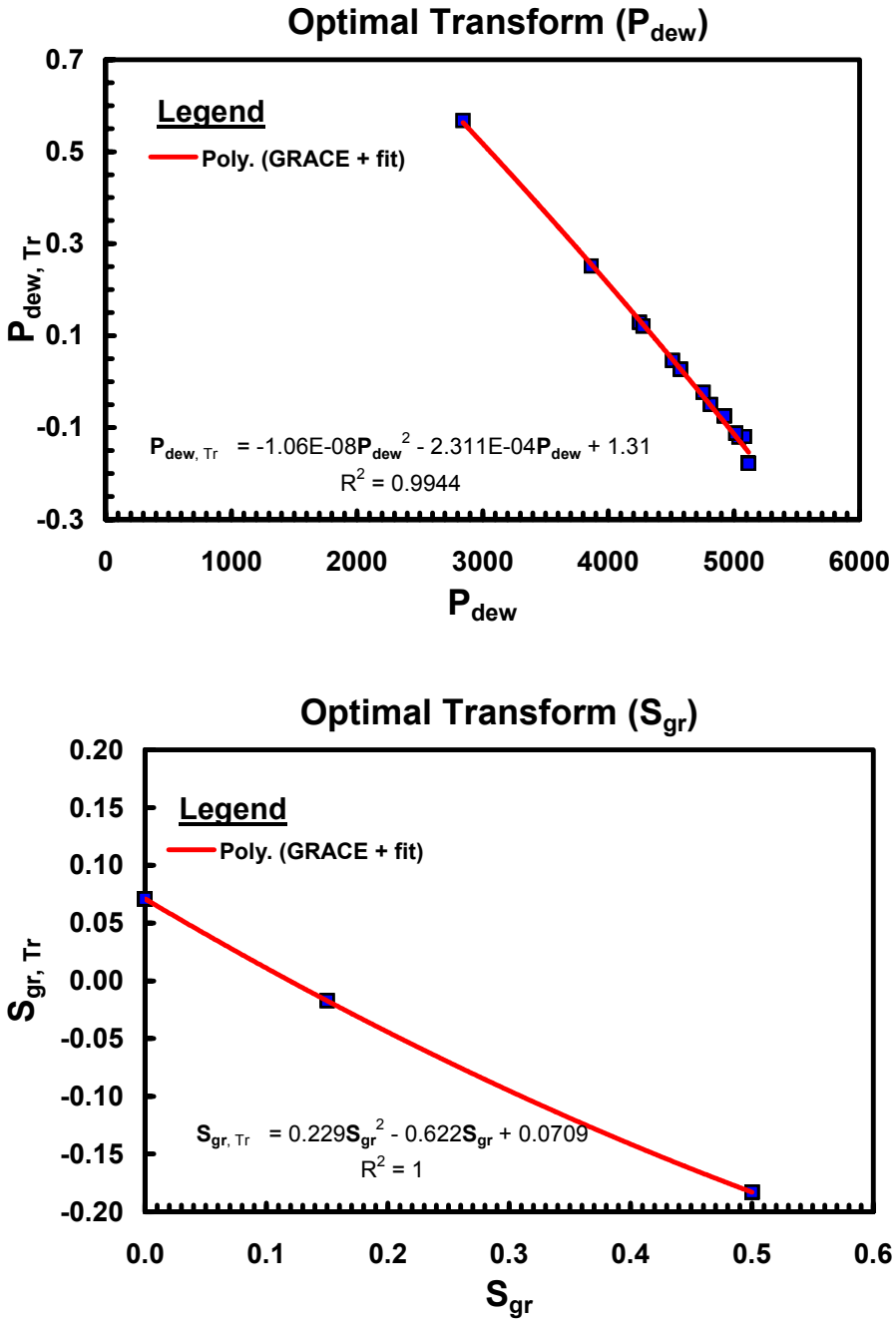

Fig. 4.11 — (Continued).

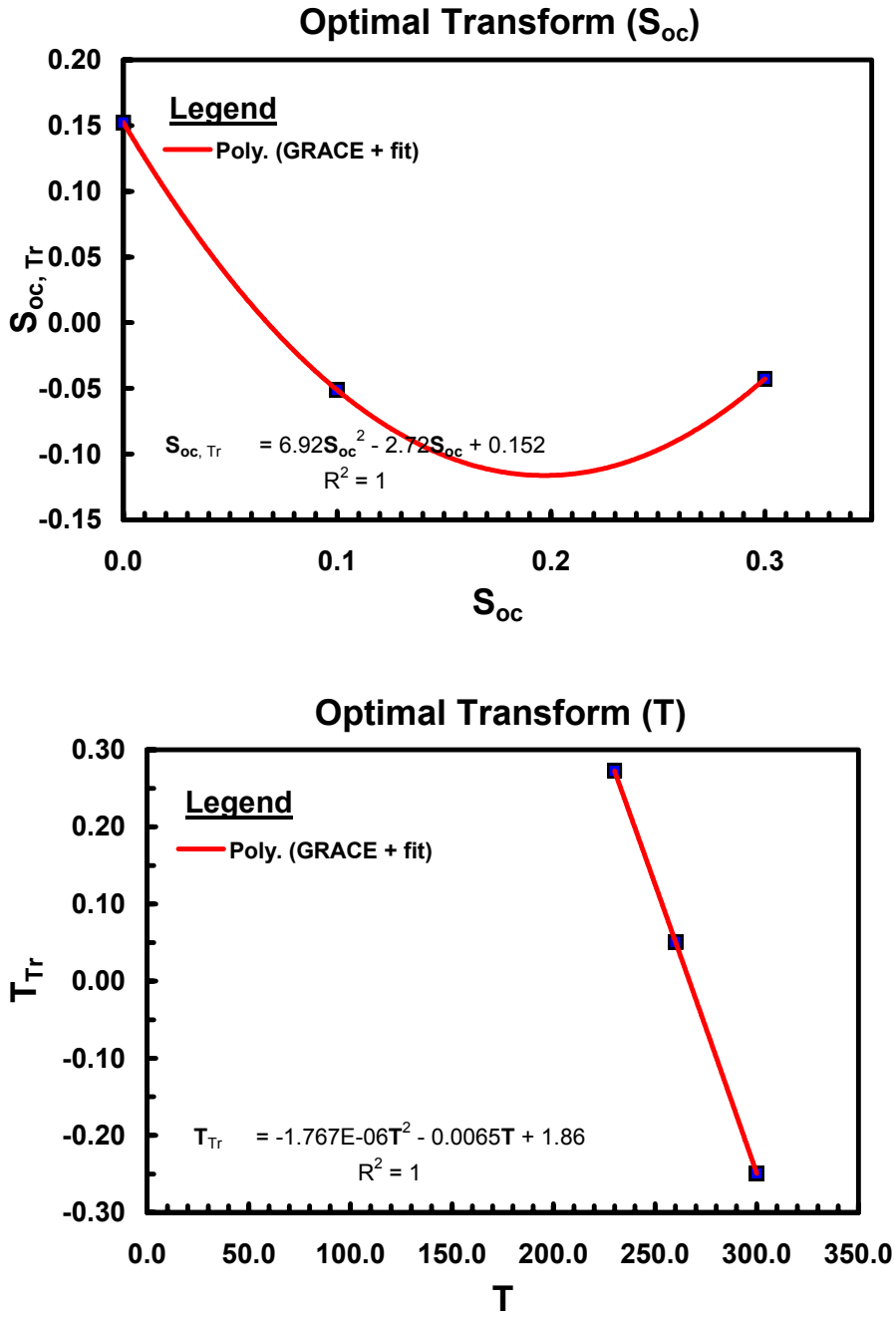

Fig. 4.11 — (Continued).

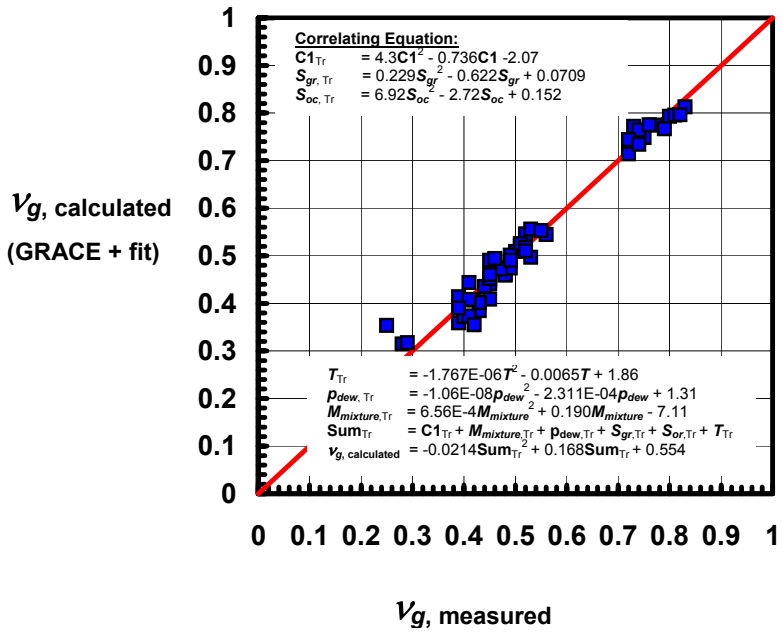

Fig. 4.12 — GRACE + polynomial regression (Case 9) — dry gas.

Comparing **Tables 4.5 and 4.6**, we observe an increase in the standard deviation as well as in the average absolute error when assuming functional approximations for the transformations (*i.e.*, the quadratic polynomials). Neverthless, as illustrated in **Fig. 4.13**, the differences in the GRACE non-parametric regression (the very best correlation) and the GRACE + quadratic polynomial regression are not substantially different.

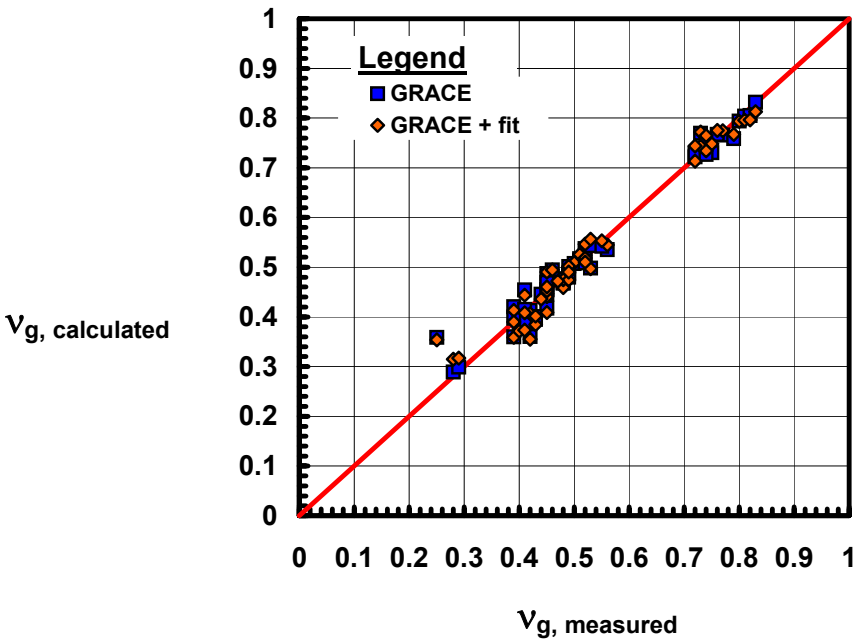

Fig. 4.13 — GRACE versus GRACE + polynomial regression (Case 9) — dry gas.

Analyzing the GRACE non-parametric regression and the GRACE plus quadratic polynomial regression results, it is clear that two distinct groups of values (ν_o and ν_g parameters) segregate — the very rich gas case (Cupiagua, Fluid 6). This observation emphasizes the importance of fluid richness characterization as part of the correlation process for the ν_o and ν_g parameters.

Two fluid richness indicators were determined previously in Chapter III — the *N*/*G* ratio and the molecular weight of the mixture. Based on our results it seems that the initial molecular weight of the mixture provides a good representation of not only the fluid richness, but also of the fluid composition when the intermediate and heavier components are not explicitly considered. This also helped us to reduce the number of independent variables in our correlation. More importantly, the initial molecular weight of the mixture is a variable that can be easily determined from a chromatographic analysis.

When comparing the results obtained using the GRACE algorithm for condensate and dry gas (**Figs. 4.6 and 4.10**), we note that the correlation of the "dry gas" case is much better (note the clustering of points about the 45 degree trend). Similar results are evident when comparing the GRACE + polynomial regression cases (**Figs. 4.8 and 4.12**). Based on these results, we believe that the variables used to correlate the ν_g parameter are appropriate and incorporate the behavior of the ν_g parameter in a unique fashion.

The fact that there is a more marked deterioration in the condensate relation for the top group of points (richest fluid) going from GRACE to GRACE plus polynomial regression suggests the need for more data

and/or the use of another variable to improve the correlation of the ν_o parameter. Nevertheless the accuracy of this correlation is good for the lower group of points (*i.e.*, the leaner gas condensate cases).

It is important to mention that as part of the optimization process we attempted to use third-order polynomial functions in order to improve the fit of the dependent variables (ν_o or ν_g). However, this was not successful — most likely because there were relatively few levels of variation in the independent variables. This suggestion implies that a thrid degree polynomial (with two inflexion points) would not improve the overall correlation significatly.

4.4 Validation

In order to test the accuracy of our correlations for the ν_o and ν_g parameters, two completely different validation cases were tested. The first case corresponds to "Example data set number 5" provided with the Eclipse 300 software and the second case to SPE 35649. Recall that we generated 10 correlations using the GRACE algorithm plus quadratic polynomials for the transform function — each of these 10 correlations were compared to the output from the Eclipse 300 case, and we note that Case 9 yielded the most accurate comparison (**Table 4.7).**

The correlation of the ν_o parameter was achieved for this simulation example — and the fluid and reservoir properties are presented in **Appendix B** (section B.1). Various condensate *IPR* curves were generated for a particular depletion ratio and as such, following the procedure outlined in Chapter III, a value of 0.22 was estimated for the ν_o parameter. The dimensional and dimensionless condensate curves for this case are presented in **Fig. 4.14**. We note that the use of a different EOS as well as a different porosity and absolute permeability profile should not affect the "dimensionless" *IPR* formulation. Also, it is important to realize that ν_o=0.22 falls within the range of ν_o values that were consider in our correlation database (**Table 4.2**).

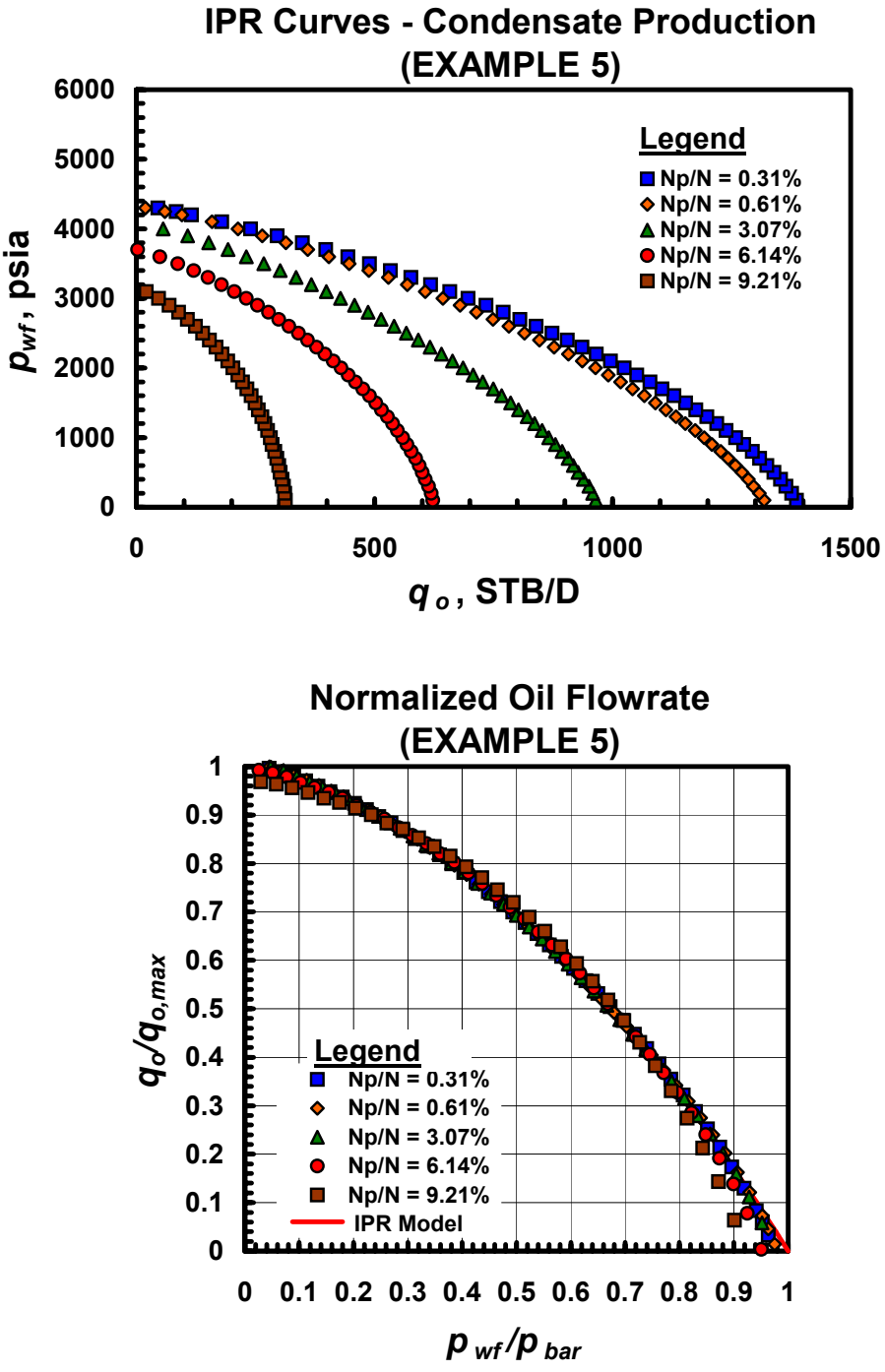

Fig. 4.14 — Example 5 — gas condensate (ν_o = 0.22 measured).

Table 4.7 shows the "predicted" v_o values obtained using the 10 different correlations. These values range from 0.28 to 0.56. Our best correlation (Case 9) predicted a v_o value equal to 0.28.

Table 4.7 — Correlation of data from example 5 (gas condensate).

	Variables														
	Independent											Dependent	Error		
	Mole fraction														
Case	C1	C2-C3	C4-C6	$C7^+$	p_{dew} (psia)	T (deg F)	S_{oc} (frac)	S_{gr} (frac)	ρ_{init} (lb_m/ft^3)	$M_{mixture}$ (lb_m/lb-mole)	N/G (STB/MSCF)	v_o	Std. Dev.	Avg. Error (%)	Calculated v_o
1	ok	ok	ok	ok	R	ok	ok	ok	ok			R	0.0500	14.45	0.56
2	ok	ok	B	ok	ok	ok	ok	ok	R	ok		R	0.042	11.75	0.35
3	B			ok	ok	ok	ok	ok	B			R	0.0560	17.60	0.40
4	ok			B	ok	ok	ok	ok	R	ok		R	0.0448	12.54	0.32
5	ok			B	ok	ok	ok	ok	R	ok	B	R	0.0436	12.05	0.31
6	ok				ok	ok	ok	ok	R	ok	ok	R	0.0437	12.15	0.29
7	ok				ok	ok	ok	ok	R	ok		R	0.0452	12.57	0.32
8	ok				ok	ok	ok	ok		ok	R	R	0.0448	12.24	0.29
9	ok				ok	ok	ok	ok		ok		R	0.0449	12.40	0.28
10					ok	ok	ok	ok	R	ok	R	R	0.0443	11.42	0.40

When analyzing **Fig. 4.15** (as well as the results presented in **Appendix B** (Section B.1.1)), an estimate of 0.28 was obtained for the v_o parameter (as opposed to the estimate of 0.22 obtained from the simulation). We note that when the value of the v_o parameter is equal to or above 0.35 (*i.e.* 0.40 or 0.50) there are considerable deviations from the dimensional *IPR* curves. We will comment that deviations due to the estimate of the v_o parameter are more evident when we consider the dimensionless form of the IPR trend.

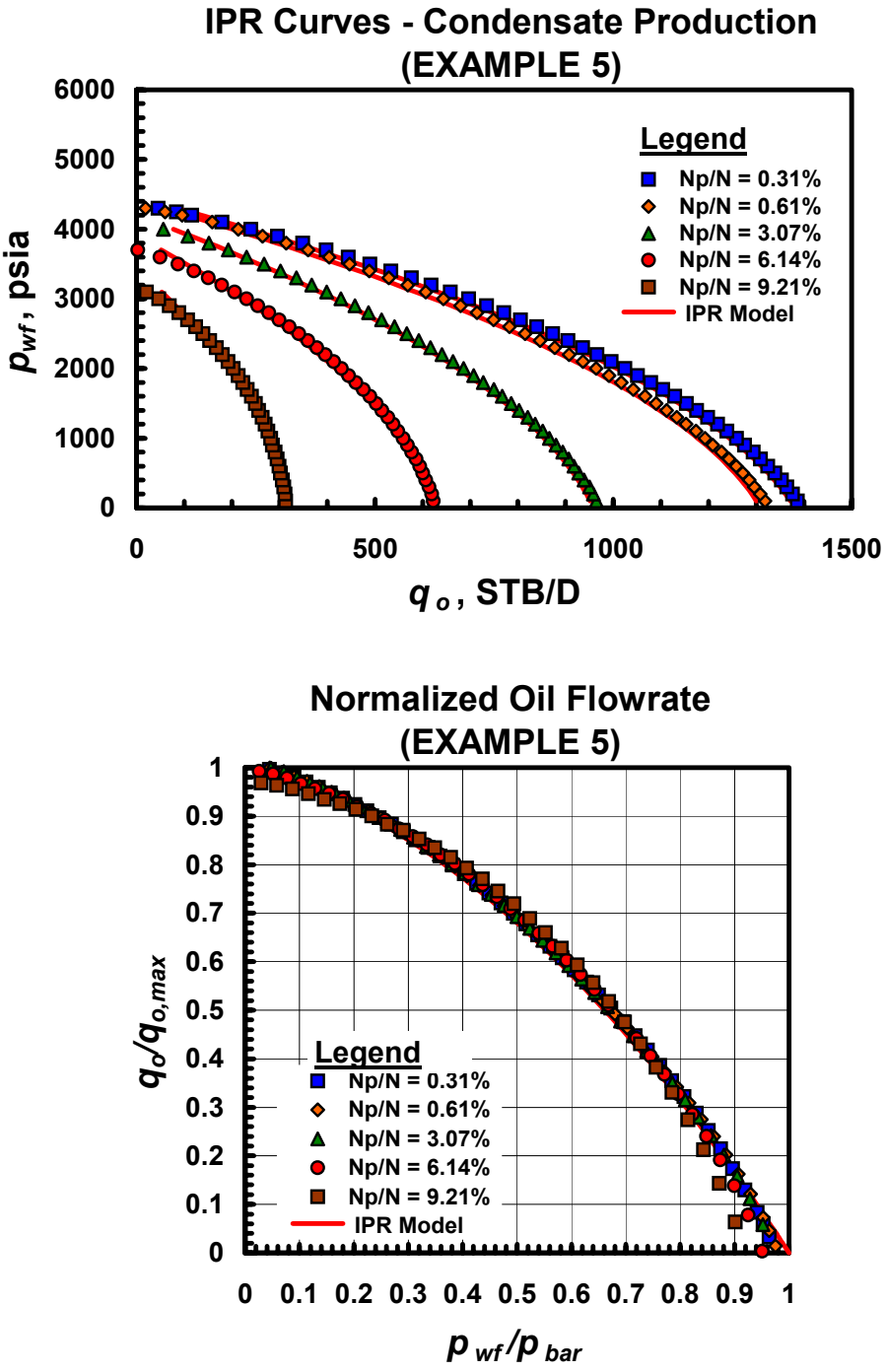

Fig. 4.15 — Example 5 — condensate real values versus calculated values (ν_o = 0.28 calculated).

The validation of the correlation for the ν_g parameter was initially performed using only the simulation case we generated (as a "blind" test using data not in the correlation database). Another validation for the gas *IPR* case was developed using the results of an independent simulation case presented in ref. 22. The complete data set taken from ref. 22 is presented in **Appendix B** (section B.2). In this case, it was not necessary to use simulation to determine the dry gas *IPR* curves, since the performance data are given (in graphical form) in the reference.

In the validation performed using data from reference 22 we note that only performance below the dewpoint was considered as we are attempting to evaluate only the flow behavior in the two- phase region. Using the same procedure we employed earlier to make the *IPR* curves dimensionless, we obtained an estimate of 0.11 for the ν_g parameter (the $\bar{p}$ and $q_{g,max}$ parameters were also successfully optimized in this effort where MS Solver was used as the regression algorithm). The dimensional and dimensionless *IPR* curves for this case are presented in **Fig. 4.16**. It is important to note that the estimate of the ν_g parameter (*i.e.*, ν_g=0.11) lies outside of the range of the ν_g values that used in our original correlation database (**Table 4.2**). In our original database the ν_g parameter ranged between 0.25 and 0.83. As a final comment, we do not believe that this situation is a significant issue (*i.e.*, our ν_g estimate lying outside the range of the original correlation) — particularly since the correlation of IPR performance is very strong (see **Fig. 4.16**).

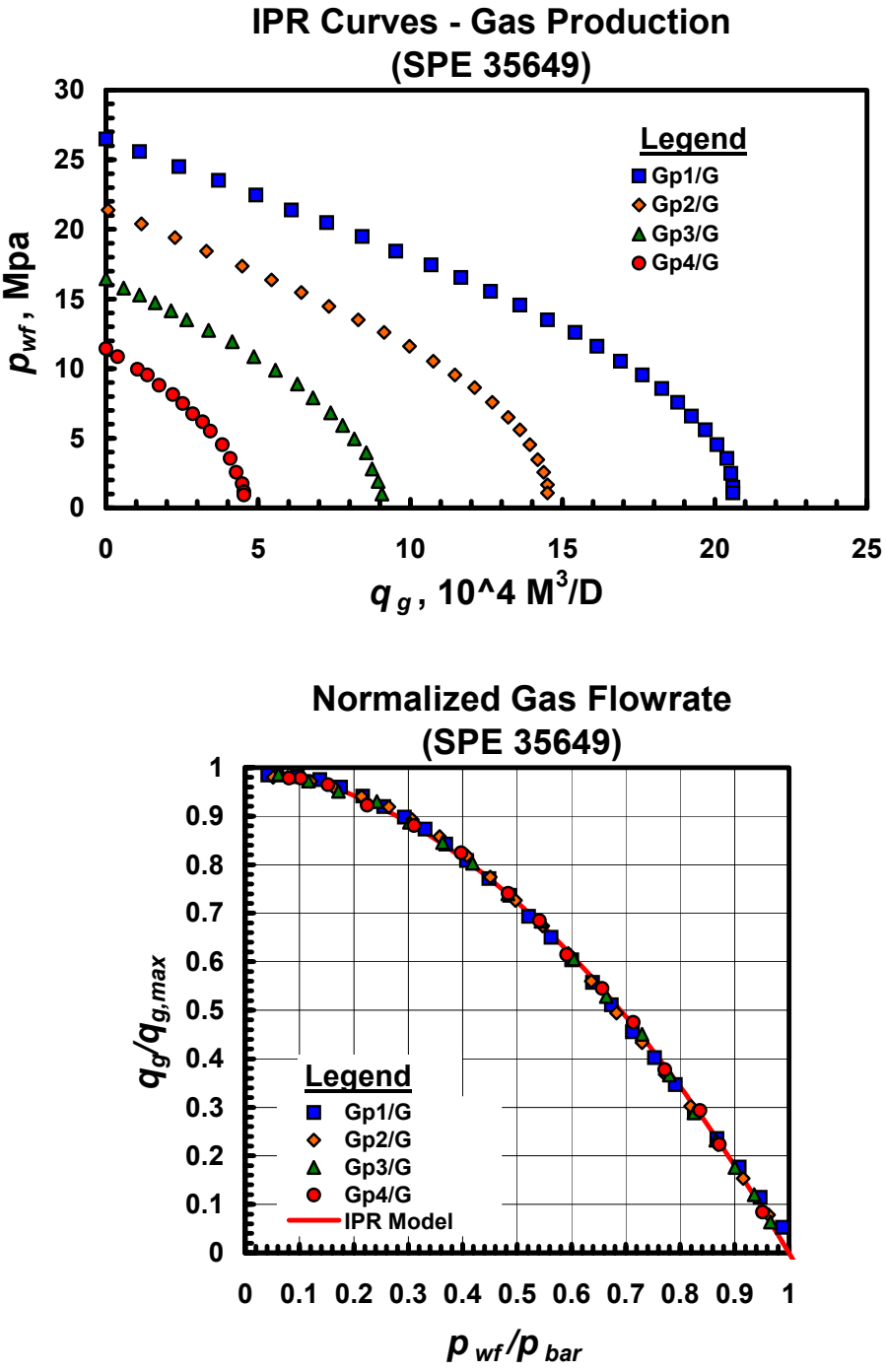

Fig. 4.16 — SPE 35649 — dry gas ($\nu_g = 0.11$ measured).

Table 4.8 presents the "predicted" ν_g values obtained using our 10 different correlations. They ν_g values range from very low values such as 0.03, to a maximum value of 0.33. Our best dry gas correlation (Case 9) predicted a value of 0.13 for the ν_g parameter.

Table 4.8 — Correlation of data from paper SPE 35649 (ref. 22).

	Variables													
	Independent										Dependent	Error		
	Mole fraction													
Case	C1	C2-C3	C4-C6	$C7^+$	p_{dew} (psia)	T (deg F)	S_{oc} (frac)	S_{gr} (frac)	ρ_{init} (lb_m/ft^3)	$M_{mixture}$ (lb_m/lb-mole)	ν_g	Std. Dev.	Avg. Error (%)	Calculated ν_g
1	ok	ok	R	ok	ok	ok	ok	ok			R	0.0303	5.11	0.04
2	ok	ok	R	R	ok	ok	ok	ok	ok		R	0.0293	5.16	0.03
3	ok	ok	VB	ok	R	ok	ok	ok		ok	ok	0.0275	4.56	0.13
4					R	ok	ok	ok		VB	ok	0.0438	7.81	0.33
5	ok			VB	ok	ok	ok	ok		ok	R	0.0281	4.70	0.12
6				ok	R	ok	ok	ok		ok	R	0.0287	4.95	0.24
7	ok			ok	ok	ok	ok	ok			R	0.0328	5.83	0.19
8	R			ok	VB	ok	ok	ok	R		R	0.0364	6.21	0.20
9	ok				ok	ok	ok	ok		ok	ok	0.0271	4.51	0.13
10	ok				R	ok	ok	ok	R	ok	R	0.0277	4.67	0.08

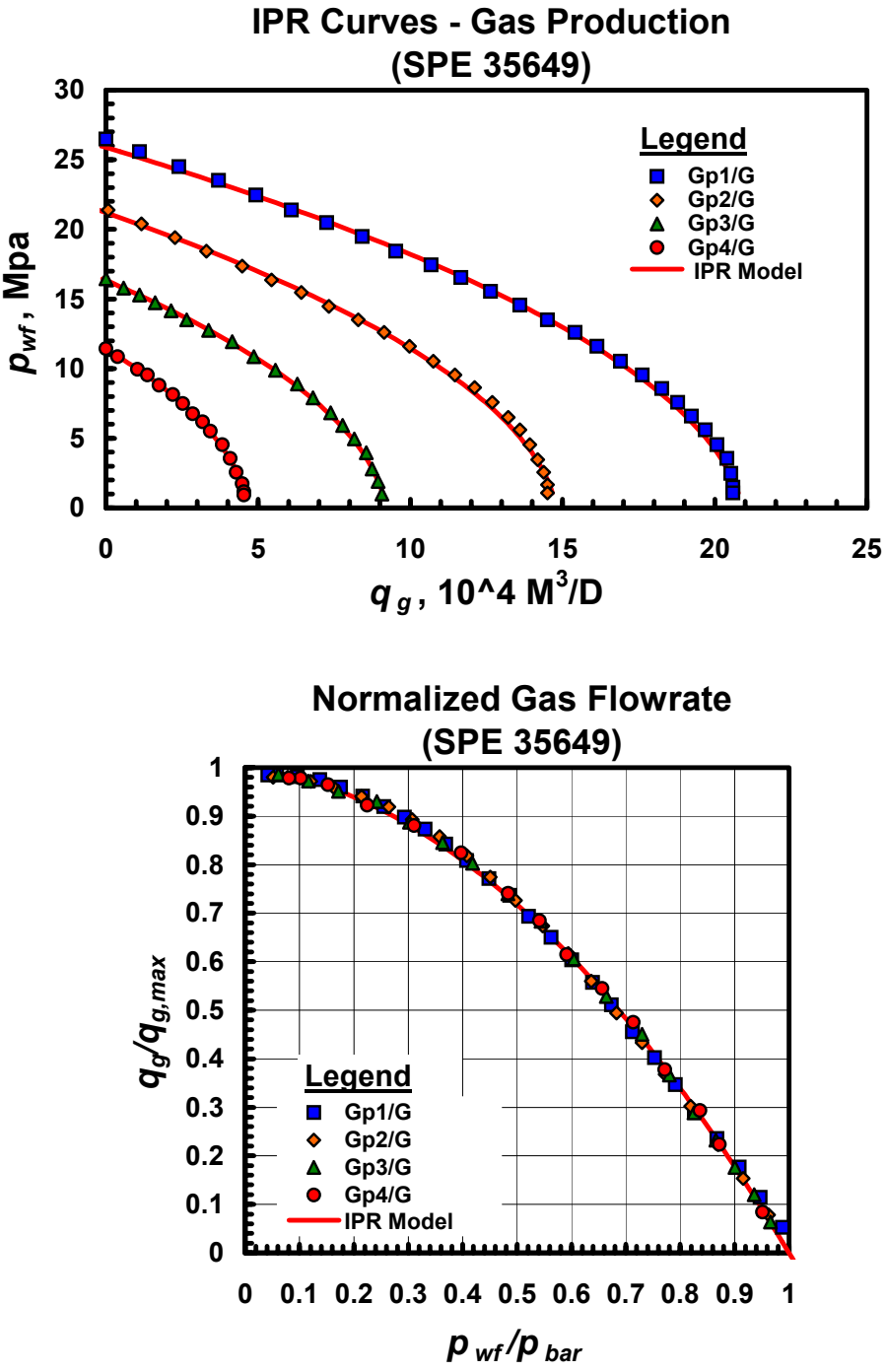

Fig. 4.17 — SPE 35649 — dry gas real values versus calculated values (ν_g = 0.13 calculated).

Comparing **Fig. 4.17** and the results presented in **Appendix B**. (section B.2.1), an estimate of 0.13 for the ν_g parameter (compared to the estimate of 0.11 obtained from simulation) gave very similar results for the dimensional and dimensionless *IPR* curves. Moreover, similar results are achieved using ν_g values of 0.03 and 0.2 (see **Appendix B**). If the estimate of the ν_g parameter is approximately 0.3 or greater, then we observe significant deviations from the dimensional *IPR* trends, where such deviations are even more apparent when viewed in the dimensionless form. It is important to recognize that our best correlation (Case 9) was used to calculate an "extrapolated" value for the ν_g parameter (*i.e.*, the ν_g=0.13 estimate), but even in this circumstance, this result does accurately reproduce the "dimensional" *IPR* curves presented in ref. 22.

As the calculated value for the ν_g parameter was out of the range of our initial database, we considered an additional case in order to validate the ν_g correlations. We again use "Example 5" from the Eclipse 300 simulation manual. As before, the dry gas *IPR* curves for the different depletion ratios were obtained from simulation, and the ν_g value was estimated to be 0.54. In this validation case the ν_g estimate of 0.54 lies within the range of ν_g values in our correlation database. The dimensional and dimensionless dry gas *IPR* curves for this case are presented in **Fig. 4.18**.

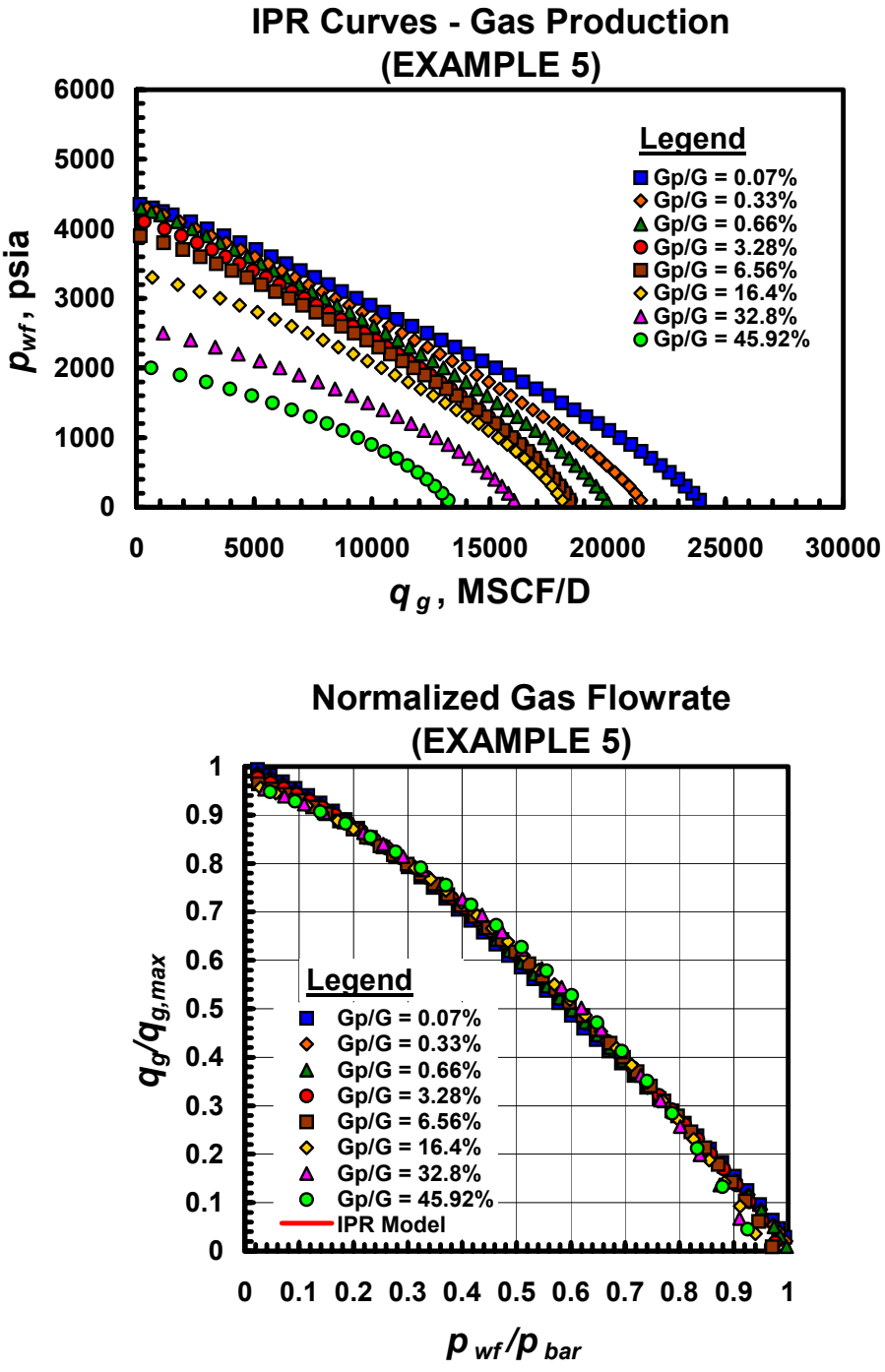

Fig. 4.18 — Example 5 — dry gas ($\nu_g = 0.54$ measured).

Table 4.9 shows the "predicted" ν_g values obtained using our 10 correlations. They results range from 0.46 to a maximum value of 0.79. Our best correlation (case 9) predicted a value of 0.49.

Table 4.9 — Correlation of data from example 5 (dry gas).

	Variables													
	Independent										Dependent	Error		
	Mole fraction													
Case	C1	C2-C3	C4-C6	$C7^+$	p_{dew} (psia)	T (deg F)	S_{oc} (frac)	S_{gr} (frac)	ρ_{init} (lb_m/ft^3)	$M_{mixture}$ (lb_m/lb-mole)	ν_g	Std. Dev.	Avg. Error (%)	Calculated ν_g
1	ok	ok	R	ok	ok	ok	ok	ok			R	0.0303	5.11	0.79
2	ok	ok	R	R	ok	ok	ok	ok	ok		R	0.0293	5.16	0.75
3	ok	ok	VB	ok	R	ok	ok	ok		ok	ok	0.0275	4.56	0.54
4					R	ok	ok	ok		VB	ok	0.0438	7.81	0.60
5	ok			VB	ok	ok	ok	ok		ok	R	0.0281	4.70	0.51
6				ok	R	ok	ok	ok		ok	R	0.0287	4.95	0.59
7	ok			ok	ok	ok	ok	ok			R	0.0328	5.83	0.68
8	R			ok	VB	ok	ok	ok	R		R	0.0364	6.21	0.46
9	ok				ok	ok	ok	ok		ok	ok	0.0271	4.51	0.49
10	ok				R	ok	ok	ok	R	ok	R	0.0277	4.67	0.47

Comparing **Fig. 4.19** and the results presented in **Appendix B** (section B.1.2), a value of 0.49 (instead of 0.54) for the ν_g parameter was found to give very similar results for the predicted dimensional and dimensionless *IPR* curves. Moreover, similar results are achieved using ν_g values of 0.45 and 0.60 (maintaining the same intercepts). We noted that the dry gas *IPR* curves appear to overlap each other and we consider this match to be very good — at very high ν_g values (near 0.80) we note that there are significant deviations which are particularly evident for the case of the dimensionless *IPR* curves.

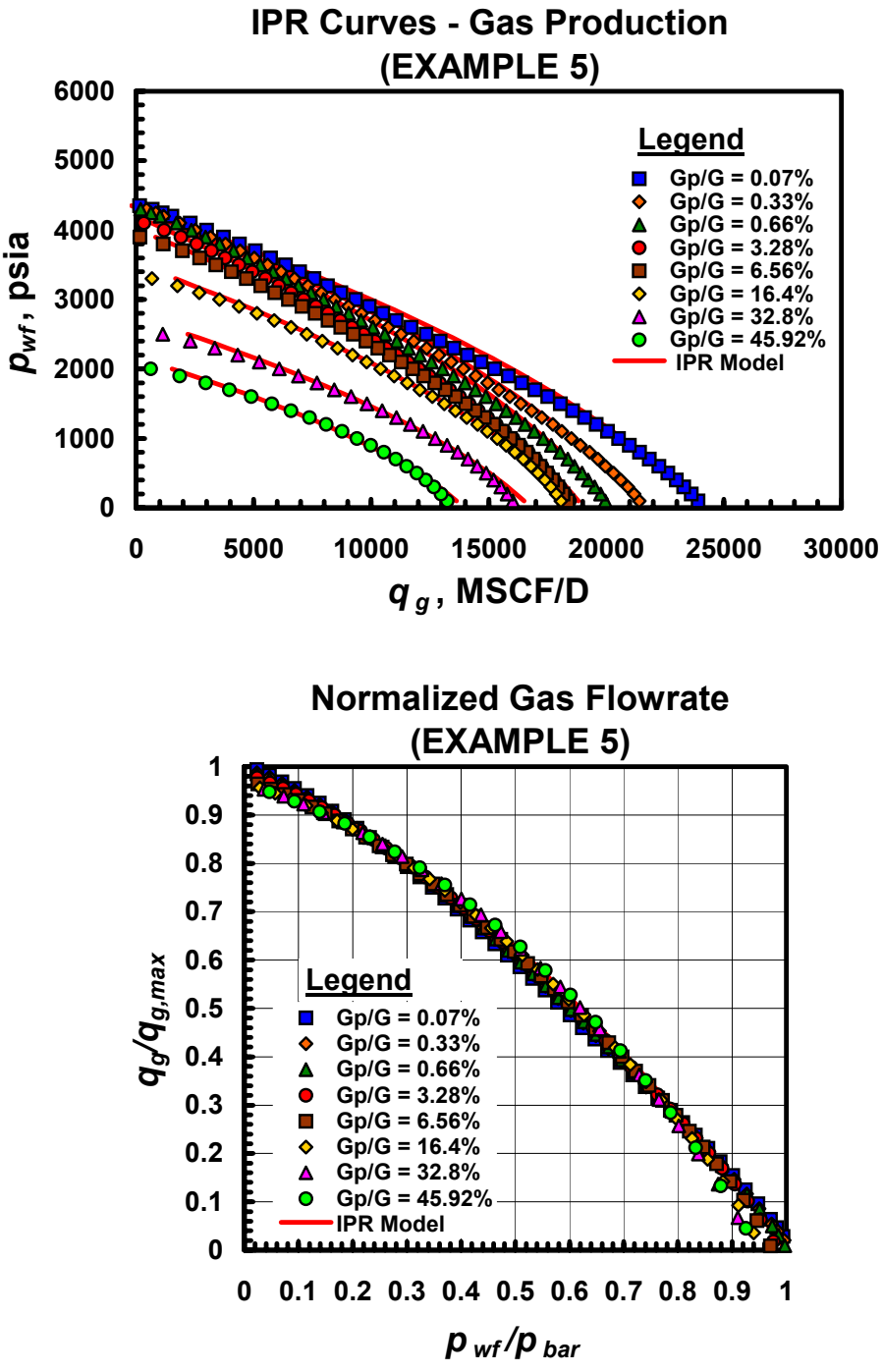

Fig. 4.19 — Example 5 — dry gas real values versus calculated values (ν_g = 0.49 calculated).

Considering the results obtained using Example 5, we observe curvature in the condensate and dry gas *IPR* curves and we note that the value of the ν_g parameter (0.54) is substantially larger than the corresponding ν_o value (0.22) for this case. This simply confirms our general observation that ν_g is generally greater than ν_o.

We also showed that a simple correlation based on reservoir and fluid properties can generate accurate estimates for the ν_o and ν_g parameters — where these parameters allow us reproduce the dimensional and dimensionless curves either for condensate or dry gas. Considering Example 5, we believe that the *IPR* correlations for condensate and gas (respectively) are accurate up to a maximum value of 12.88 percent for the condensate depletion ratio (N_p/N) and to a maximum value of 65.76 percent for the dry gas depletion ratio (G_p/G).

We would comment that the results of this work suggest that there seems to be a range of "good" values for the ν_o and/or ν_g parameters rather than a single unique value. When developing the condensate *IPR* curves for Example 5, $0.22<\nu_o<0.35$ values showed reasonable comparison. Similarly, for $0.03<\nu_g<0.2$ we find that satisfactory *IPR* curves can be developed for the data given in ref. 22. And, for the cases presented in Example 5, we found that for $0.45<\nu_g<0.60$ we obtain representative matches of the IPR trends for the dry gas case.

Based on this work we conclude there is no single, unique "best" correlation for the ν_o and/or ν_g parameters. Our "Case 9" correlation provides the best statistical correlation of the database values, but there are several other correlations, which give comparable results. We believe that a larger population of cases (*i.e.*, the ν_o and ν_g values as well as the associated data) will help to define better correlations — and we recommend that future research be conducted along this path.

4.5 Calibration

In this section we outline a procedure for applying the modified Vogel relationship to calculate a specific *IPR* trend, either for condensates or dry gases. The ν_o and ν_g parameters are calculated corresponding to a particular condensate system using a selected correlation (*e.g.*, in our work, we have typically used the correlation known as "Case 9"). At this point it is necessary to obtain estimates of the intercepts for a particular depletion case. The "y" intercept ($\bar{p}$) is the average reservoir pressure and can be estimated using data from a pressure transient test at the specific depletion stage. The "x" intercept (*i.e.* $q_{o,max}$ or $q_{g,max}$) can be calculated using production test data (*i.e.* $q_{o,g}$ and p_{wf}).

To show the details of this procedure we selected 3 cases which have previously been discussed. Case 16 corresponds to the richest condensate fluid (Cupiagua), we then consider the case of data from ref. 22, and finally we consider a simulated case (Example 5).

In the first case (Case 16) we used the ν_o value determined using the procedures outlined in Chapter III. For the last two cases we used the calculated ν_g values estimated in the previous section using our best correlation (Case 9). In all three cases the reservoir pressure was assumed known.

For each case, three different maximum rates were calculated using three different production tests ($q_{o,g}$ and p_{wf}) and the modified Vogel relationship (condensate or dry gas). We note that each maximum rate represents a different calibration for the same *IPR* curve. In other words, each calibration has the same "y" intercept (*i.e.*, the same reservoir pressure) — but each calibration has a different "x" intercept. **Tables 4.10, 4.11, and 4.12** show the results of the calibrations for the three given cases. The maximum absolute error between the calculated maximum rate and the defined (or actual) maximum rate was 5.3 percent.

In **Figs. 4.20 to 4.22** we show the *IPR* curves generated using the 3 different calibrations for each case. In all three cases, there seem to be small differences in the generated *IPR* curves when the bottomhole pressure achieved in the production test is less than half of the reservoir pressure at the selected depletion stage. Specifically, we only observed substantial deviations in the generated *IPR* curves when the bottomhole pressure was very high (*e.g.*, the case given in ref. 22).

Based on our previous results we can conclude that after the ν_o and ν_g parameters are estimated using our best correlation (Case 9), the tuning of the modified Vogel relationship for a particular depletion ratio can be achieved using the reservoir pressure from a pressure transient test and the rates from a production test ($q_{o,g}$ and p_{wf}). We recommend that the flowing bottomhole pressure during the production test be held to a value less than half of the reservoir pressure. Using this profile the results of the predicted *IPR* curves should be accurate and representative.

Table 4.10— Case16 — Condensate IPR, richest condensate fluid (Cupiagua).

Initial data required				
$\bar{p}$ (psia)	4898.75			
$\nu_{o,\text{ measured}}$	0.61			
$q_{o,max}$ calculation				
	$q_{o,max}$ (STB/D)			
Real value	546.97			
		Production tests		Abs. error (%)
		p_{wf} (psia)	1200	
Calibration 1	550.56	q_a (STB/D)	455.409	0.66
		p_{wf} (psia)	2400	
Calibration 2	545.33	q_a (STB/D)	331.31	0.30
		p_{wf} (psia)	3600	
Calibration 3	535.98	q_a (STB/D)	182.825	2.01

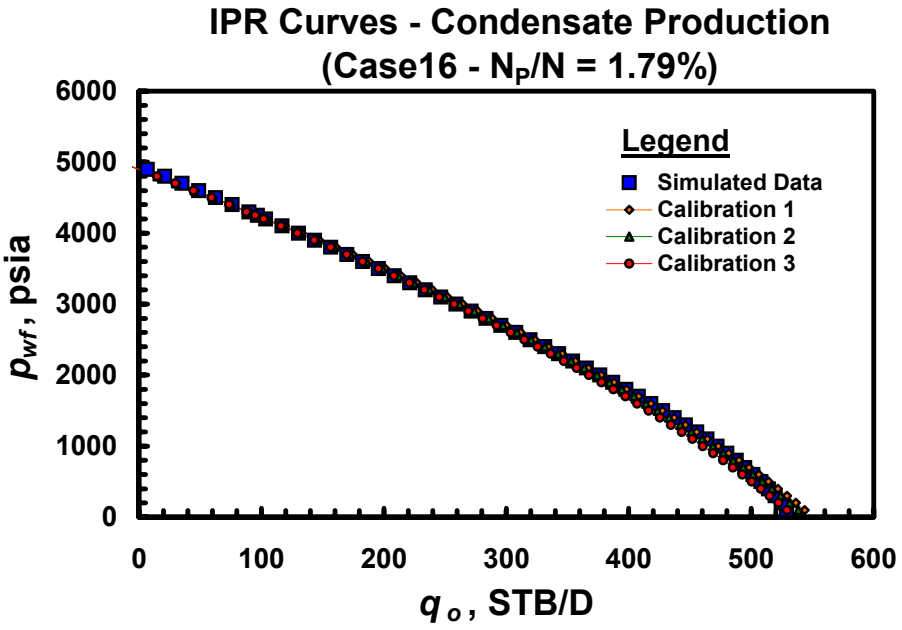

Fig. 4.20 — Case16 (Cupiagua).

Table 4.11— SPE 35649 — dry gas IPR.

Initial data required				
$\overline{p}$ (MPa)	26.48			
$v_{g,\text{ calculated}}$	0.13			
$q_{g,max}$ calculation				
	$q_{g,max}$ (10^4M^3/D)			
Real value	20.60			
		Production tests		Abs. error (%)
		p_{wf}(Mpa)	5.60274	
Calibration 1	21.09	q_g (10^4M^3/D)	19.6891	2.40
		p_{wf}(Mpa)	12.589	
Calibration 2	20.79	q_g (10^4M^3/D)	15.4145	0.93
		p_{wf}(Mpa)	18.4247	
Calibration 3	19.50	q_g (10^4M^3/D)	9.52073	5.34

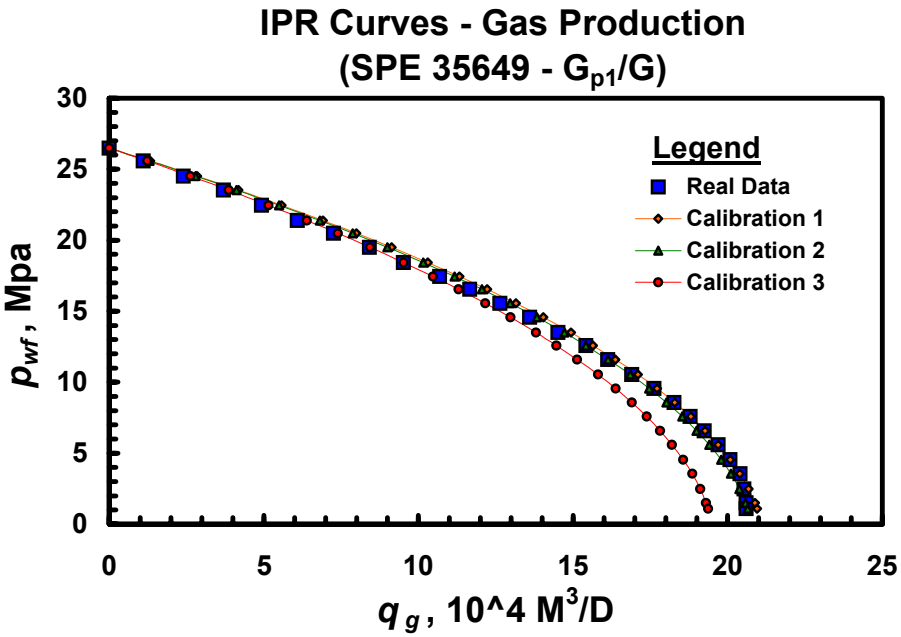

Fig. 4.21 — SPE 35649.

Table 4.12— Example 5 — dry gas IPR.

Initial data required				
$\overline{p}$ (psia)	4016.54			
$v_{g,\text{ calculated}}$	0.49			
$q_{g,max}$ calculation				
	$q_{g,max}$ (Mscf/D)			
Real value	19047.34			
		Production tests		error (%)
		p_{wf}(psia)	1000	
Calibration 1	18818.43	q_g (Mscf/D)	15927.8	1.20
		p_{wf}(psia)	2000	
Calibration 2	18688.79	q_g (Mscf/D)	11765.7	1.88
		p_{wf}(psia)	3000	
Calibration 3	18547.44	q_g (Mscf/D)	6482.28	2.62

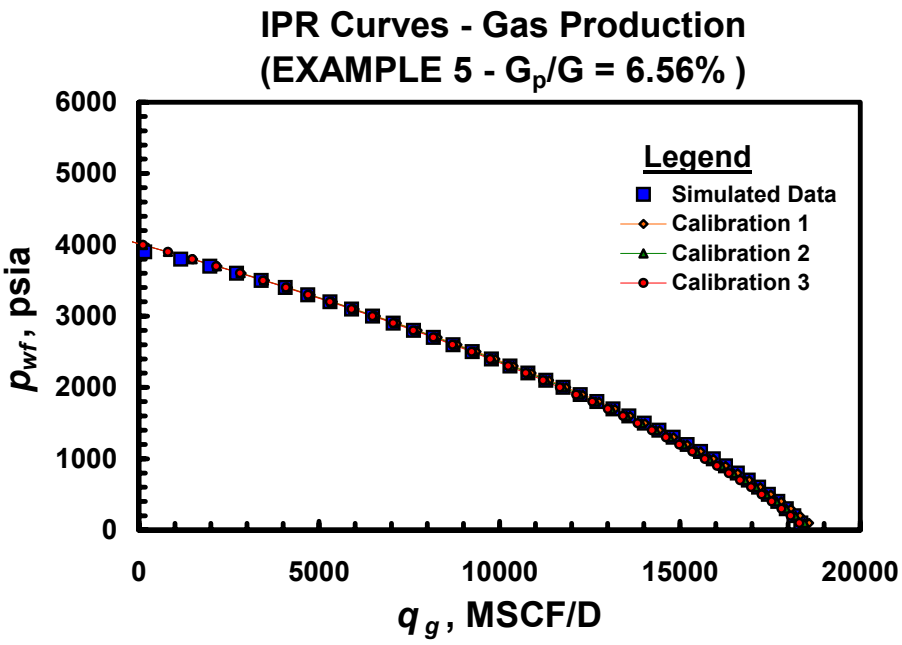

Fig. 4.22 — Example 5.

CHAPTER V

CONCLUSIONS AND RECOMMENDATIONS

5.1 Conclusions

1. A simple method (modified Vogel correlation) was developed to calculated gas condensate well deliverability. This approach allows us to estimate future performance of gas condensate reservoir systems without resorting to the use of simulation.
2. The modified Vogel correlation permitted the development of "dimensionless" *IPR* curves for condensates and dry gases.
3. Unlike the (original) Vogel correlation for solution gas-drive reservoirs, the ν_o and ν_g parameters are not unique for different gas condensate systems (these parameters vary with the fluid and reservoir properties). The ν_o and ν_g can be presumed constant for a given condensate system — that is, these parameters do not vary with depletion stage (N_p/N or G_p/G).
4. In a practical sense, the determination of the exact value of the ν_o and ν_g parameters is not critical. We find that there is an acceptable margin of error in the parameters (as much as 10-20 percent) within which we do not observe significant changes in the computed *IPR* trends.
5. Using a non-parametric correlation technique, we correlated the values of the ν_o and ν_g parameters using the following independent variables: C1, p_{dew}, T, S_{oc}, S_{gr} and $M_{mixture}$ — where these independent variables were identified to be the most influential parameters. These non-parametric correlations are considered to be both representative and accurate.
6. It is important to note that our correlation of the ν_o and ν_g parameters may not be unique because our choice of independent variables (C1, p_{dew}, T, S_{oc}, S_{gr} and $M_{mixture}$) is not complete. In particular, we have approximated the fluid composition by use of the initial mixture properties and we have represented the relative permeability effects using the S_{oc} and S_{gi} variables. Other variables (or combinations of variables) may include additional information that would improve such correlations.

5.2 Recommendations

1. It is important to consider/investigate the influence of other variables that may affect deliverability in gas condensate reservoir systems.This work is based solely on cases of simulated reservoir performance — field data should be tested against the results/methodology proposed in this work.
3. The influence of flowrate (and/or viscosity) on relative permeability should be considered for the case of gas condensate reservoir systems (Henderson and Danesh model[27]).

NOMENCLATURE

Variables

A	=	Drainage area of well, sq ft
B_g	=	Gas formation volume factor, scf/rcf
B_o	=	Condensate (oil) formation volume factor, RB/STB
C_A	=	Shape constant or factor, dimensionless
C1	=	C1 mole fraction, dimensionless
C2-C3	=	C1 to C2 mole fraction, dimensionless
C4-C6	=	C4 to C6 mole fraction, dimensionless
$C7^+$	=	C7 plus mole fraction, dimensionless
G	=	Original gas-in-place, BSCF
G_p	=	Cumulative gas production, MSCF
G_p/G	=	Gas depletion ratio, percentage
GOR	=	Gas oil ratio, scf/STB
h	=	Formation thickness, ft
J_o	=	Residual condensate (oil) function for optimization, fraction
J_g	=	Residual gas function for optimization, fraction
k	=	Formation permeability, md
k_{rg}	=	Relative permeability to gas, fraction
k_{ro}	=	Relative permeability to condensate, fraction
M_i	=	Molecular weight of individual component, lb_m/lb-mole
$M_{mixture}$	=	Molecular weight of the fluid mixture, lb_m/lb-mole
n	=	Exponent of back-pressure curve
N	=	Original condensate (oil)-in-place, MMSTB
N_p	=	Cumulative condensate (oil) production, STB
N_p/N	=	Condensate (oil) depletion ratio, percentage
N/G	=	Original condensate in-place over original gas -in-place, STB/MSCF
$\bar{p}$	=	Average reservoir pressure, psia or Mpa (text and figures)
p_{bar}	=	Average reservoir pressure, psia (figures)
p_{ci}	=	Critical pressure of individual component, psia
p_{dew}	=	Dewpoint pressure, psia
$p_{pc}\_C7^+$	=	Pseudocritical pressure of the C7 plus fraction, psia
$\bar{p}_R$	=	Average reservoir pressure, psia

Variables (continued)

p_{wf} = Flowing bottomhole pressure, psia

q_g = Gas flowrate, MSCF/D

$q_{g,max}$ = Maximum gas flowrate, MSCF/D

q_o = Condensate (oil) flowrate, STB/D

$q_{o,g}$ = Condensate (oil) flowrate (STB/D) or gas flowrate (MSCF/D)

$q_{o,g,max}$ = Maximum condensate flowrate (STB/D) or maximum gas flowrate (MSCF/D)

$q_{o,max}$ = Maximum condensate (oil) flowrate, STB/D

r_e = Reservoir drainage radius, ft

r_w = Wellbore radius, ft

R_s = Solution gas-oil ratio, scf/STB

s = Radial flow skin factor, dimensionless

S_{gr} = Residual gas saturation, fraction

S_o = Condensate saturation, fraction

S_{oc} = Critical condensate saturation, fraction

S_{wi} = Critical condensate saturation, fraction

T = Reservoir temperature, deg F

$T_b\_C7^+$ = Boiling temperature of the C7 plus fraction, deg R

T_{ci} = Critical temperature of individual component, deg R

$T_{pc}\_C7^+$ = Pseudocritical temperature of the C7 plus fraction, deg R

z = Gas law deviation factor (or gas compressibility factor), dimensionless

Other symbols

γ = Euler's constant (0.577216 ....)

γ_g = Gas specific gravity, dimensionless

μ_g = Gas viscosity, cp

μ_o = Condensate (oil) viscosity, cp

ν = Oil *IPR* parameter in a solution gas-drive reservoir (for Eq. 1.16 and Eq. 1.20), dimensionless

ν_g = Gas *IPR* parameter (for Eq. 3.5), dimensionless

ν_o = Condensate *IPR* parameter (for Eq. 3.1), dimensionless

$\nu_{o,g}$ = Condensate *IPR* parameter or gas *IPR* parameter, dimensionless

ρ_{init} = Fluid density at the dewpoint pressure (initial density), lb_m/ft^3

$\check{z}_i$ = Mole fraction of individual component, dimensionless

REFERENCES

1. Evinger, H.H. and Muskat, M.: "Calculation of Theoretical Productivity Factor," *Trans.* AIME (1942) **146**, 126-139.
2. Rawlins, E.L. and Schellhardt, M.A.: *Backpressure Data on Natural Gas Wells and Their Application to Production Practices*, Monograph Series, USBM (1935) 7.
3. Gilbert, W.E.: "Flowing and Gas-Lift Well Performance," *Drill. and Prod. Prac.*, API (1954) 126.
4. Raghavan, R.: *Well Test Analysis*, Prentice Hall Petroleum Engineering Series, Englewood Cliffs, New Jersey (1993) 513-514.
5. Fetkovich, M.J.: "The Isochronal Testing of Oil Wells," paper SPE 4529 presented at the 1973 SPE Annual Fall Meeting, Las Vegas, Nevada, 30 September-3 October.
6. Vogel, J.V.: "Inflow Performance Relationships for Solution-Gas Drive Wells," *JPT* (January 1968), 83
7. Richardson, J.M. and Shaw A.H: "Two-Rate *IPR* Testing — A Practical Production Tool," *JCPT*, (March-April 1982) 57-61.
8. Seidle, J.P. and Erikson, D.J.: "Use of Vogel's Inflow Performance Relation for Coal Wells," paper SPE 26201 presented at the 1993 SPE Gas Technology Symposium, Calgary, Alberta, Canada, 28-30 June.
9. Wiggins, M.L., Russell, J.E., Jennings, J.W.: "Analytical Development of Vogel-Type Inflow Performance Relationships," *SPE Journal* (December 1996) 355-362.
10. Fussell, D.D.: "Single-Well Performance Predictions for Gas Condensate Reservoirs," *JPT* (July 1973) 860-870.
11. O'Dell, H.G. and Miller, R.N.: "Successfully Cycling a Low Permeability, High-Yield Gas Condensate Reservoirs," *JPT* (January 1967) 41-44.
12. Fevang, O. and Whitson, C.H.: "Modelling Gas-Condensate Well Deliverability," paper SPE 30714 presented at the 1995 SPE Annual Technical Conference and Exhibition, Dallas, 22-25 October.
13. Roussennac, B.: *Gas Condensate Well Analysis*, M.S. Thesis, Stanford University, California, June 2001.
14. Fevang, O., Kameshwar, S., and Whitson, C. H.: "Guidelines for Choosing Compositional and Black-Oil Models for Volatile Oil and Gas-Condensate Reservoirs," paper SPE 63087 presented at the 2000 SPE Annual Technical Conference and Exhibition, Dallas, Texas, 1-4 October.
15. Malachowski, M.A., Yanosik, M.A., and Saldana, M.A.: "Simulation of Well Productivity Losses Due to Near Well Condensate Accumulation in Field Scale Simulations," paper SPE 30715 presented at the 1995 SPE Annual Technical Conference and Exhibition, Dallas, Texas, 22-25 October.

16. Zapata, F.: *Impact of Relative Permeability Models on Fluid Flow Behavior for Gas Condensate Reservoirs*, M.S. Thesis Texas A&M University, College Station, August 2002.
17. Jaramillo, J.M.: *Vertical Composition Gradient Effects on Original Hydrocarbon in Place Volumes and Liquid Recovery for Volatile Oil and Gas Condensate Reservoirs*, M.S. Thesis Texas A&M University, College Station, December 2000.
18. Lohrenz, J., Bray, B.G., and Clark, C.R.: "Calculating Viscosities of Reservoir Fluids from Their Compositions," *JPT* (October 1964) 1171-76.
19. Guerra, A.: *Analysis of the Dynamics of Saturation and Pressure Close to the Wellbore for Condensate Reservoirs as a Tool to Optimize Liquid Production*, M.S. Thesis Texas A&M University, College Station, May 2001.
20. Pedersen, K.S., Thomssen, P., and Fredenslund, A.: "C7+ Fraction Characterization, Characterization of Gas Condensates Mixtures," *Advances in Thermodynamics*, Vol. 1 (1989), Mansoori, G.A. ed., Taylor and Francis, New York, 137-152.
21. McCain, W.D. Jr.: *The Properties of Petroleum Fluids*, second edition, PennWell Publishing Co. Inc., Tulsa, Oklahoma (1990) 129-164.
22. Xiong, Y., Sun, Le., Sun Li., and Li S.: "A New Method for Predicting the Law of Unsteady Flow Through Porous Medium on a Gas Condensate Well," paper SPE 35649 presented at the 1996 SPE Program Conference, Calgary, Canada, 28 April- 1 May.
23. Microsoft Excel 2000, Vers. 9.0.3821 SR-1, Microsoft Corporation (1999).
24. McCain, W.D. Jr., Soto B. R., Valko, P.P., and Blasingame, T.A.: "Correlation of Bubblepoint Pressures for Reservoir Oils — A Comparative Study," paper SPE 51086 presented at the 1998 SPE Eastern Regional Conference and Exhibition, Pittsburgh, Pennsylvania, 9-11 November.
25. Whitson, C.H., and Brule, M.R.: *Phase Behavior*, Monograph Series, SPE, Richardson, Texas (2000) 23-26.
26. Lee, J. and Wattenbarger, R.A.: *Gas Reservoir Engineering,* first printing, Textbook Series, Society of Petroleum Engineers, Richardson, Texas (1996) 3-7.
27. Henderson, G. D., Danesh, A., Tehrani, D.H., Al-Shaidi, S., and Peden, J.M.: "Measurement and Correlation of Gas Condensate Relative Permeability by the Steady-State Method," *SPE Journal* (June 1996) 191-201.
28. Camacho-V. R. G. and Raghavan, R: "Inflow Performance Relationships for Solution-Gas-Drive Reservoirs," *JPT* (May 1989) 541-550.

APPENDIX A

INVENTORY OF *IPR* CASES DEVELOPED FOR GAS CONDENSATE RESERVOIRS

In this appendix we provide an inventory of the various inflow performance relationships (or *IPR* functions) generated for a gas condensate reservoir producing at conditions near or below the dewpoint pressure.

Table A.1 — IPR Correlation Results from Compositional Reservoir Simulation — Gas Condensate Reservoir Systems.

Case	k_r set	Fluid set	S_{oc} (frac)	S_{gr} (frac)	p_{dew} (psia)	T (deg F)	N/G (STB/ MSCF)	Mole Fraction C1 (frac)	C2-C3 (frac)	C4-C6 (frac)	$C7^+$ (frac)	ρ_{init} (lb_m/ft^3)	$M_{mixture}$ (lb_m/ lb-mole)
1	1	1	0.10	0.00	4278	260	0.1094	0.896	0.000	0.030	0.074	15.431	26.00
2	2	1	0.10	0.00	4278	260	0.1094	0.896	0.000	0.030	0.074	15.431	26.00
3	3	1	0.10	0.00	4278	260	0.1094	0.896	0.000	0.030	0.074	15.431	26.00
4	4	1	0.10	0.50	4278	260	0.1094	0.896	0.000	0.030	0.074	15.431	26.00
5	5	1	0.00	0.00	4278	260	0.1094	0.896	0.000	0.030	0.074	15.431	26.00
6	1	2	0.10	0.00	4575	260	0.1541	0.870	0.000	0.030	0.100	18.705	29.10
7	1	3	0.10	0.00	2845	260	0.0388	0.956	0.000	0.015	0.029	12.551	20.08
8	1	4	0.10	0.00	4814	260	0.1800	0.870	0.000	0.015	0.115	19.833	30.23
9	1	5	0.10	0.00	5015	260	0.1578	0.690	0.131	0.047	0.082	24.352	34.85
10	4	5	0.10	0.50	5015	260	0.1578	0.690	0.131	0.047	0.082	24.352	34.85
11	5	5	0.00	0.00	5015	260	0.1578	0.690	0.131	0.047	0.082	24.352	34.85
12	4	5	0.10	0.50	5040	230	0.1578	0.690	0.131	0.047	0.082	25.791	34.85
13	4	5	0.10	0.50	4925	300	0.1578	0.690	0.131	0.047	0.082	22.570	34.85
14	4	6	0.10	0.50	5113	260	0.2655	0.617	0.146	0.067	0.121	30.635	44.35
15	4	6	0.10	0.50	5084	230	0.2655	0.617	0.146	0.067	0.121	33.289	44.35
16	4	6	0.10	0.50	5117	300	0.2655	0.617	0.146	0.067	0.121	36.078	44.35
17	1	5	0.10	0.00	5040	230	0.1578	0.690	0.131	0.047	0.082	25.791	34.85
18	2	5	0.10	0.00	5015	260	0.1578	0.690	0.131	0.047	0.082	24.352	34.85
19	3	5	0.10	0.00	5015	260	0.1578	0.690	0.131	0.047	0.082	24.352	34.85
20	2	5	0.10	0.00	5040	230	0.1578	0.690	0.131	0.047	0.082	25.791	34.85
21	3	5	0.10	0.00	5040	230	0.1578	0.690	0.131	0.047	0.082	25.791	34.85
22	1	5	0.10	0.00	4925	300	0.1578	0.690	0.131	0.047	0.082	22.570	34.85
23	2	5	0.10	0.00	4925	300	0.1578	0.690	0.131	0.047	0.082	22.570	34.85
24	3	5	0.10	0.00	4925	300	0.1578	0.690	0.131	0.047	0.082	22.570	34.85
25	5	5	0.00	0.00	4925	300	0.1578	0.690	0.131	0.047	0.082	22.570	34.85
26	1	6	0.10	0.00	5113	260	0.2655	0.617	0.146	0.067	0.121	30.635	44.35
27	5	6	0.00	0.00	5113	260	0.2655	0.617	0.146	0.067	0.121	30.635	44.35
28	1	6	0.10	0.00	5084	230	0.2655	0.617	0.146	0.067	0.121	33.289	44.35
29	5	6	0.00	0.00	5084	230	0.2655	0.617	0.146	0.067	0.121	33.289	44.35
30	1	6	0.10	0.00	5117	300	0.2655	0.617	0.146	0.067	0.121	36.078	44.35
31	5	6	0.00	0.00	5117	300	0.2655	0.617	0.146	0.067	0.121	36.078	44.35
32	4	2	0.10	0.50	4575	260	0.1541	0.870	0.000	0.030	0.100	18.705	29.10
33	5	2	0.00	0.00	4575	260	0.1541	0.870	0.000	0.030	0.100	18.705	29.10
34	5	3	0.00	0.00	2845	260	0.0388	0.956	0.000	0.015	0.029	12.551	20.08
35	4	4	0.10	0.50	4814	260	0.1800	0.870	0.000	0.015	0.115	19.833	30.23
36	5	4	0.00	0.00	4814	260	0.1800	0.870	0.000	0.015	0.115	19.833	30.23
37	1	1	0.10	0.00	4512	230	0.1094	0.896	0.000	0.030	0.074	17.613	26.00
38	4	1	0.10	0.50	4512	230	0.1094	0.896	0.000	0.030	0.074	17.613	26.00
39	5	1	0.00	0.00	4512	230	0.1094	0.896	0.000	0.030	0.074	17.613	26.00
40	1	1	0.10	0.00	3864	300	0.1094	0.896	0.000	0.030	0.074	15.469	26.00
41	4	1	0.10	0.50	3864	300	0.1094	0.896	0.000	0.030	0.074	15.469	26.00
42	5	1	0.00	0.00	3864	300	0.1094	0.896	0.000	0.030	0.074	15.469	26.00
43	1	2	0.10	0.00	4755	230	0.1541	0.870	0.000	0.030	0.100	19.778	29.10
44	4	2	0.10	0.50	4755	230	0.1541	0.870	0.000	0.030	0.100	19.778	29.10
45	5	2	0.00	0.00	4755	230	0.1541	0.870	0.000	0.030	0.100	19.778	29.10
46	1	2	0.10	0.00	4249	300	0.1541	0.870	0.000	0.030	0.100	17.428	29.10
47	4	2	0.10	0.50	4249	300	0.1541	0.870	0.000	0.030	0.100	17.428	29.10
48	5	2	0.00	0.00	4249	300	0.1541	0.870	0.000	0.030	0.100	17.428	29.10
49	6	1	0.30	0.00	4278	260	0.1094	0.896	0.000	0.030	0.074	15.431	26.00
50	6	2	0.30	0.00	4575	260	0.1541	0.870	0.000	0.030	0.100	18.705	29.10

Table A.1 — IPR Correlation Results from Compositional Reservoir Simulation — Gas Condensate Reservoir Systems. (continued)

Case	k_r set	Fluid set	S_{oc} (frac)	S_{gr} (frac)	p_{dew} (psia)	T (deg F)	N/G (STB/ MSCF)	Mole Fraction C1 (frac)	C2-C3 (frac)	C4-C6 (frac)	$C7^+$ (frac)	ρ_{init} (lb_m/ft^3)	$M_{mixture}$ (lb_m/ lb-mole)
51	6	5	0.30	0.00	5015	260	0.1578	0.690	0.131	0.047	0.082	24.352	34.85
52	6	6	0.30	0.00	5113	260	0.2655	0.617	0.146	0.067	0.121	30.635	44.35
53	6	6	0.30	0.00	5084	230	0.2655	0.617	0.146	0.067	0.121	33.289	44.35
54	6	6	0.30	0.00	5117	300	0.2655	0.617	0.146	0.067	0.121	36.078	44.35
55	6	1	0.30	0.00	3864	300	0.1094	0.896	0.000	0.030	0.074	15.469	26.00
56	6	5	0.30	0.00	4925	300	0.1578	0.690	0.131	0.047	0.082	22.570	34.85
57	7	1	0.30	0.15	4278	260	0.1094	0.896	0.000	0.030	0.074	15.431	26.00
58	7	1	0.30	0.15	3864	300	0.1094	0.896	0.000	0.030	0.074	15.469	26.00
59	7	5	0.30	0.15	5015	260	0.1578	0.690	0.131	0.047	0.082	24.352	34.85
60	7	5	0.30	0.15	4925	300	0.1578	0.690	0.131	0.047	0.082	22.570	34.85
61	7	6	0.30	0.15	5100	260	0.2655	0.617	0.146	0.067	0.121	30.635	44.35
62	7	6	0.30	0.15	5117	300	0.2655	0.617	0.146	0.067	0.121	36.078	44.35

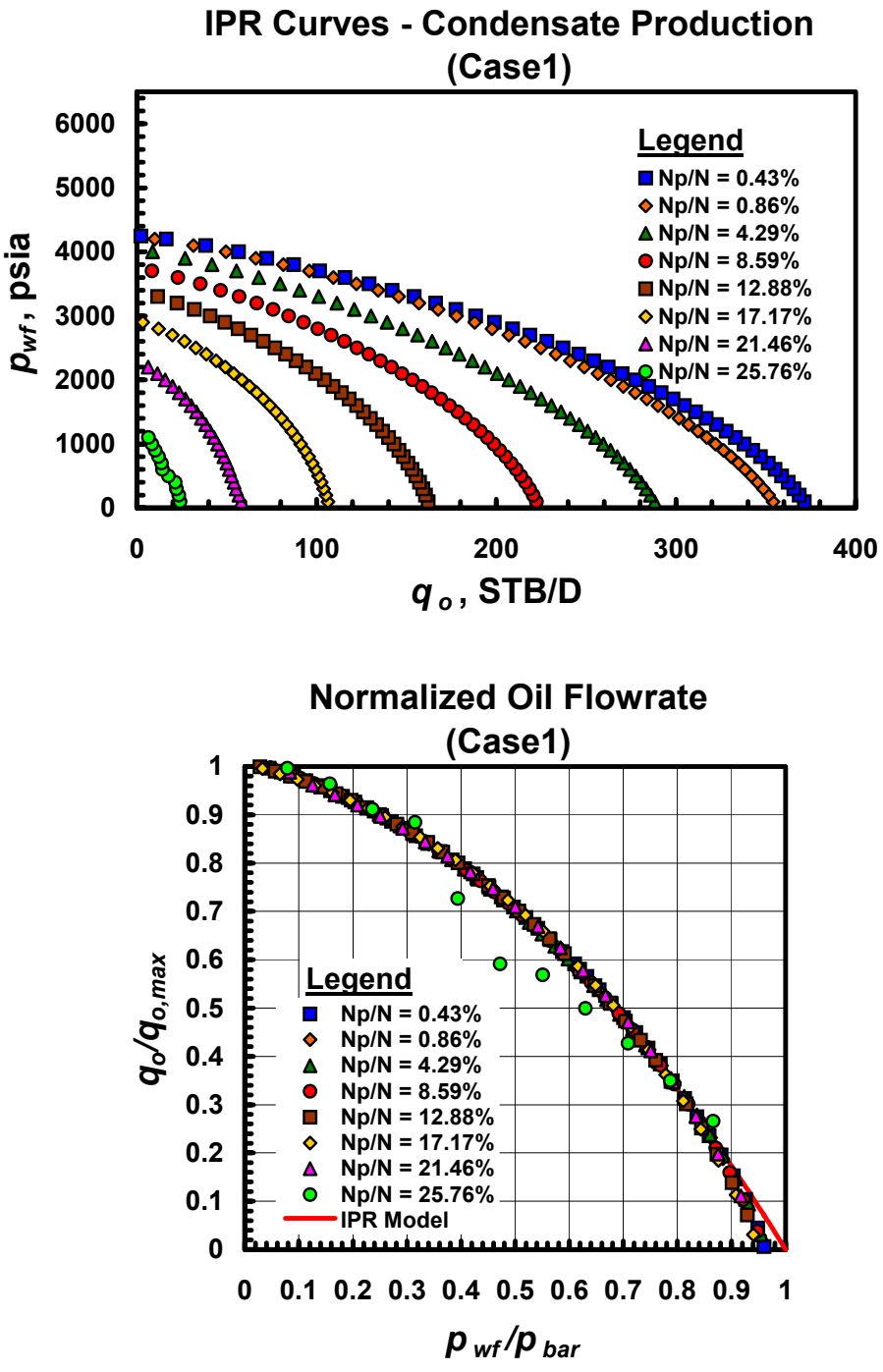

Fig. A.1.a — Dimensional and dimensionless IPR trends for Case 1 — gas condensate performance trends.

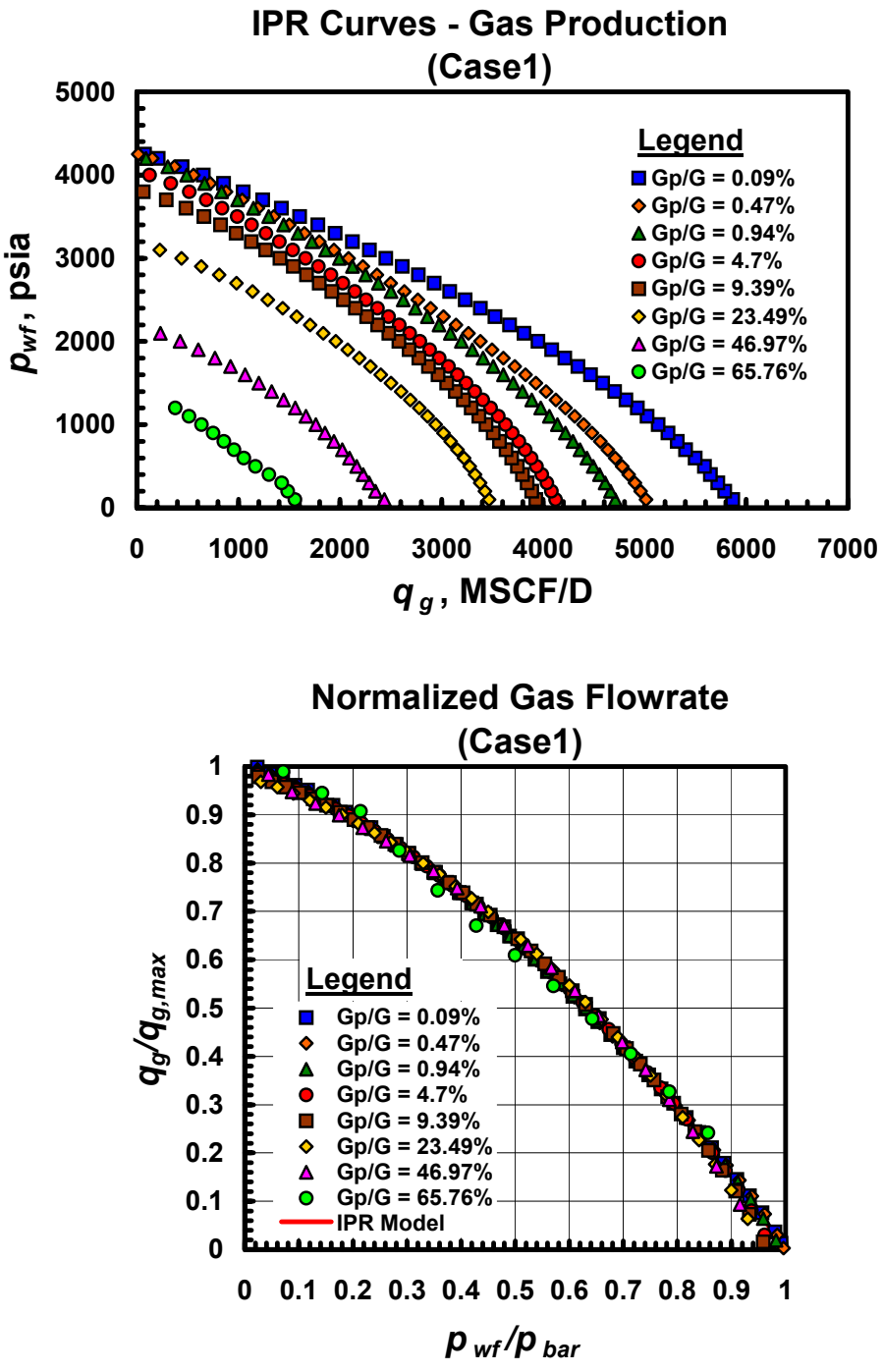

Fig. A.1.b — Dimensional and dimensionless IPR trends for Case 1 — gas performance trends.

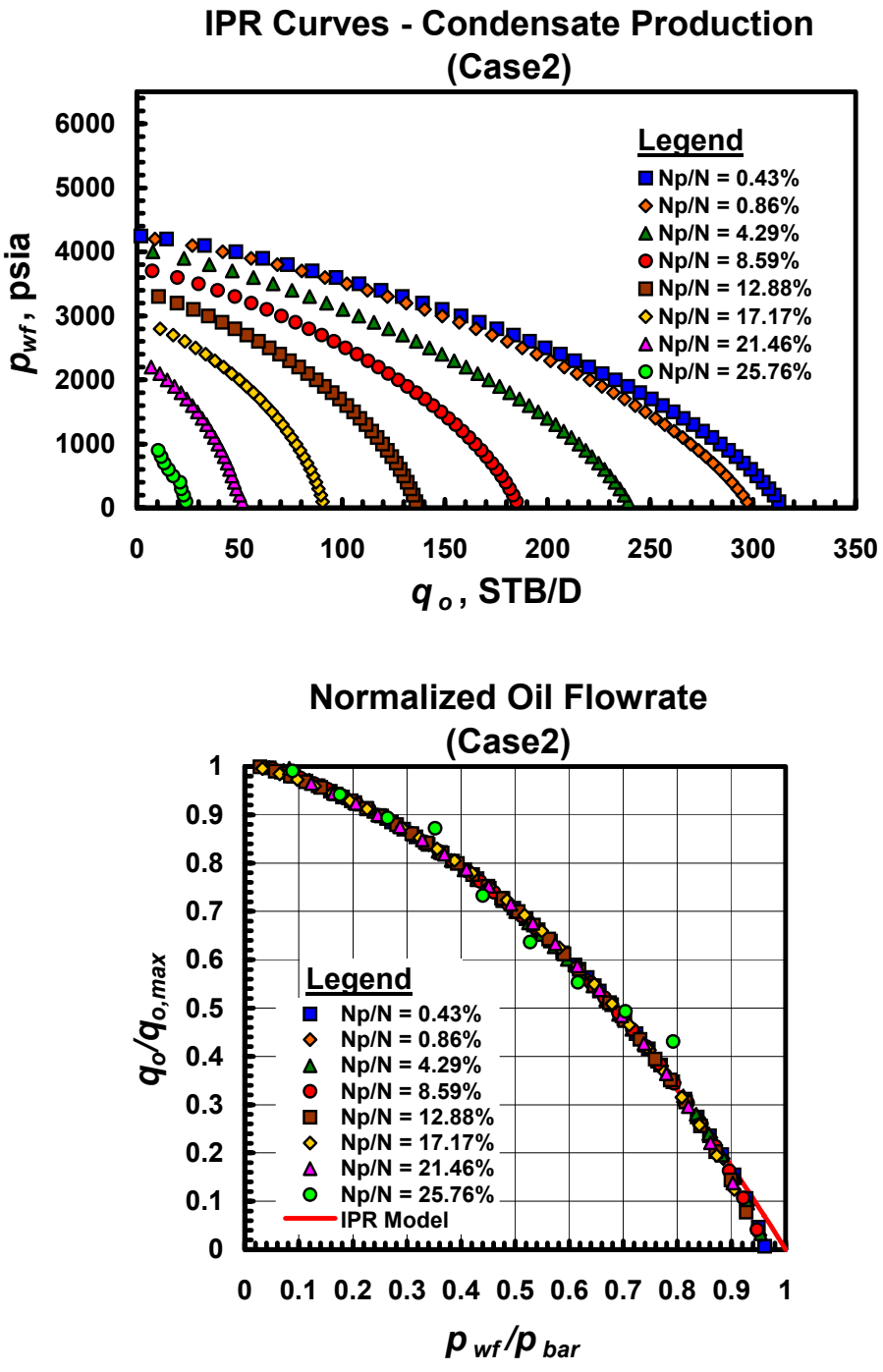

Fig. A.2.a — Dimensional and dimensionless IPR trends for Case 2 — gas condensate performance trends.

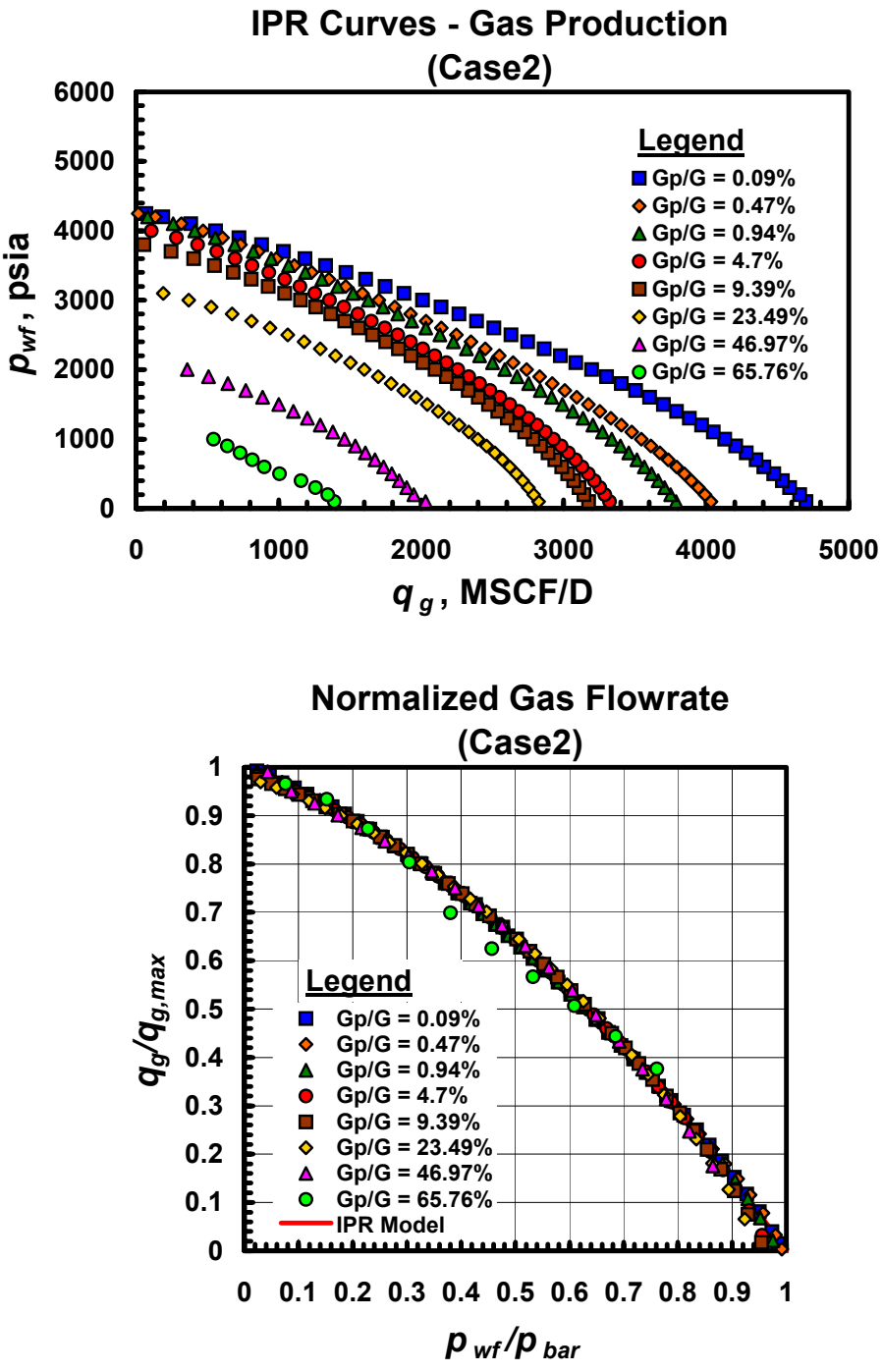

Fig. A.2.b — Dimensional and dimensionless IPR trends for Case 2 — gas performance trends.

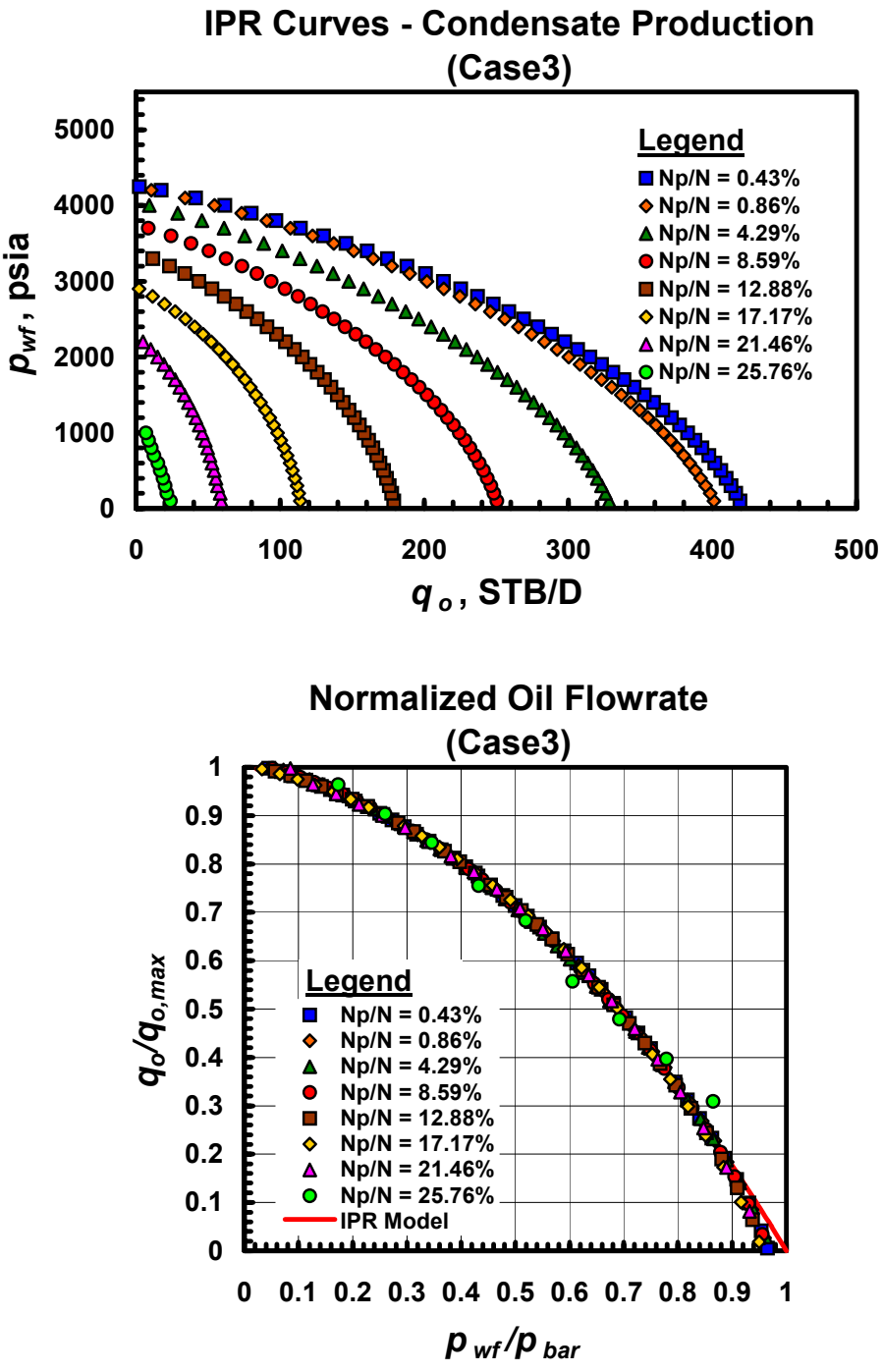

Fig. A.3.a — Dimensional and dimensionless IPR trends for Case 3 — gas condensate performance trends.

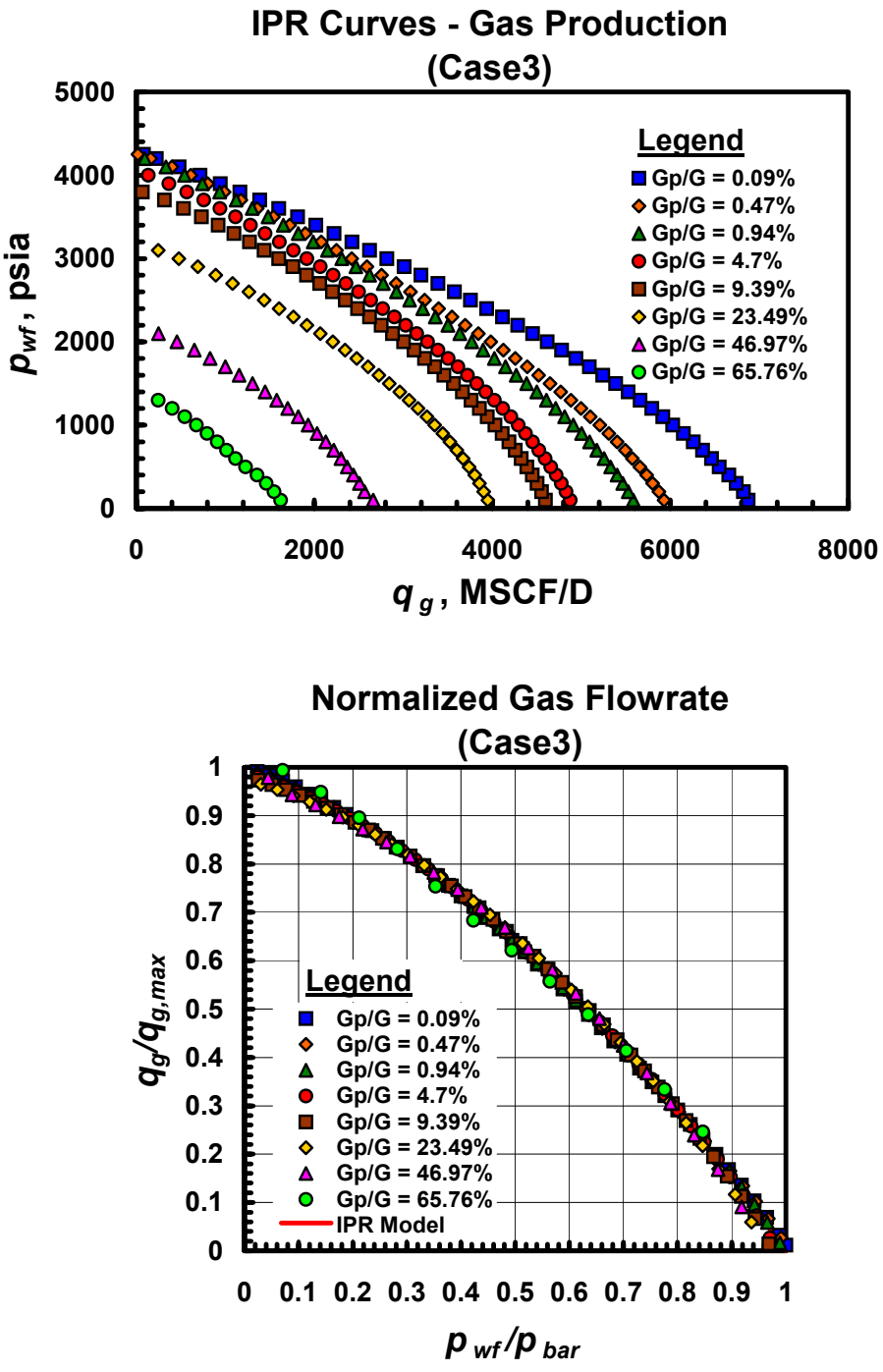

Fig. A.3.b — Dimensional and dimensionless IPR trends for Case 3 — gas performance trends.

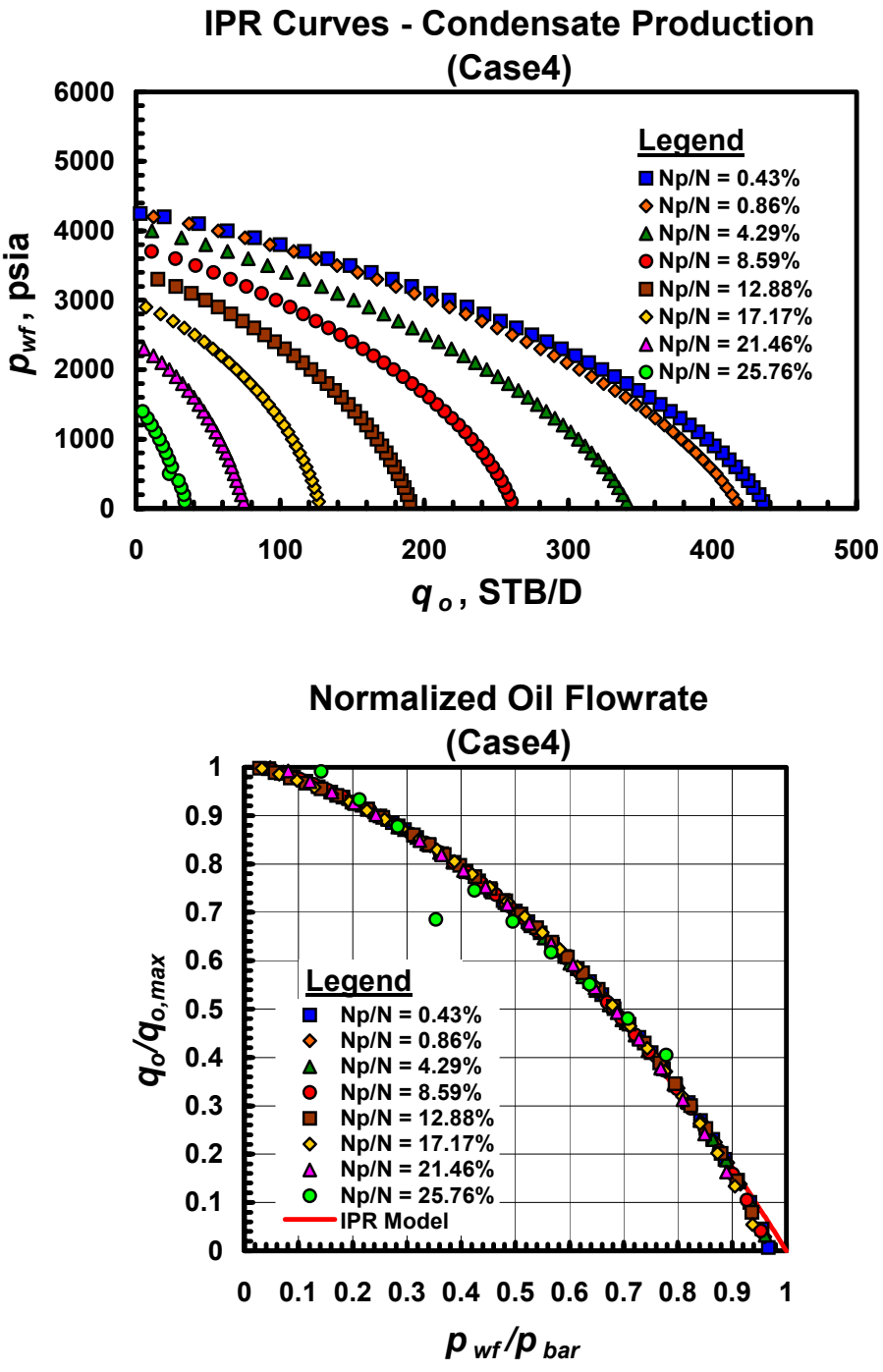

Fig. A.4.a — Dimensional and dimensionless IPR trends for Case 4 — gas condensate performance trends.

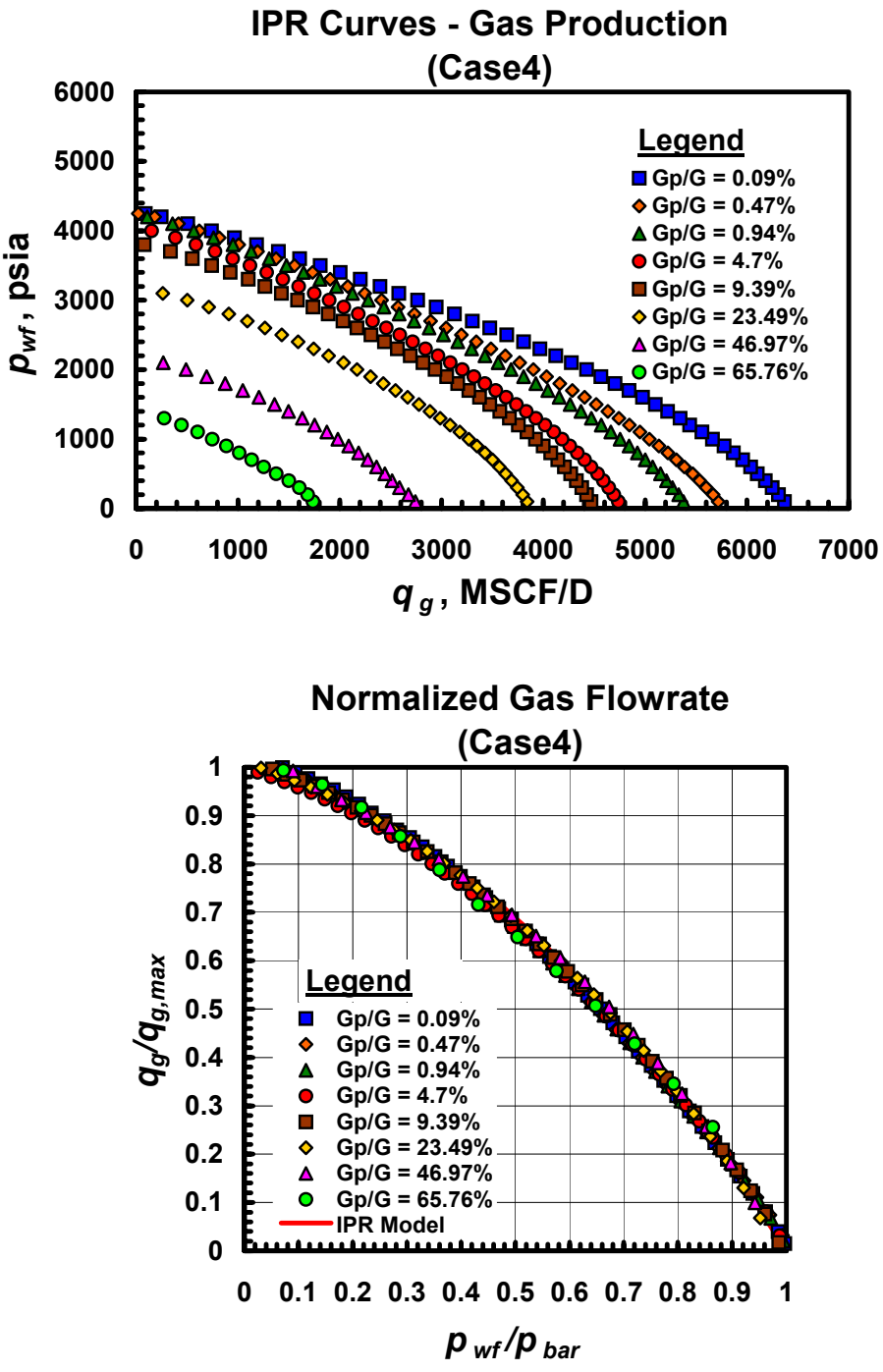

Fig. A.4.b — Dimensional and dimensionless IPR trends for Case 4 — gas performance trends.

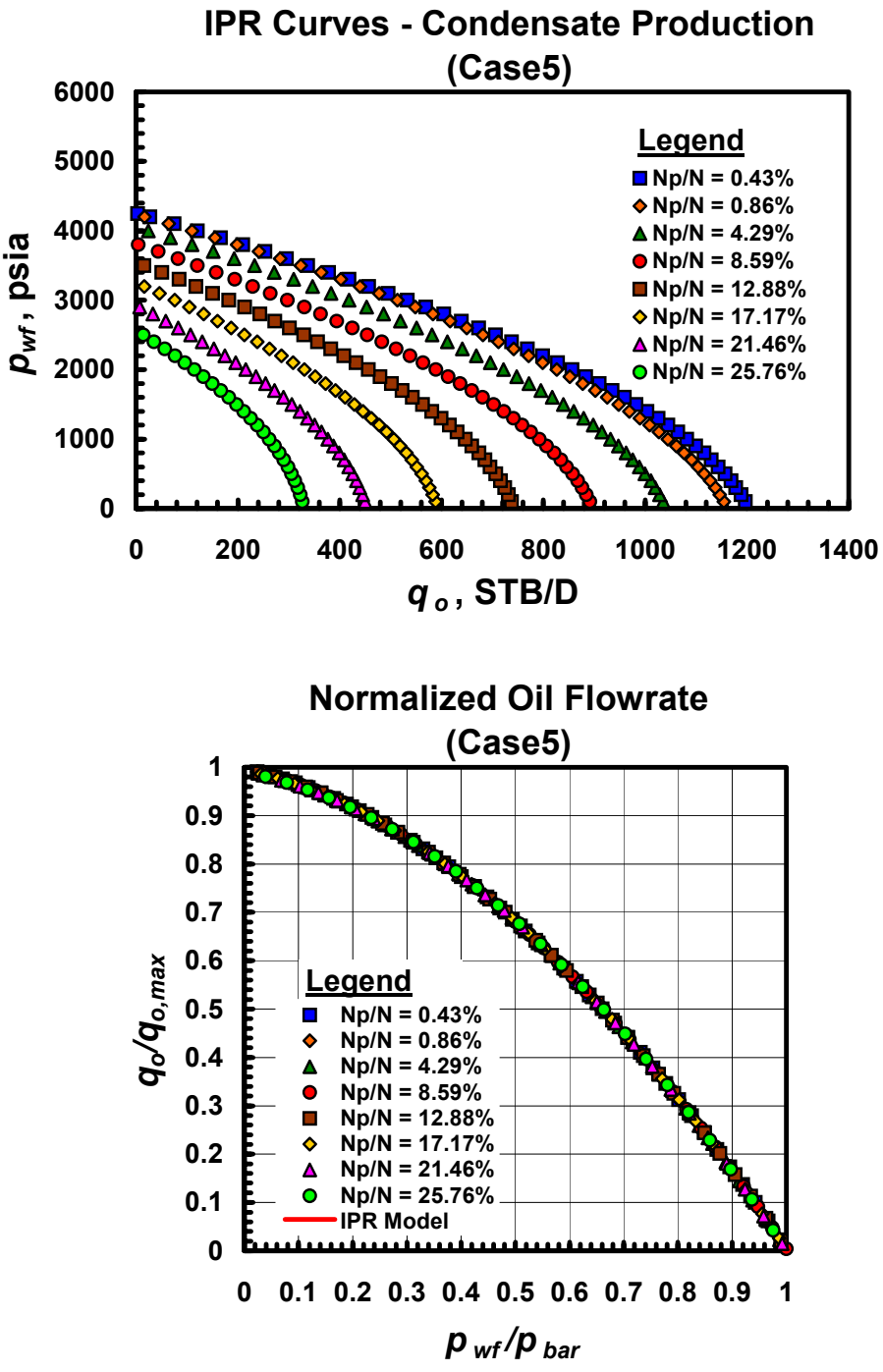

Fig. A.5.a — Dimensional and dimensionless IPR trends for Case 5 — gas condensate performance trends.

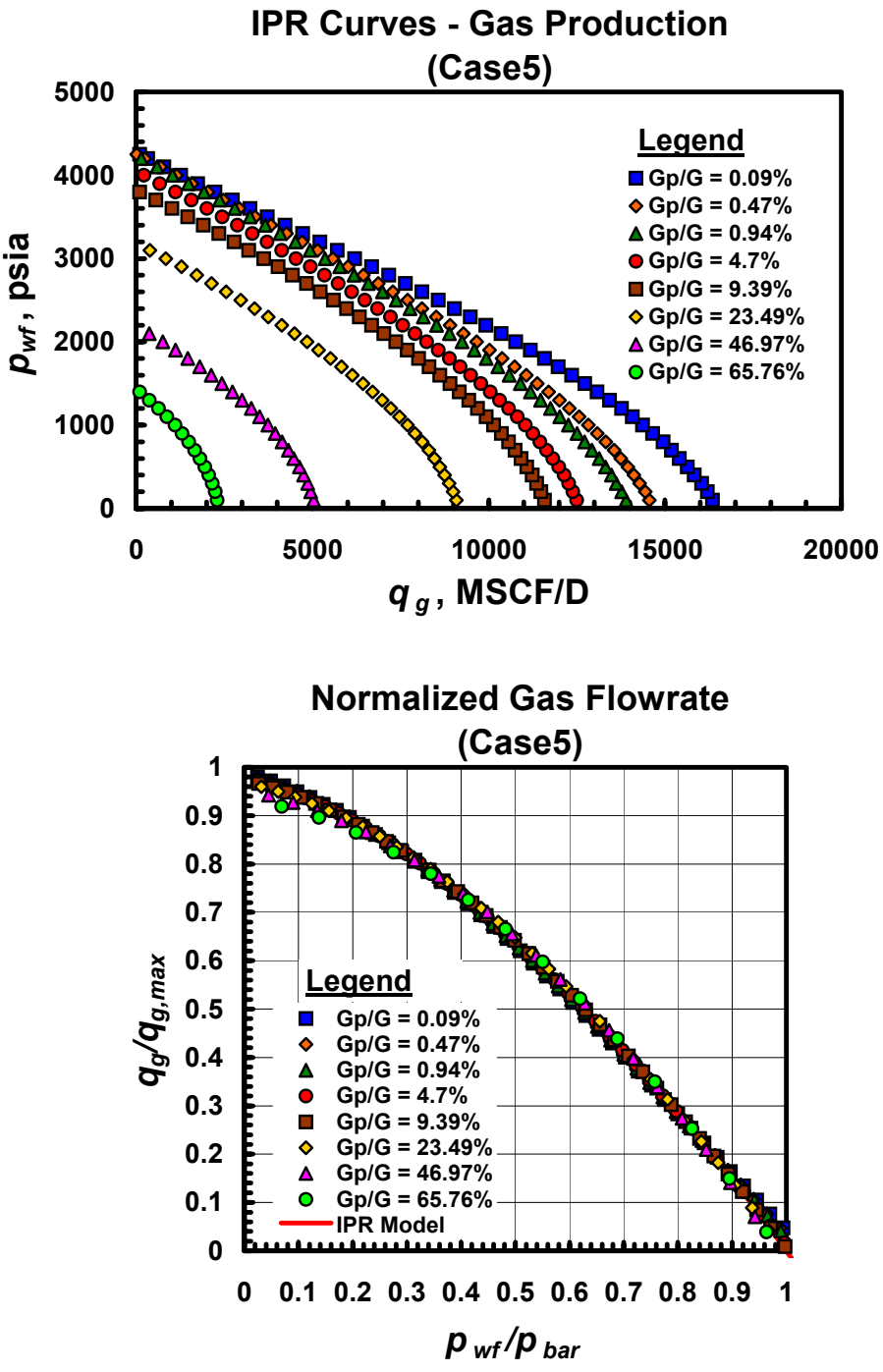

Fig. A.5.b — Dimensional and dimensionless IPR trends for Case 5 — gas performance trends.

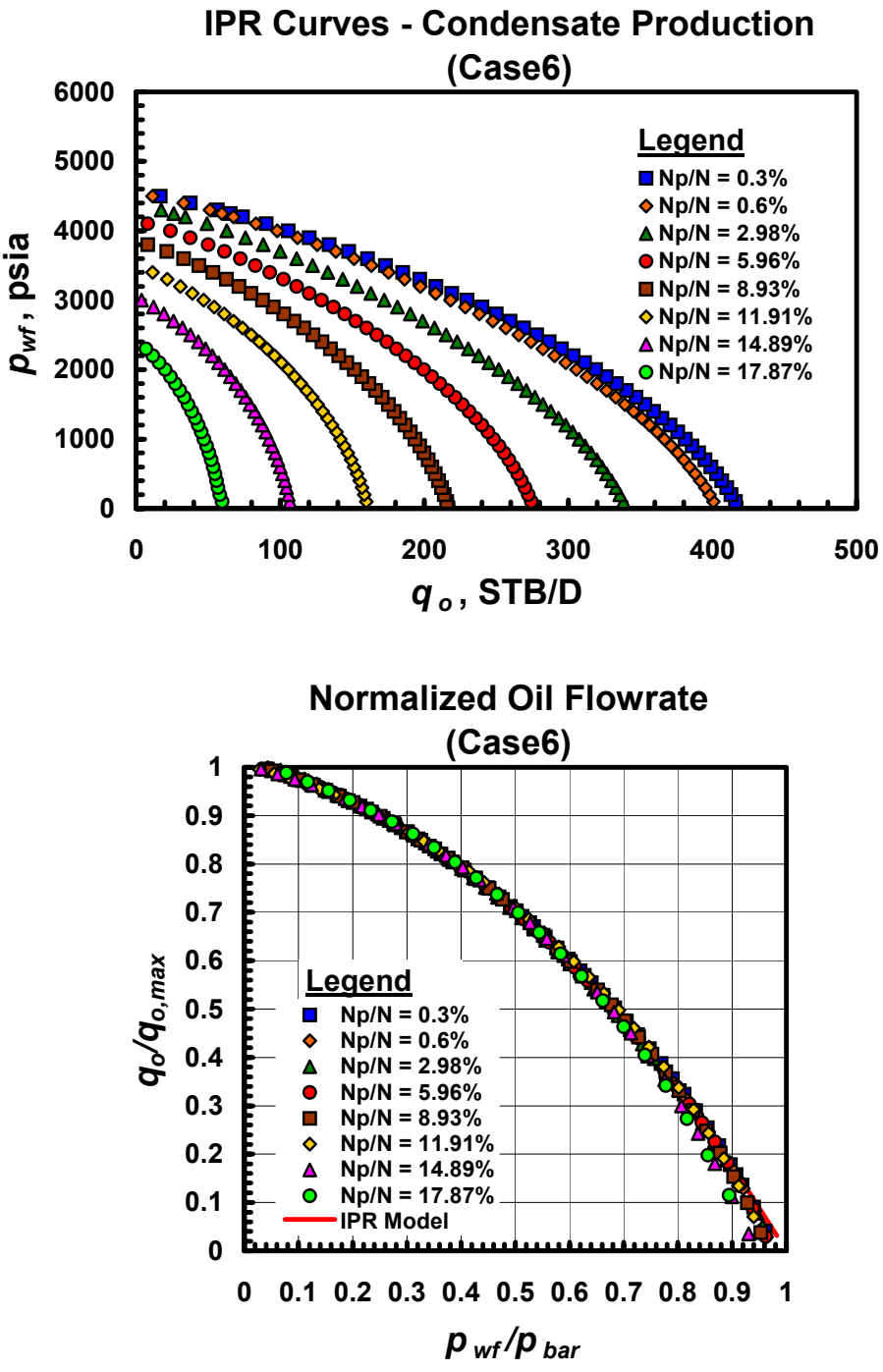

Fig. A.6.a — Dimensional and dimensionless IPR trends for Case 6 — gas condensate performance trends.

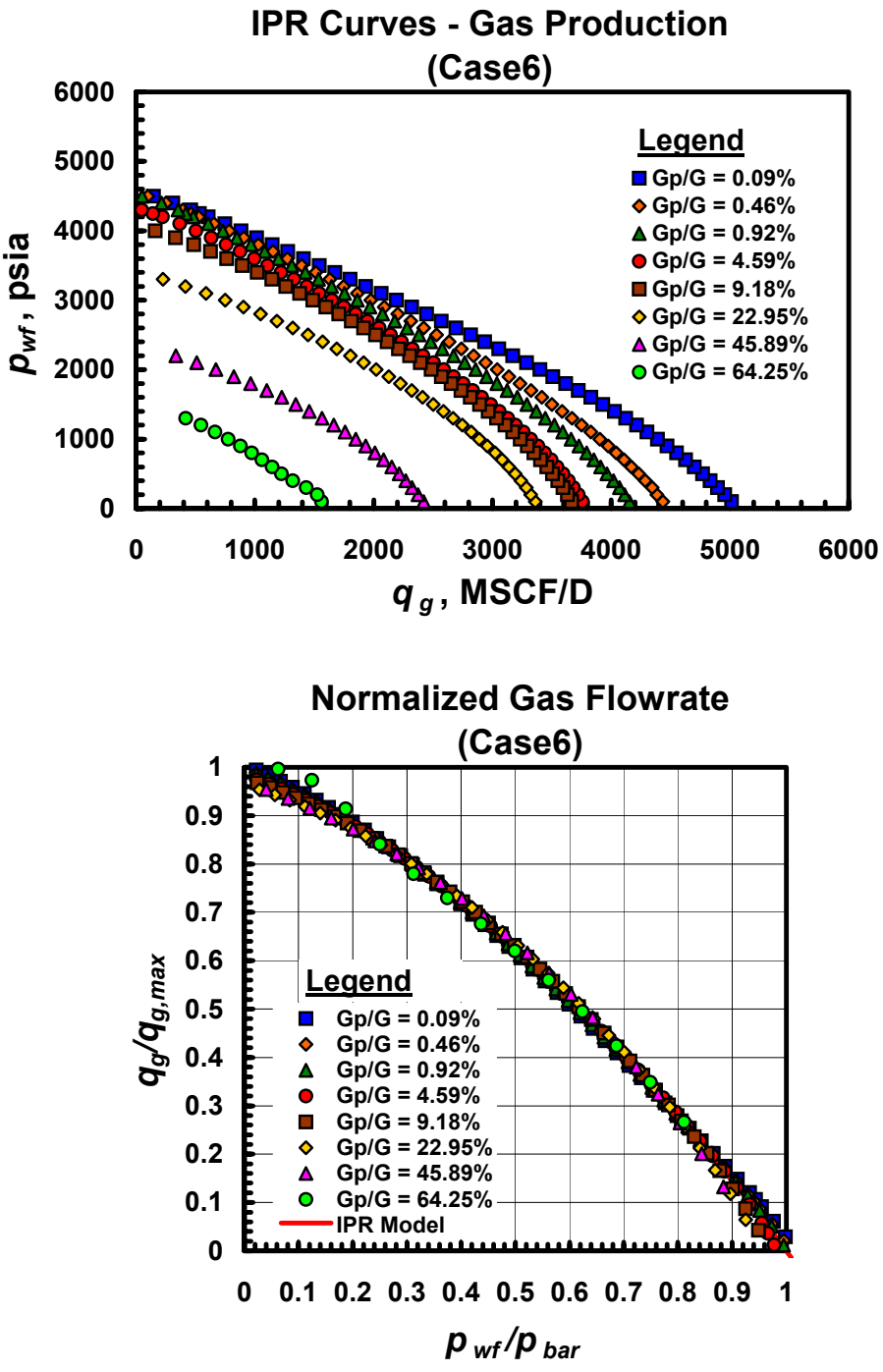

Fig. A.6.b — Dimensional and dimensionless IPR trends for Case 6 — gas performance trends.

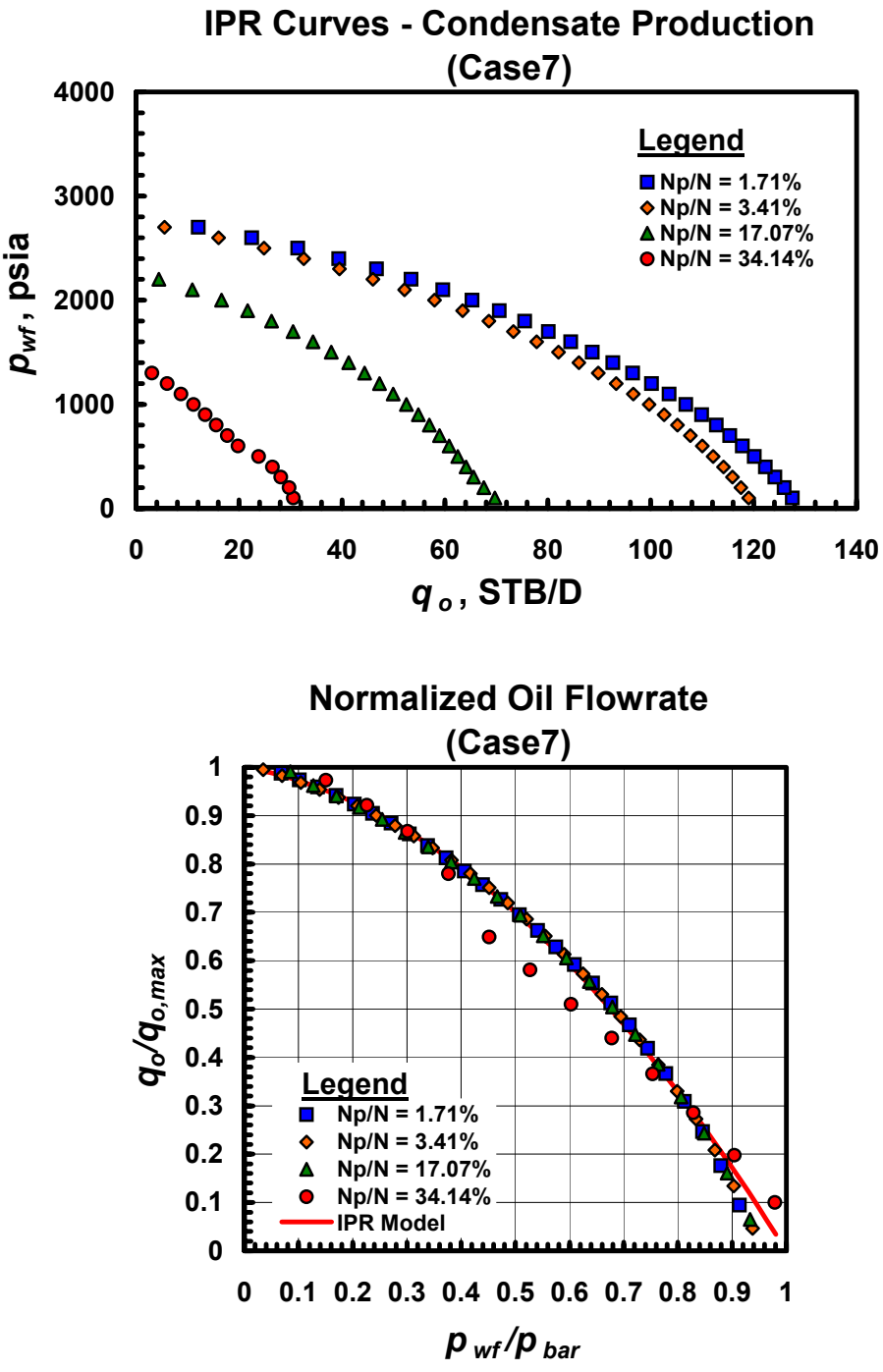

Fig. A.7.a — Dimensional and dimensionless IPR trends for Case 7 — gas condensate performance trends.

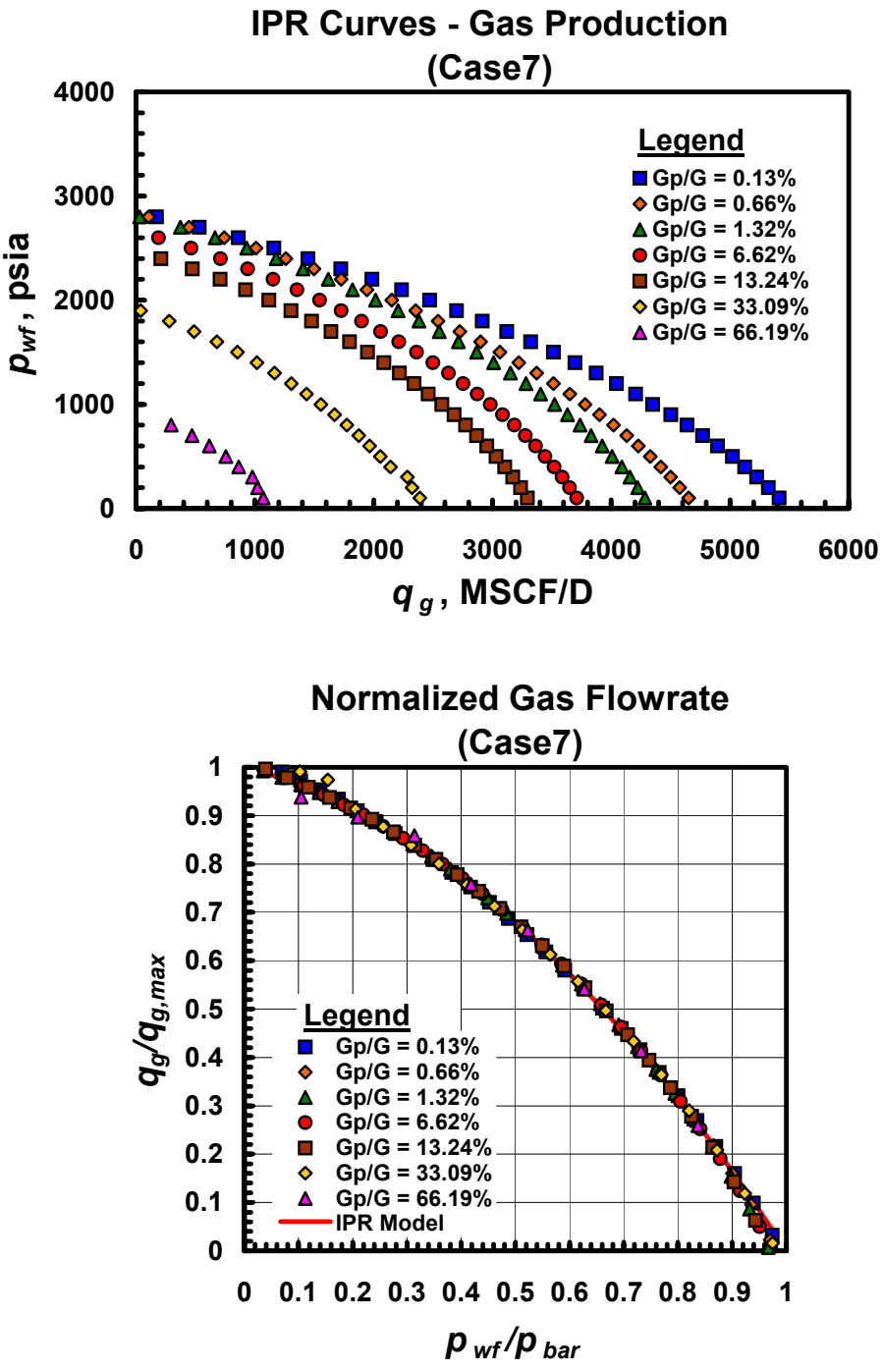

Fig. A.7.b — Dimensional and dimensionless IPR trends for Case 7 — gas performance trends.

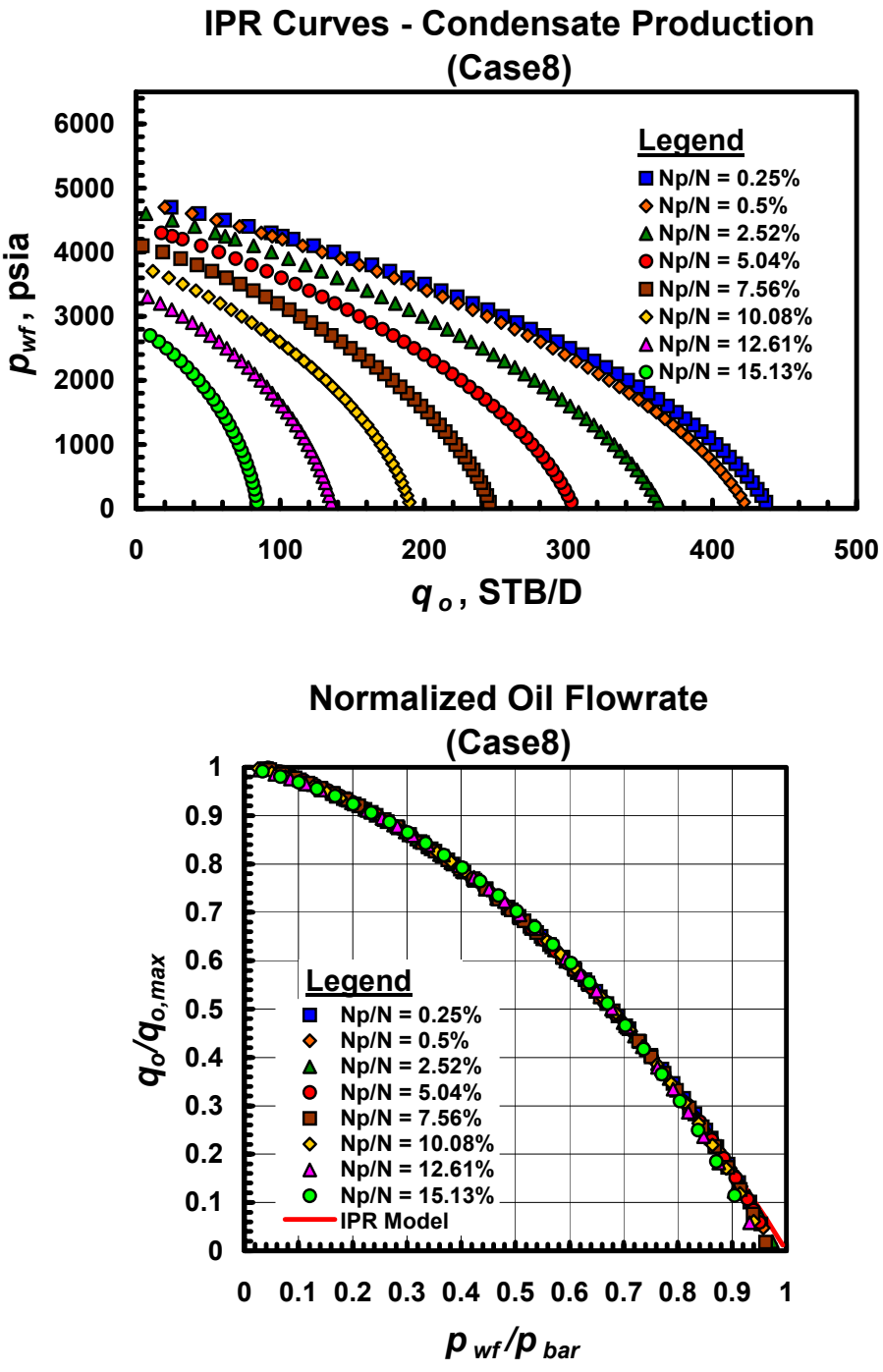

Fig. A.8.a — Dimensional and dimensionless IPR trends for Case 8 — gas condensate performance trends.

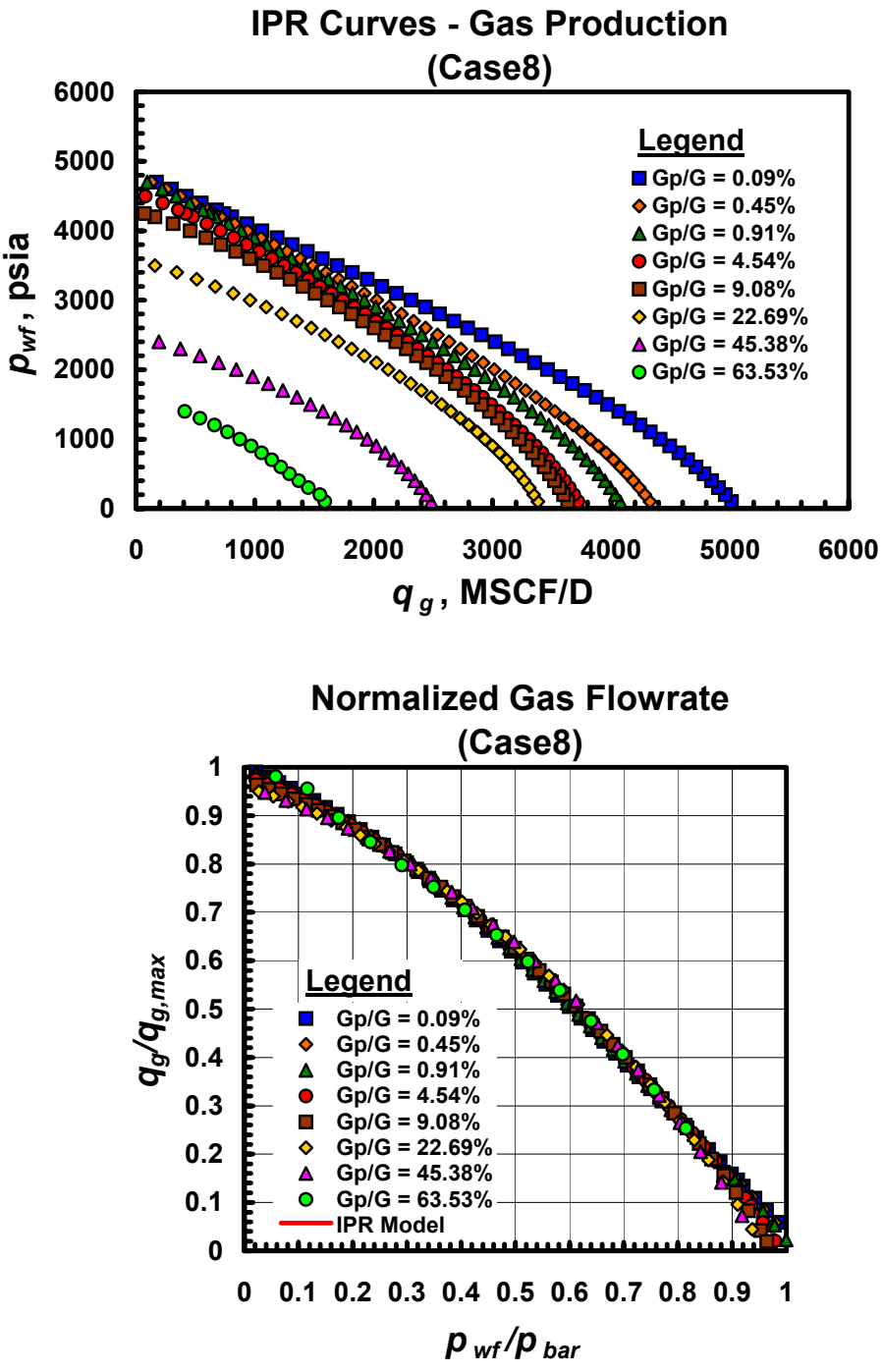

Fig. A.8.b — Dimensional and dimensionless IPR trends for Case 8 — gas performance trends.

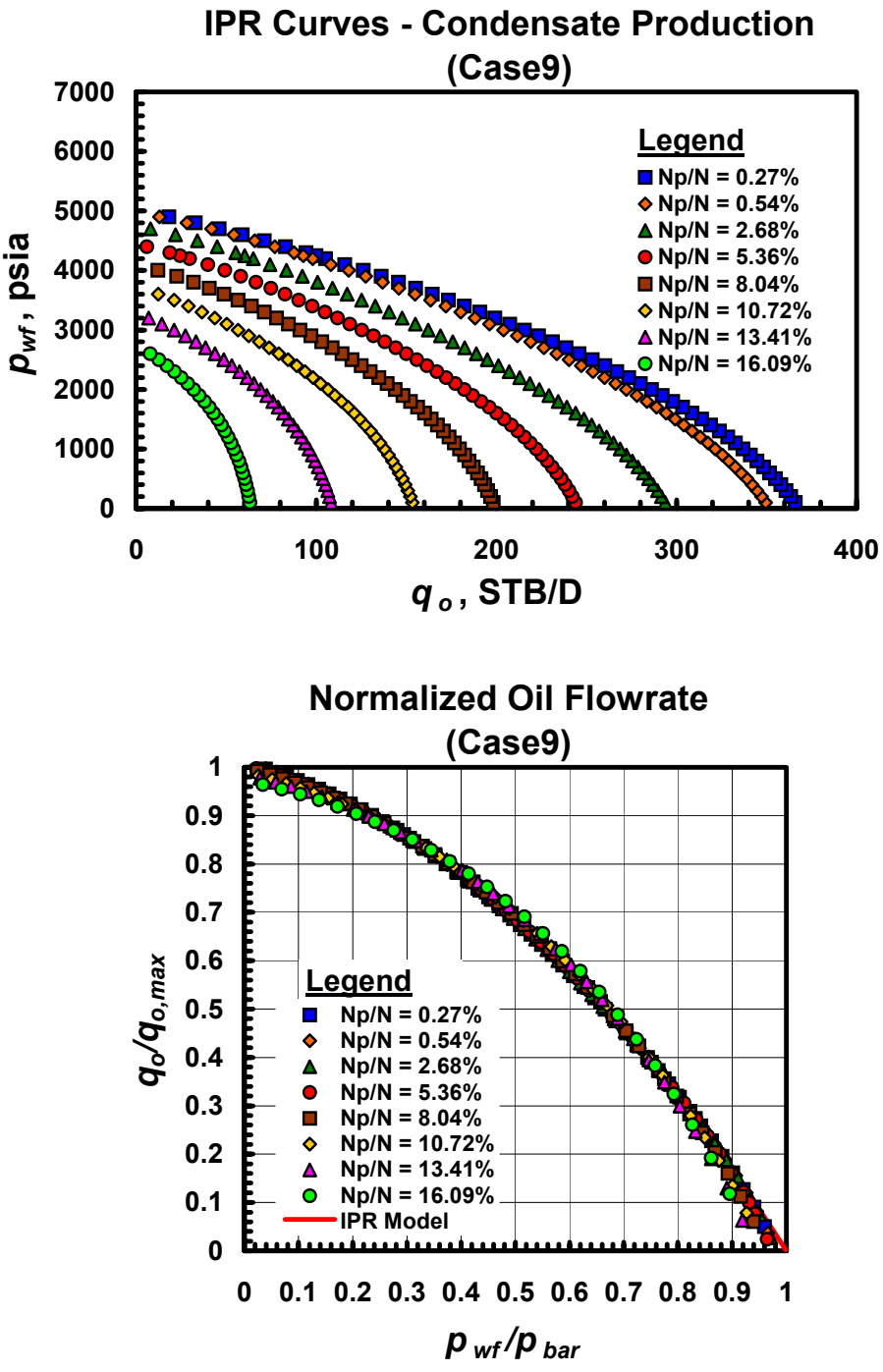

Fig. A.9.a — Dimensional and dimensionless IPR trends for Case 9 — gas condensate performance trends.

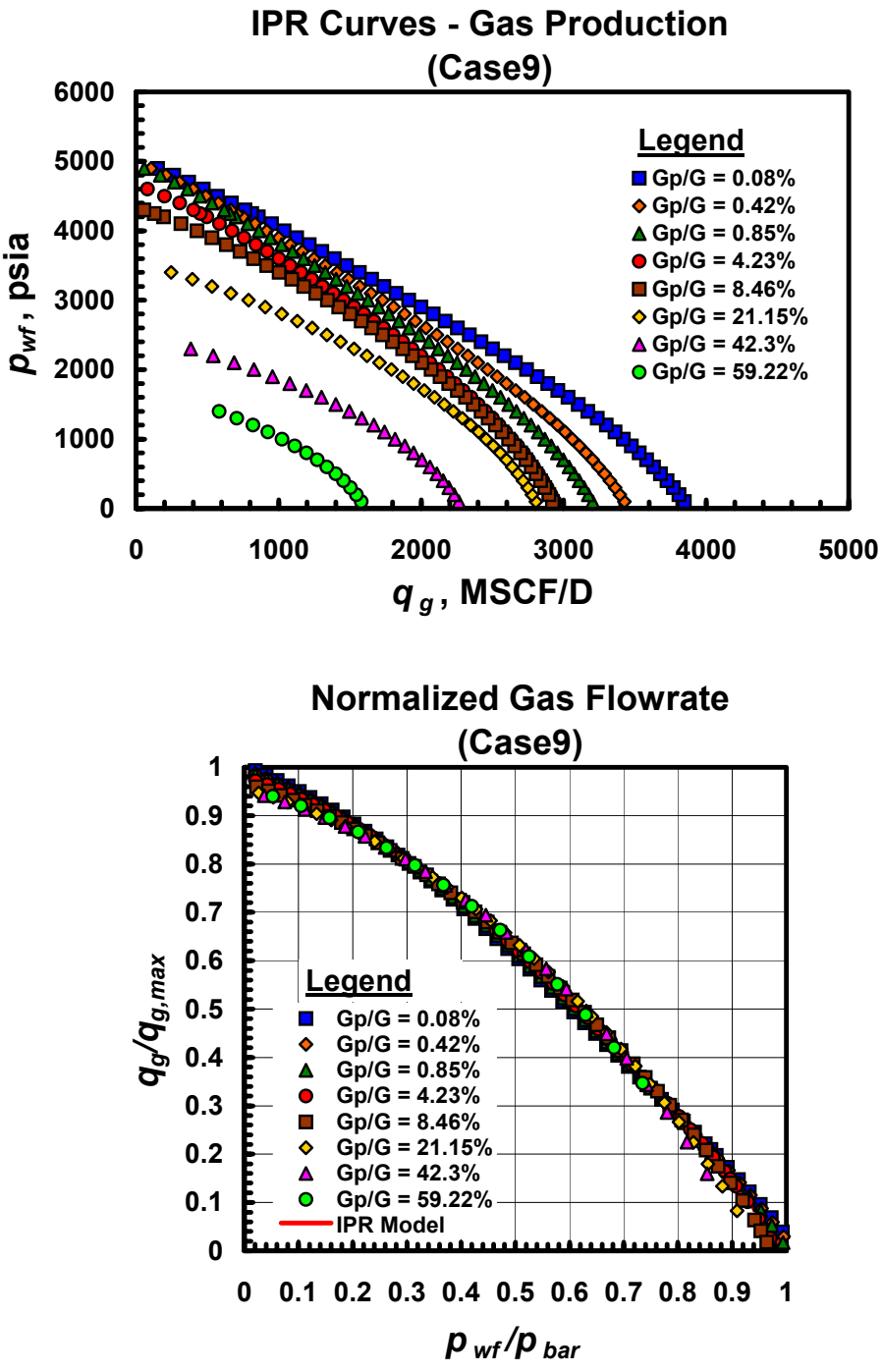

Fig. A.9.b — Dimensional and dimensionless IPR trends for Case 9 — gas performance trends.

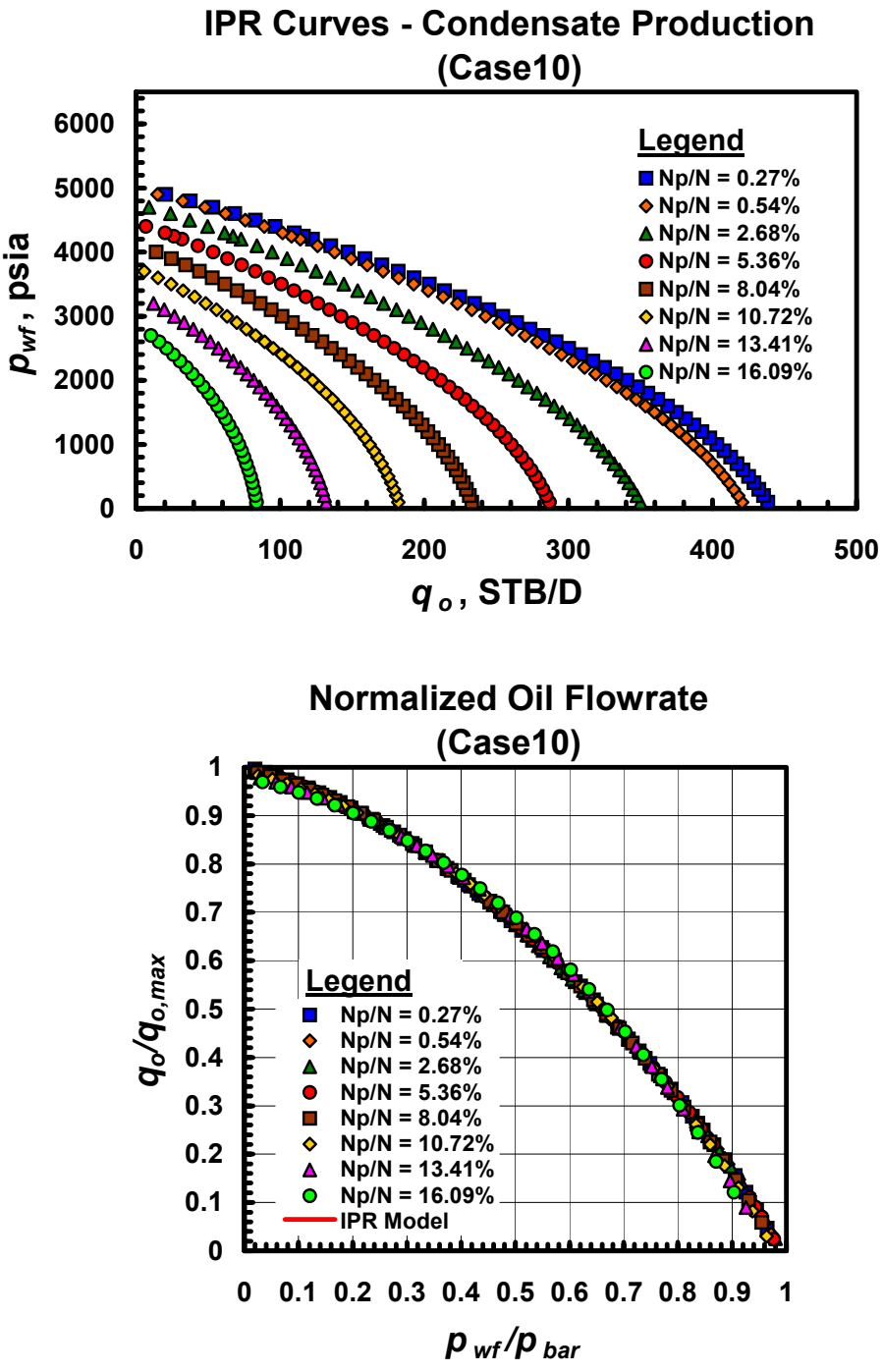

Fig. A.10.a — Dimensional and dimensionless IPR trends for Case 10 — gas condensate performance trends.

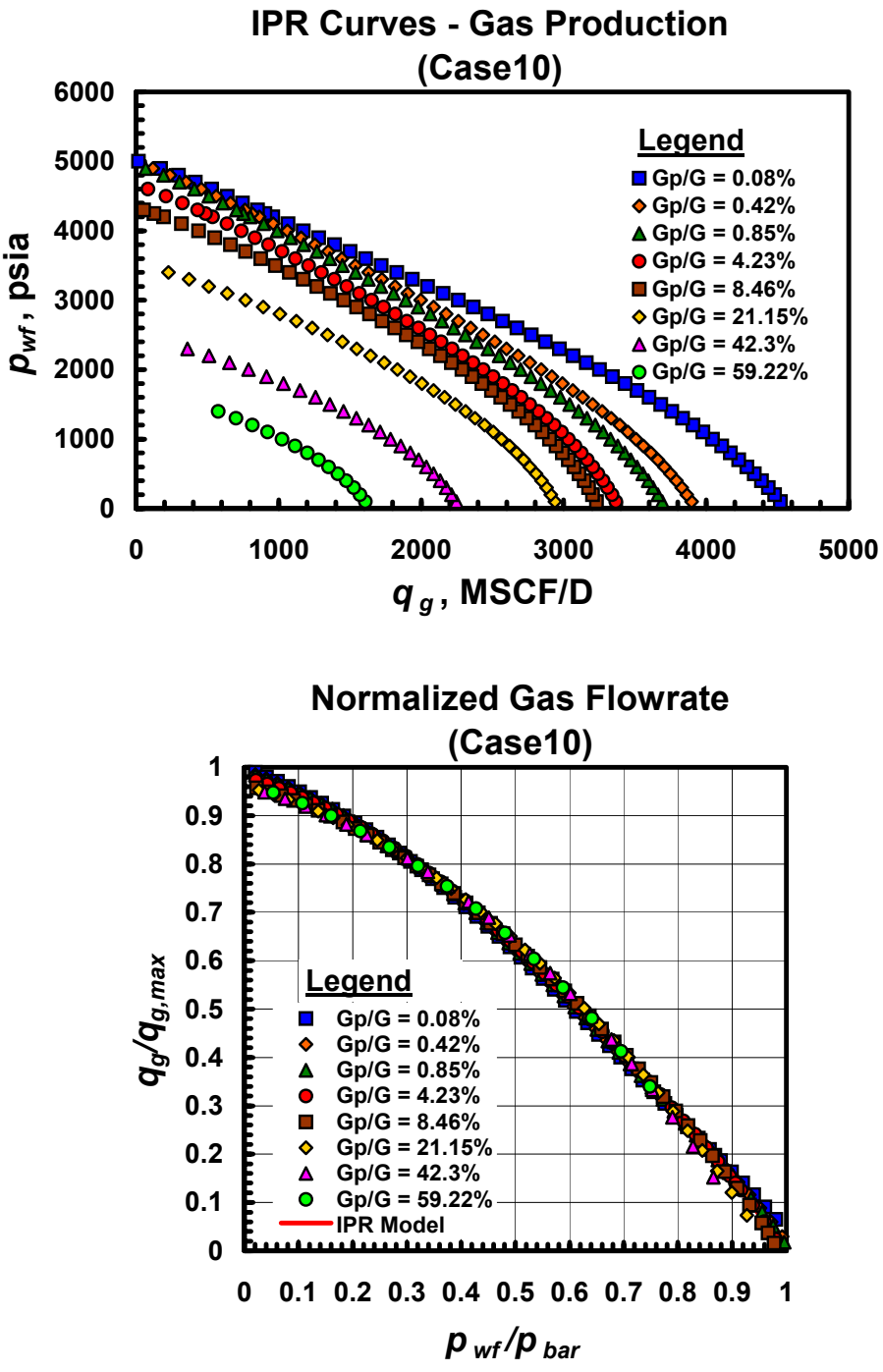

Fig. A.10.b — Dimensional and dimensionless IPR trends for Case 10 — gas performance trends.

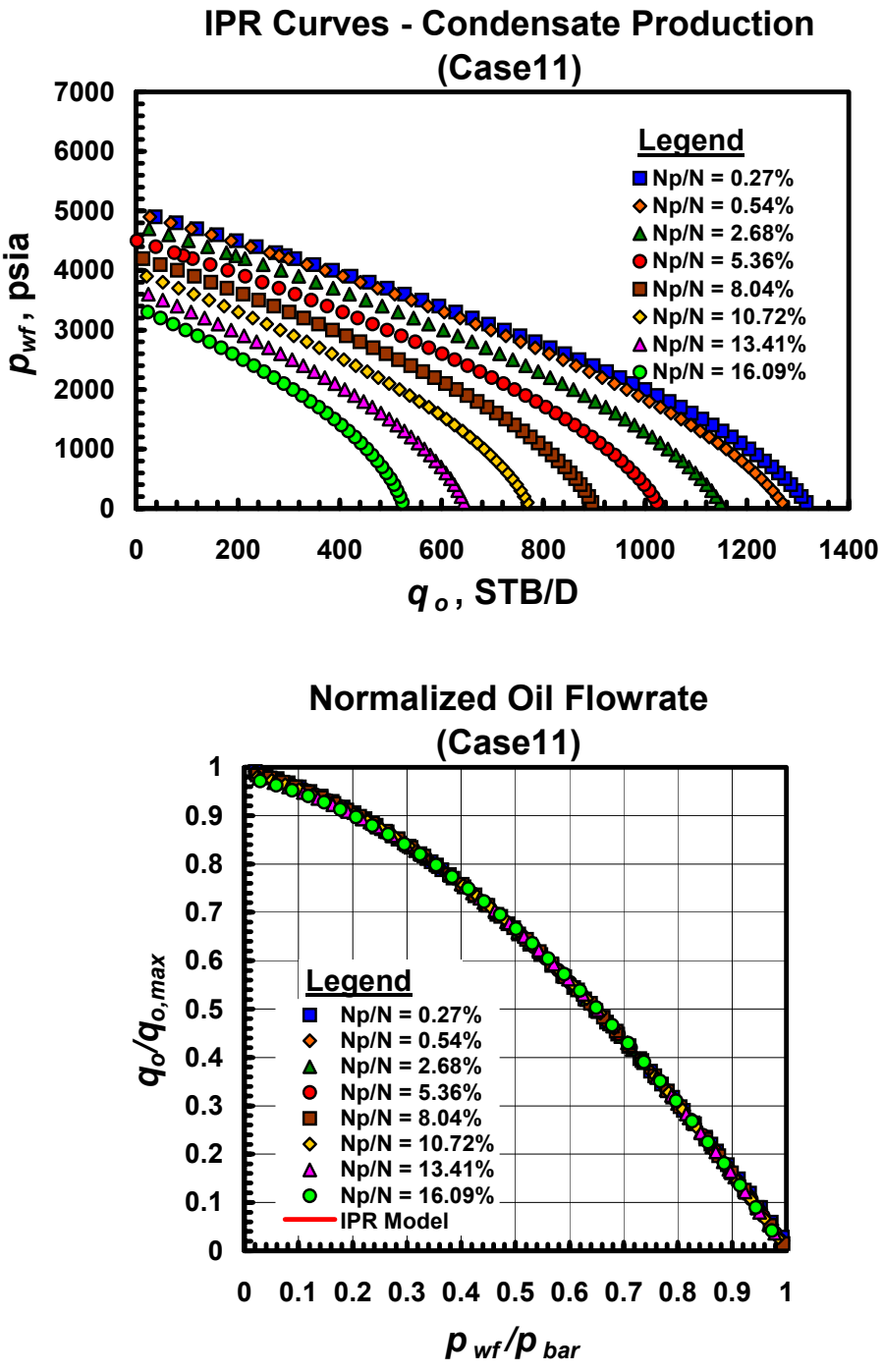

Fig. A.11.a — Dimensional and dimensionless IPR trends for Case 11 — gas condensate performance trends.

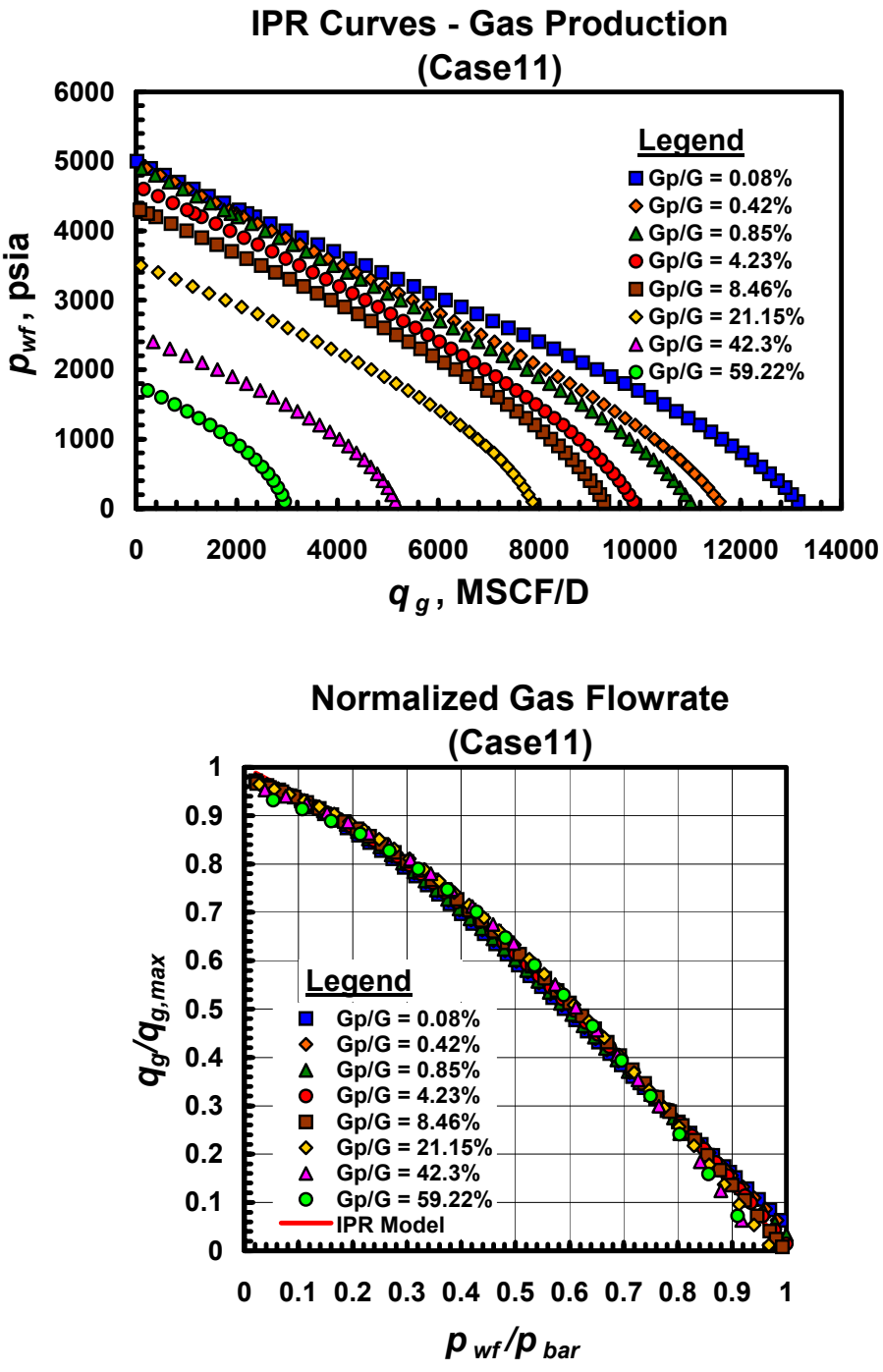

Fig. A.11.b — Dimensional and dimensionless IPR trends for Case 11 — gas performance trends.

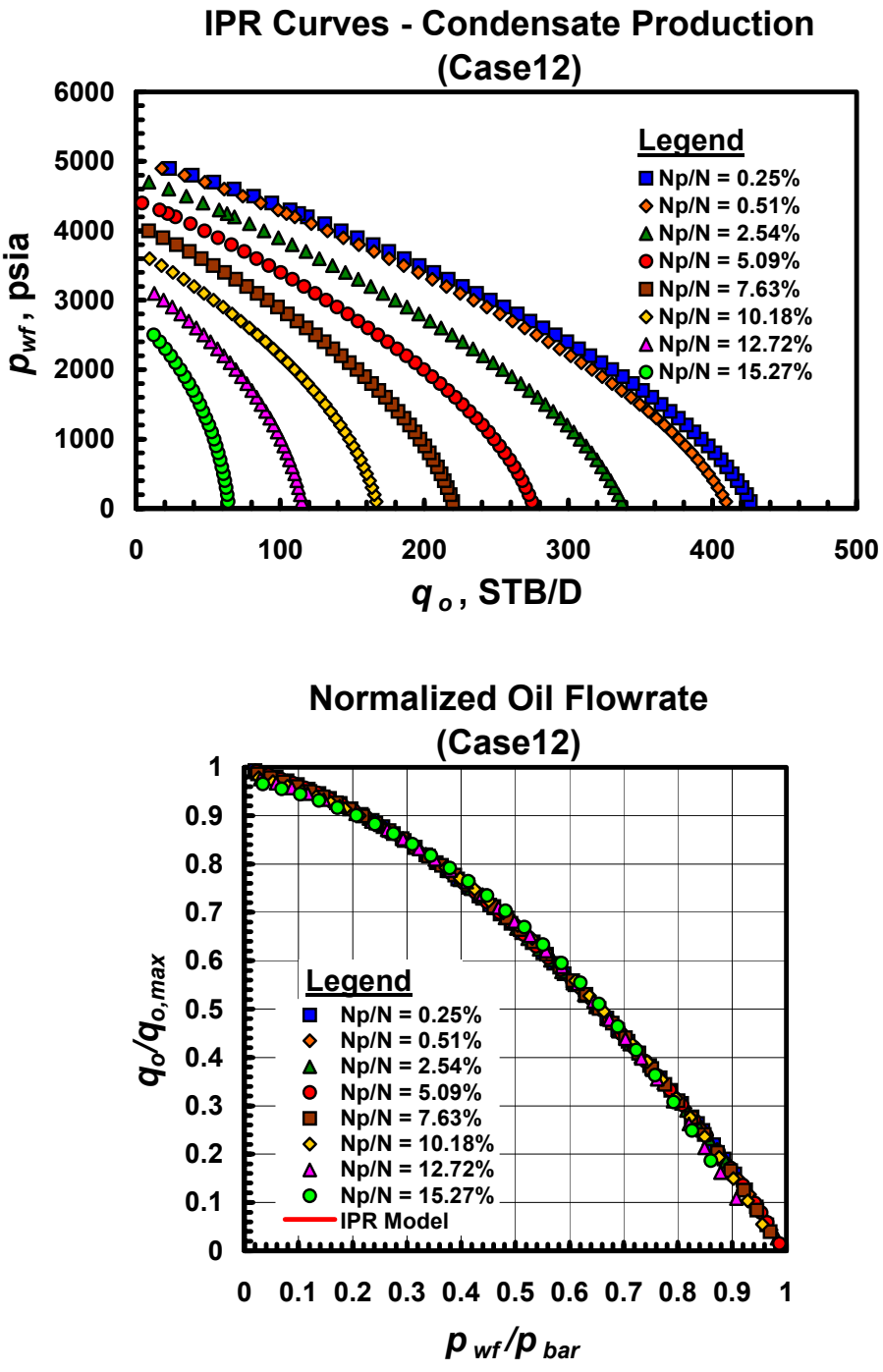

Fig. A.12.a — Dimensional and dimensionless IPR trends for Case 12 — gas condensate performance trends.

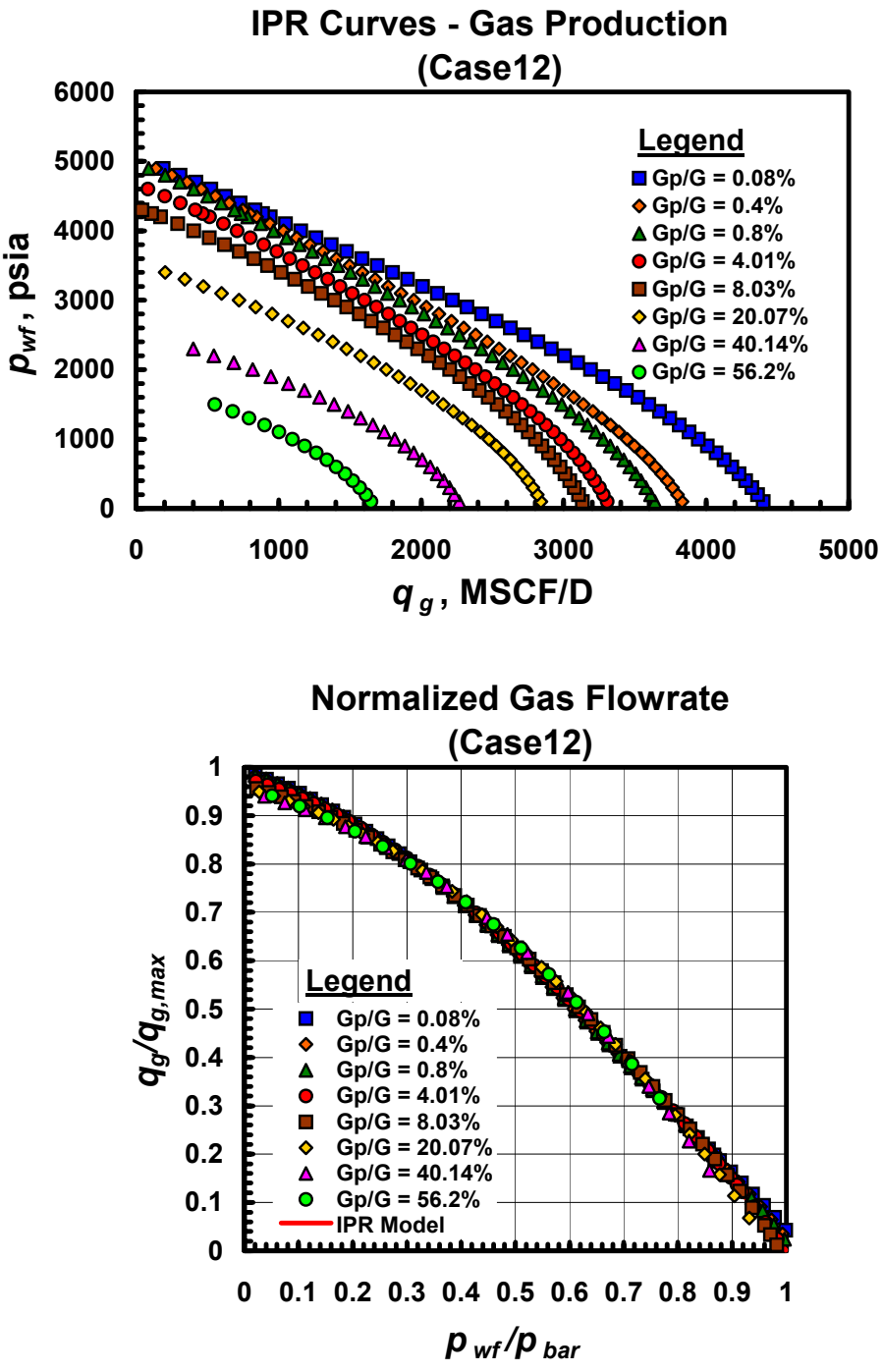

Fig. A.12.b — Dimensional and dimensionless IPR trends for Case 12 — gas performance trends.

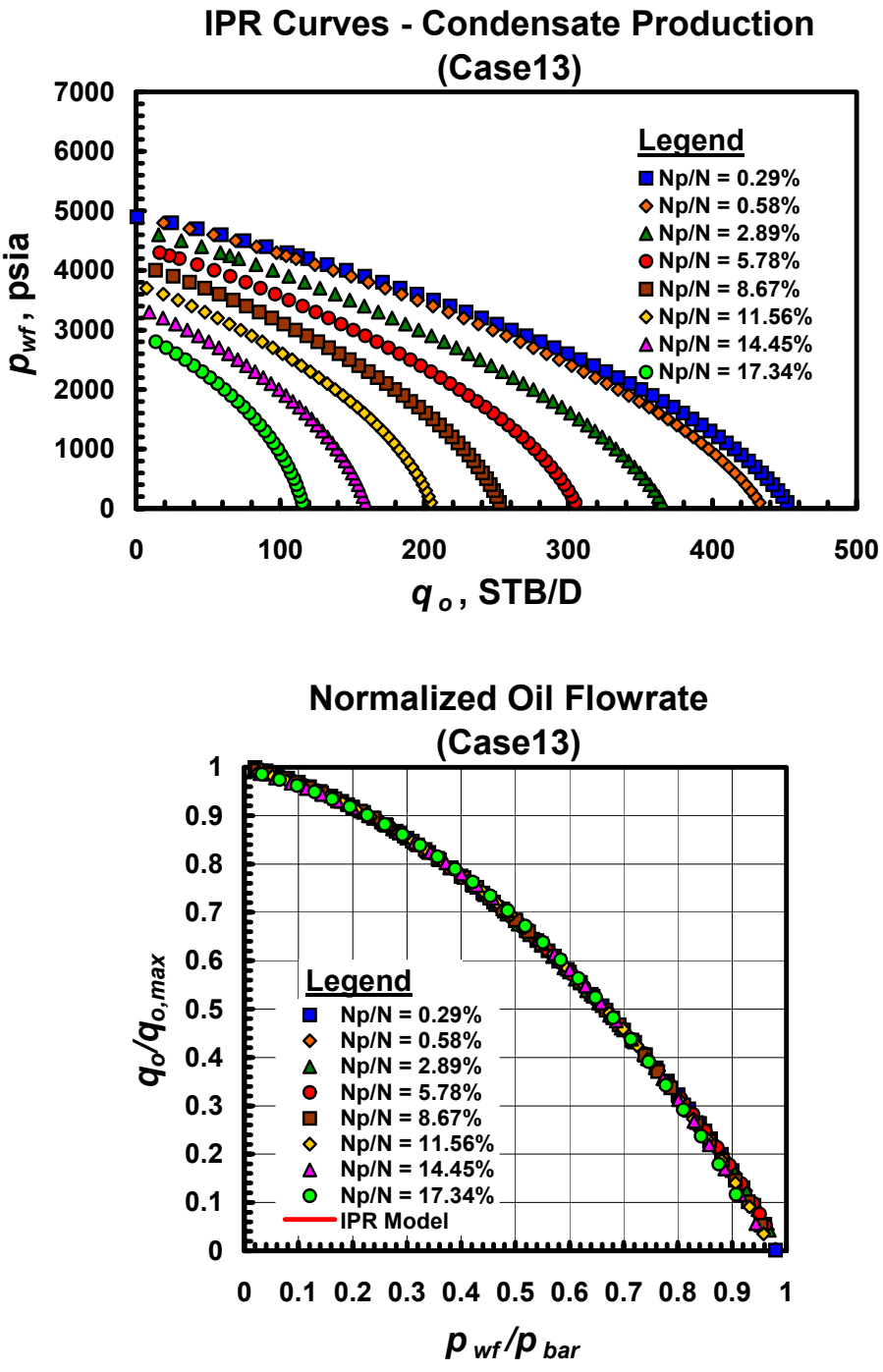

Fig. A.13.a — Dimensional and dimensionless IPR trends for Case 13 — gas condensate performance trends.

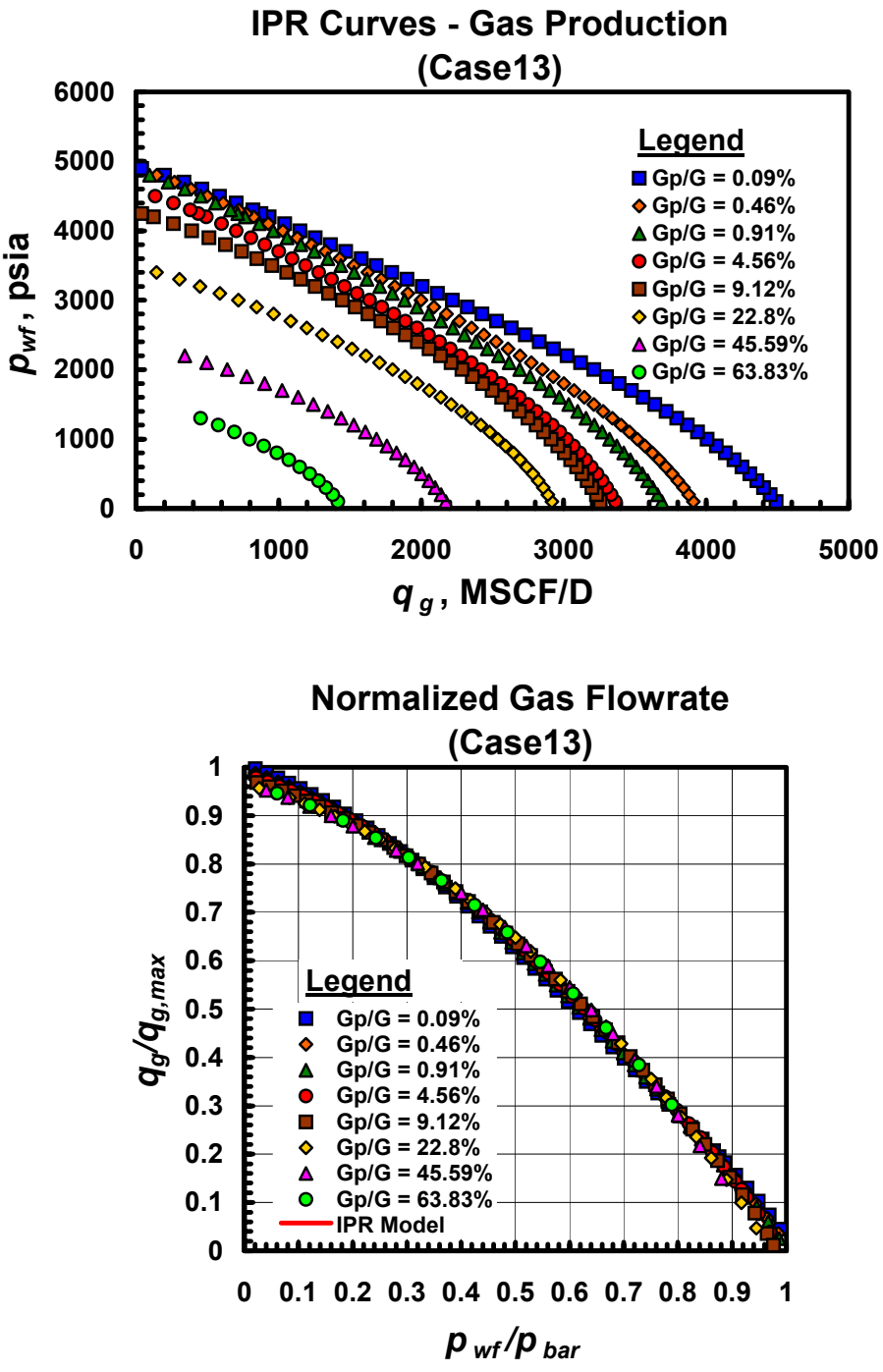

Fig. A.13.b — Dimensional and dimensionless IPR trends for Case 13 — gas performance trends.

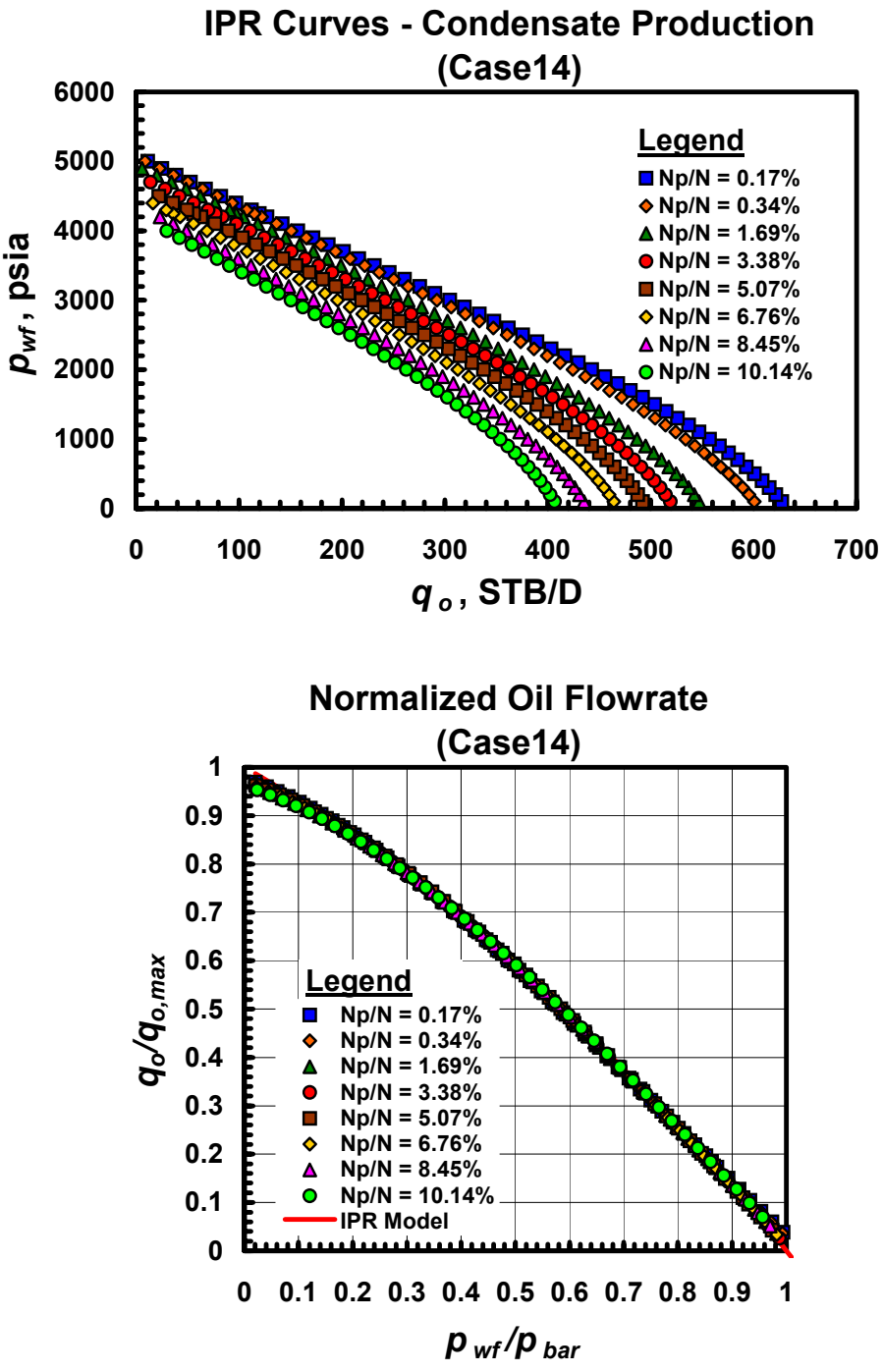

Fig. A.14.a — Dimensional and dimensionless IPR trends for Case 14 — gas condensate performance trends.

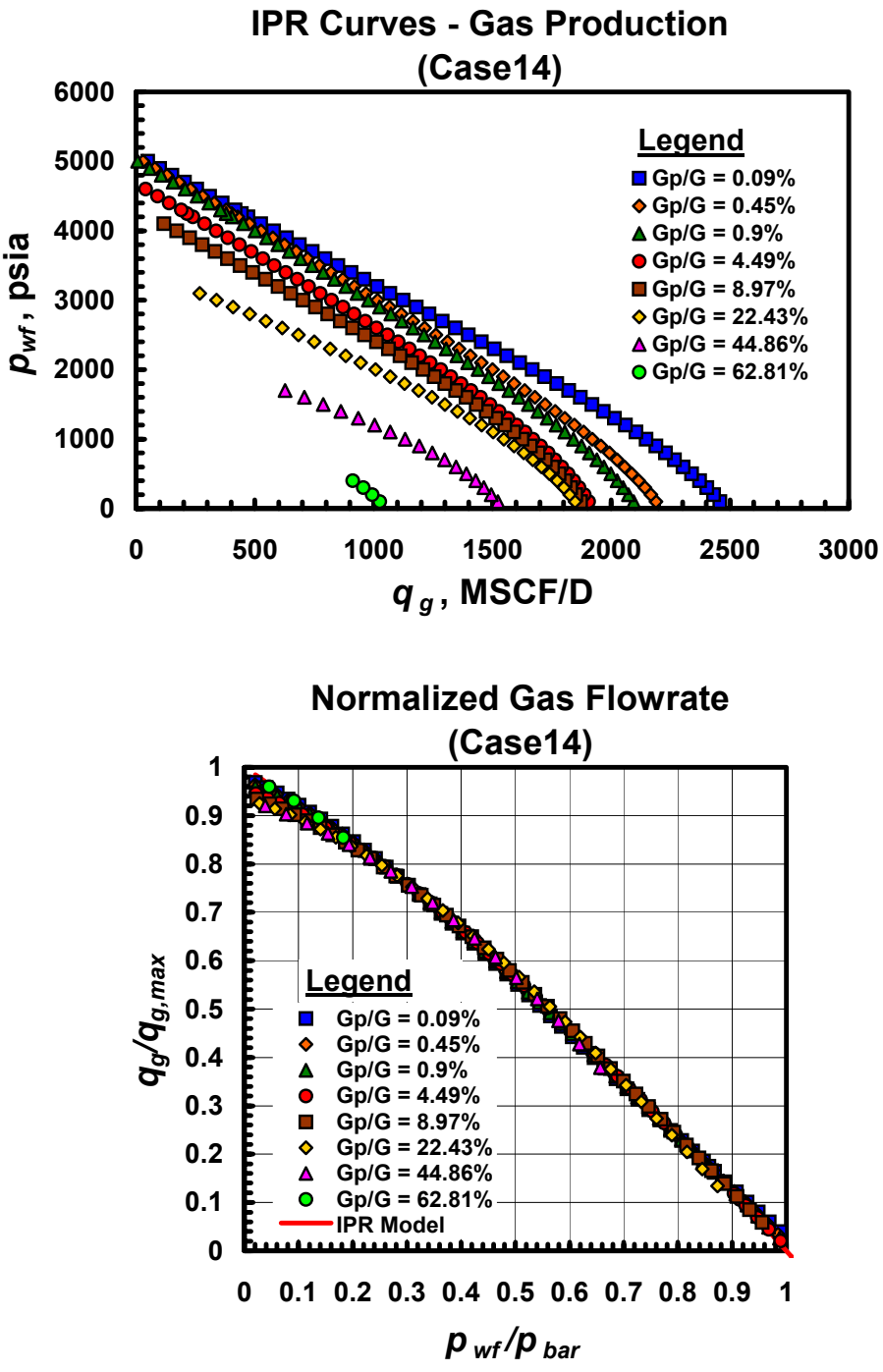

Fig. A.14.b — Dimensional and dimensionless IPR trends for Case 14 — gas performance trends.

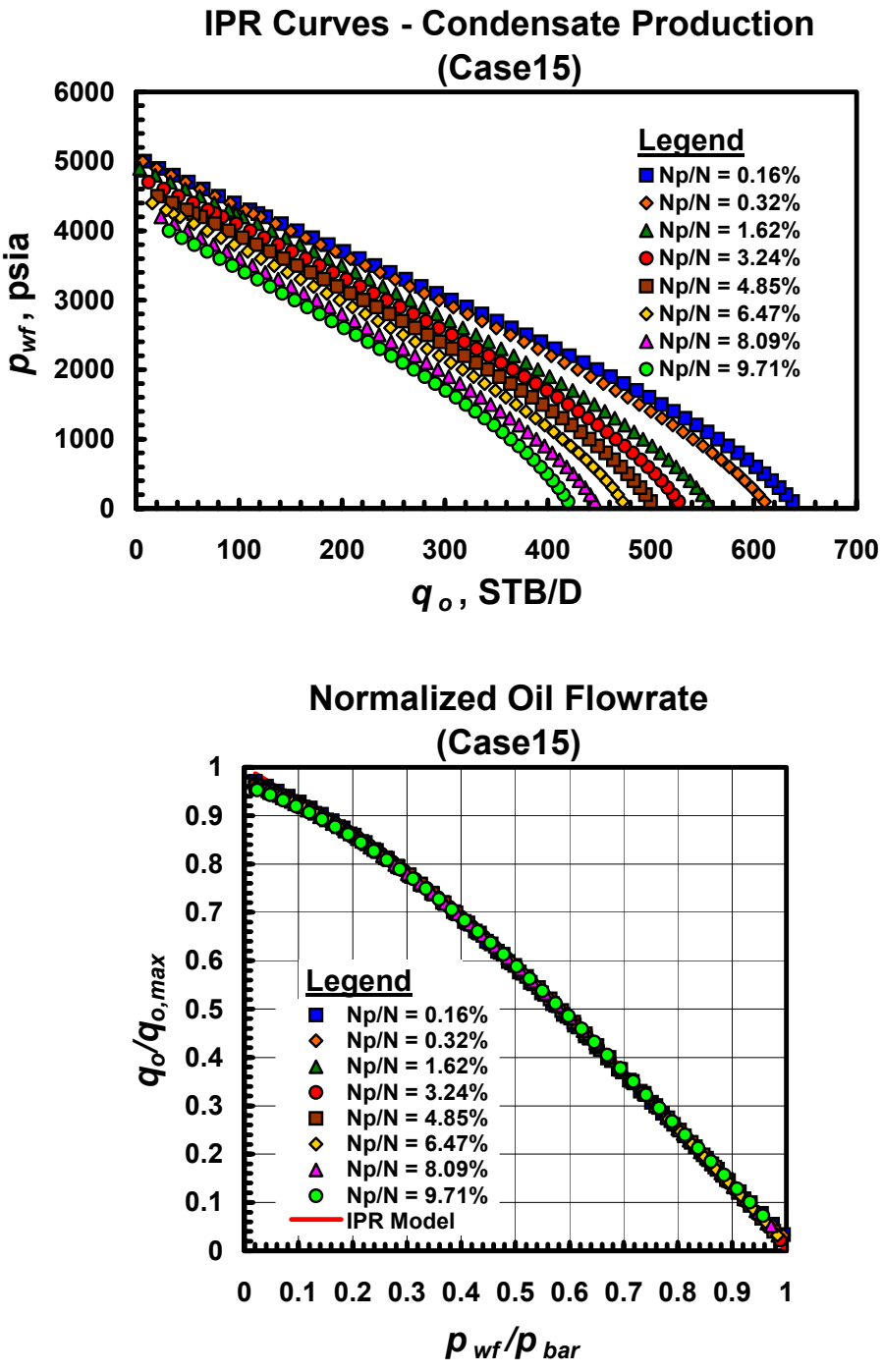

Fig. A.15.a — Dimensional and dimensionless IPR trends for Case 15 — gas condensate performance trends.

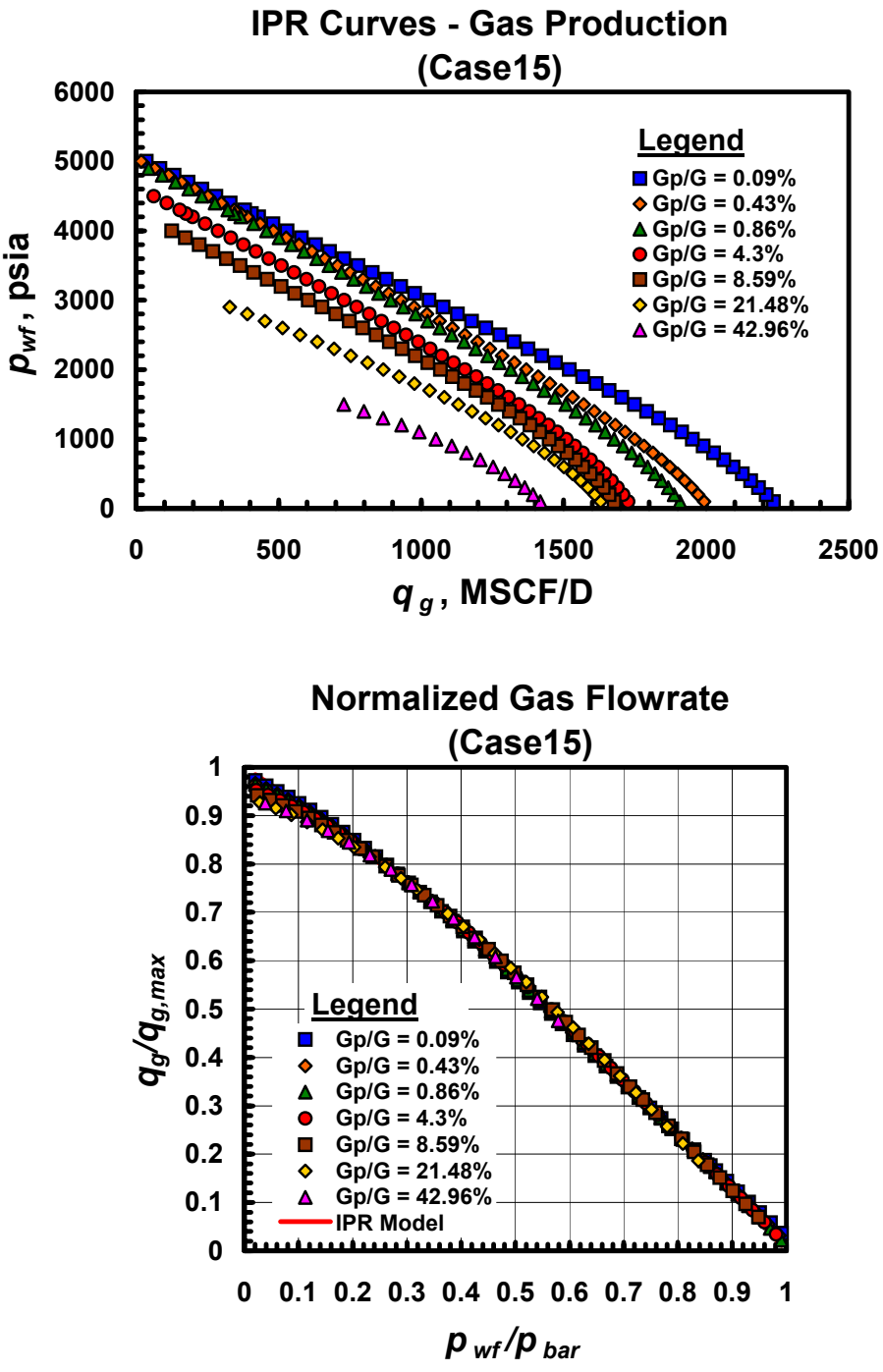

Fig. A.15.b — Dimensional and dimensionless IPR trends for Case 15 — gas performance trends.

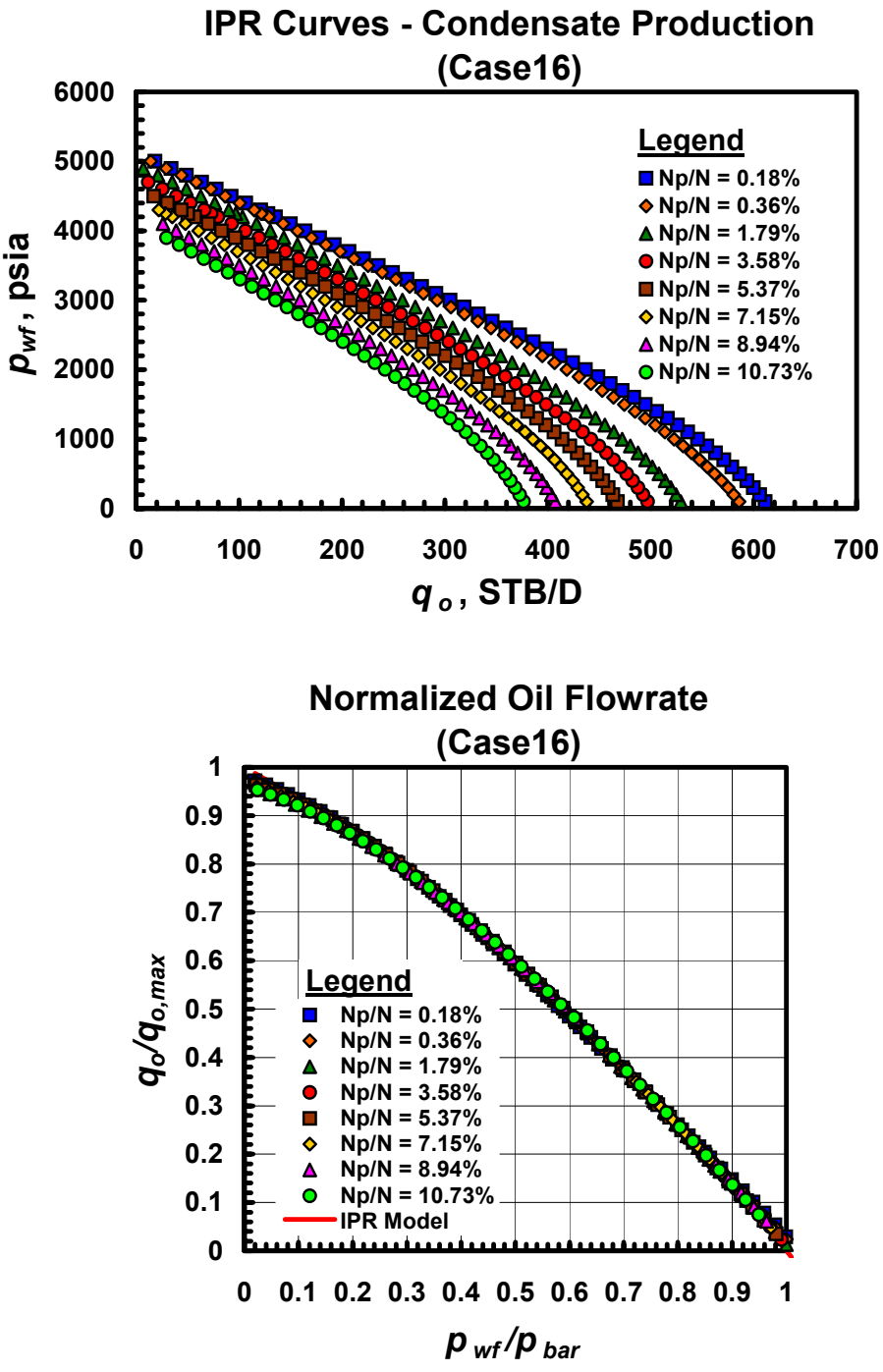

Fig. A.16.a — Dimensional and dimensionless IPR trends for Case 16 — gas condensate performance trends.

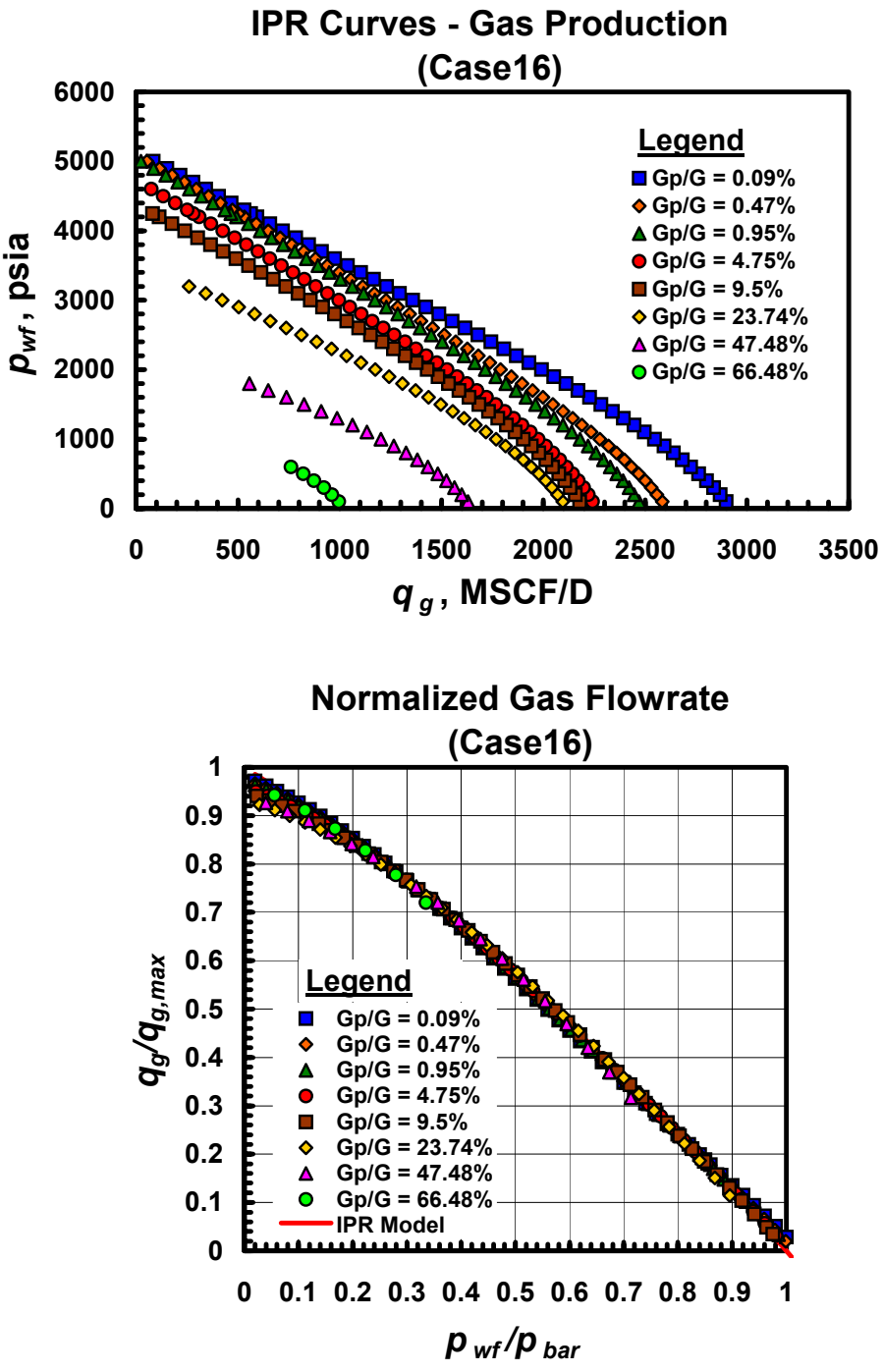

Fig. A.16.b — Dimensional and dimensionless IPR trends for Case 16 — gas performance trends.

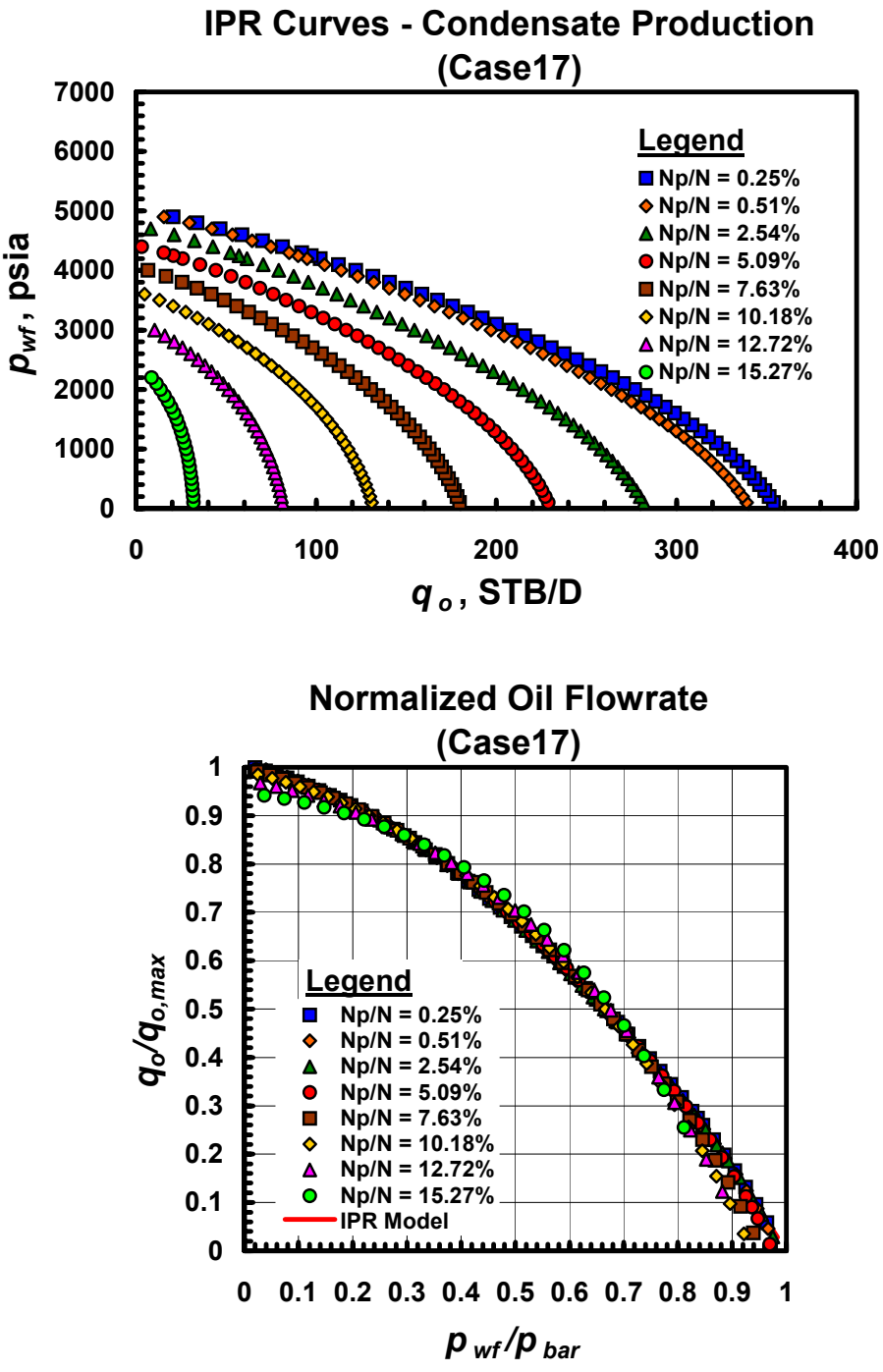

Fig. A.17.a — Dimensional and dimensionless IPR trends for Case 17 — gas condensate performance trends.

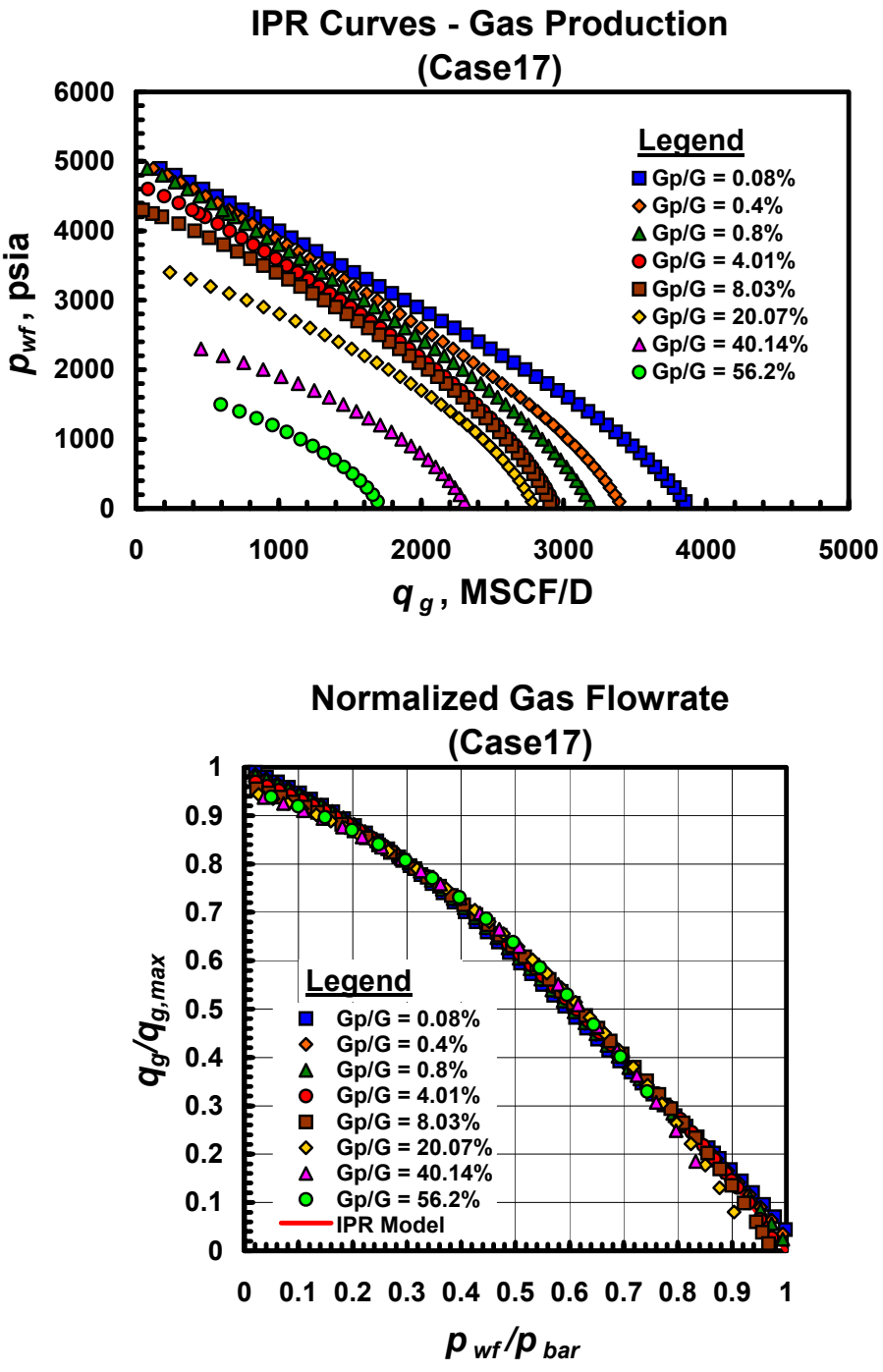

Fig. A.17.b — Dimensional and dimensionless IPR trends for Case 17 — gas performance trends.

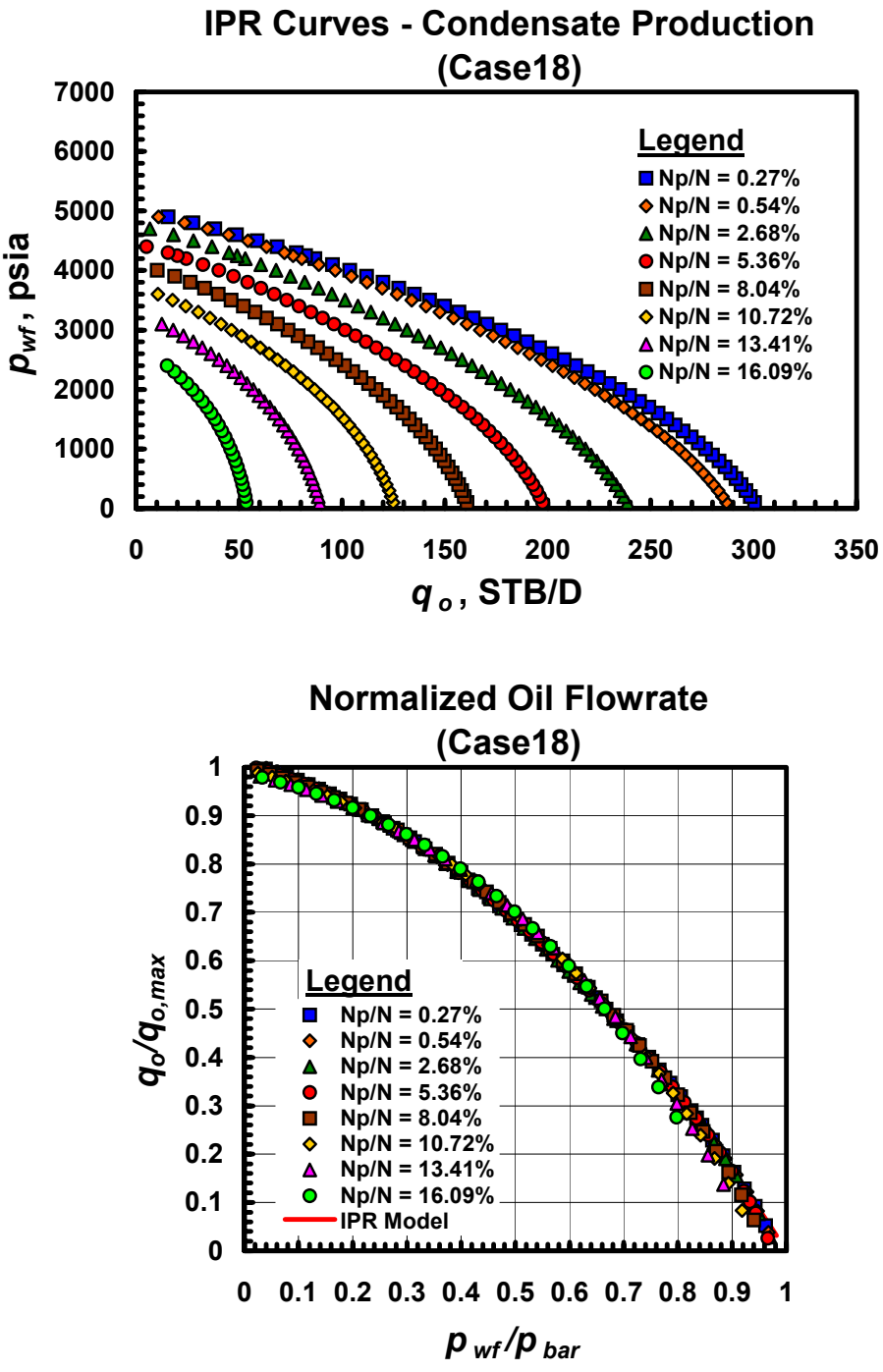

Fig. A.18.a — Dimensional and dimensionless IPR trends for Case 18 — gas condensate performance trends.

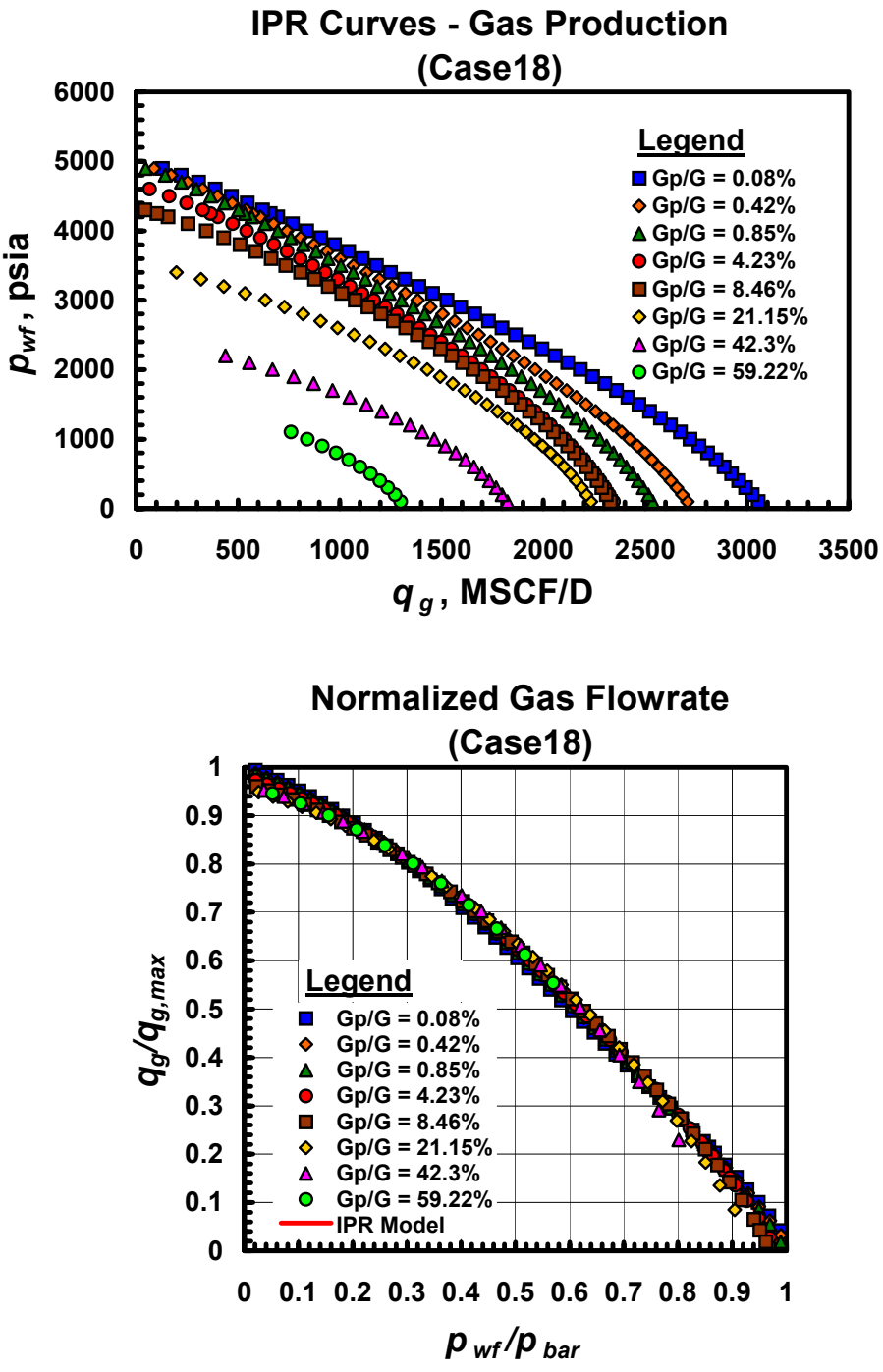

Fig. A.18.b — Dimensional and dimensionless IPR trends for Case 18 — gas performance trends.

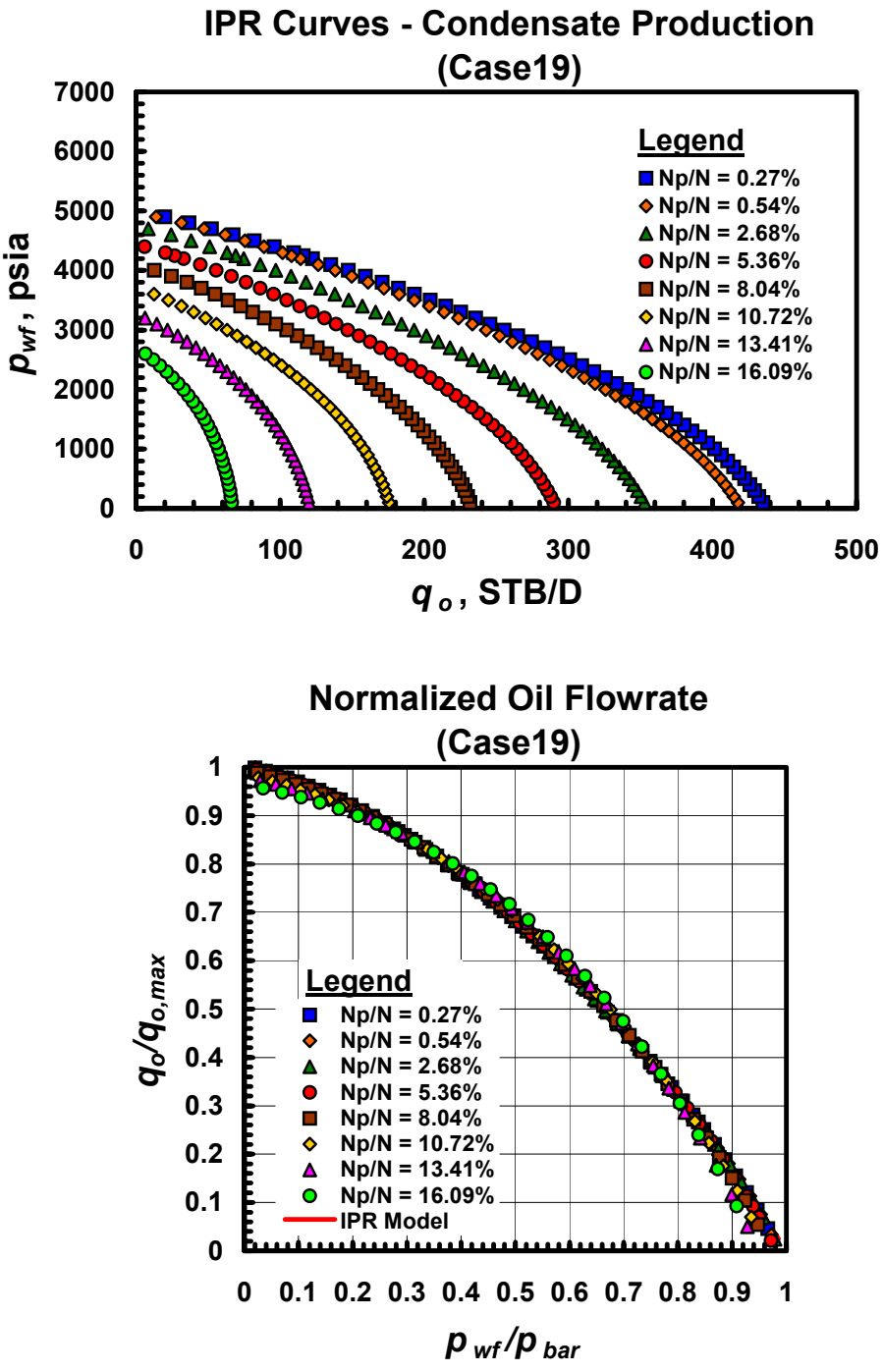

Fig. A.19.a — Dimensional and dimensionless IPR trends for Case 19 — gas condensate performance trends.

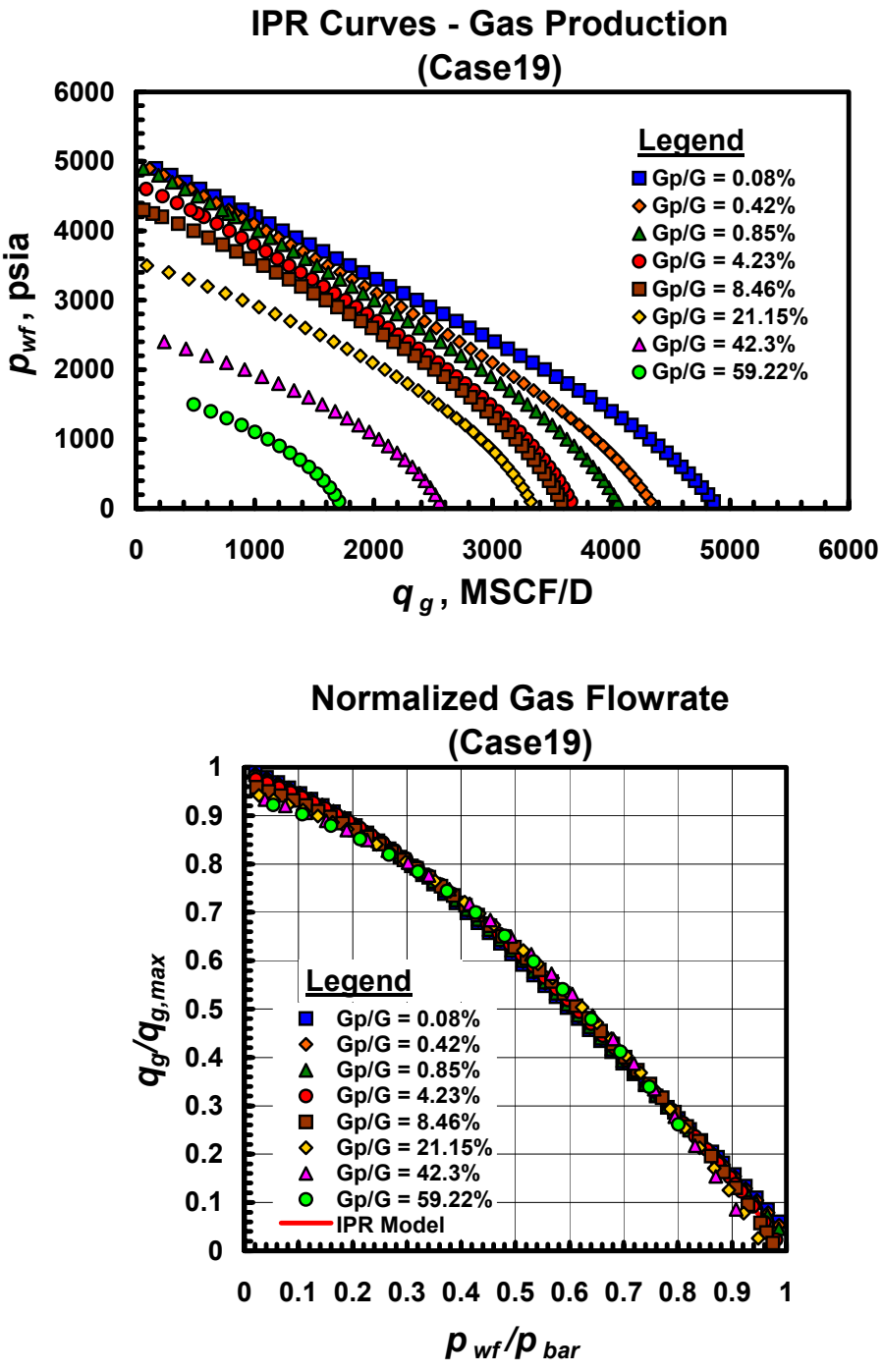

Fig. A.19.b — Dimensional and dimensionless IPR trends for Case 19 — gas performance trends.

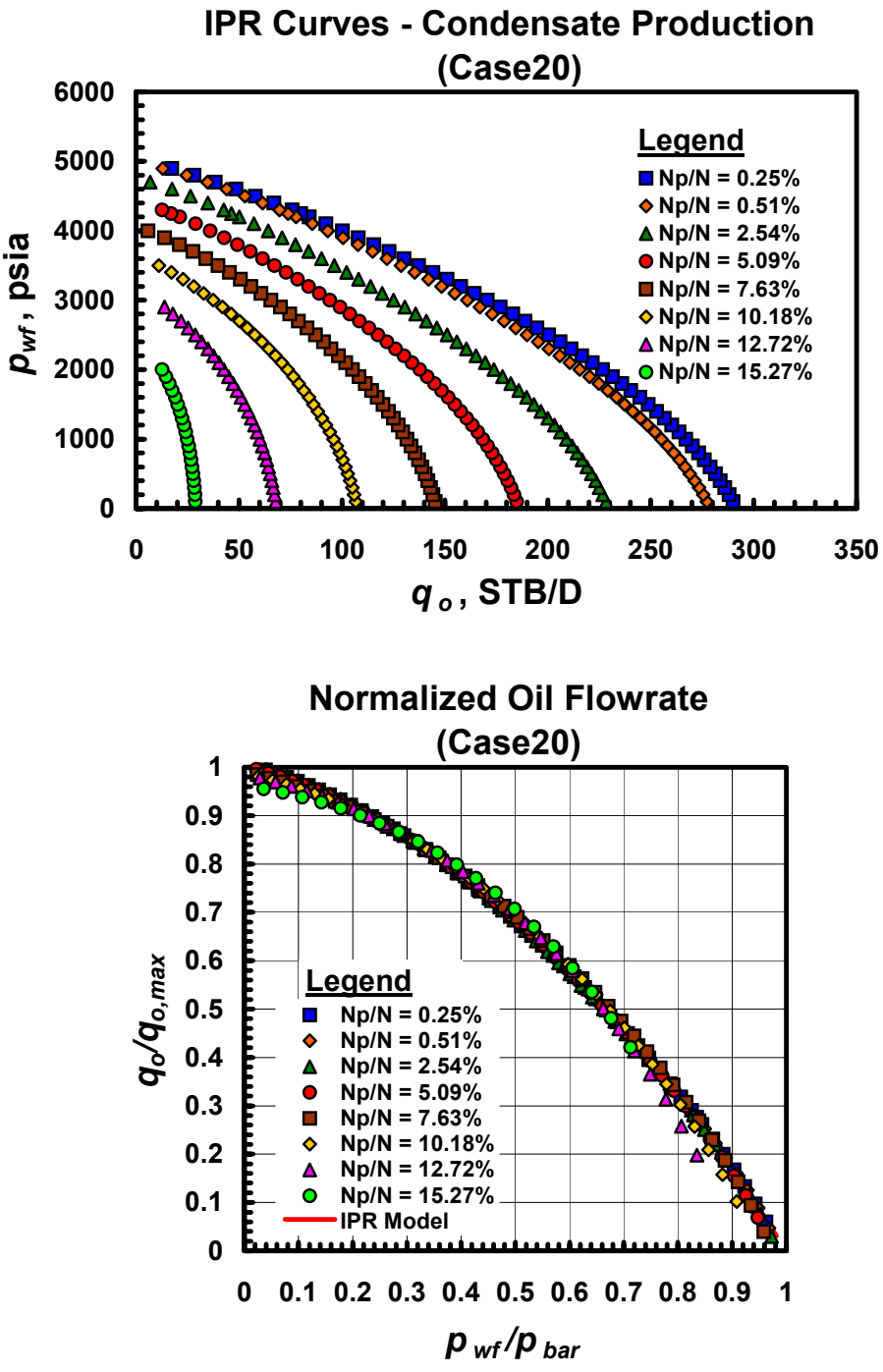

Fig. A.20.a — Dimensional and dimensionless IPR trends for Case 20 — gas condensate performance trends.

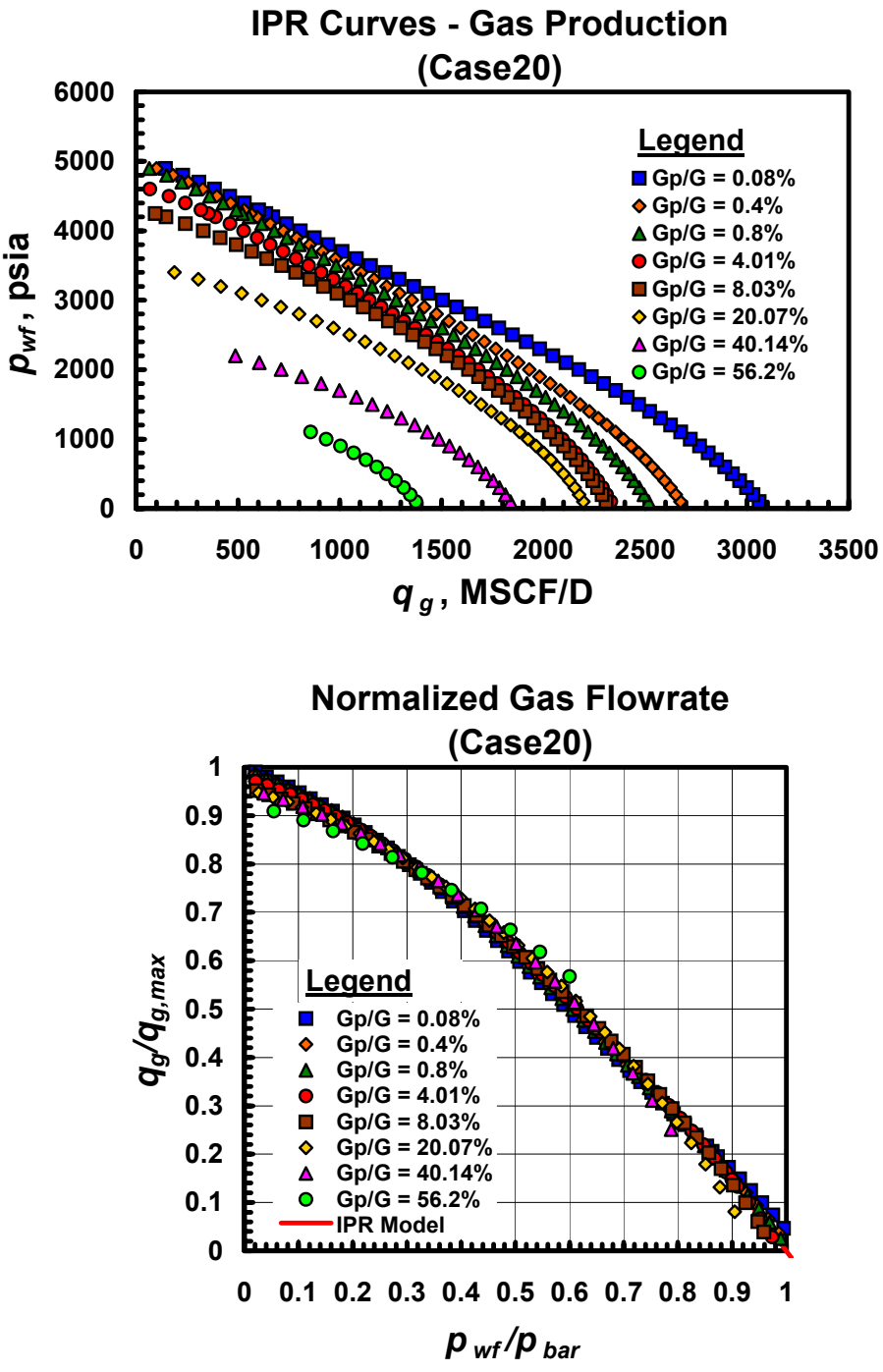

Fig. A.20.b — Dimensional and dimensionless IPR trends for Case 20 — gas performance trends.

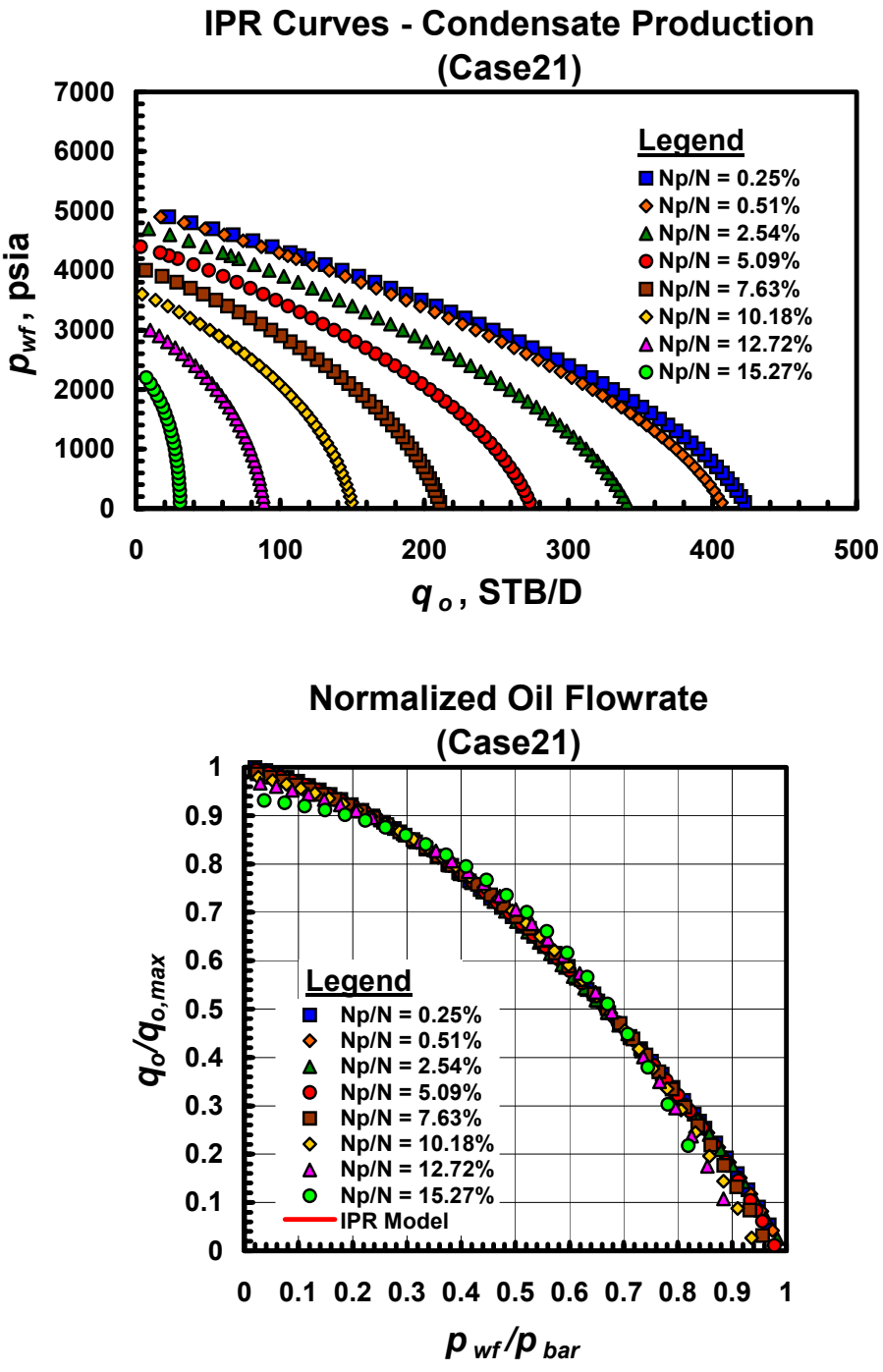

Fig. A.21.a — Dimensional and dimensionless IPR trends for Case 21 — gas condensate performance trends.

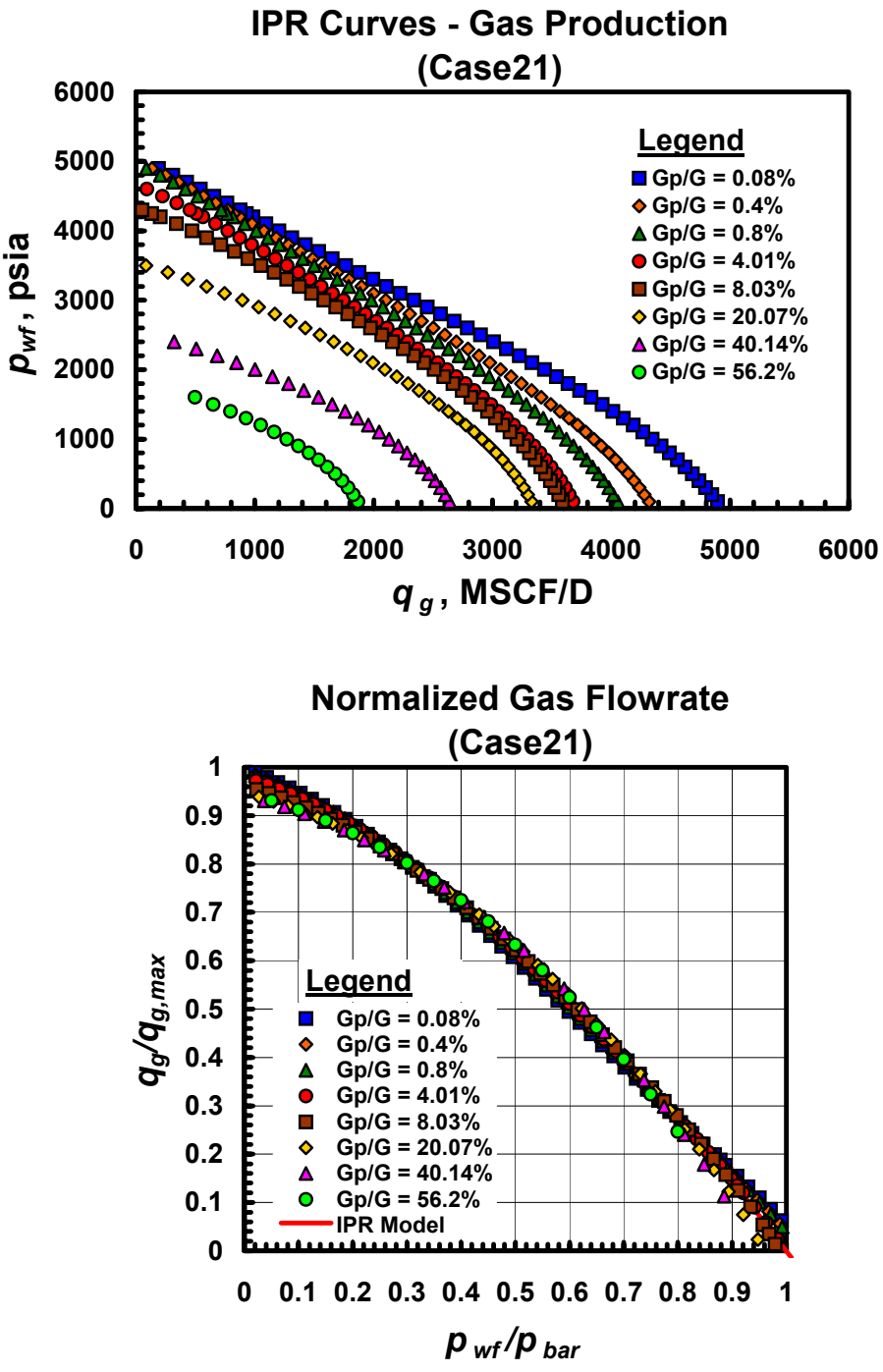

Fig. A.21.b — Dimensional and dimensionless IPR trends for Case 21 — gas performance trends.

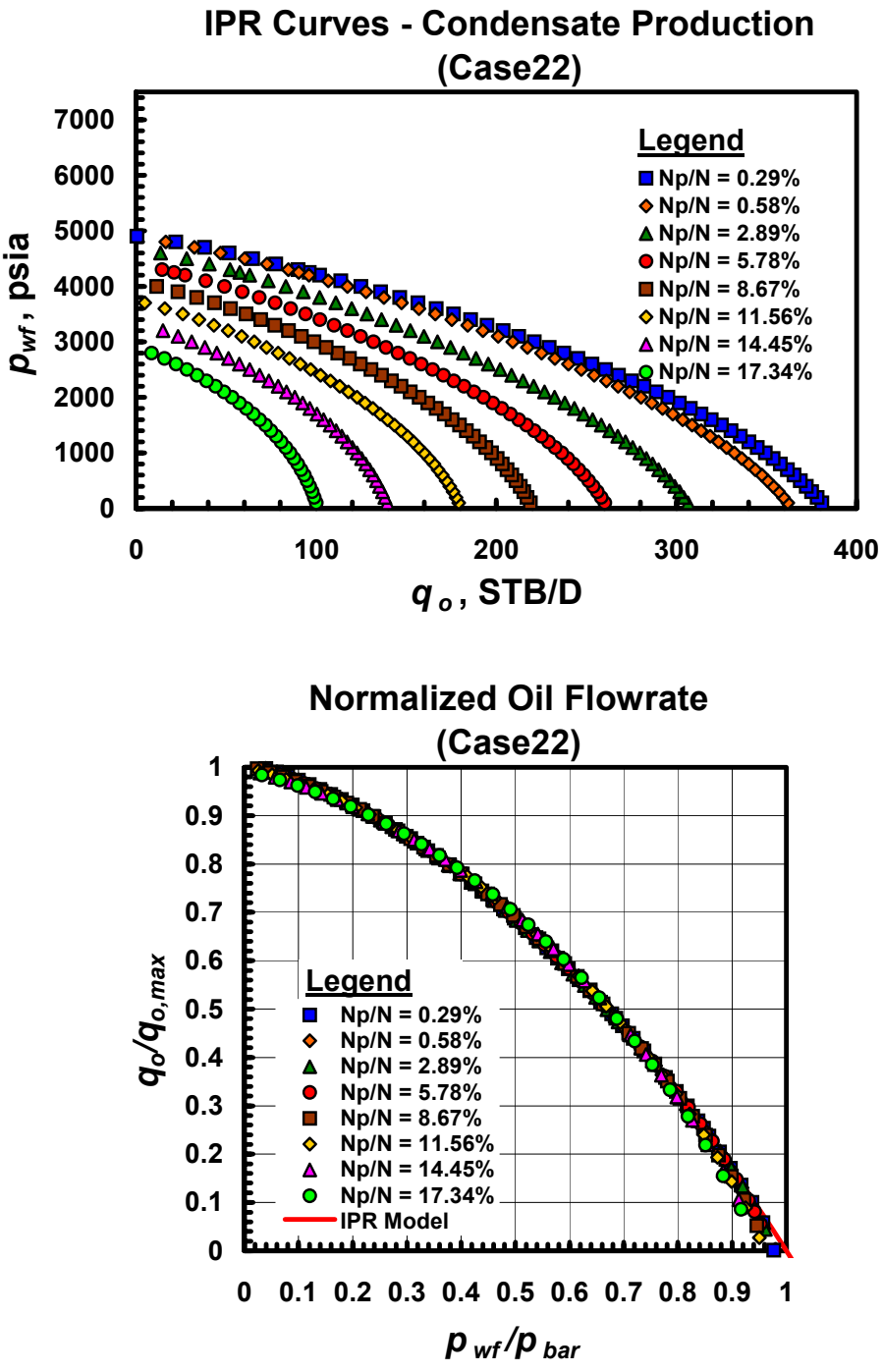

Fig. A.22.a — Dimensional and dimensionless IPR trends for Case 22 — gas condensate performance trends.

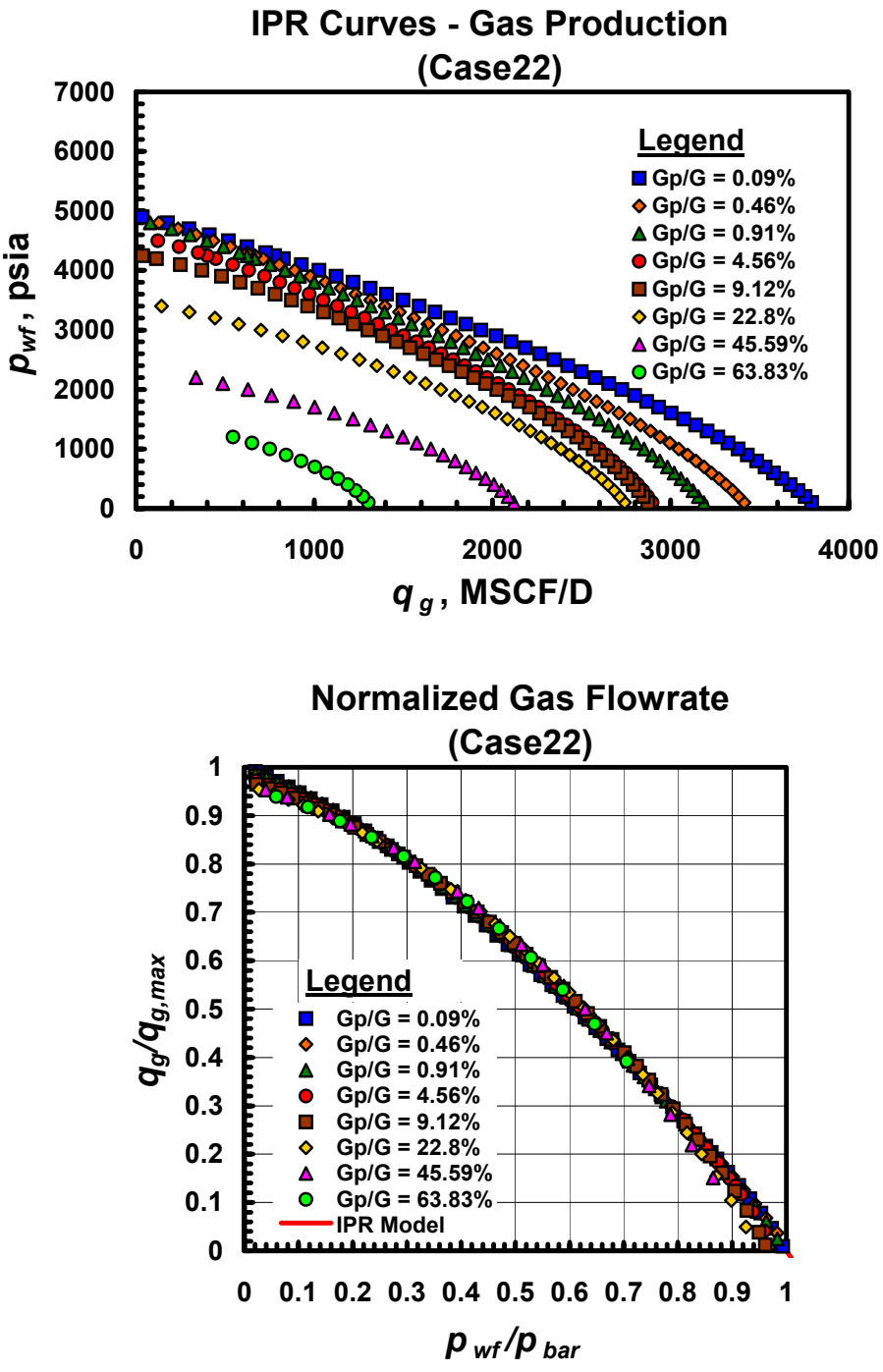

Fig. A.22.b — Dimensional and dimensionless IPR trends for Case 22 — gas performance trends.

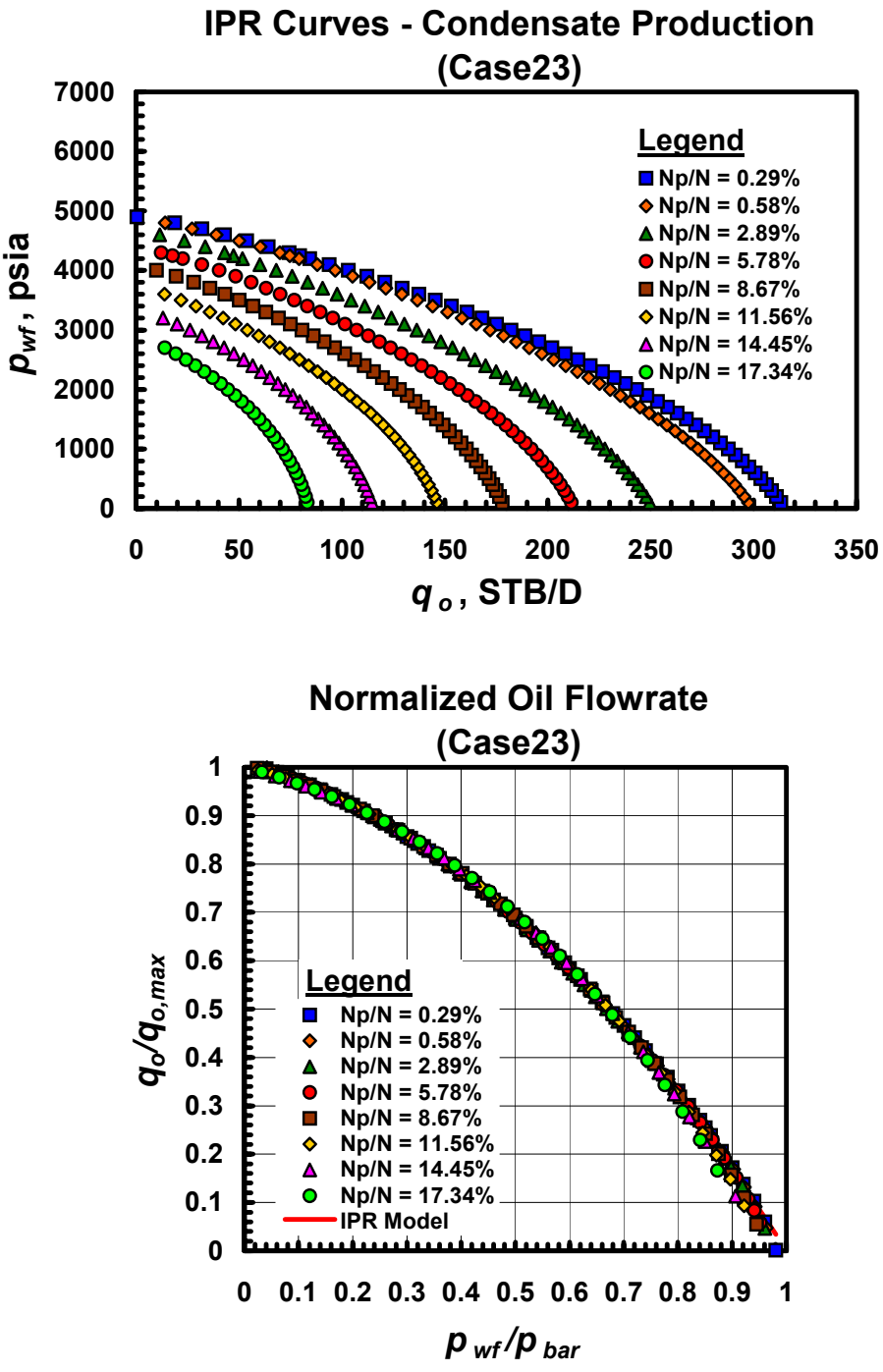

Fig. A.23.a — Dimensional and dimensionless IPR trends for Case 23 — gas condensate performance trends.

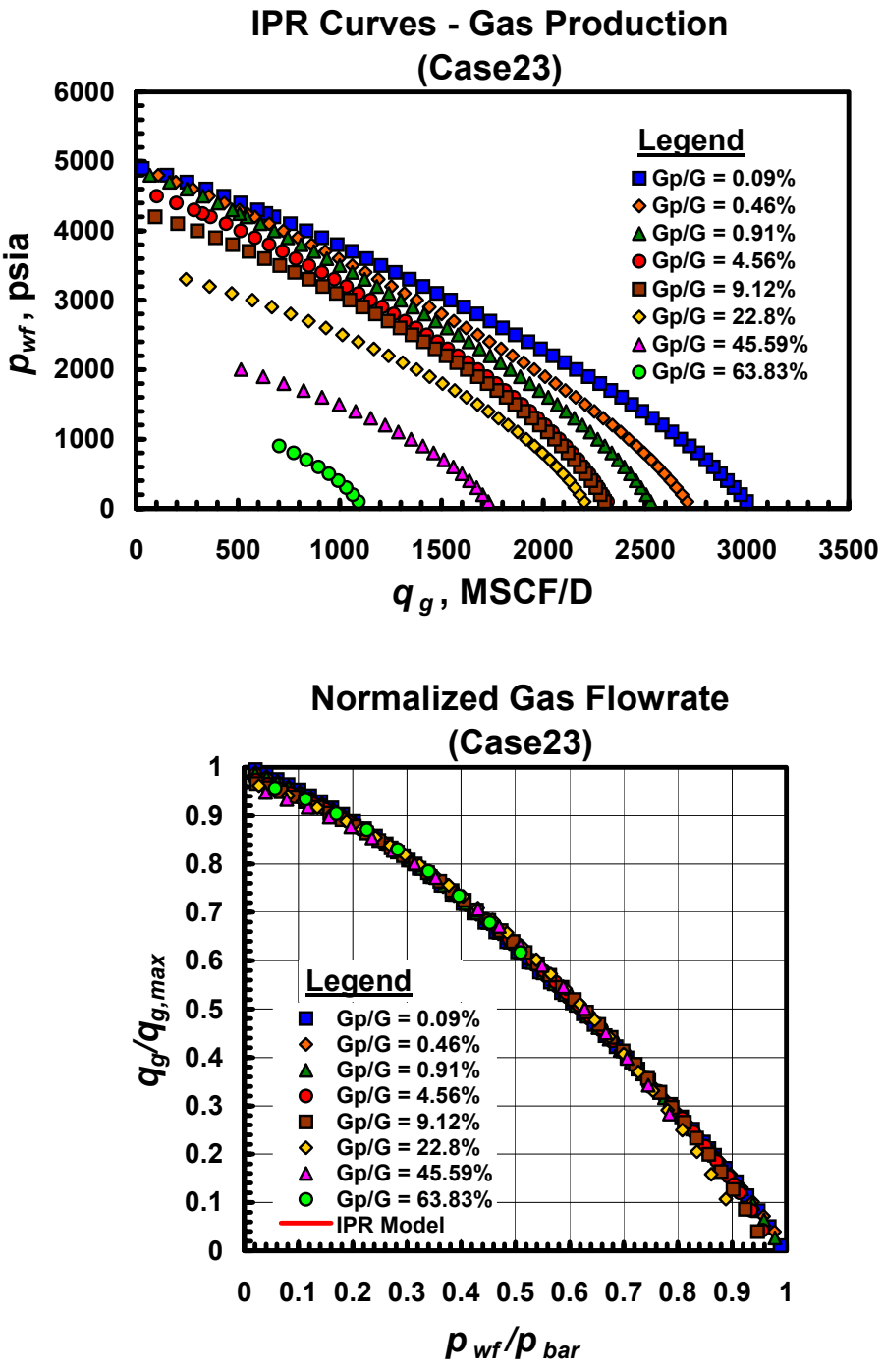

Fig. A.23.b — Dimensional and dimensionless IPR trends for Case 23 — gas performance trends.

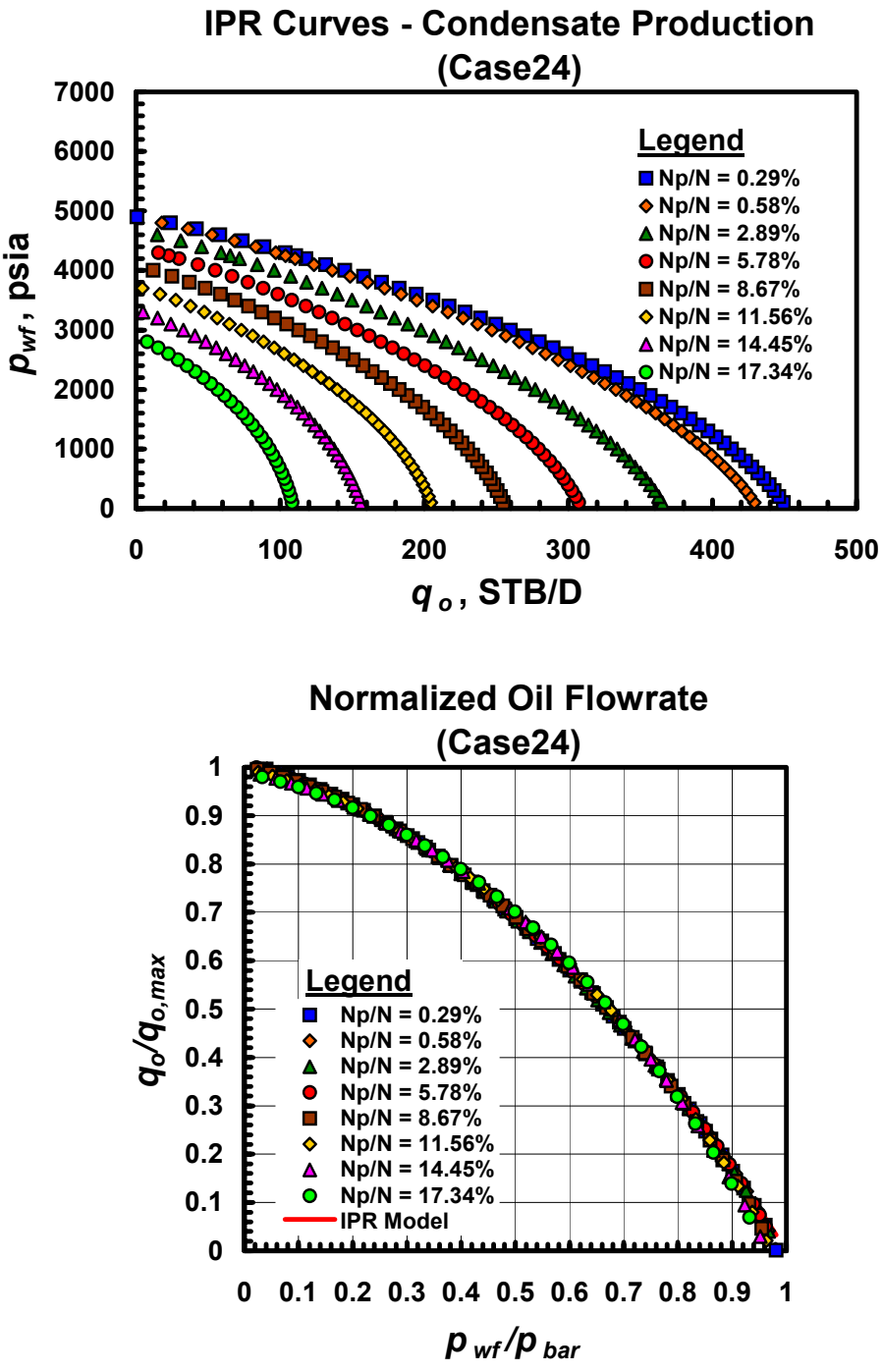

Fig. A.24.a — Dimensional and dimensionless IPR trends for Case 24 — gas condensate performance trends.

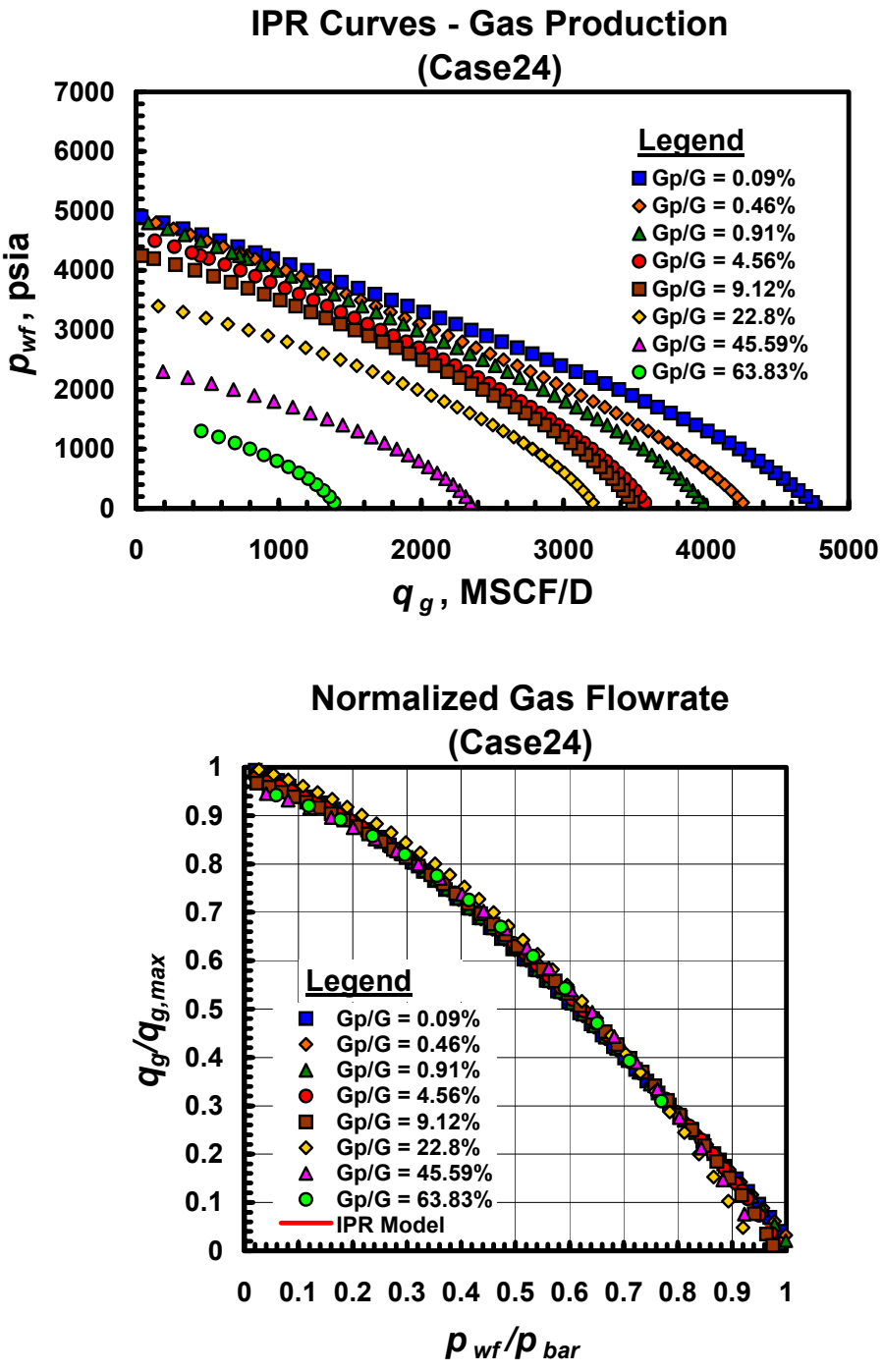

Fig. A.24.b — Dimensional and dimensionless IPR trends for Case 24 — gas performance trends.

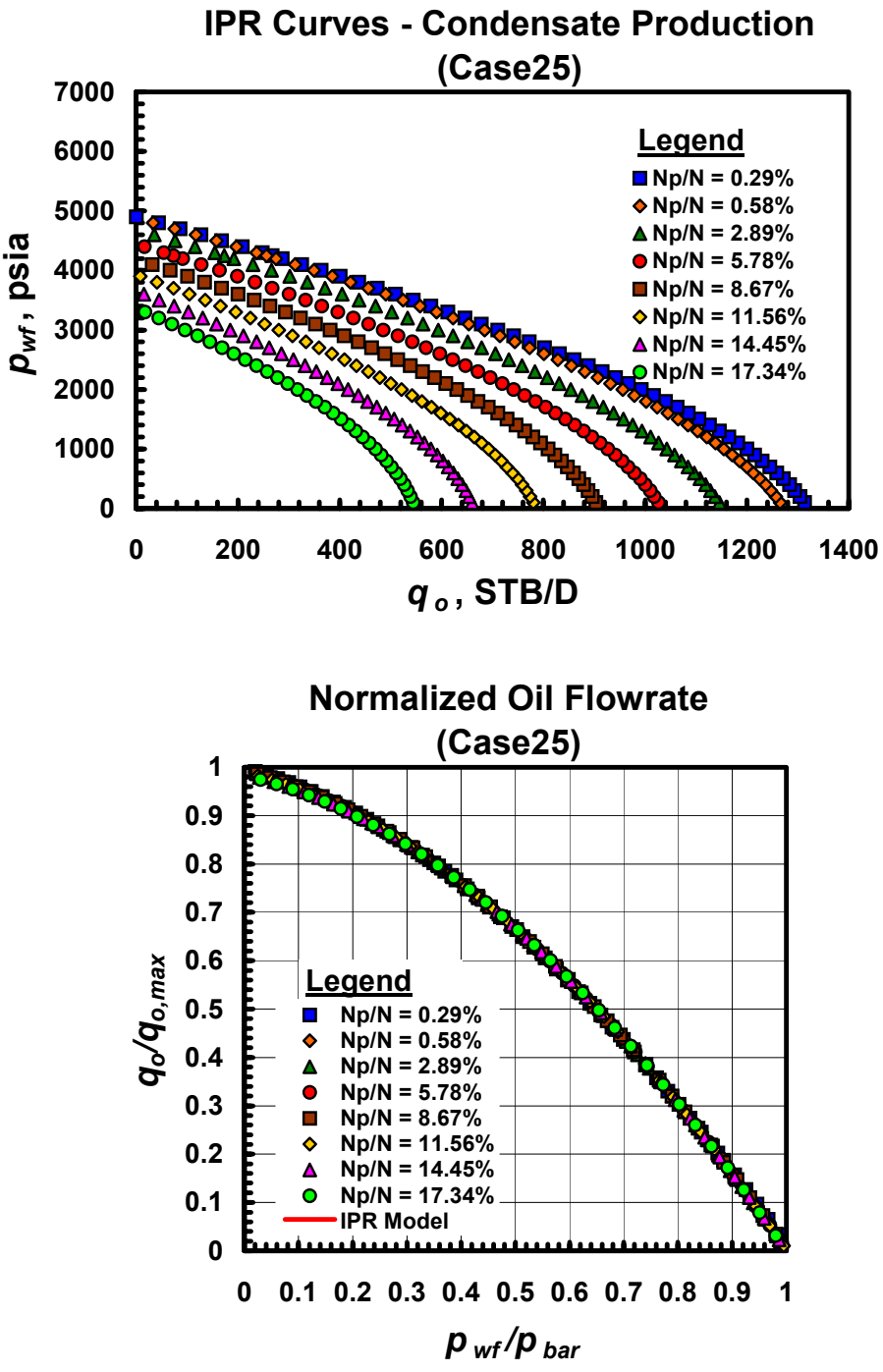

Fig. A.25.a — Dimensional and dimensionless IPR trends for Case 25 — gas condensate performance trends.

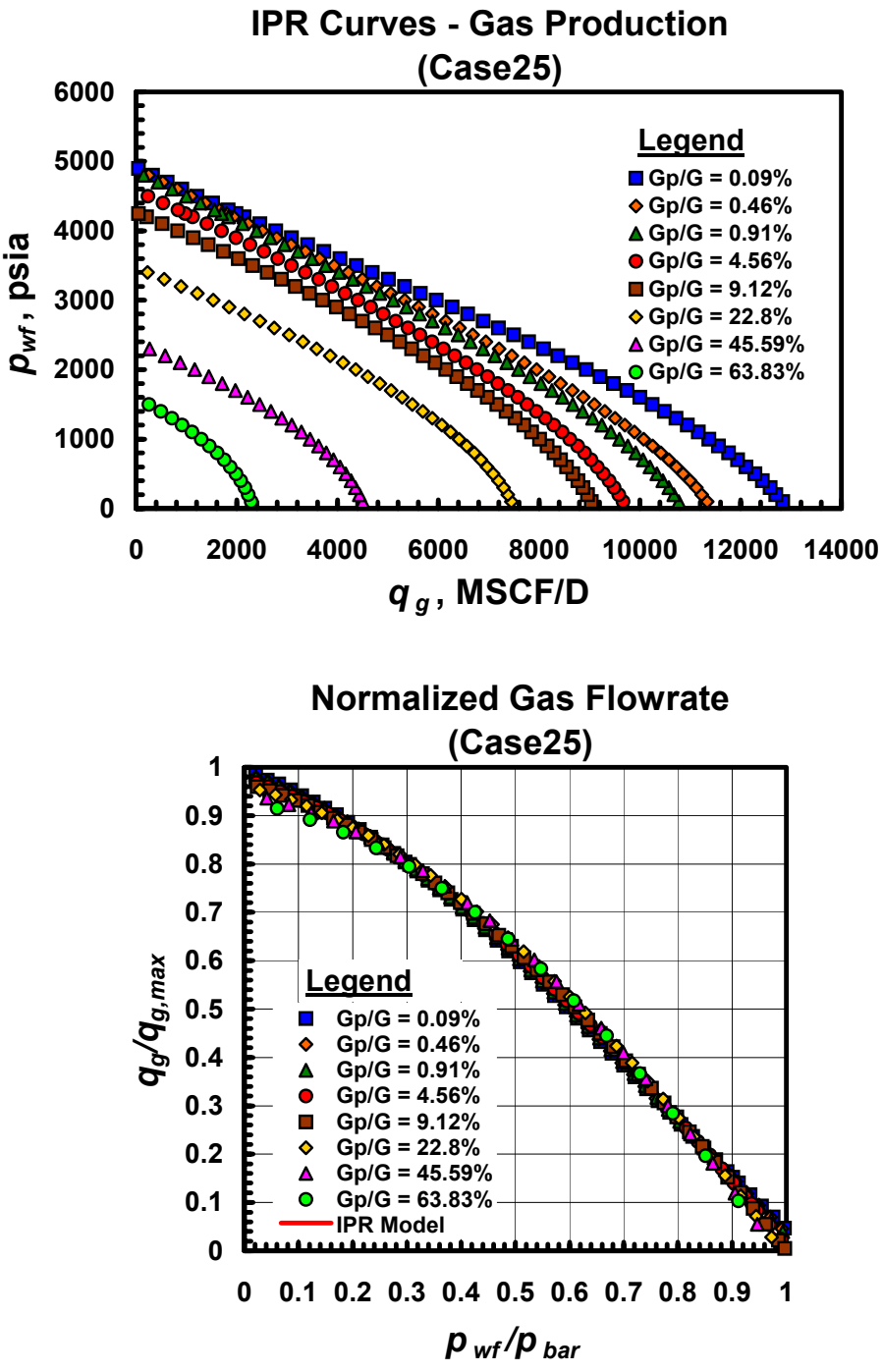

Fig. A.25.b — Dimensional and dimensionless IPR trends for Case 25 — gas performance trends.

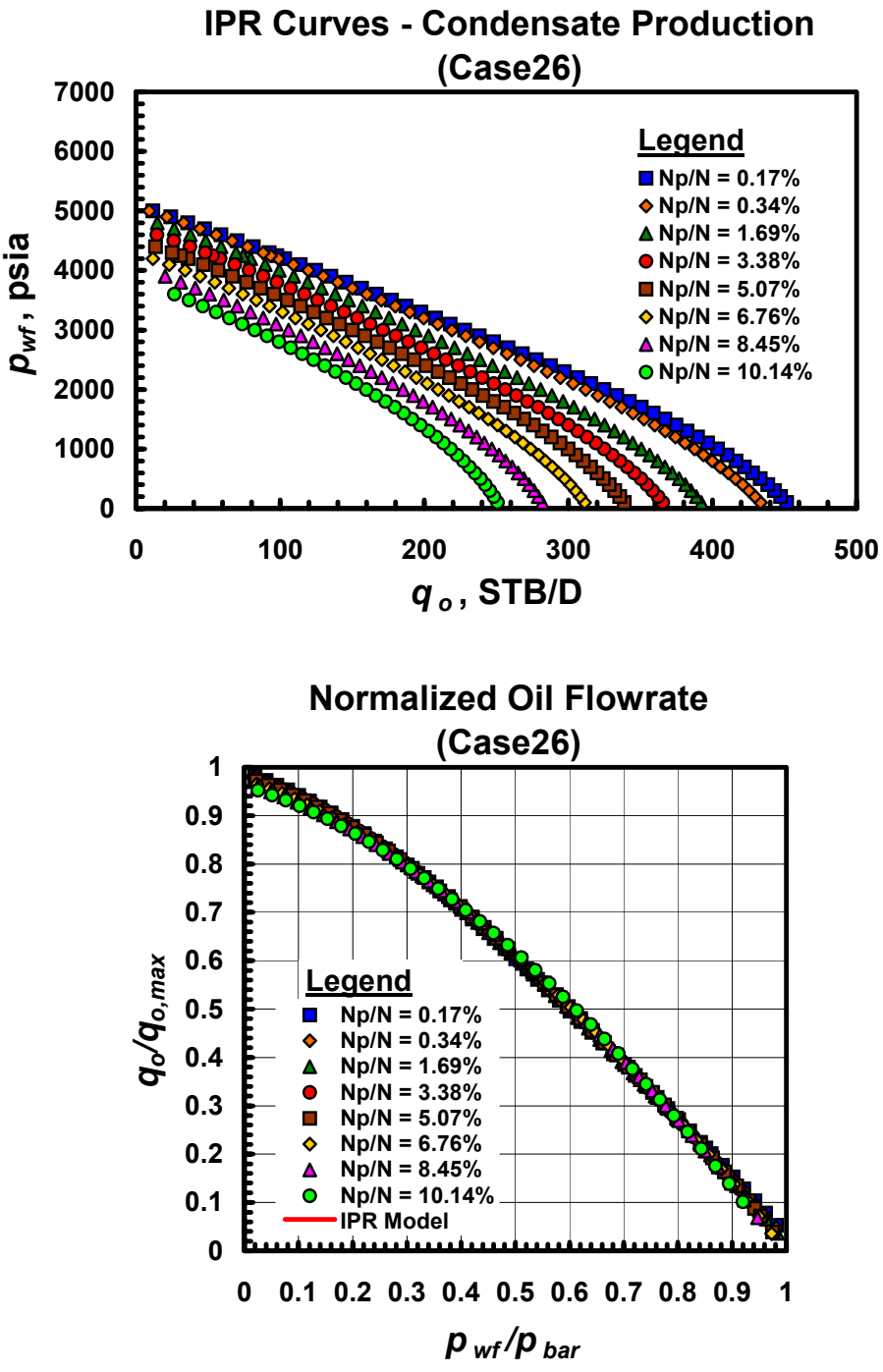

Fig. A.26.a — Dimensional and dimensionless IPR trends for Case 26 — gas condensate performance trends.

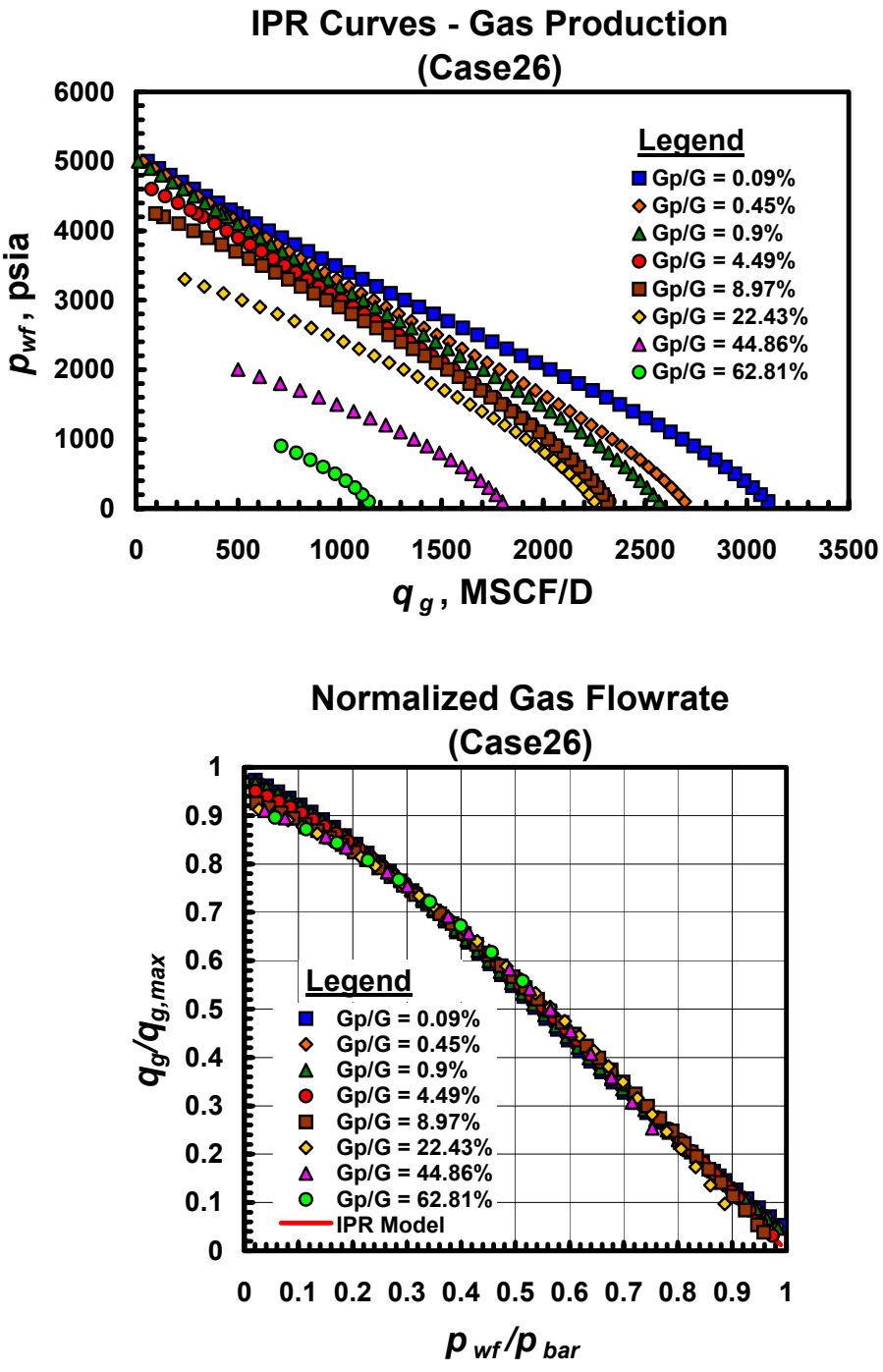

Fig. A.26.b — Dimensional and dimensionless IPR trends for Case 26 — gas performance trends.

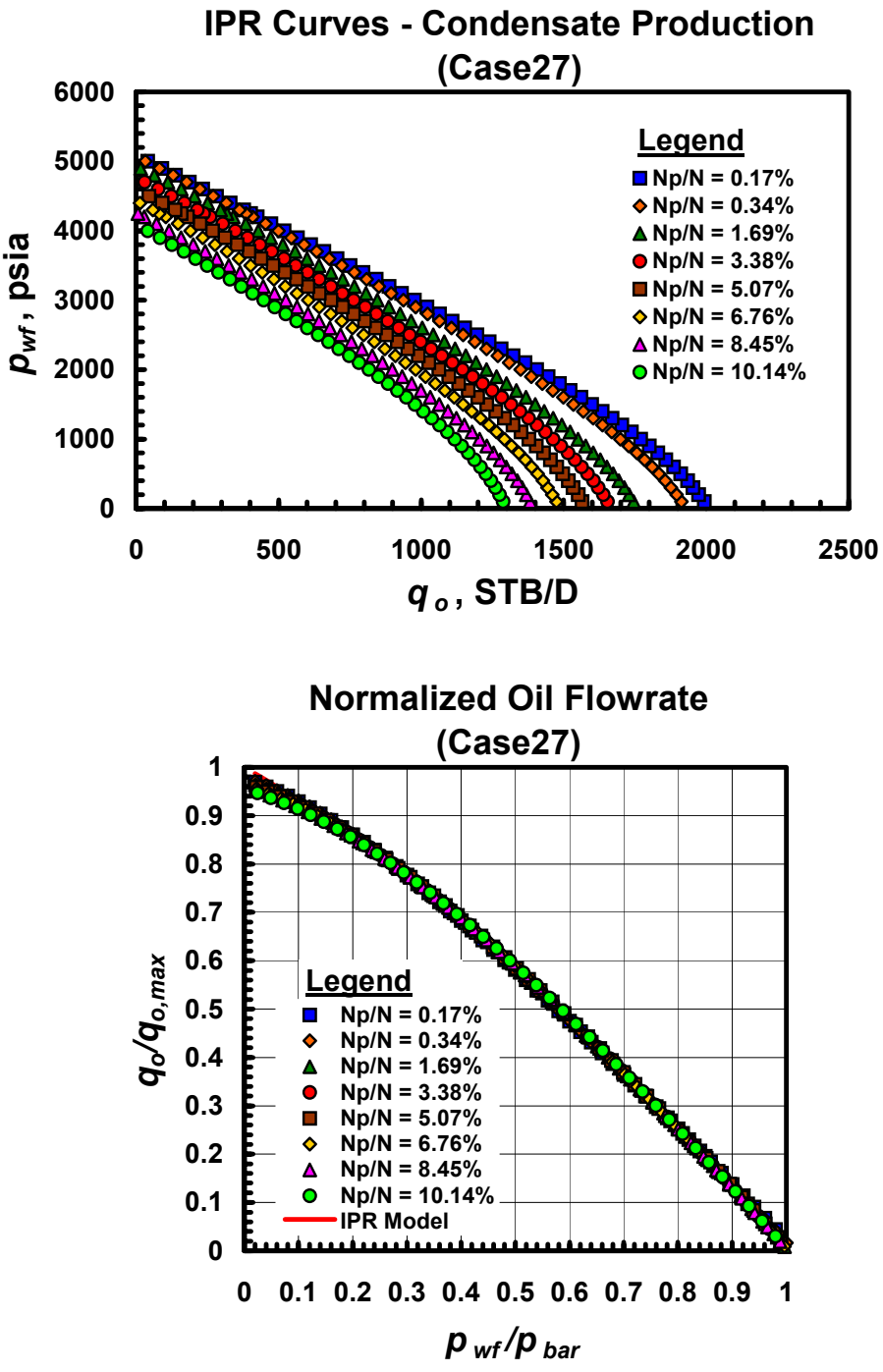

Fig. A.27.a — Dimensional and dimensionless IPR trends for Case 27 — gas condensate performance trends.

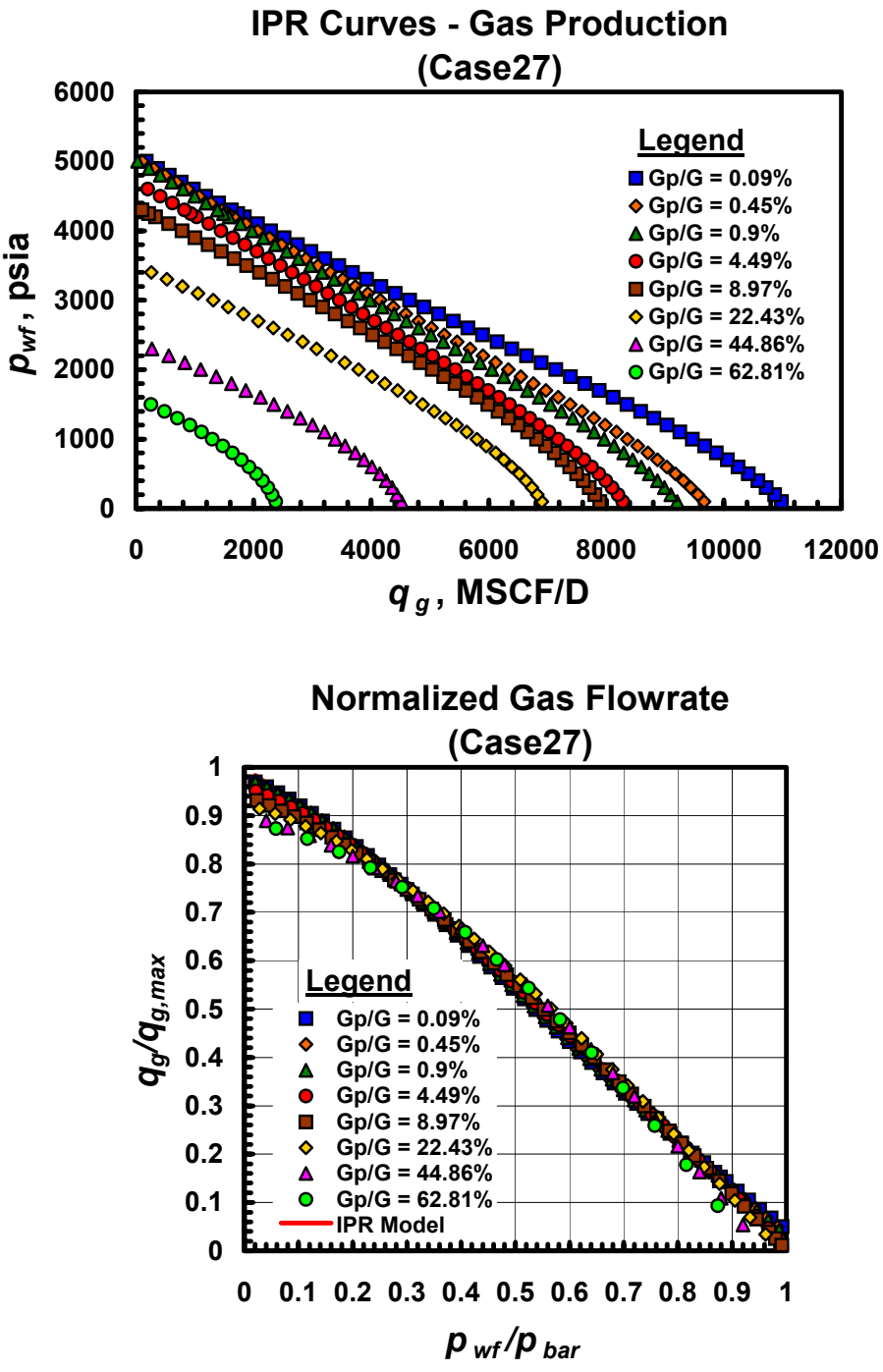

Fig. A.27.b — Dimensional and dimensionless IPR trends for Case 27 — gas performance trends.

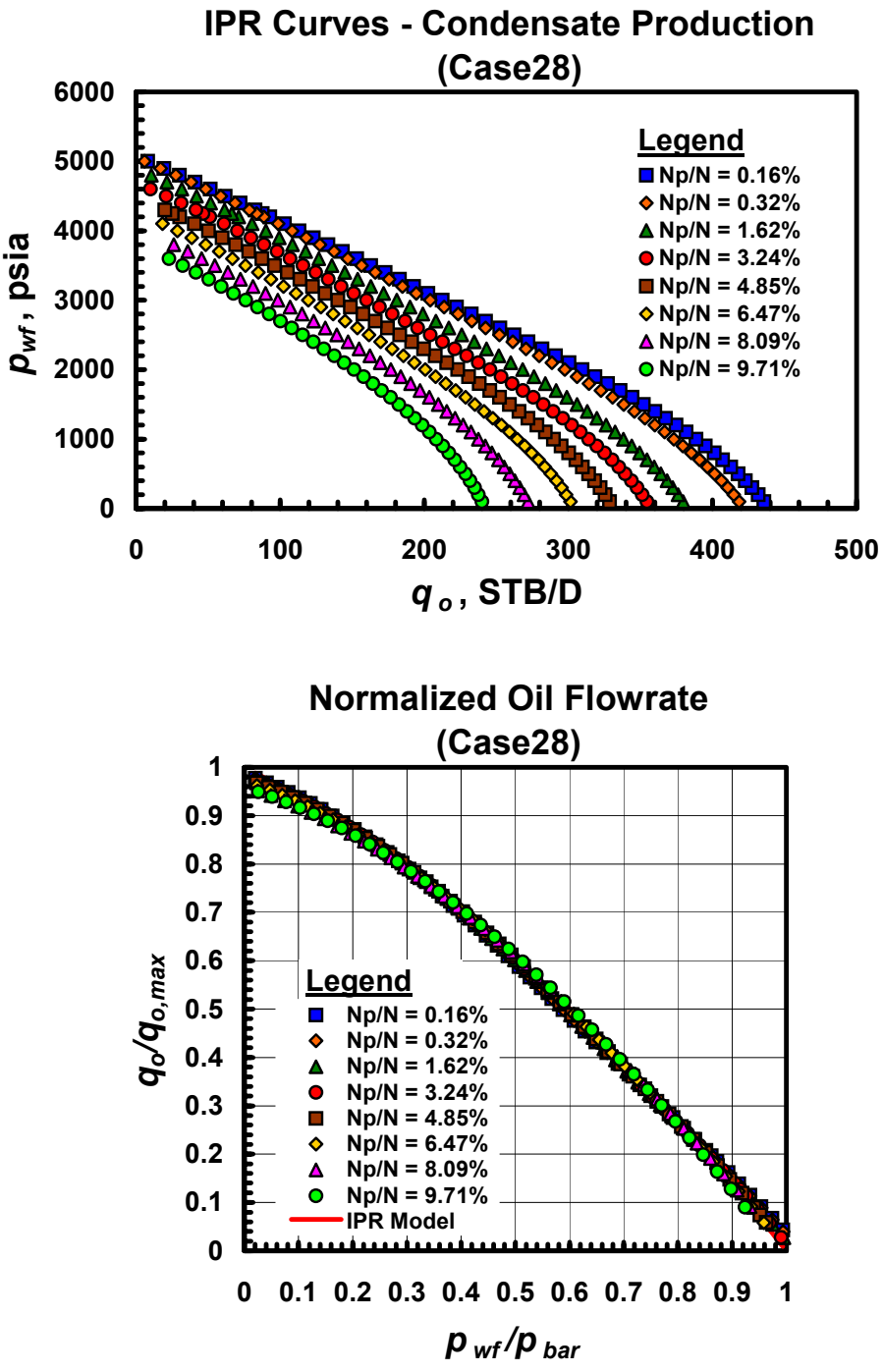

Fig. A.28.a — Dimensional and dimensionless IPR trends for Case 28 — gas condensate performance trends.

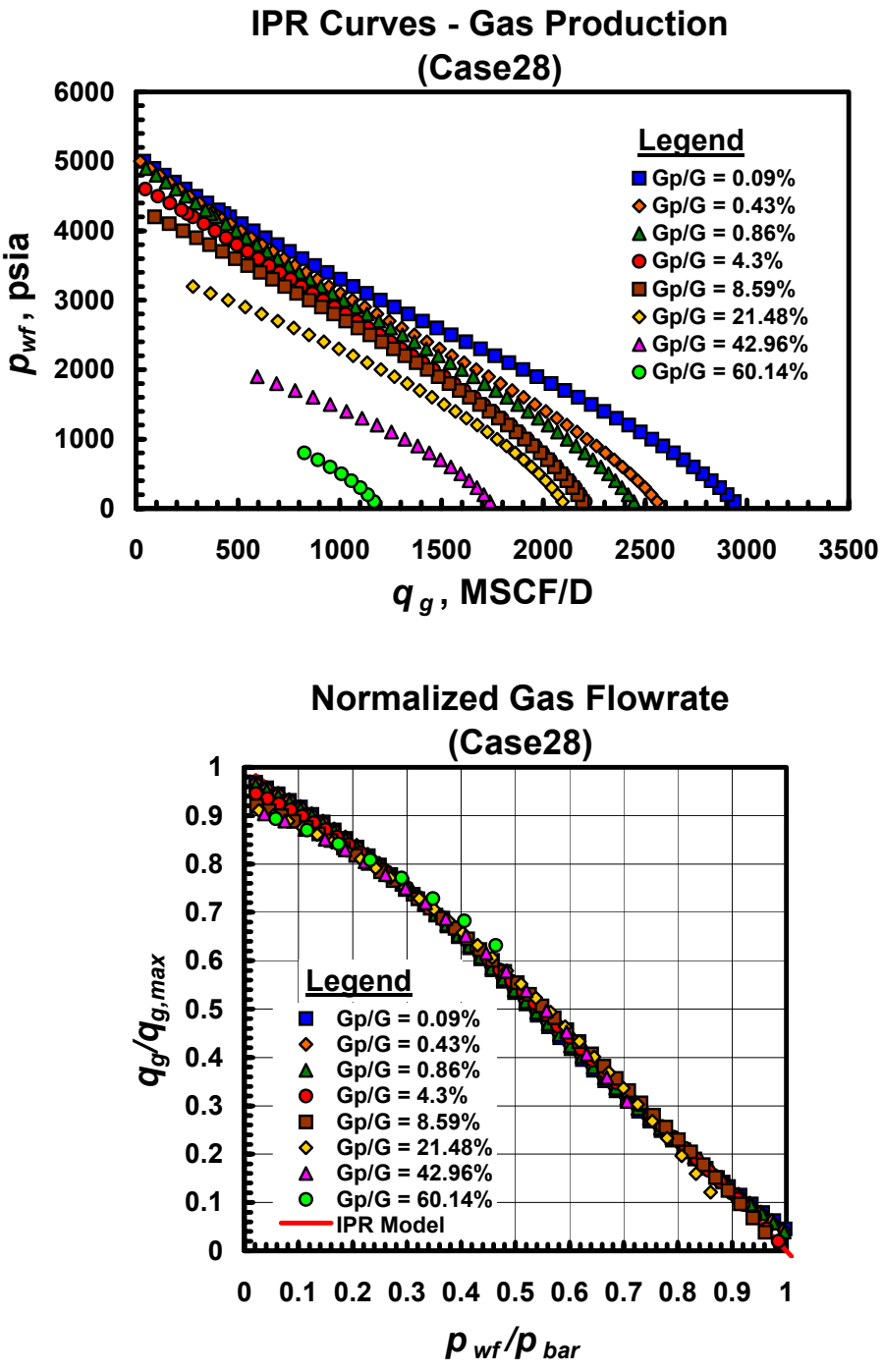

Fig. A.28.b — Dimensional and dimensionless IPR trends for Case 28 — gas performance trends.

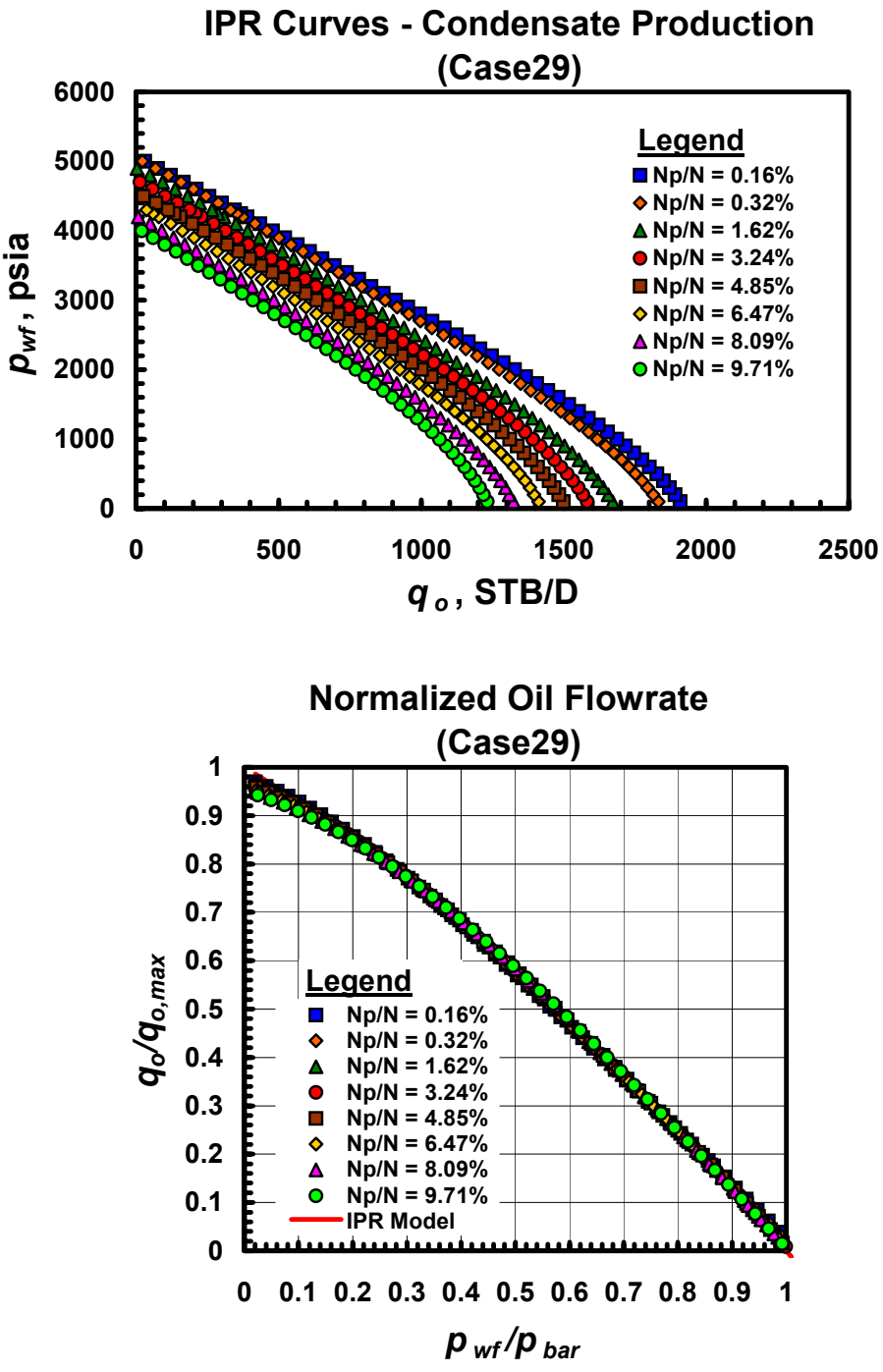

Fig. A.29.a — Dimensional and dimensionless IPR trends for Case 29 — gas condensate performance trends.

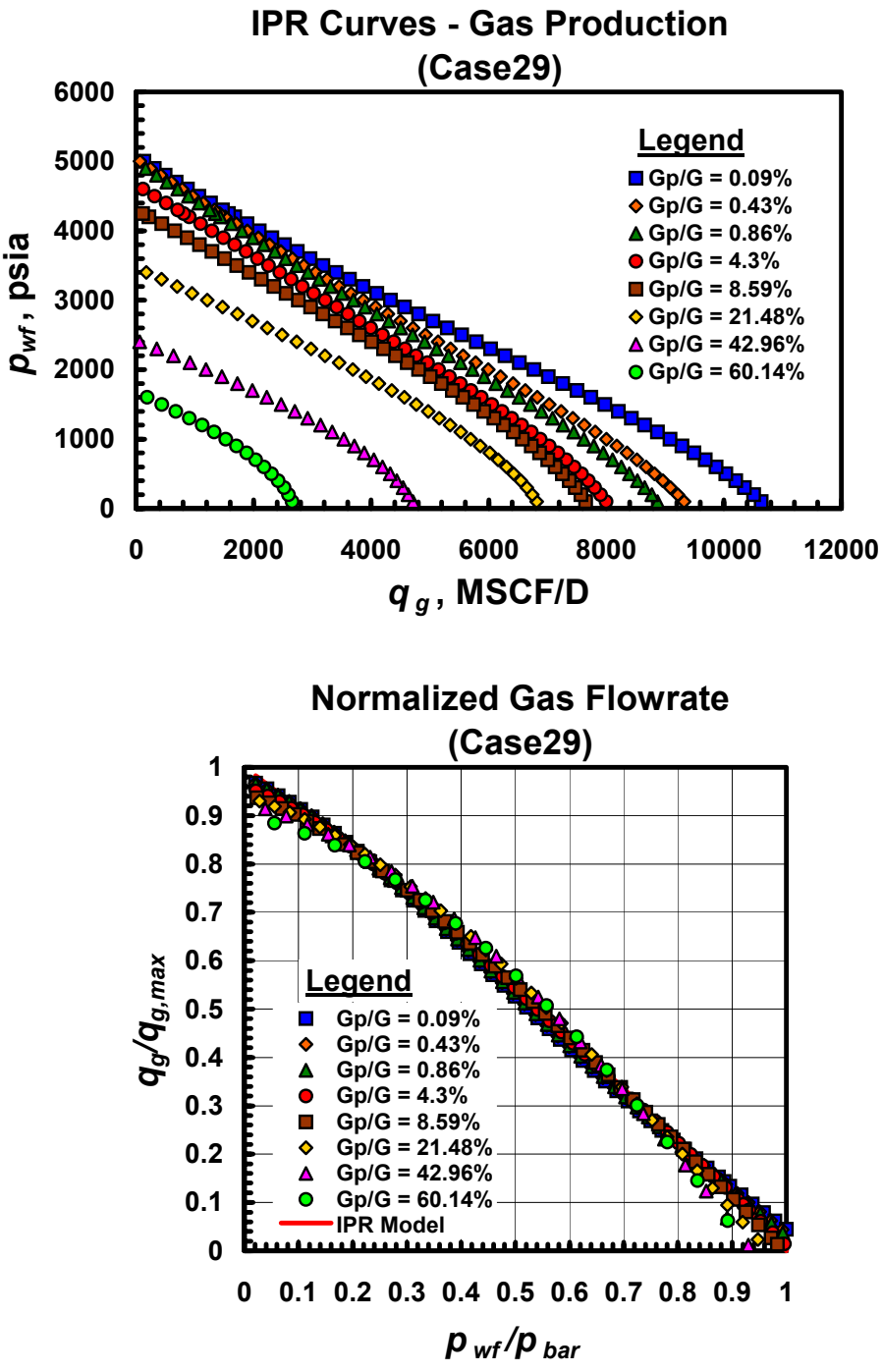

Fig. A.29.b — Dimensional and dimensionless IPR trends for Case 29 — gas performance trends.

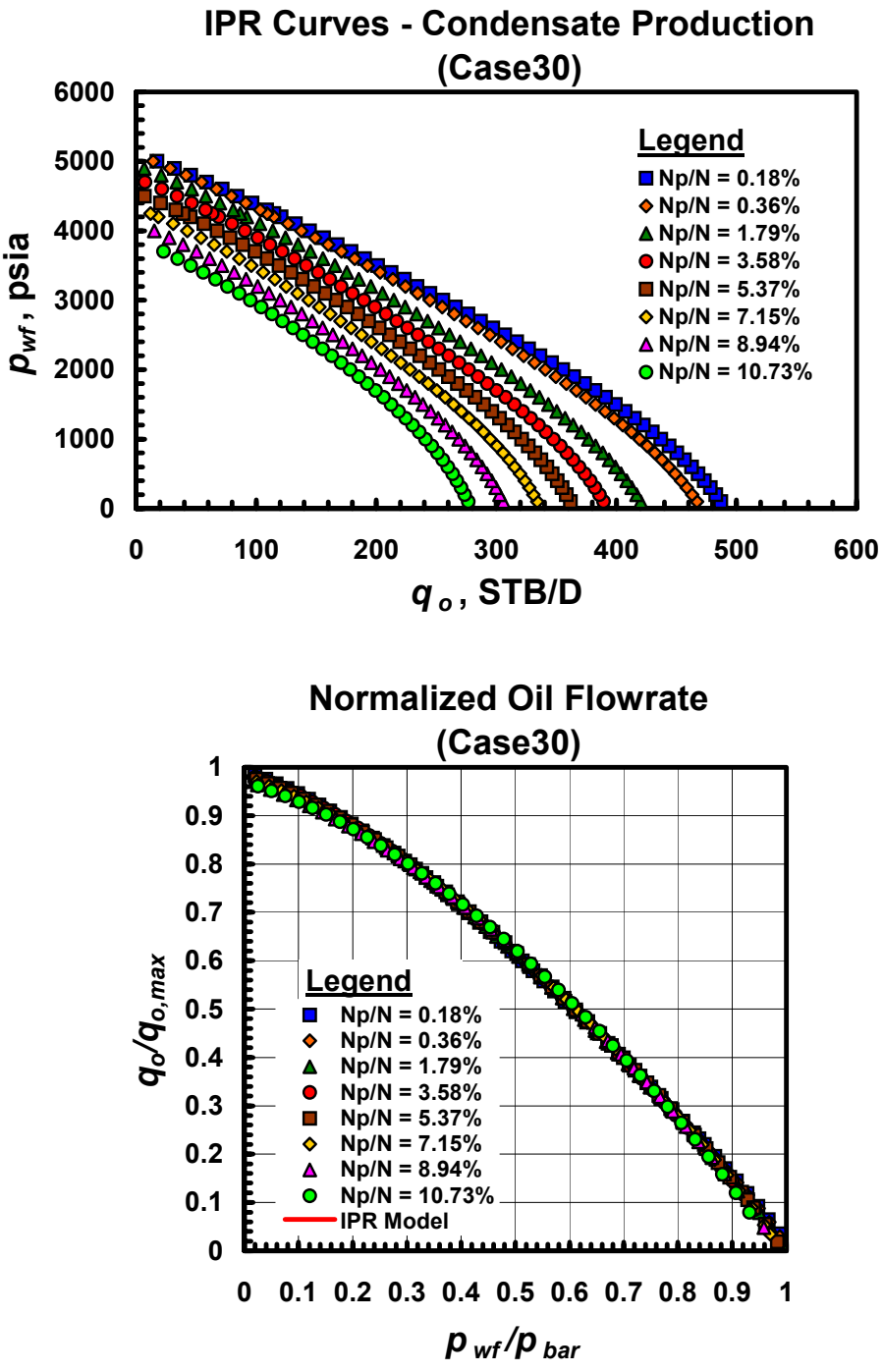

Fig. A.30.a — Dimensional and dimensionless IPR trends for Case 30 — gas condensate performance trends.

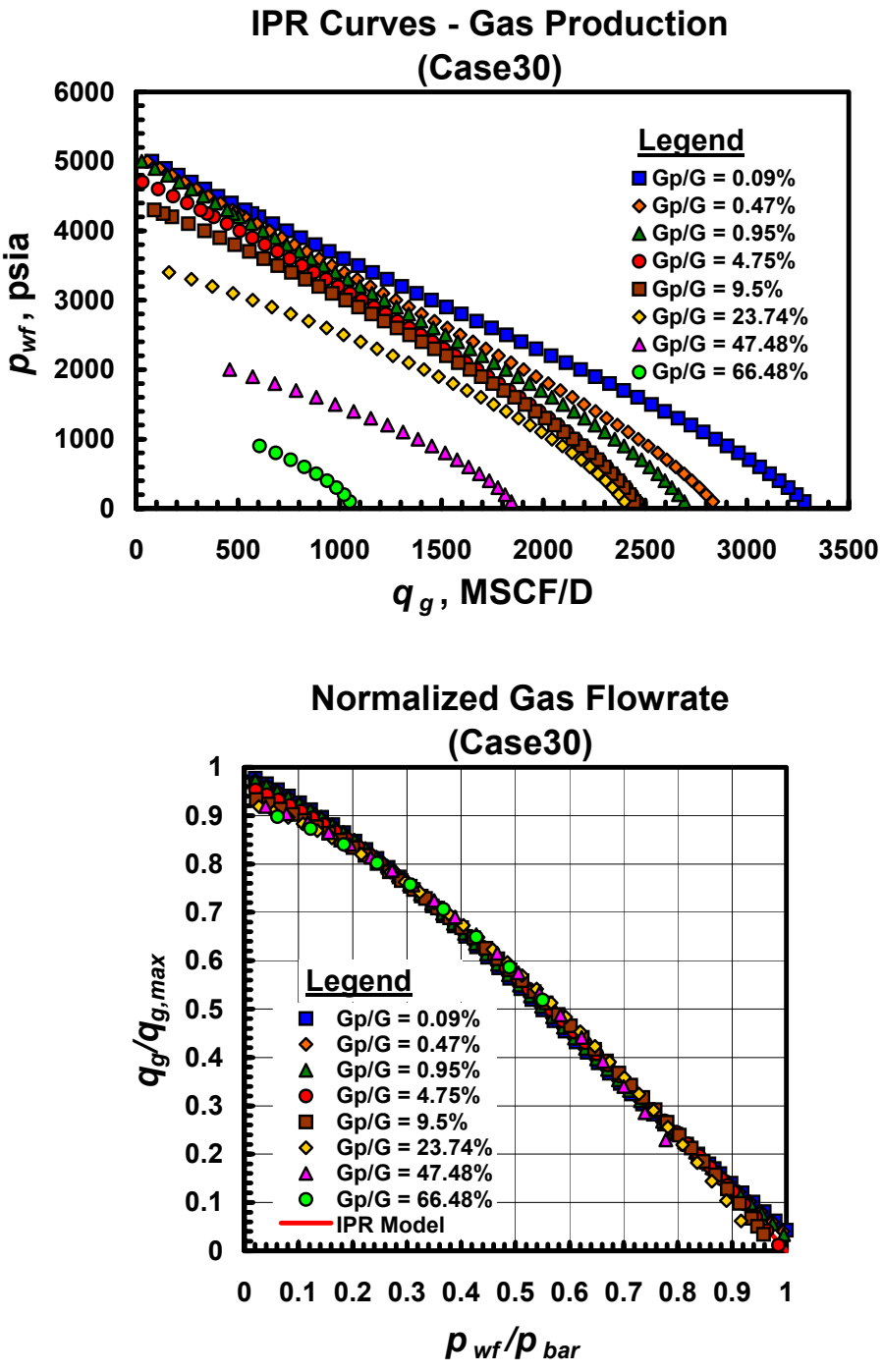

Fig. A.30.b — Dimensional and dimensionless IPR trends for Case 30 — gas performance trends.

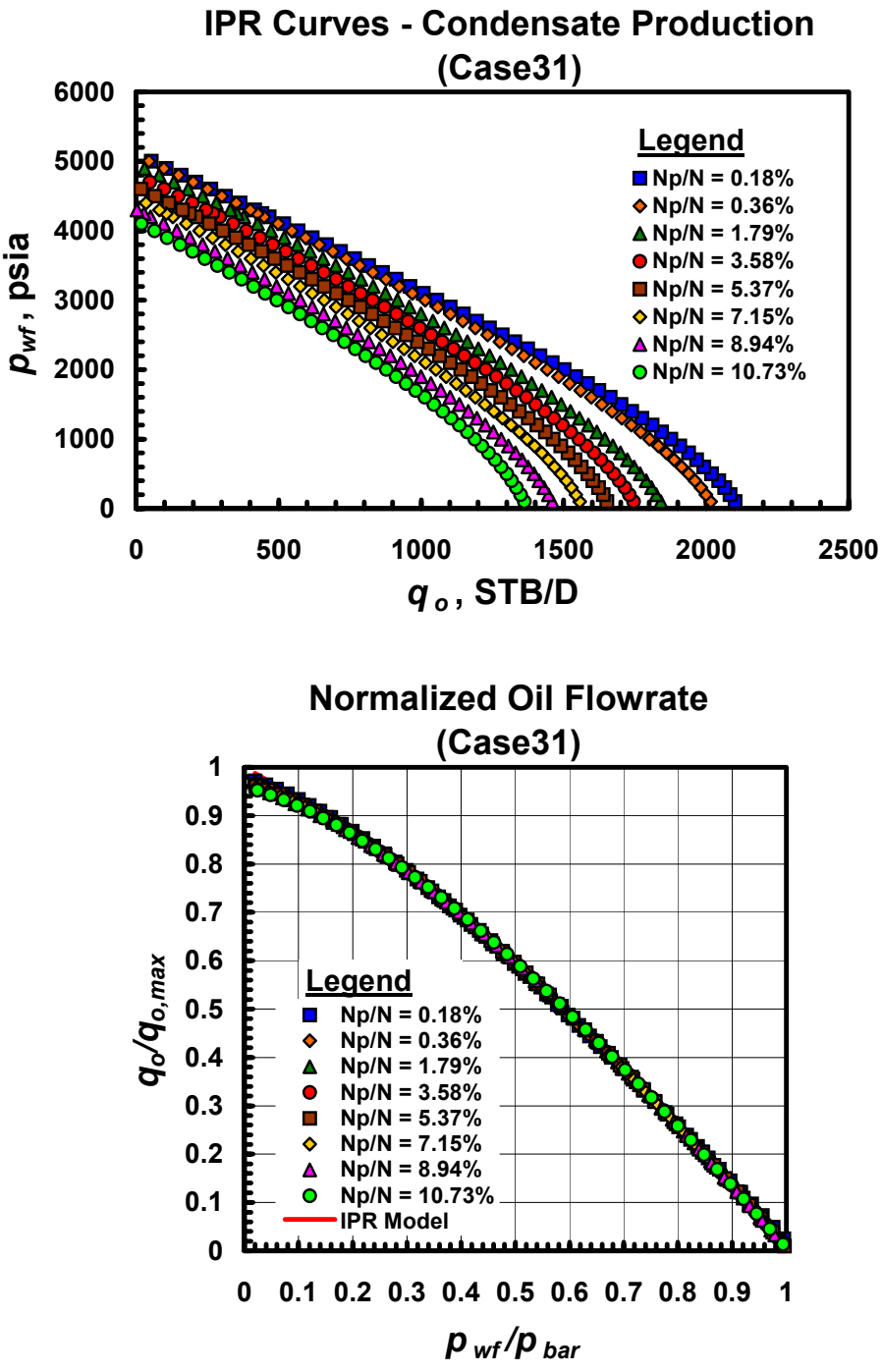

Fig. A.31.a — Dimensional and dimensionless IPR trends for Case 31 — gas condensate performance trends.

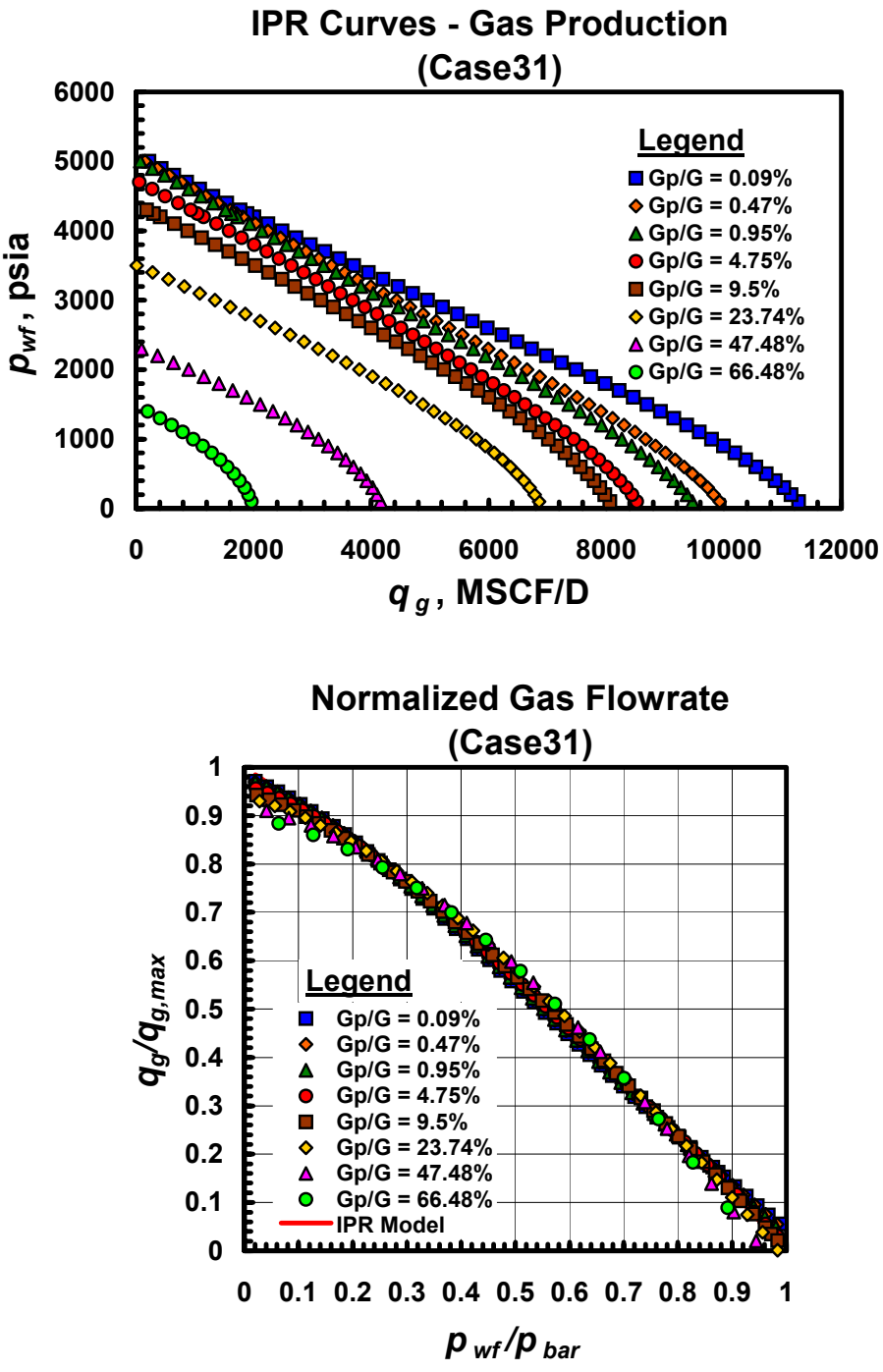

Fig. A.31.b — Dimensional and dimensionless IPR trends for Case 31 — gas performance trends.

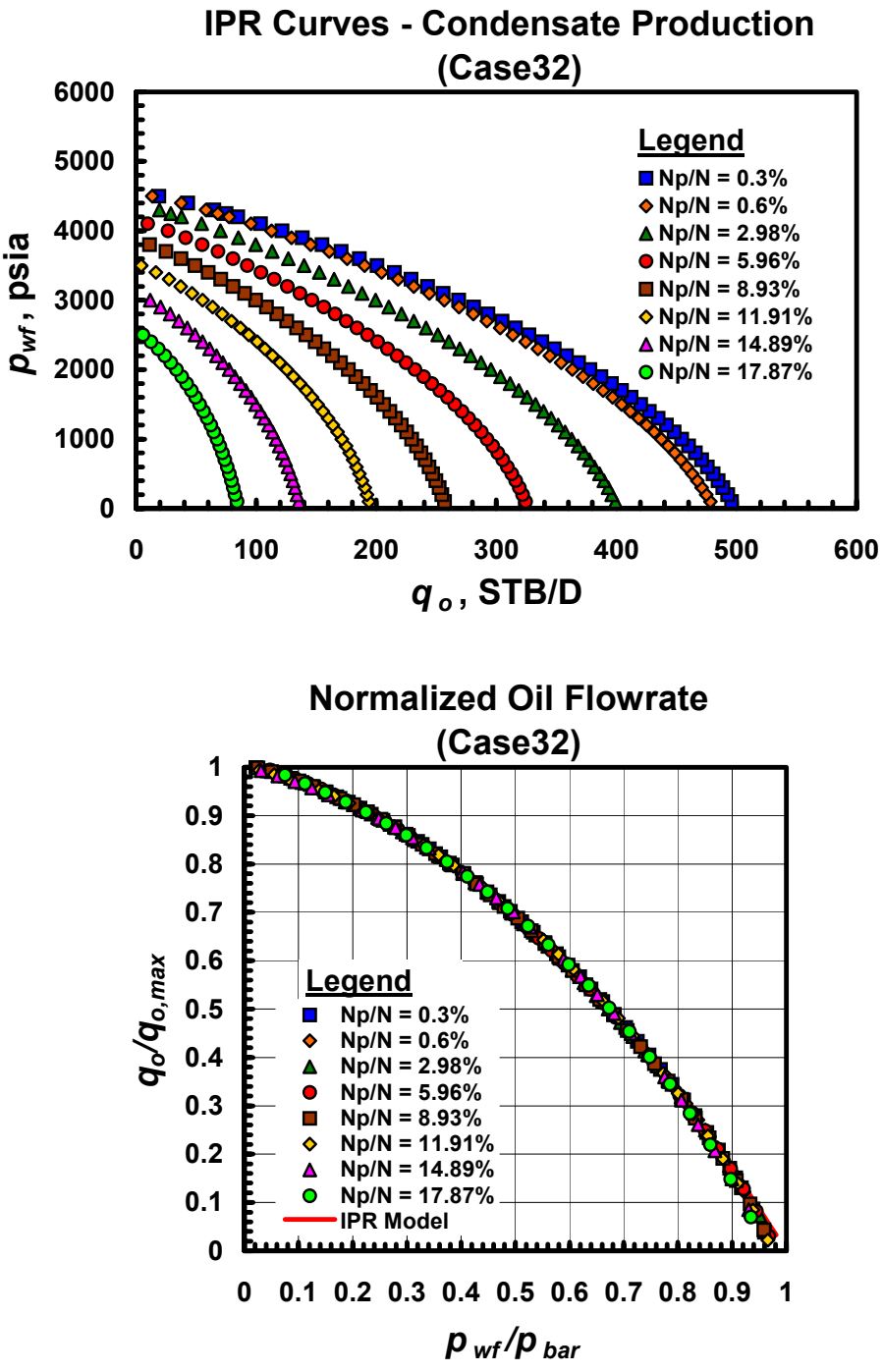

Fig. A.32.a — Dimensional and dimensionless IPR trends for Case 32 — gas condensate performance trends.

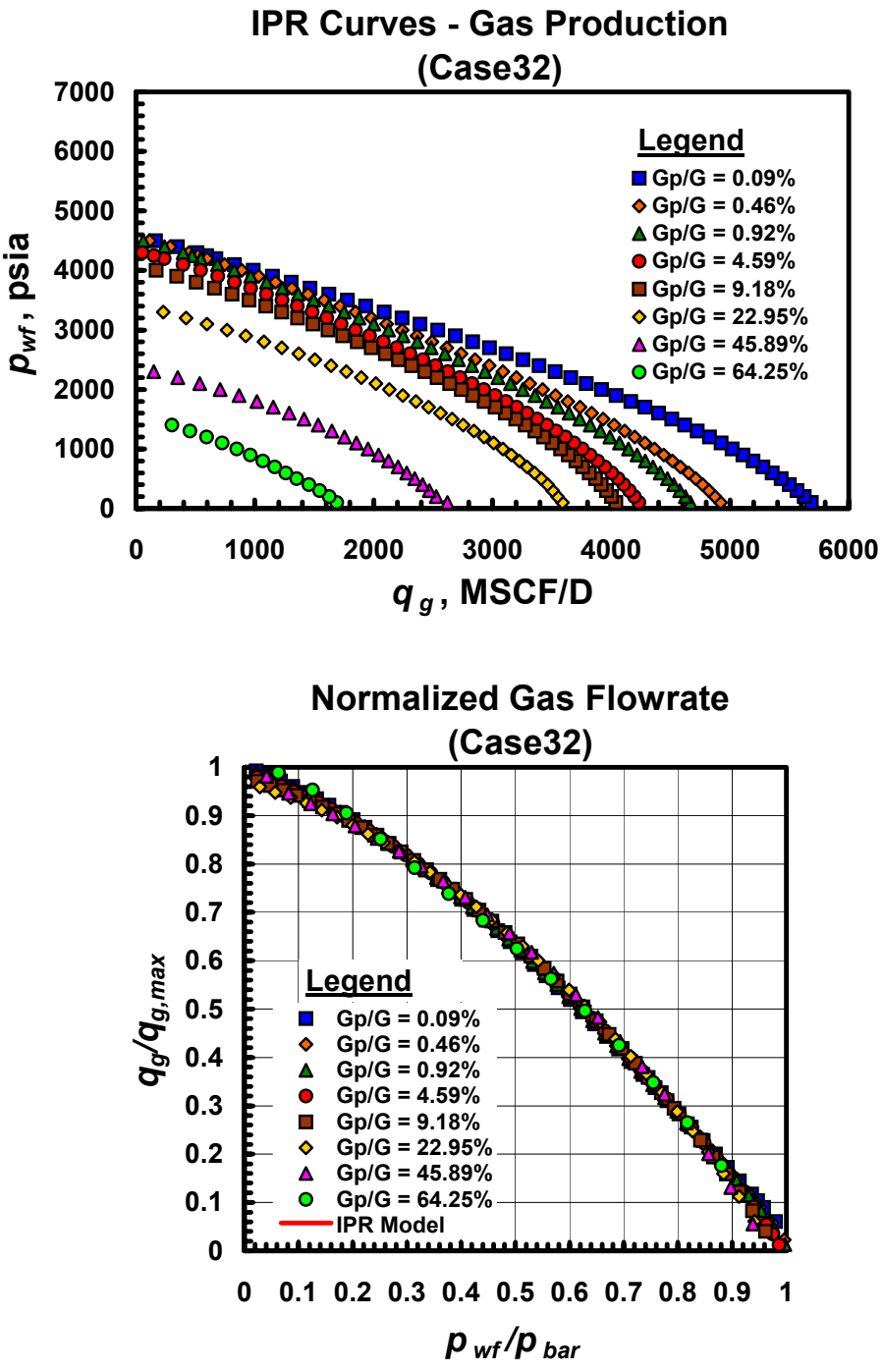

Fig. A.32.b — Dimensional and dimensionless IPR trends for Case 32 — gas performance trends.

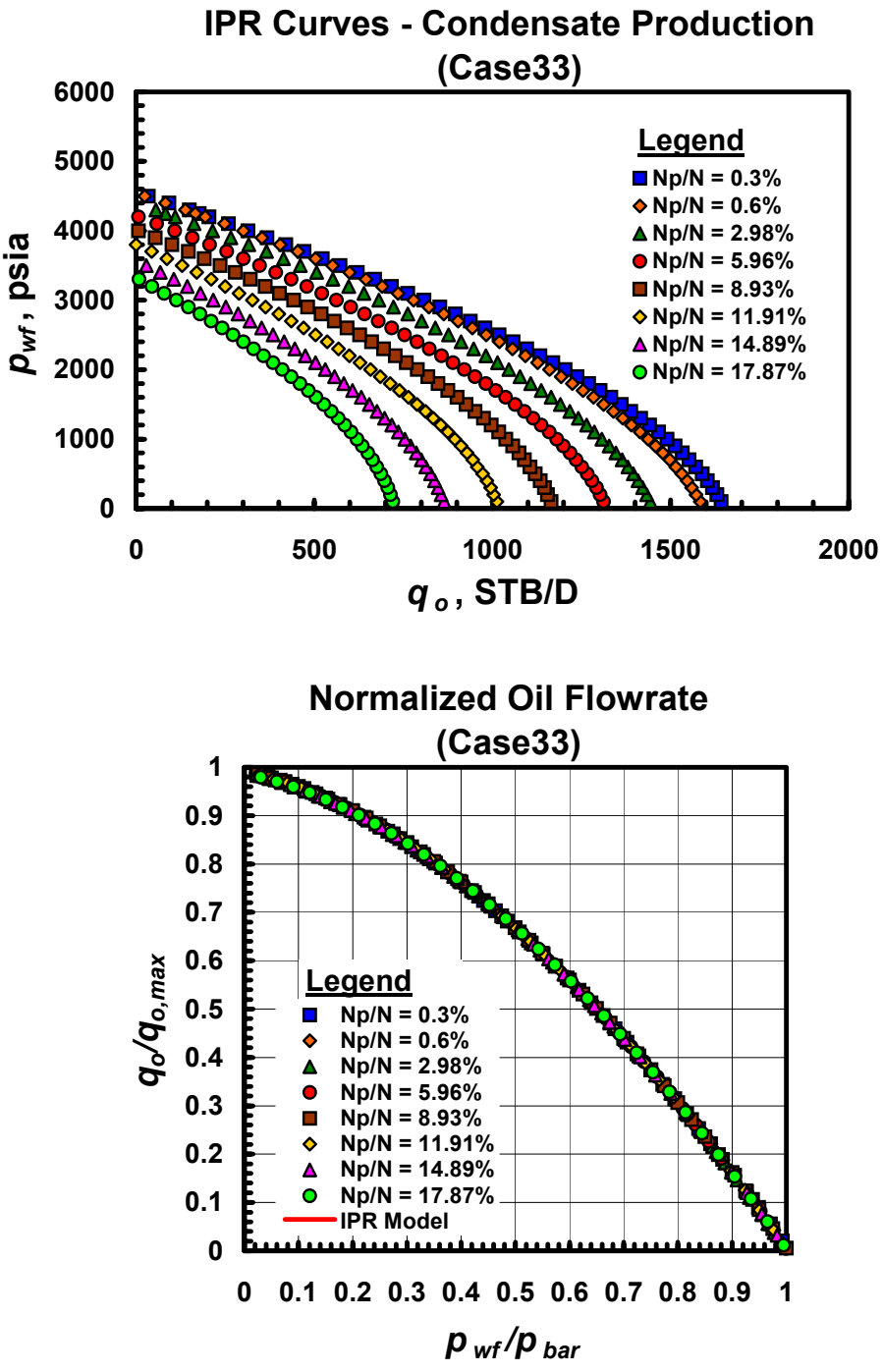

Fig. A.33.a — Dimensional and dimensionless IPR trends for Case 33 — gas condensate performance trends.

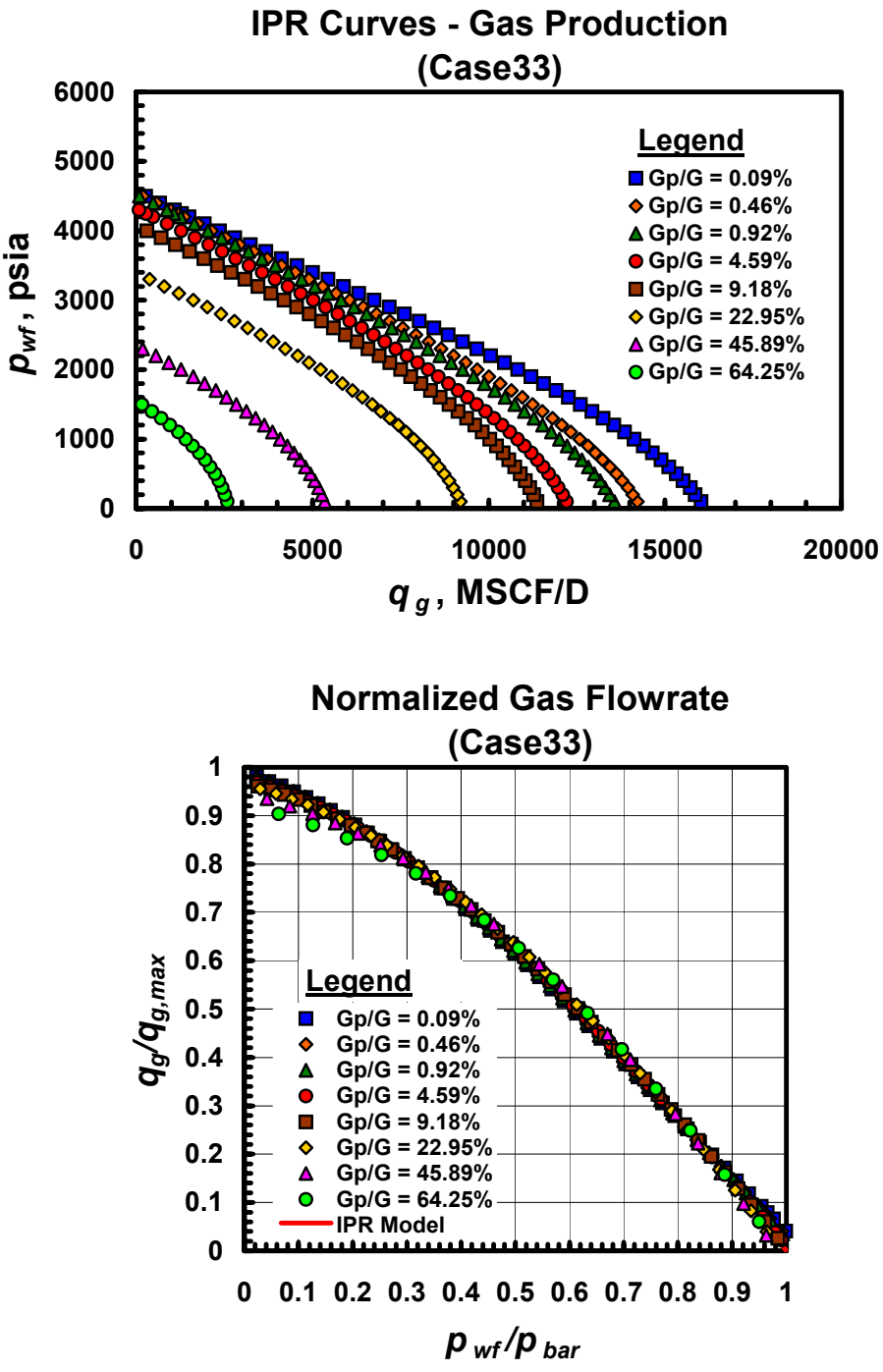

Fig. A.33.b — Dimensional and dimensionless IPR trends for Case 33 — gas performance trends.

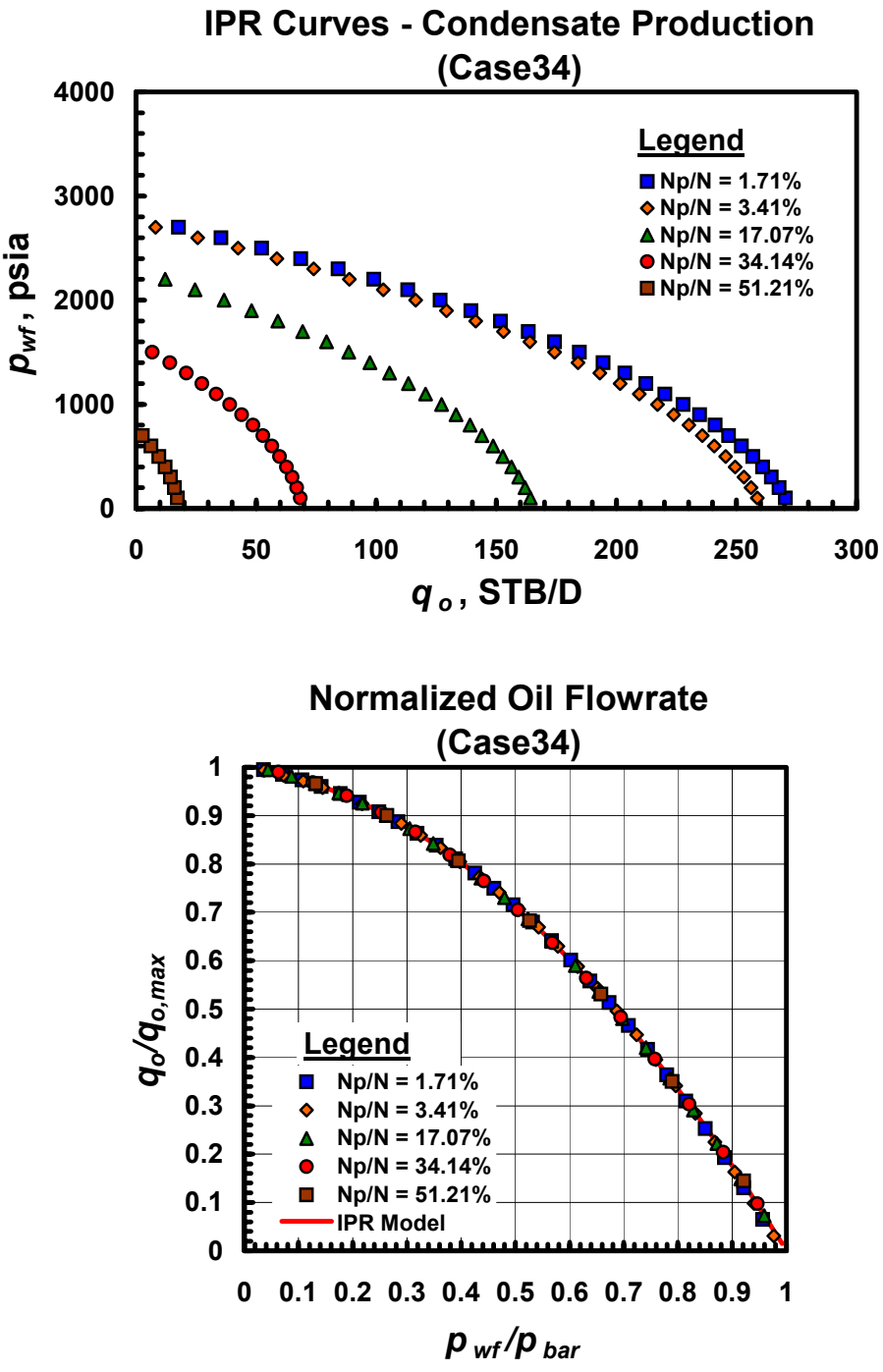

Fig. A.34.a — Dimensional and dimensionless IPR trends for Case 34 — gas condensate performance trends.

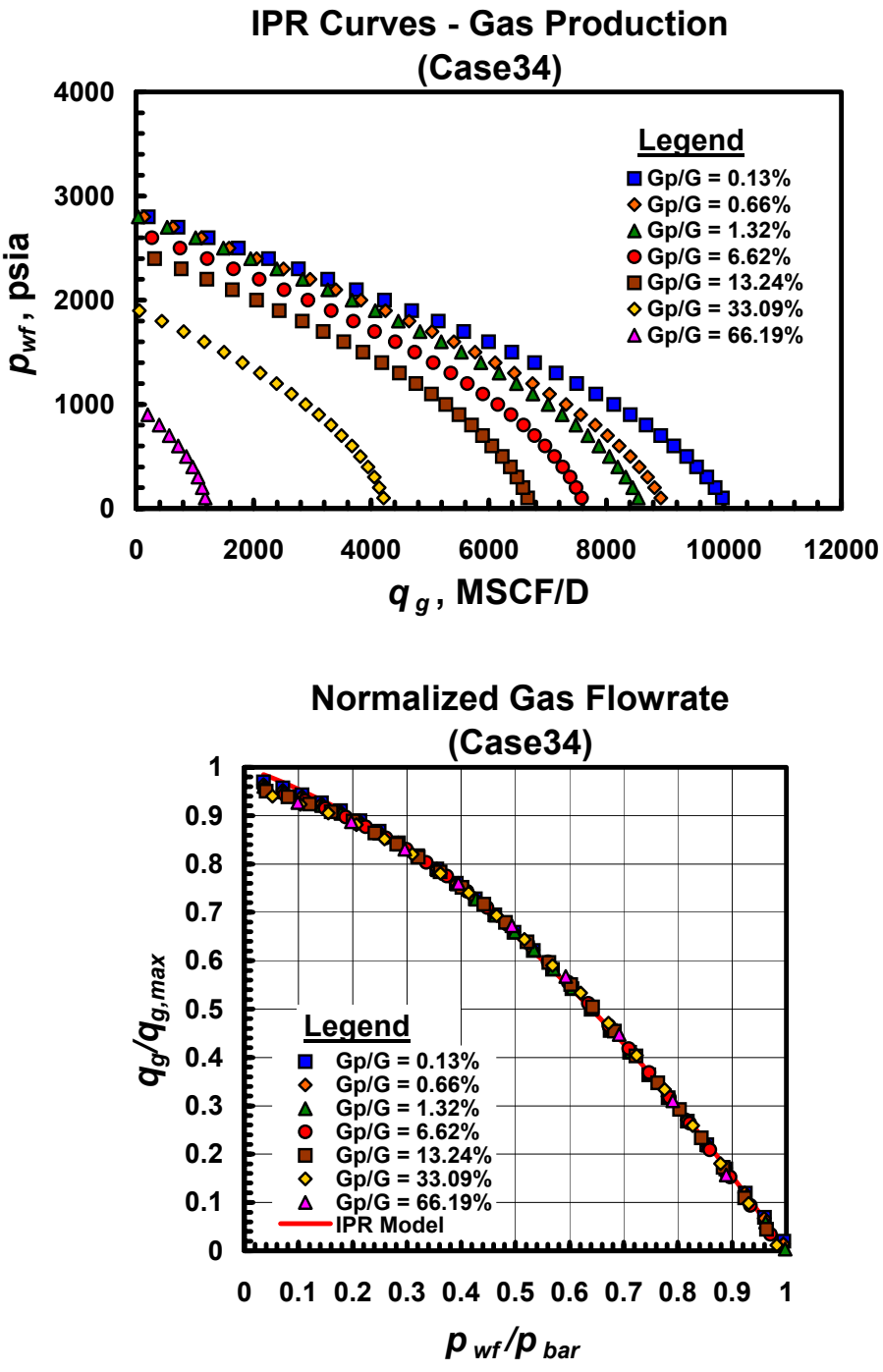

Fig. A.34.b — Dimensional and dimensionless IPR trends for Case 34 — gas performance trends.

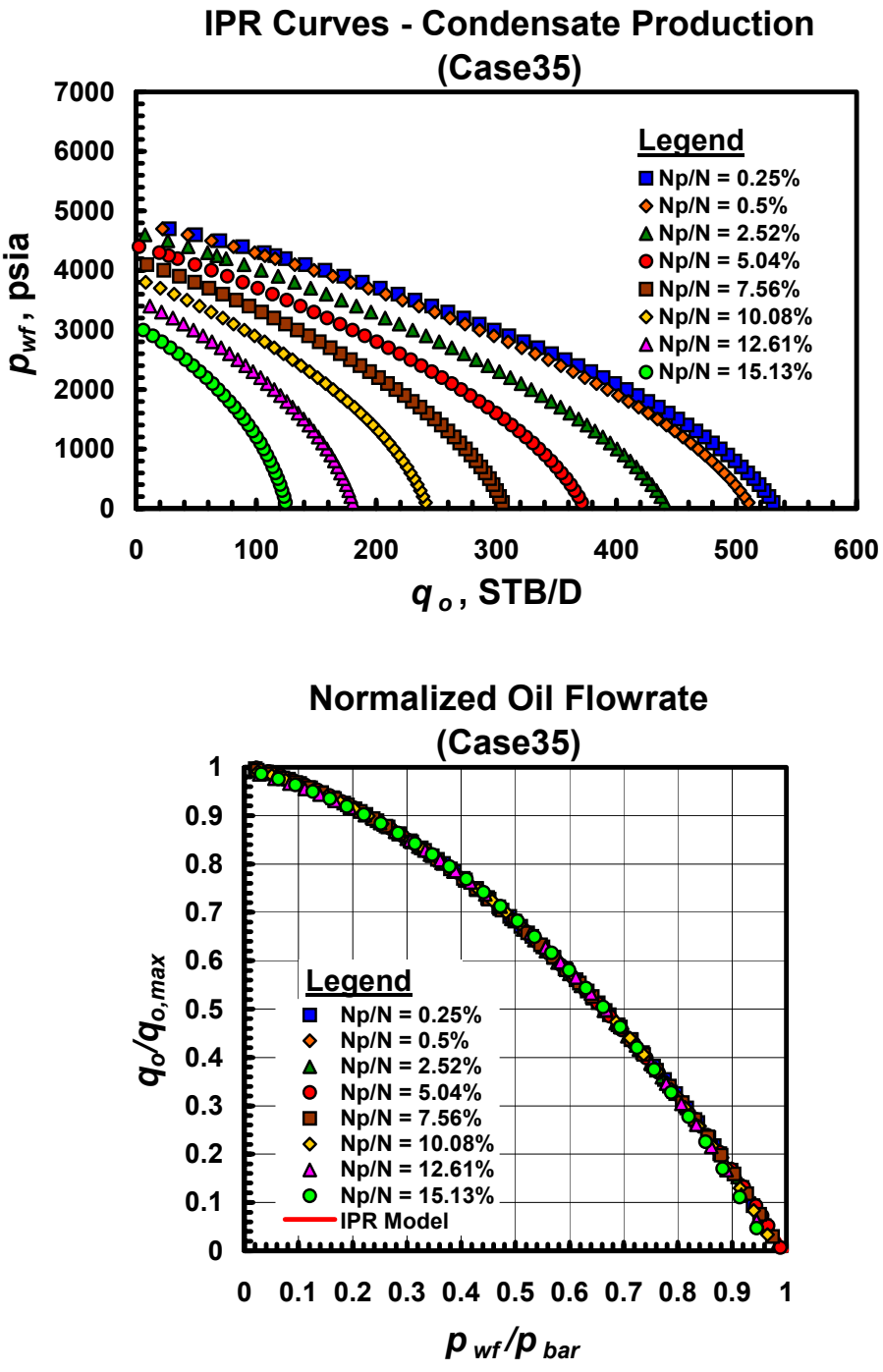

Fig. A.35.a — Dimensional and dimensionless IPR trends for Case 35 — gas condensate performance trends.

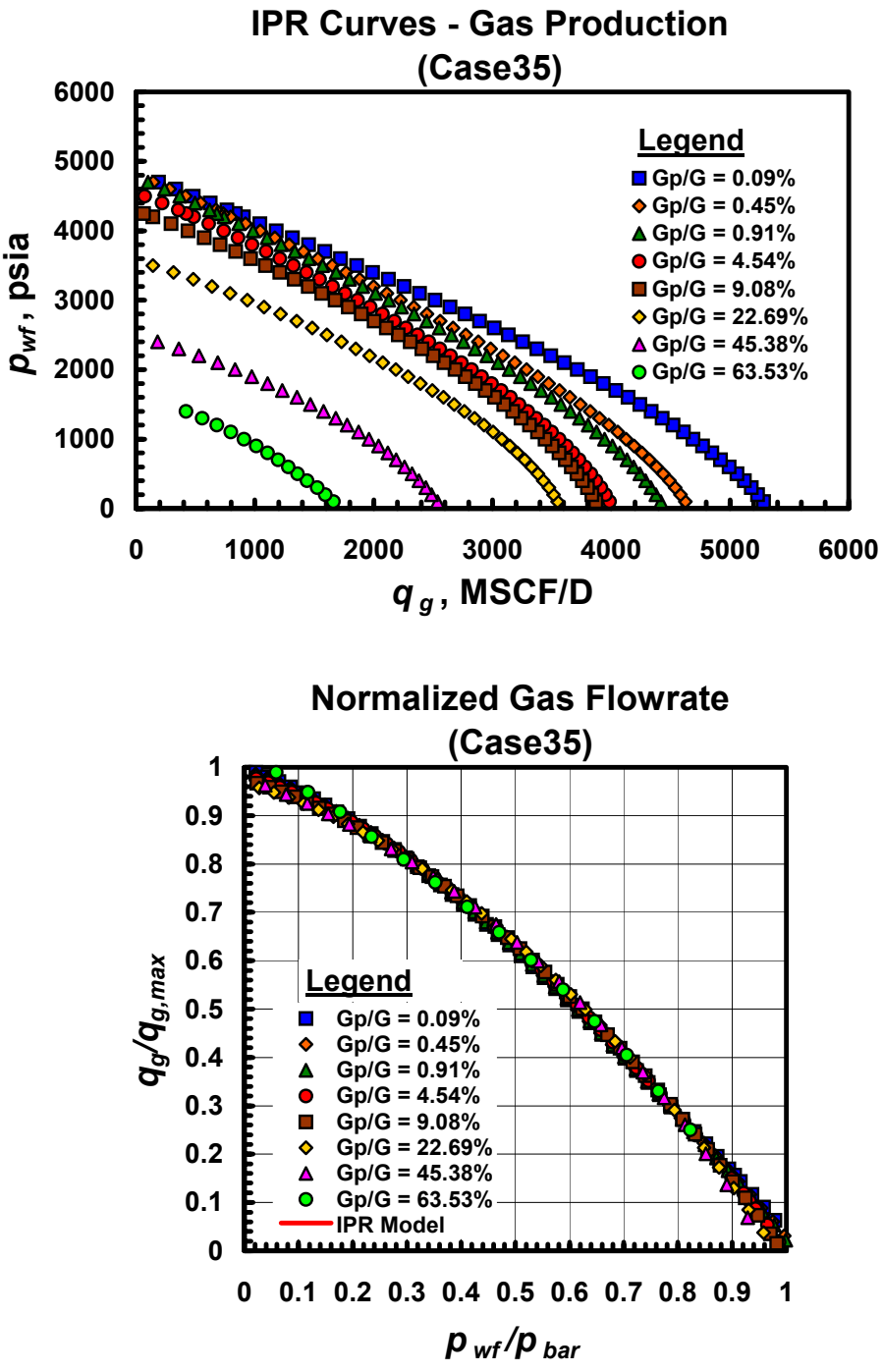

Fig. A.35.b — Dimensional and dimensionless IPR trends for Case 35 — gas performance trends.

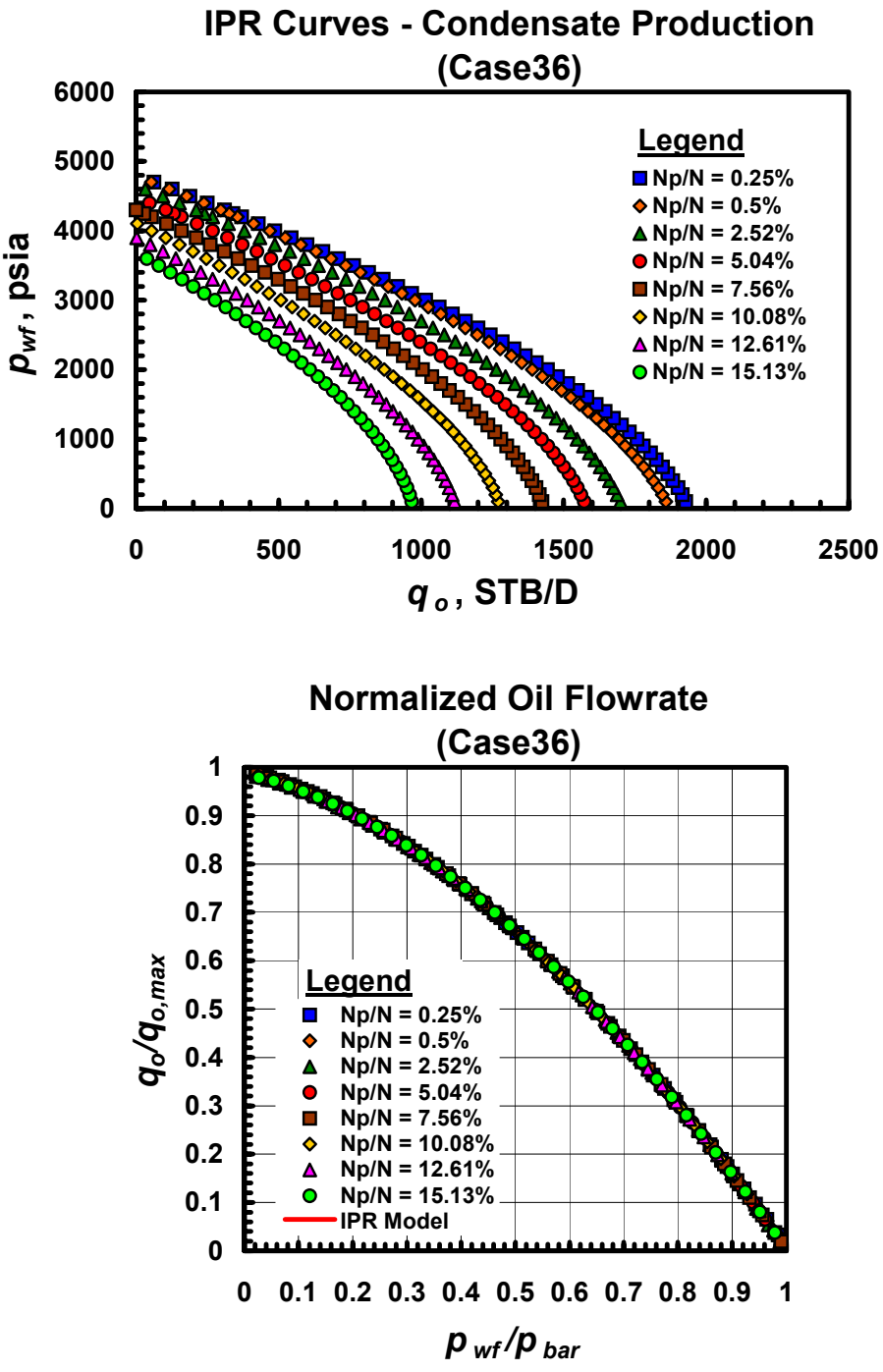

Fig. A.36.a — Dimensional and dimensionless IPR trends for Case 36 — gas condensate performance trends.

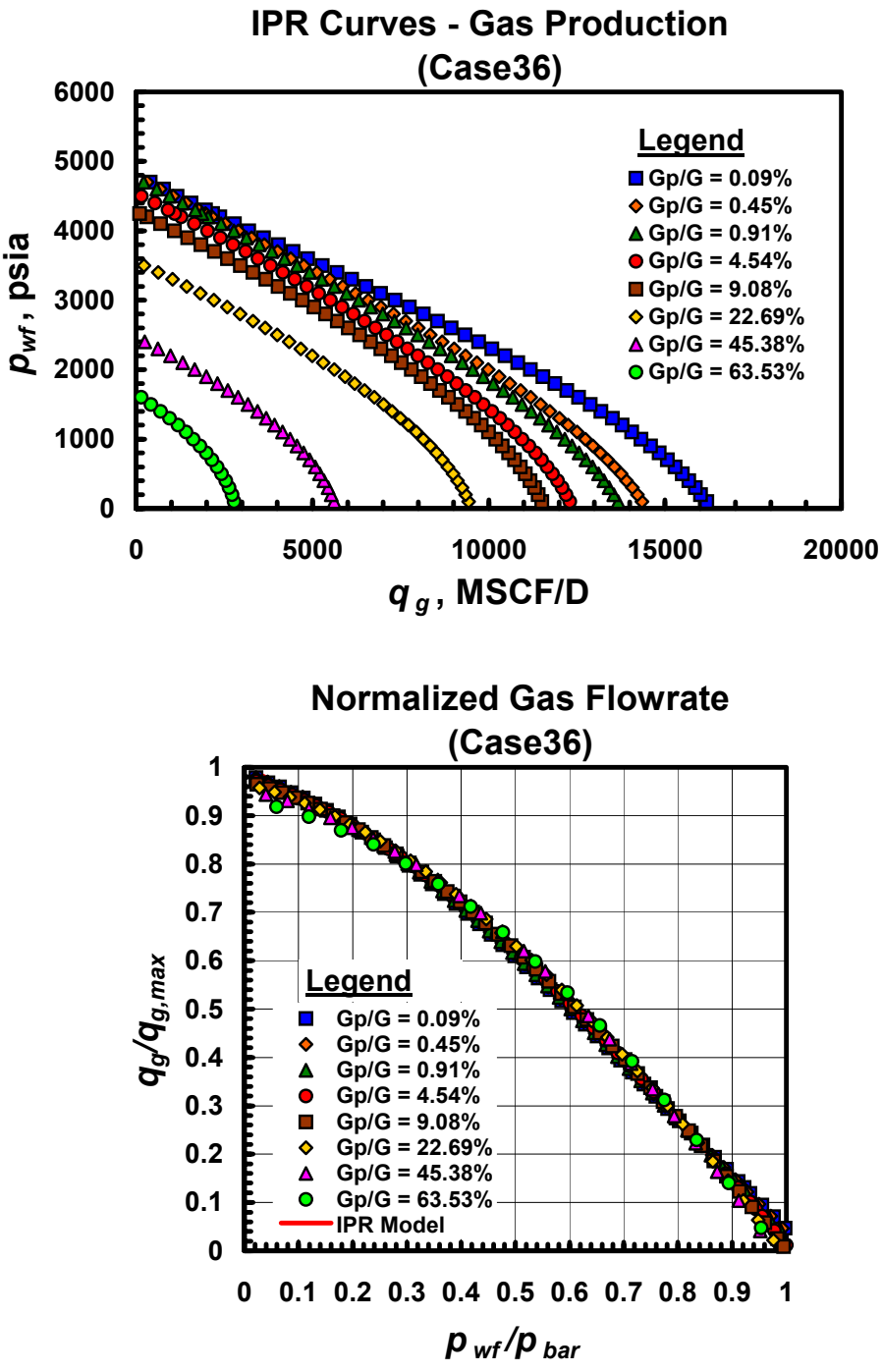

Fig. A.36.b — Dimensional and dimensionless IPR trends for Case 36 — gas performance trends.

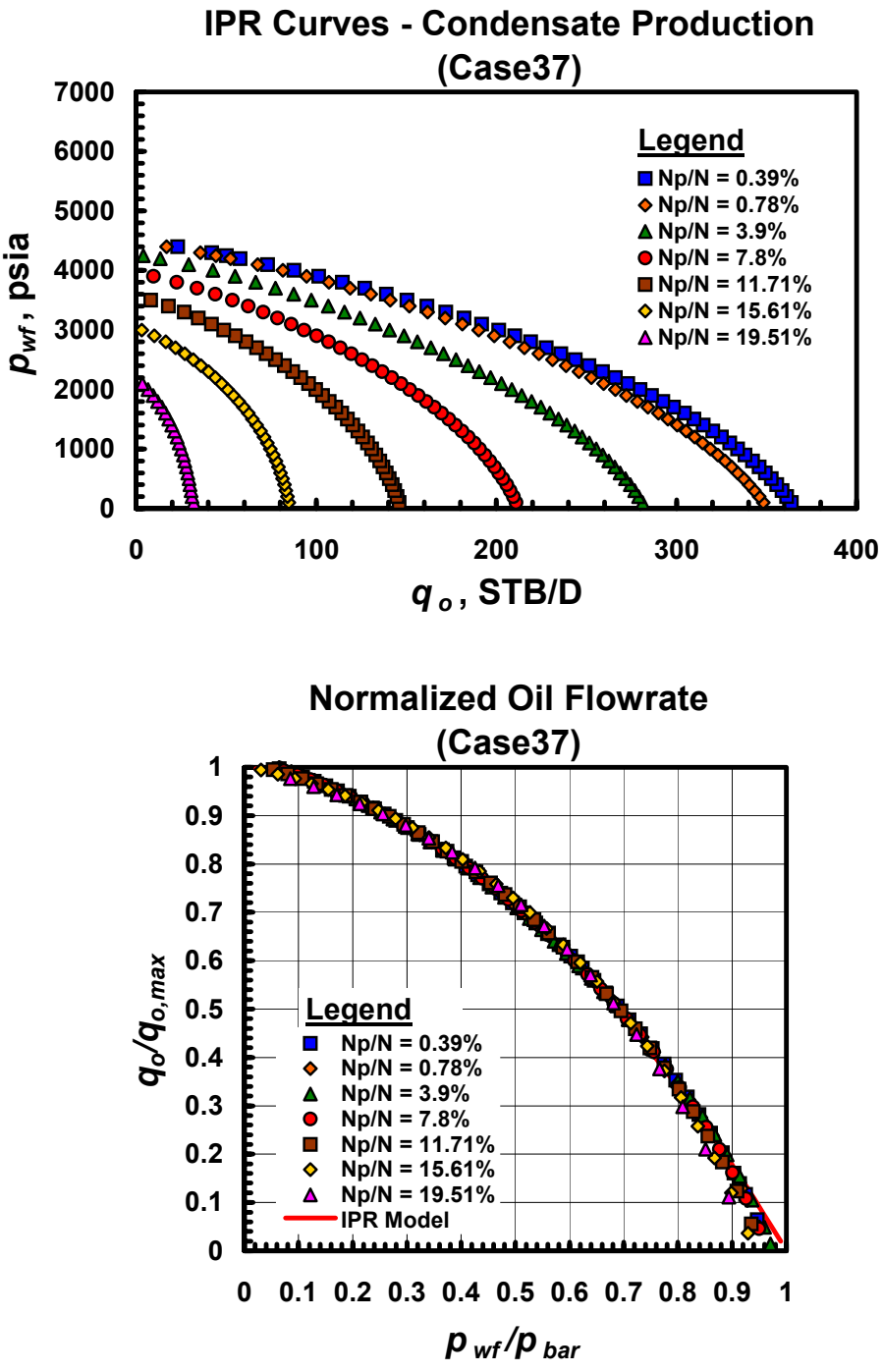

Fig. A.37.a — Dimensional and dimensionless IPR trends for Case 37 — gas condensate performance trends.

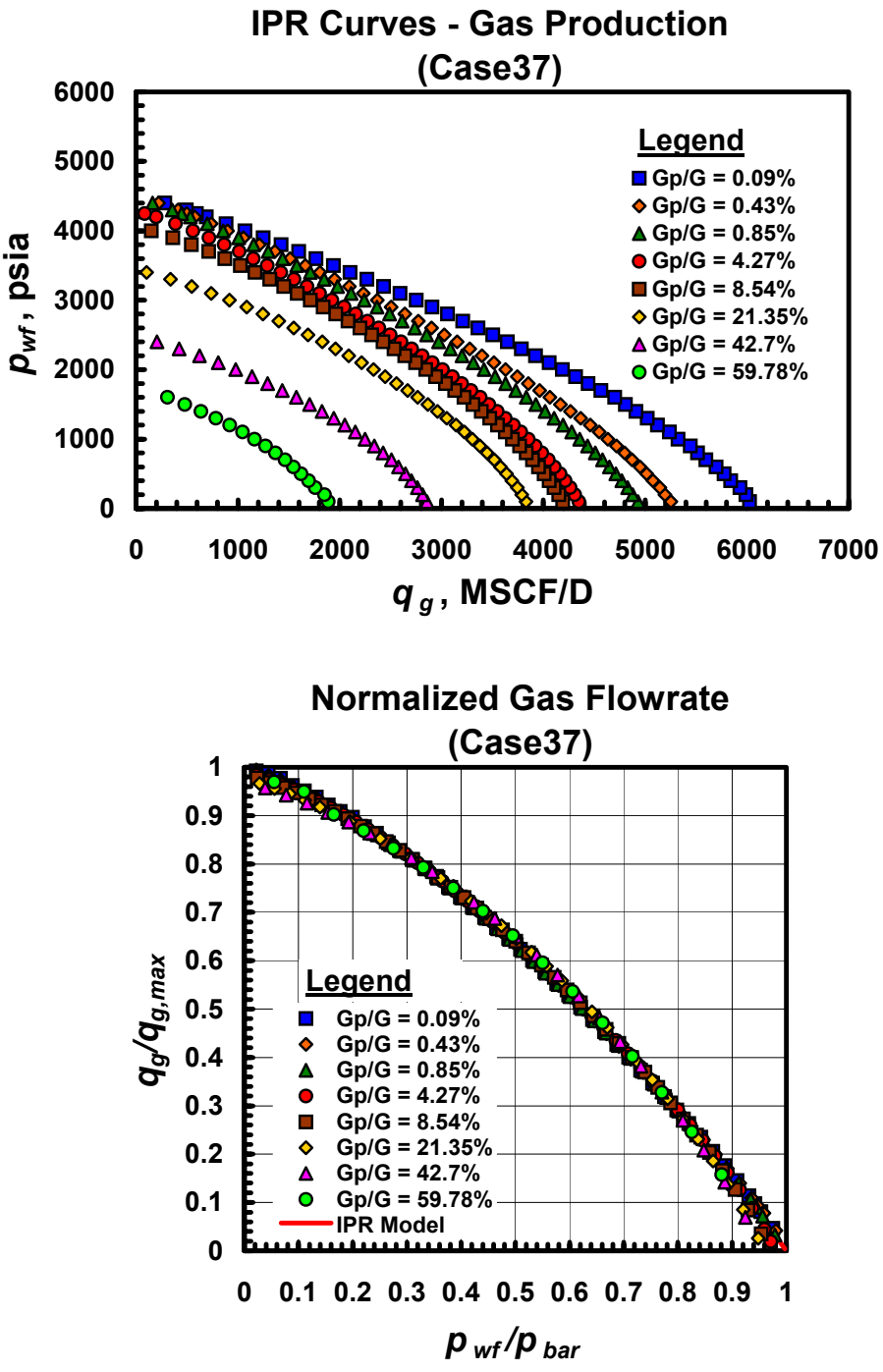

Fig. A.37.b — Dimensional and dimensionless IPR trends for Case 37 — gas performance trends.

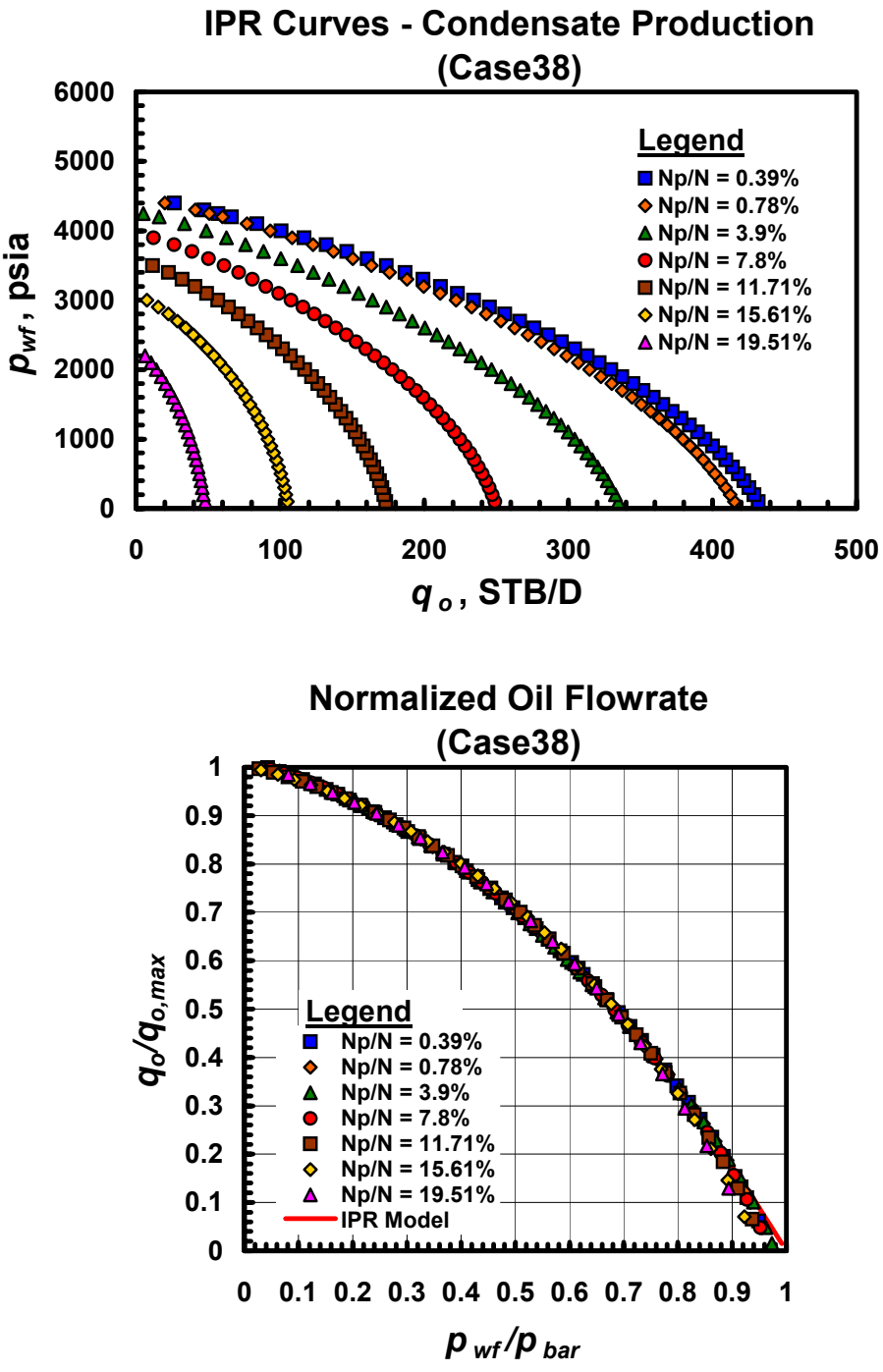

Fig. A.38.a — Dimensional and dimensionless IPR trends for Case 38 — gas condensate performance trends.

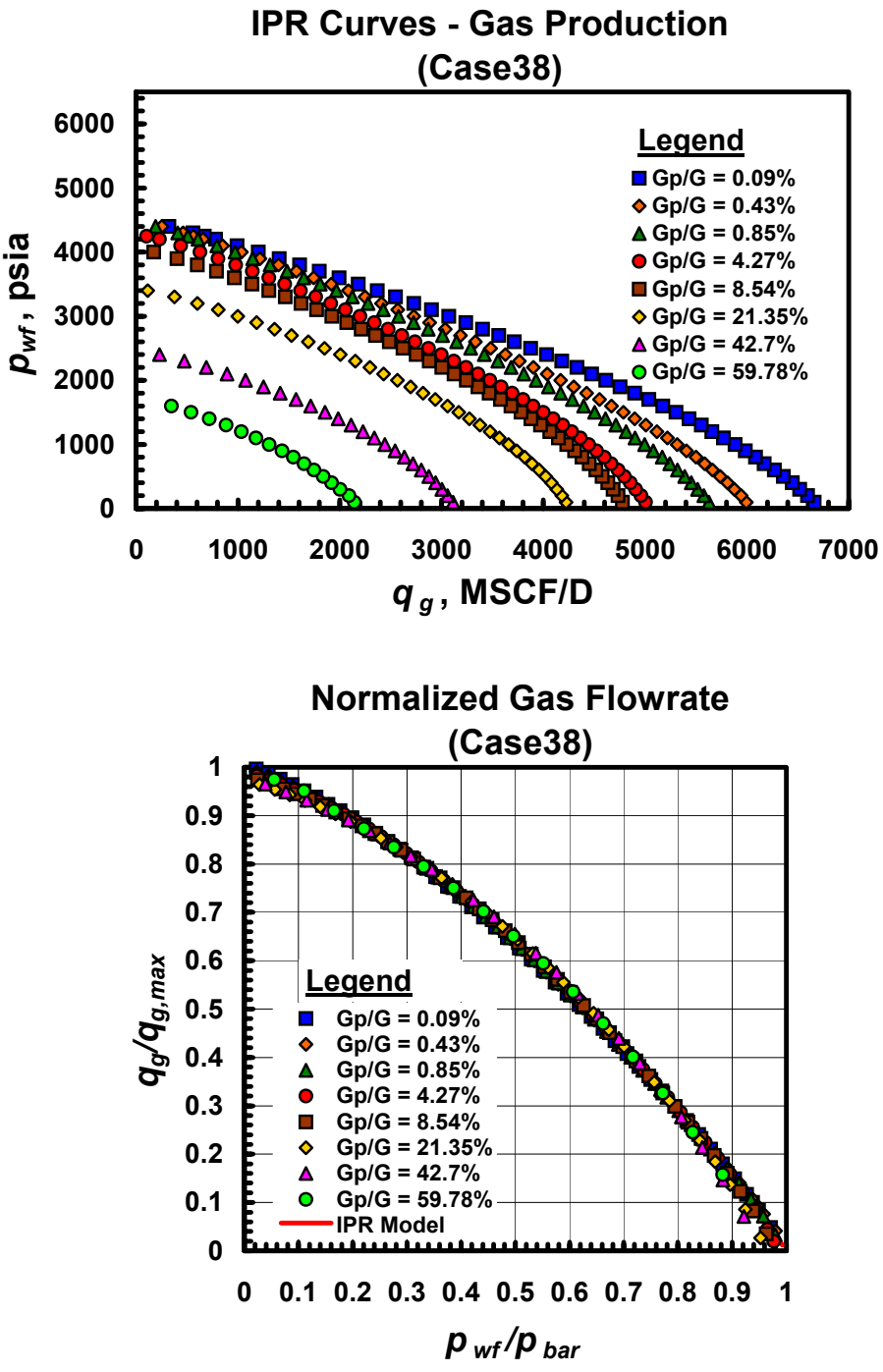

Fig. A.38.b — Dimensional and dimensionless IPR trends for Case 38 — gas performance trends.

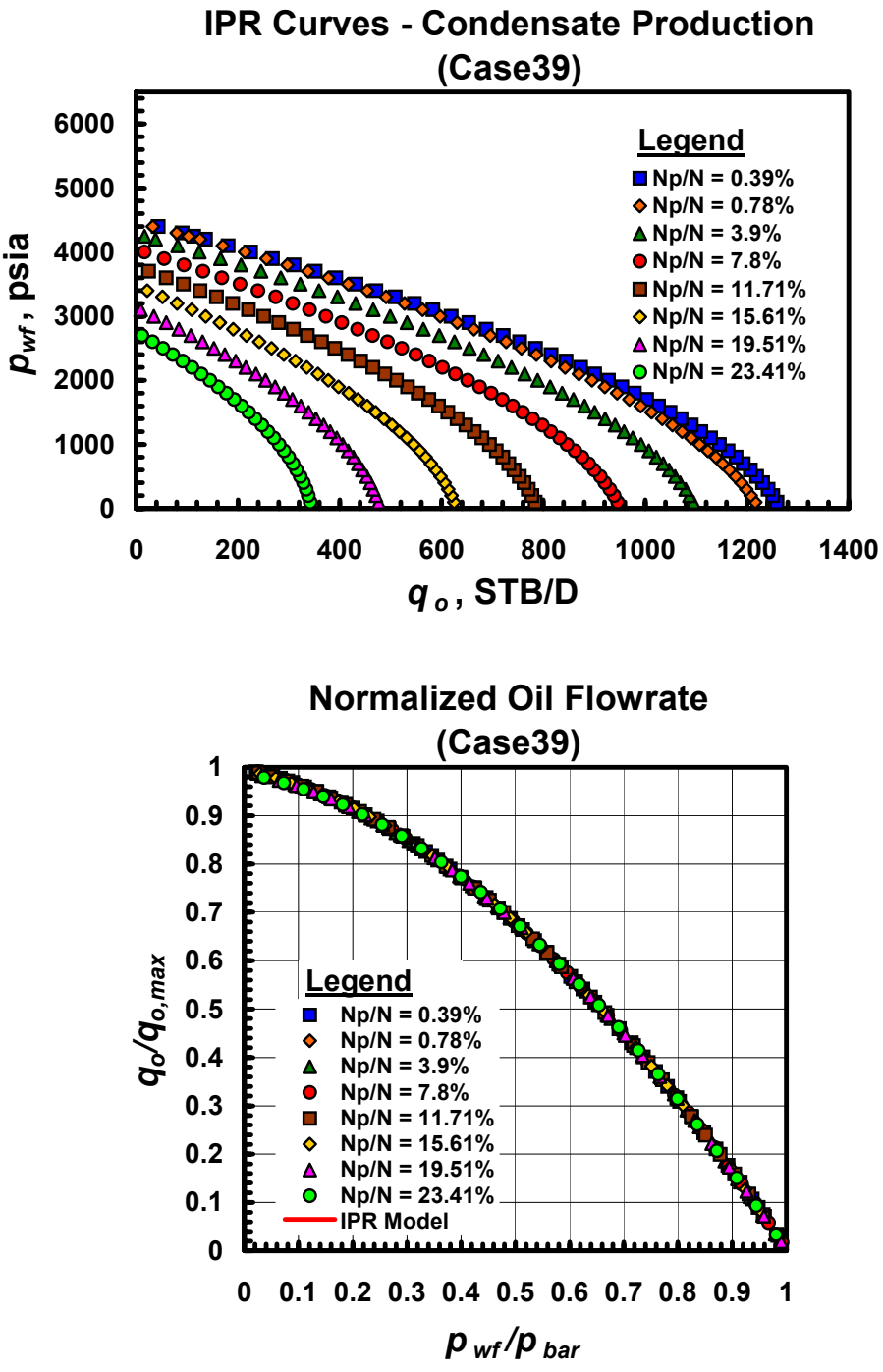

Fig. A.39.a — Dimensional and dimensionless IPR trends for Case 39 — gas condensate performance trends.

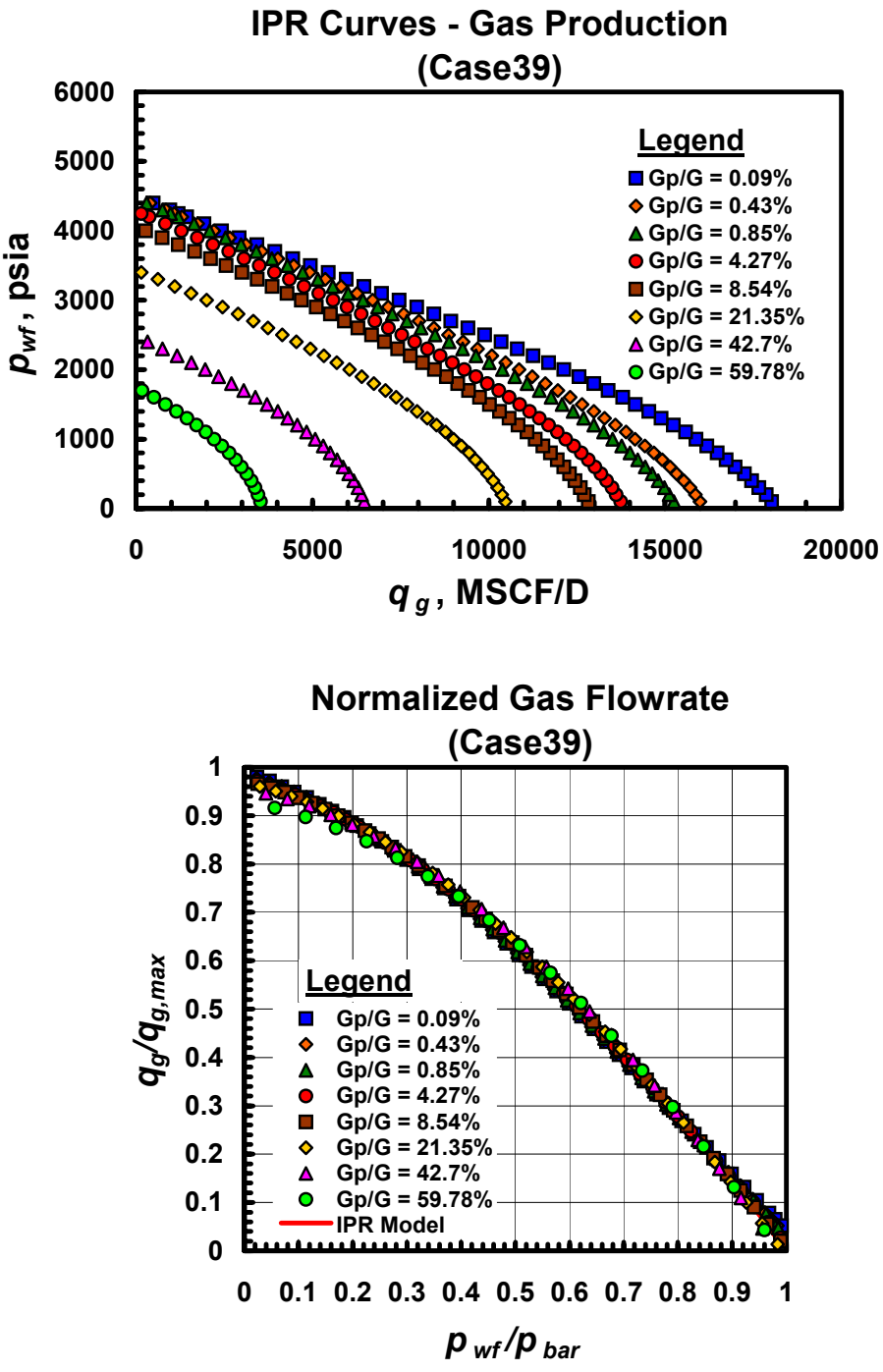

Fig. A.39.b — Dimensional and dimensionless IPR trends for Case 39 — gas performance trends.

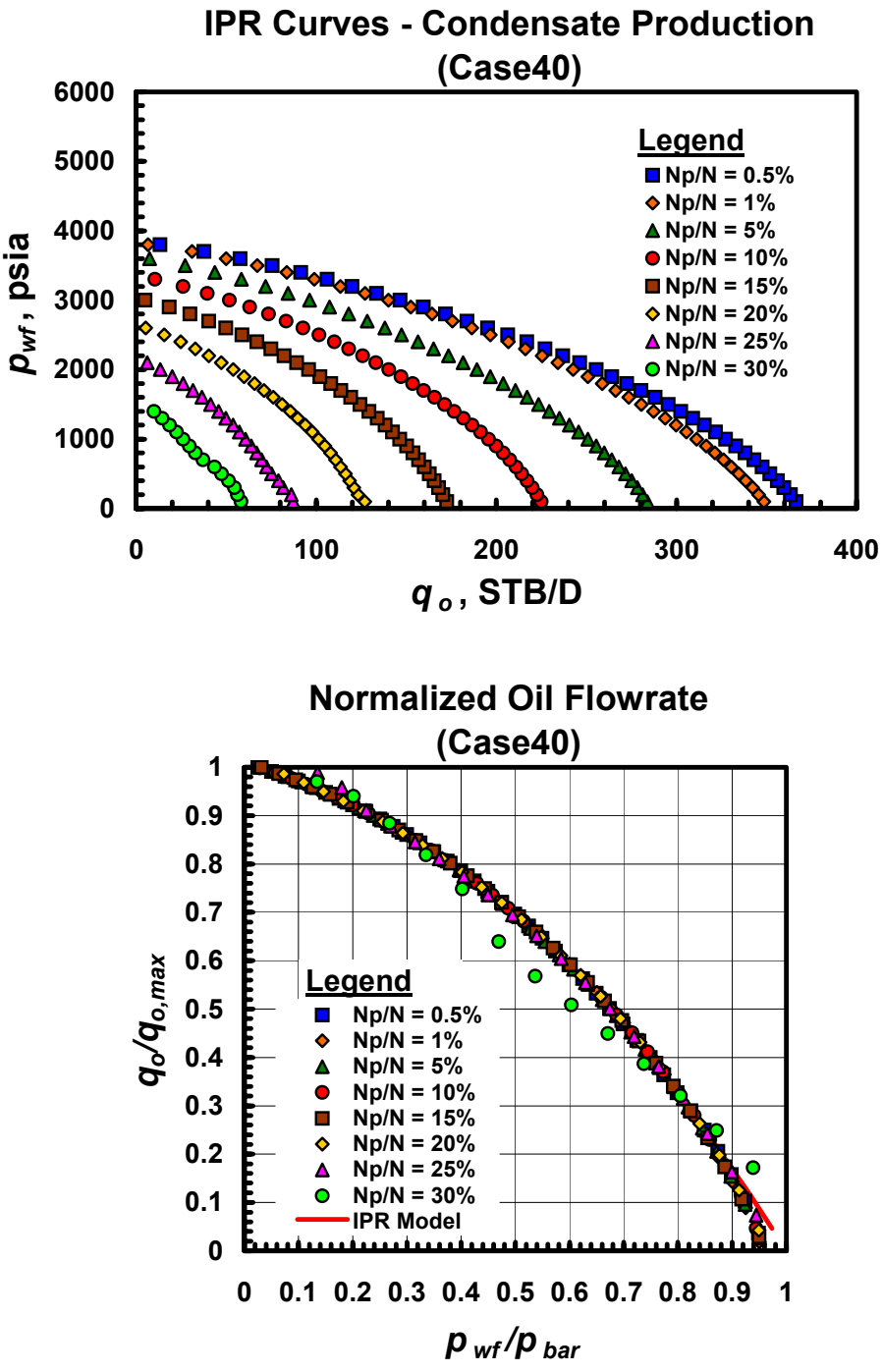

Fig. A.40.a — Dimensional and dimensionless IPR trends for Case 40 — gas condensate performance trends.

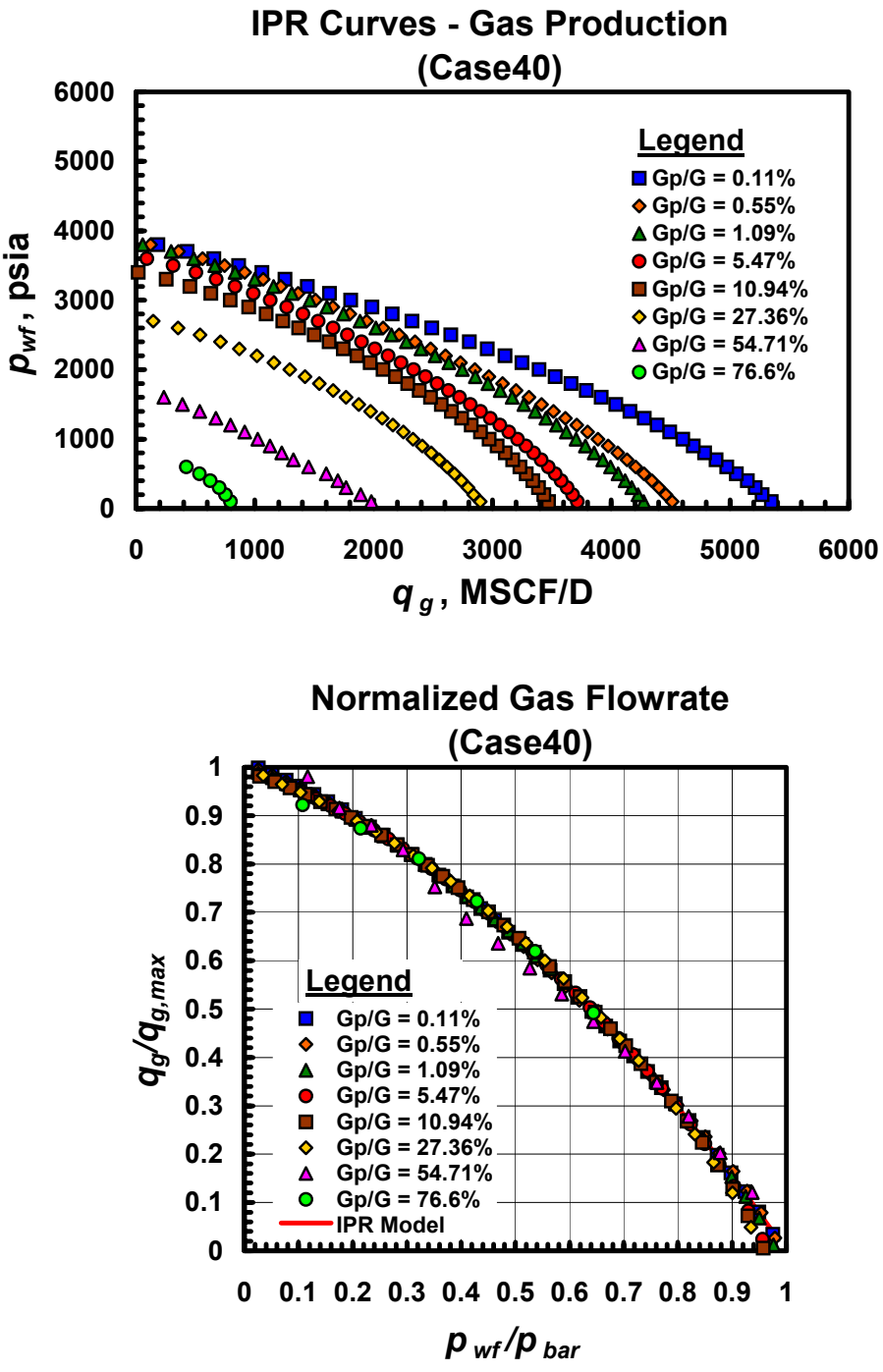

Fig. A.40.b — Dimensional and dimensionless IPR trends for Case 40 — gas performance trends.

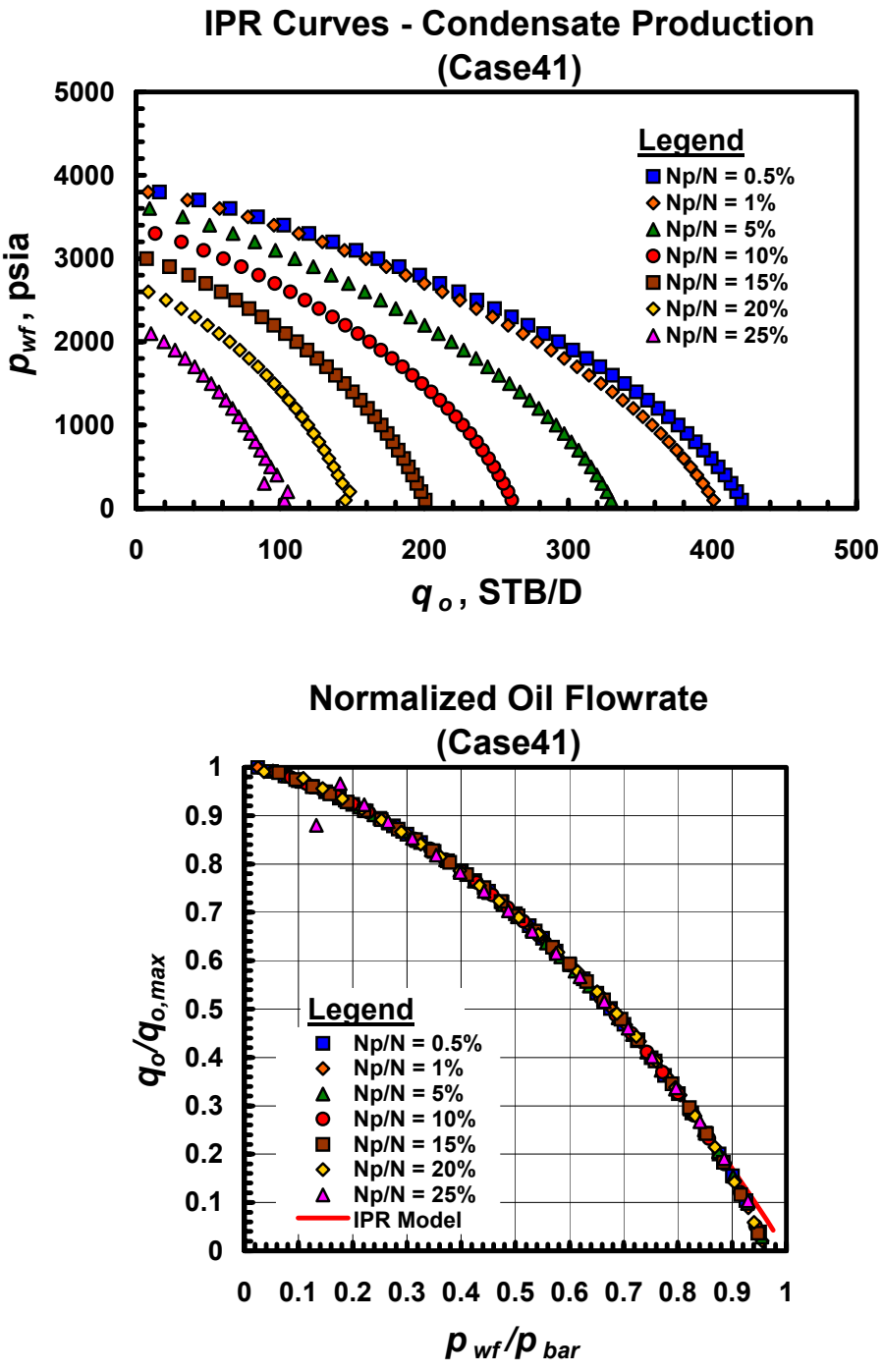

Fig. A.41.a — Dimensional and dimensionless IPR trends for Case 41 — gas condensate performance trends.

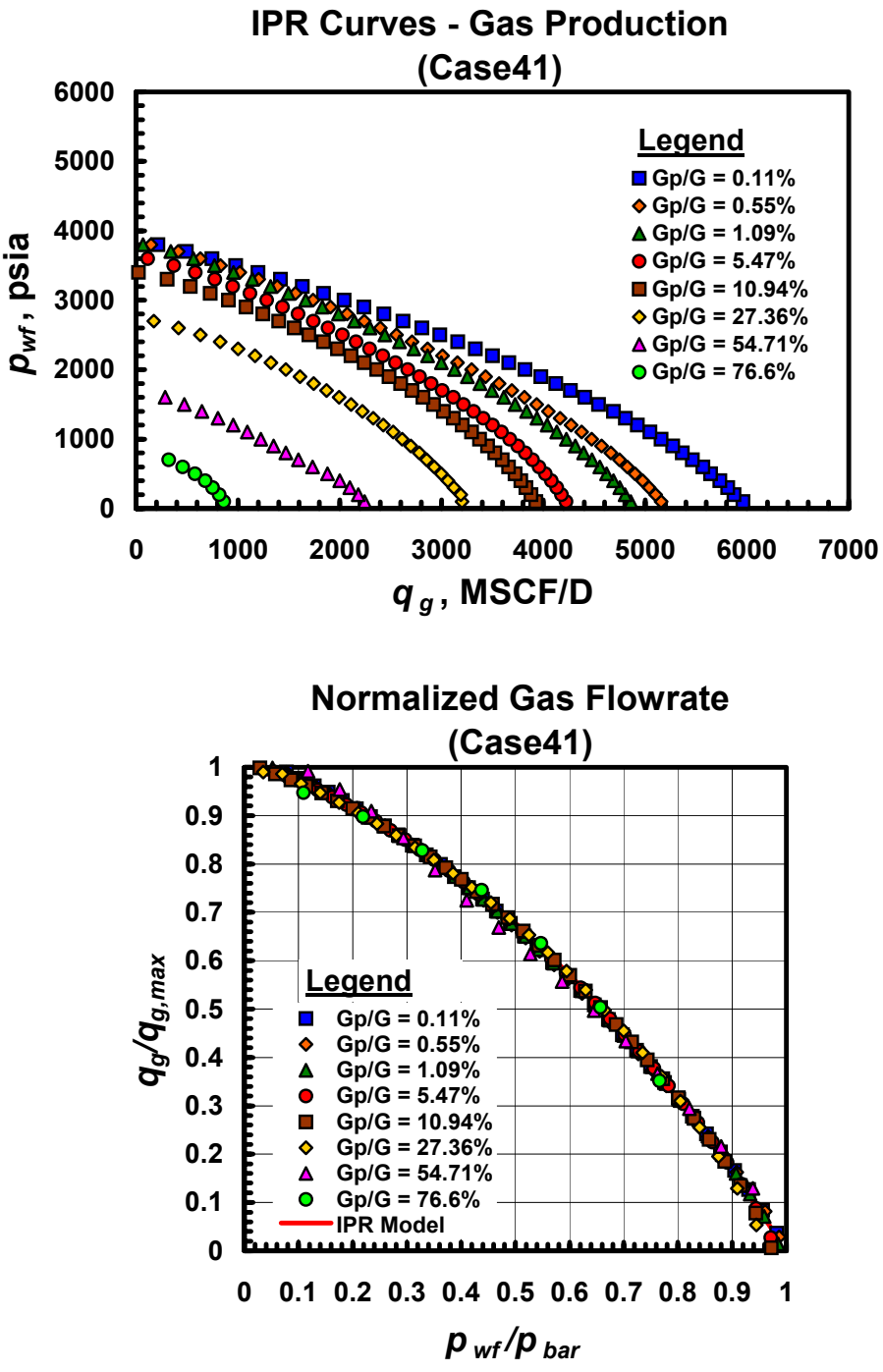

Fig. A.41.b — Dimensional and dimensionless IPR trends for Case 41 — gas performance trends.

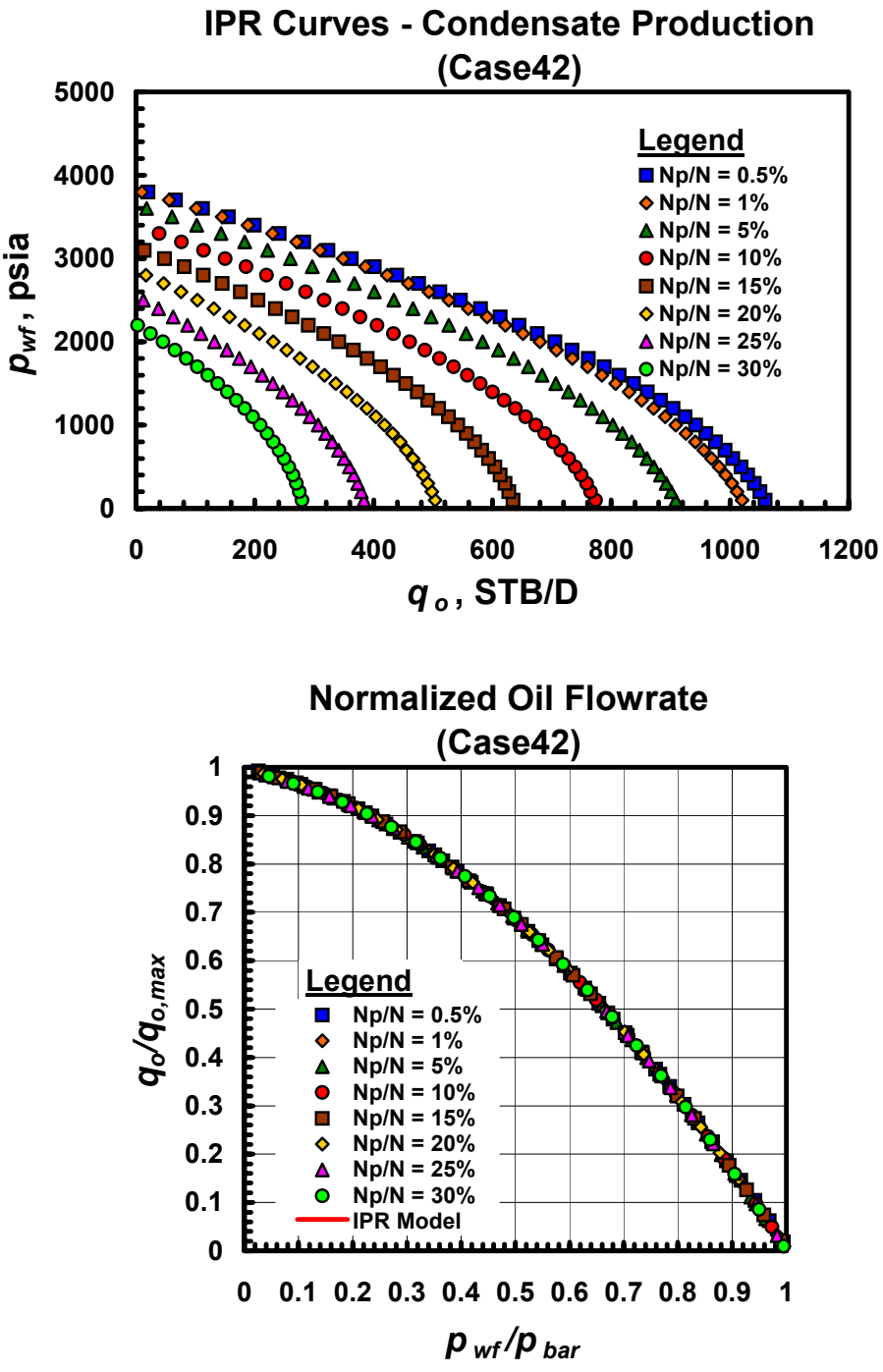

Fig. A.42.a — Dimensional and dimensionless IPR trends for Case 42 — gas condensate performance trends.

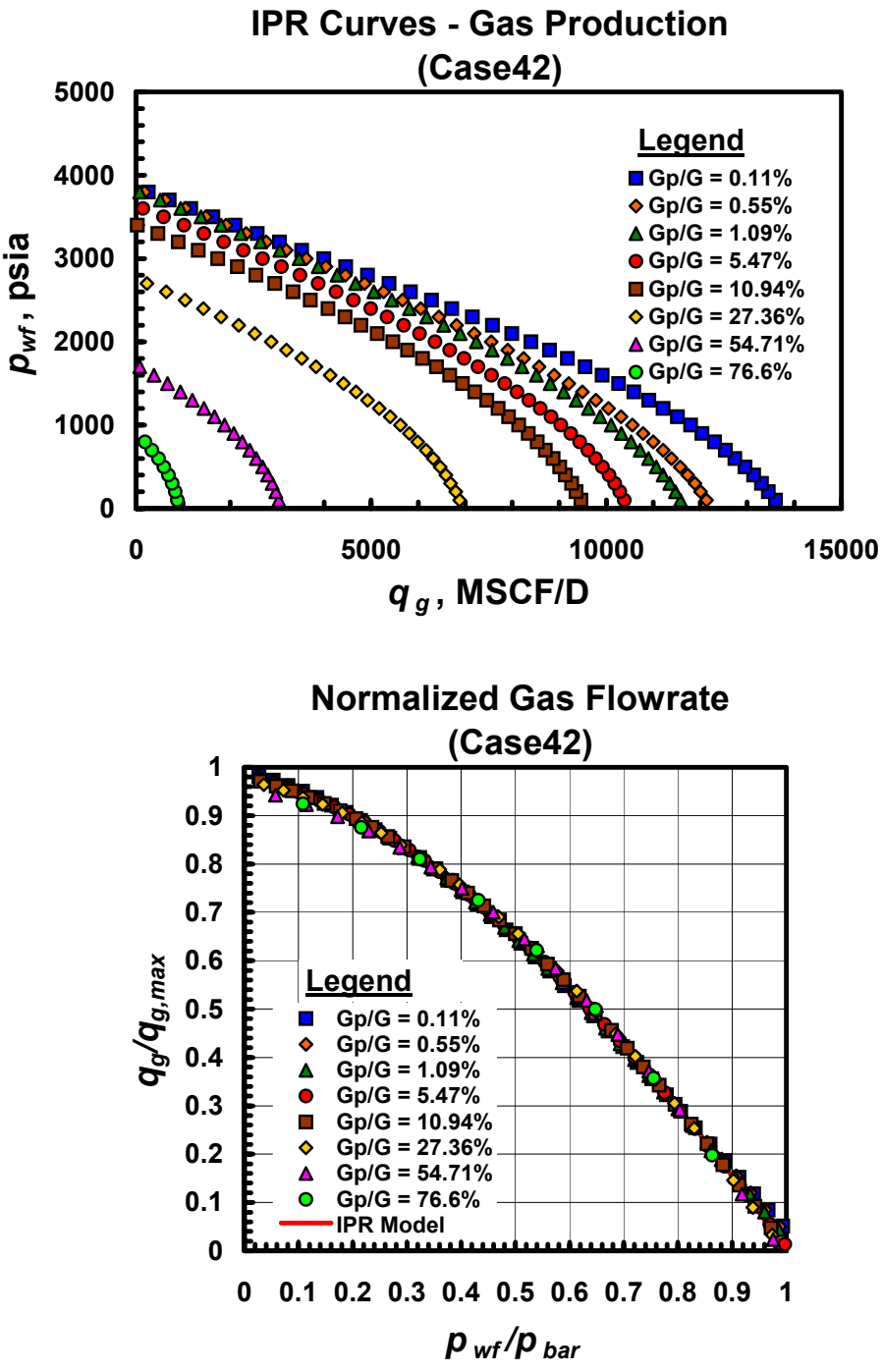

Fig. A.42.b — Dimensional and dimensionless IPR trends for Case 42 — gas performance trends.

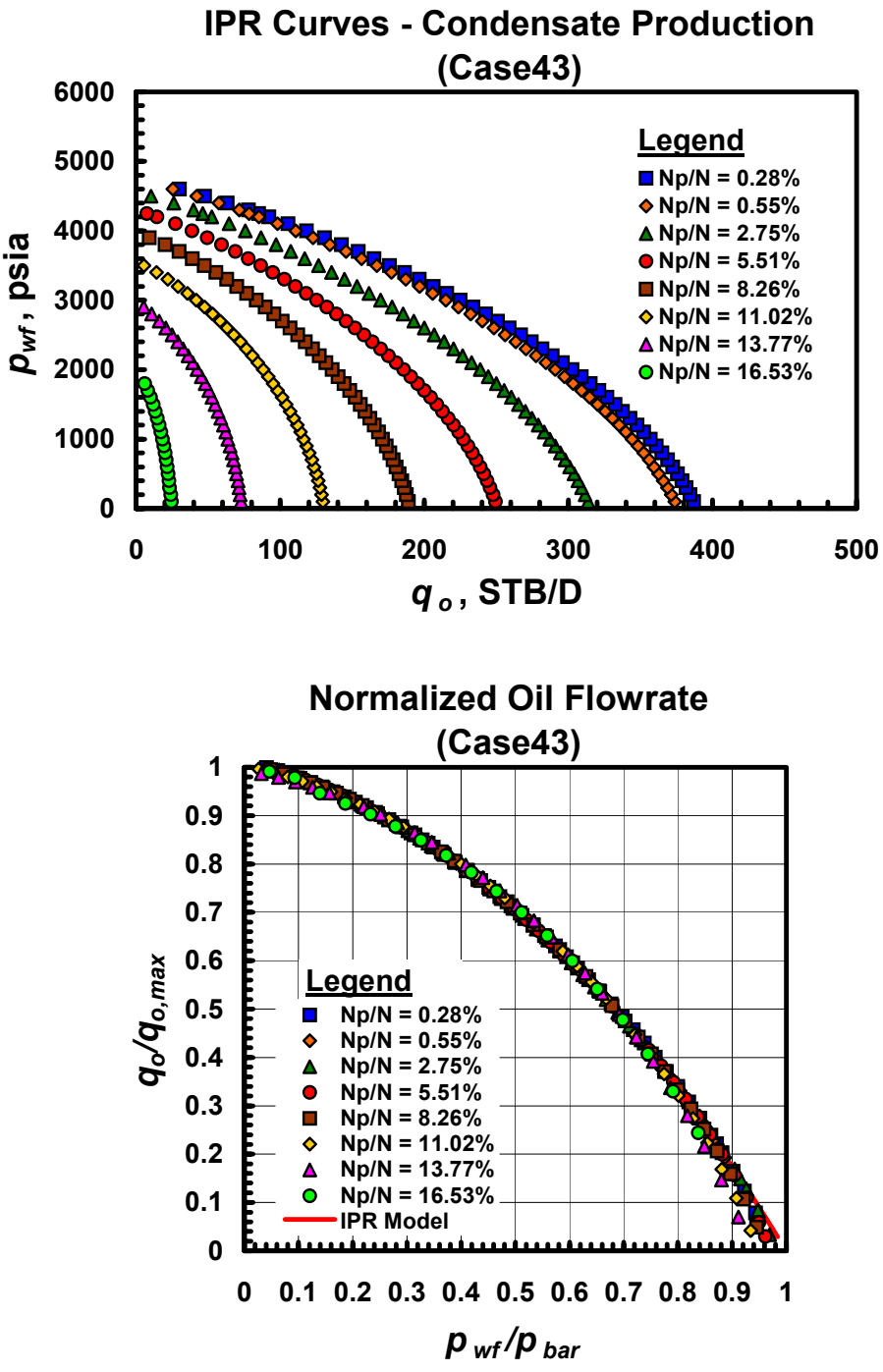

Fig. A.43.a — Dimensional and dimensionless IPR trends for Case 43 — gas condensate performance trends.

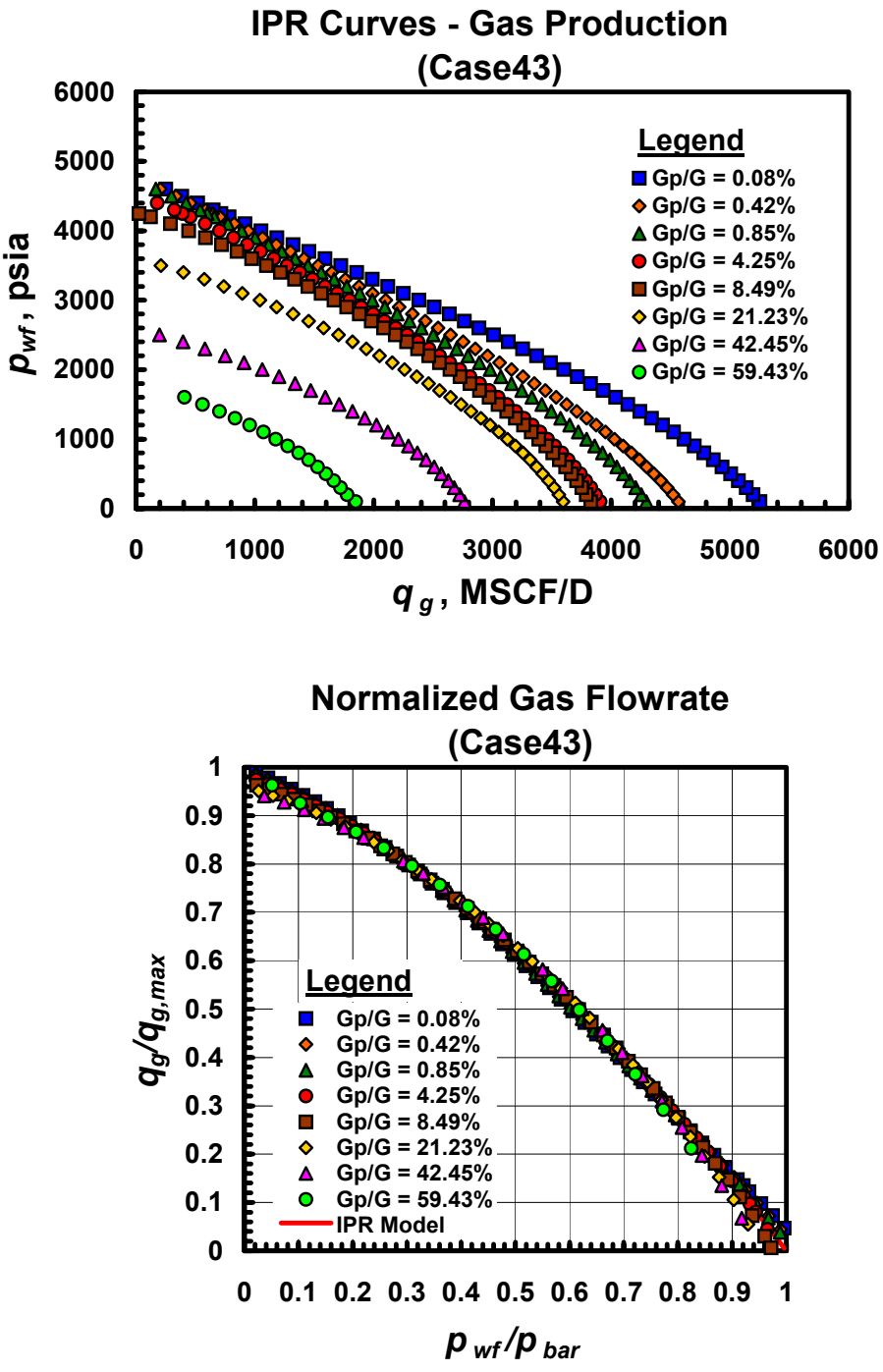

Fig. A.43.b — Dimensional and dimensionless IPR trends for Case 43 — gas performance trends.

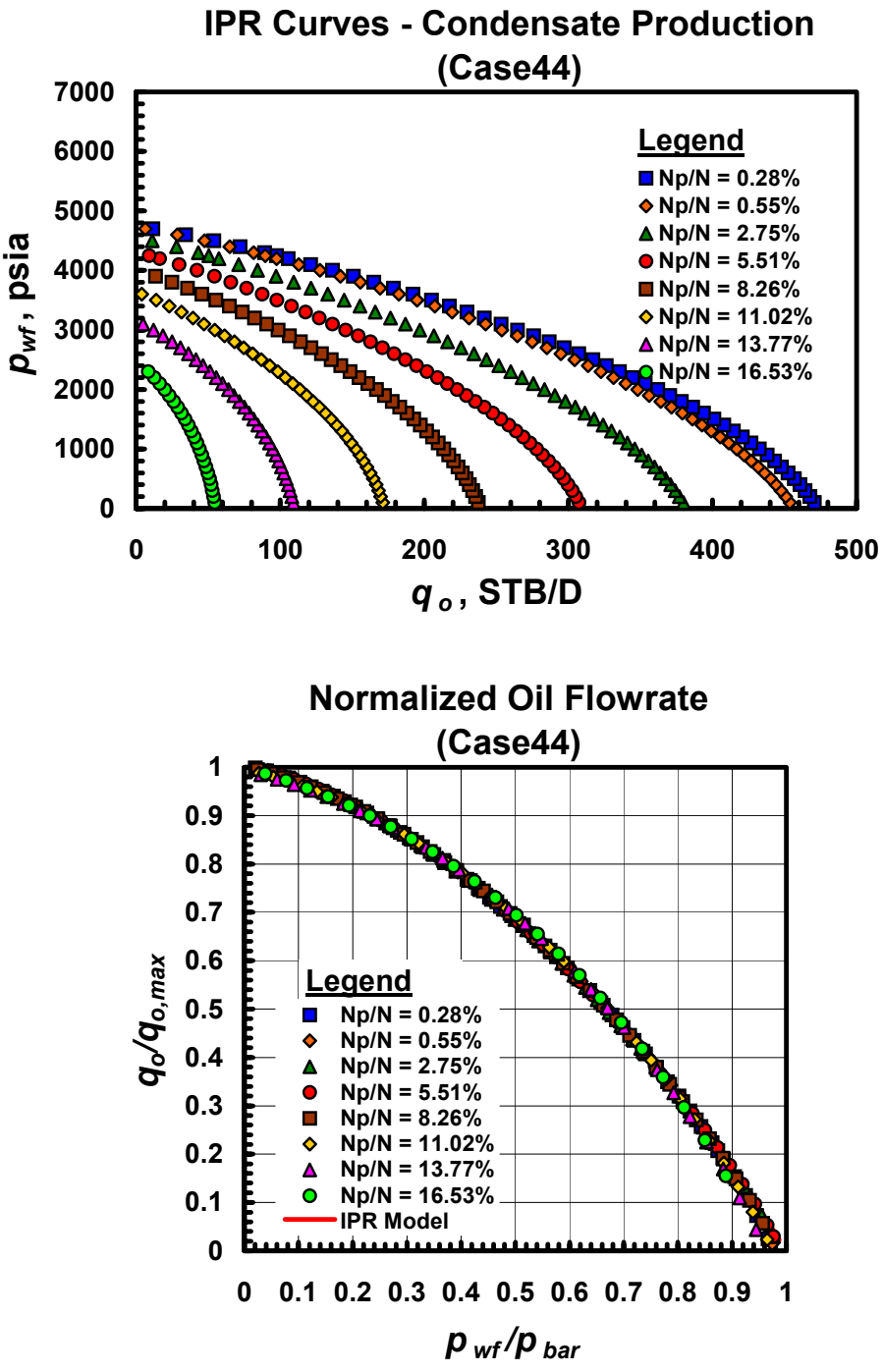

Fig. A.44.a — Dimensional and dimensionless IPR trends for Case 44 — gas condensate performance trends.

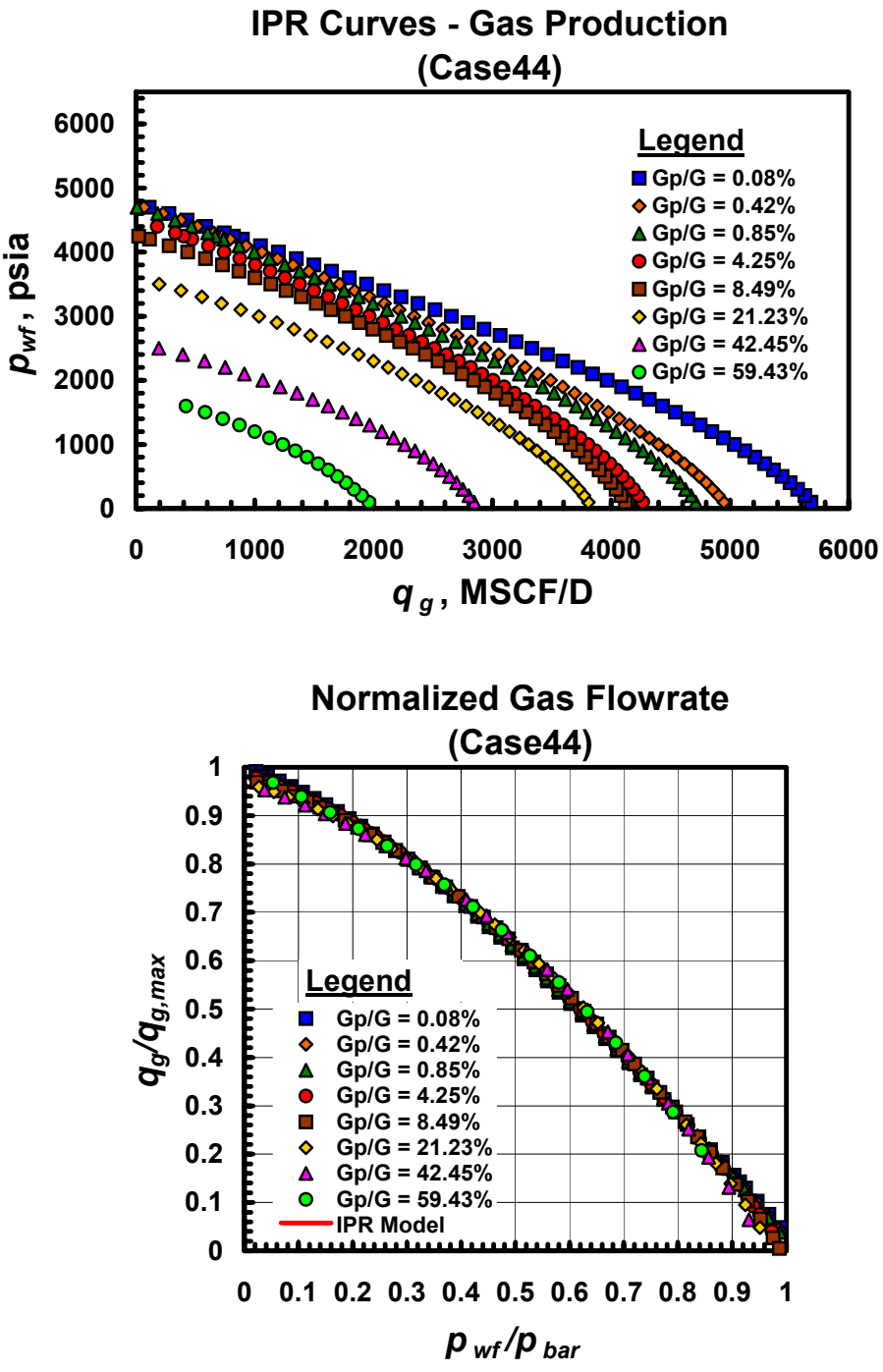

Fig. A.44.b — Dimensional and dimensionless IPR trends for Case 44 — gas performance trends.

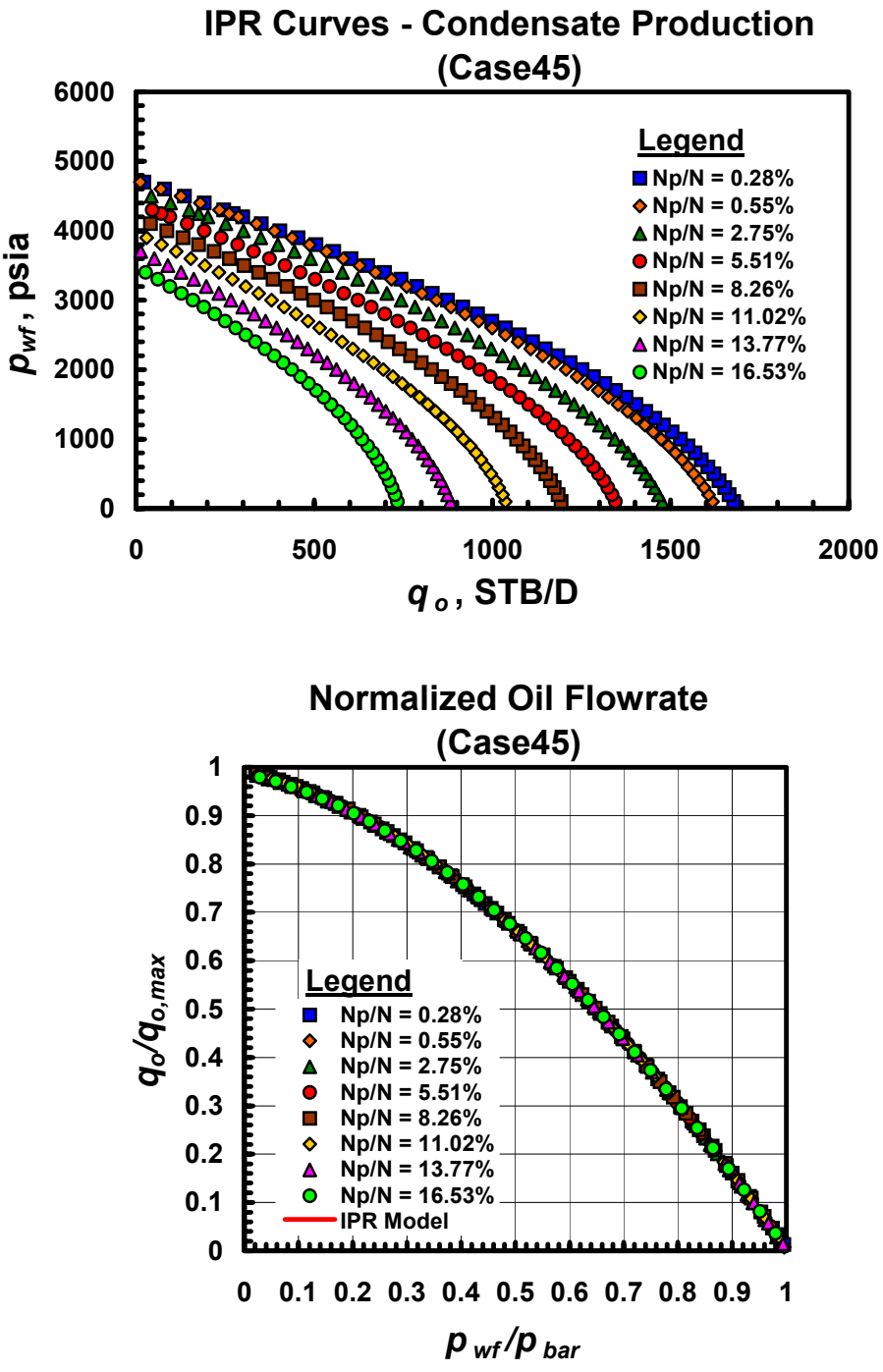

Fig. A.45.a — Dimensional and dimensionless IPR trends for Case 45 — gas condensate performance trends.

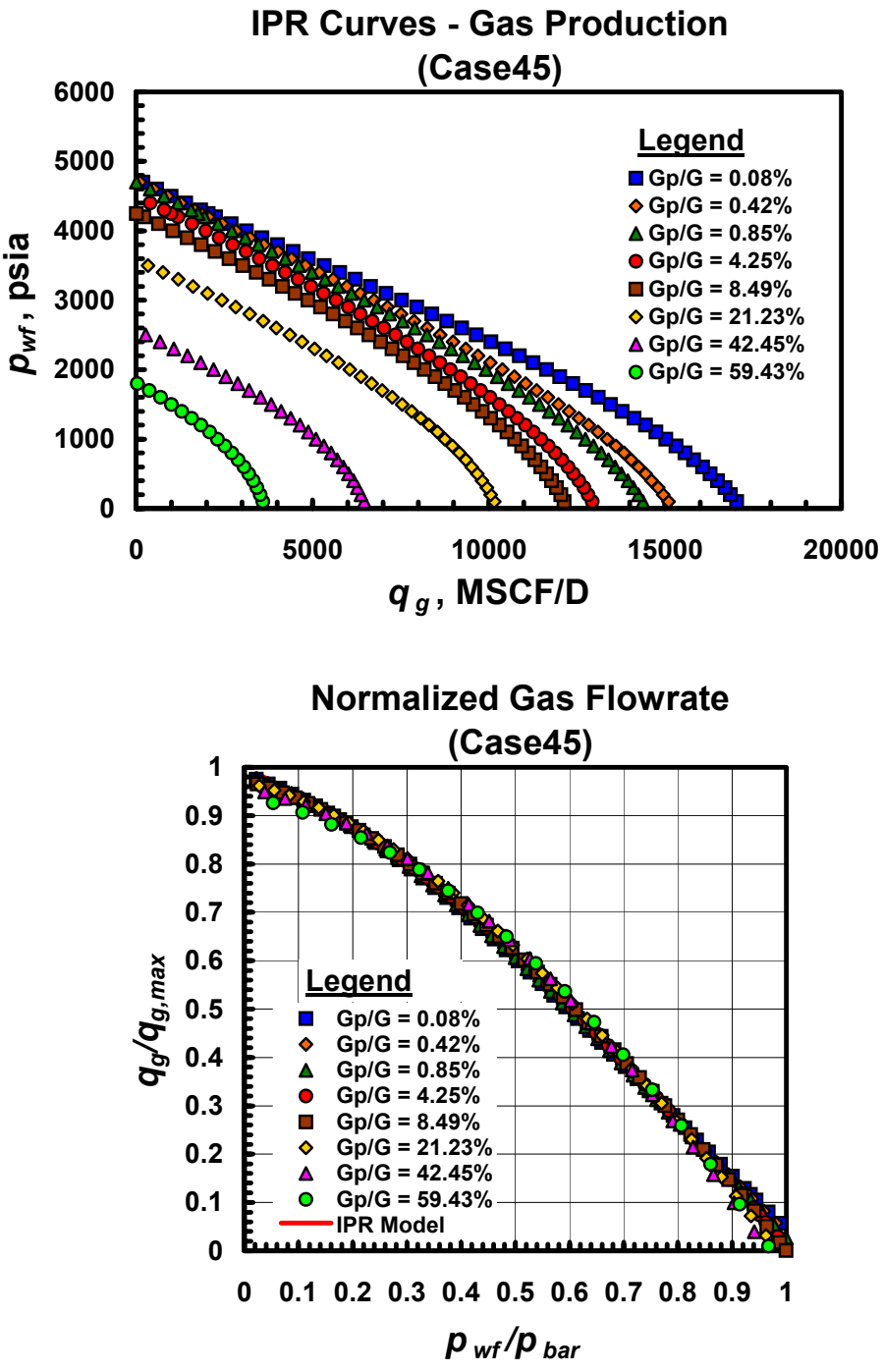

Fig. A.45.b — Dimensional and dimensionless IPR trends for Case 45 — gas performance trends.

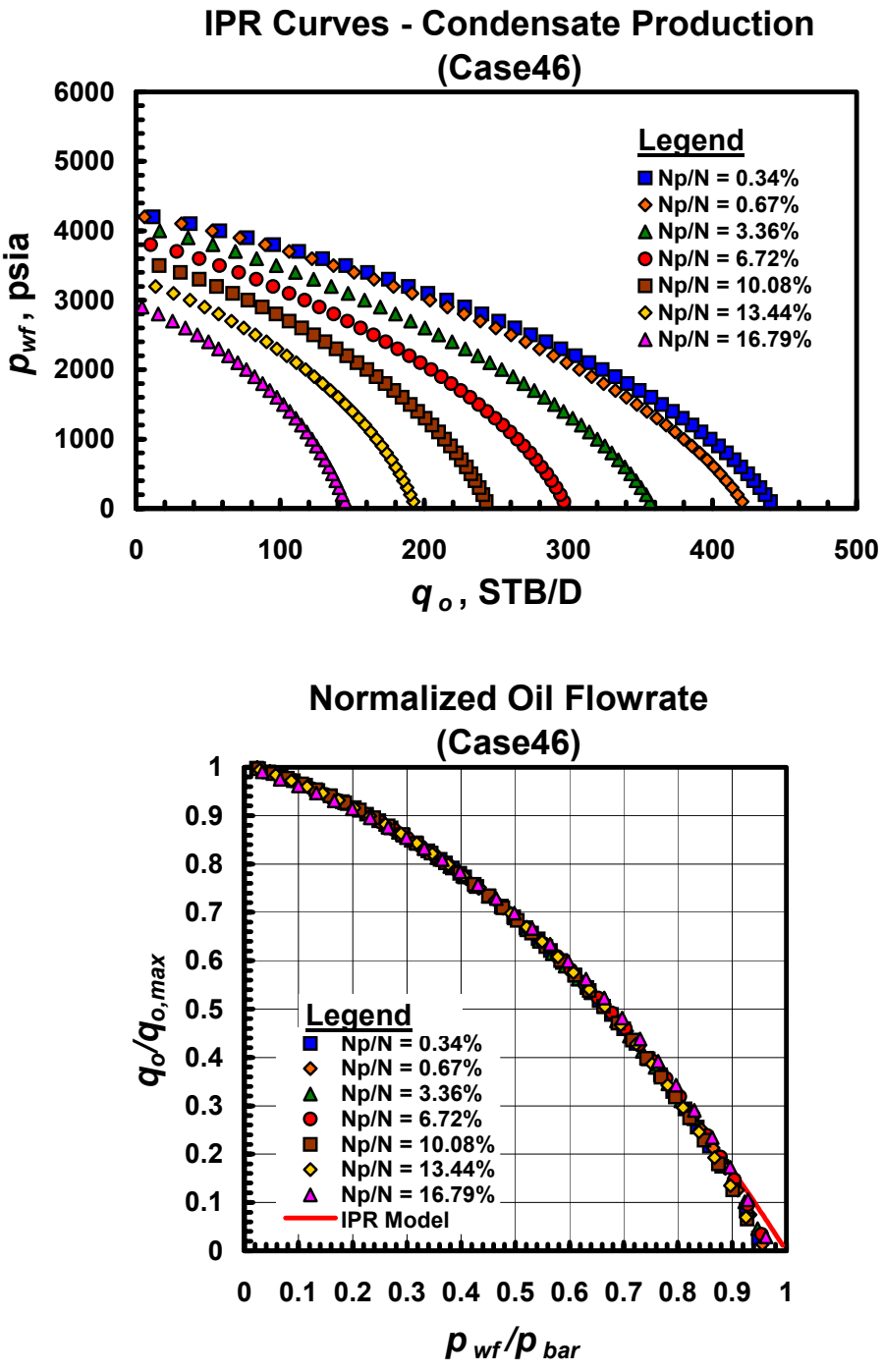

Fig. A.46.a — Dimensional and dimensionless IPR trends for Case 46 — gas condensate performance trends.

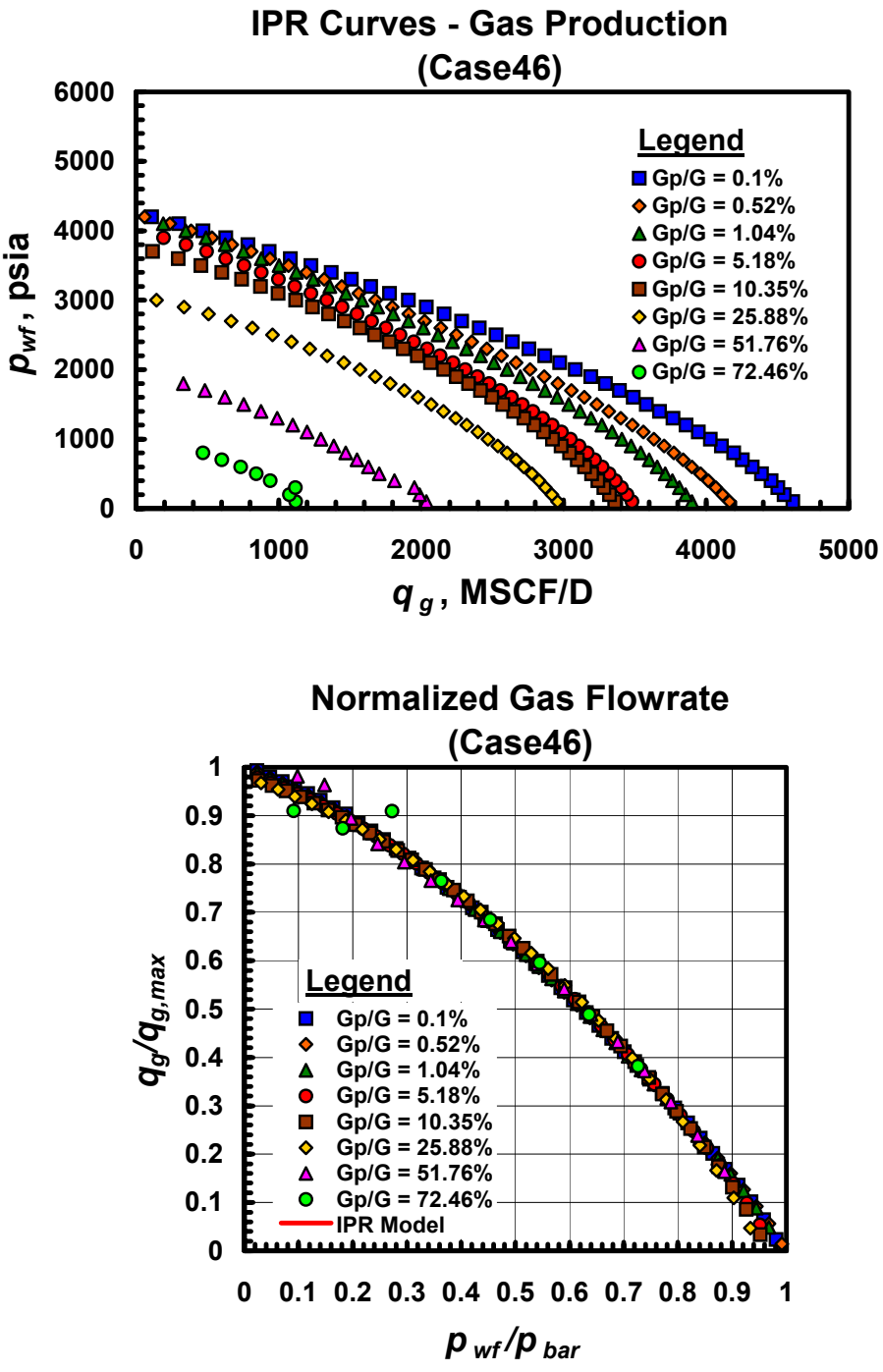

Fig. A.46.b — Dimensional and dimensionless IPR trends for Case 46 — gas performance trends.

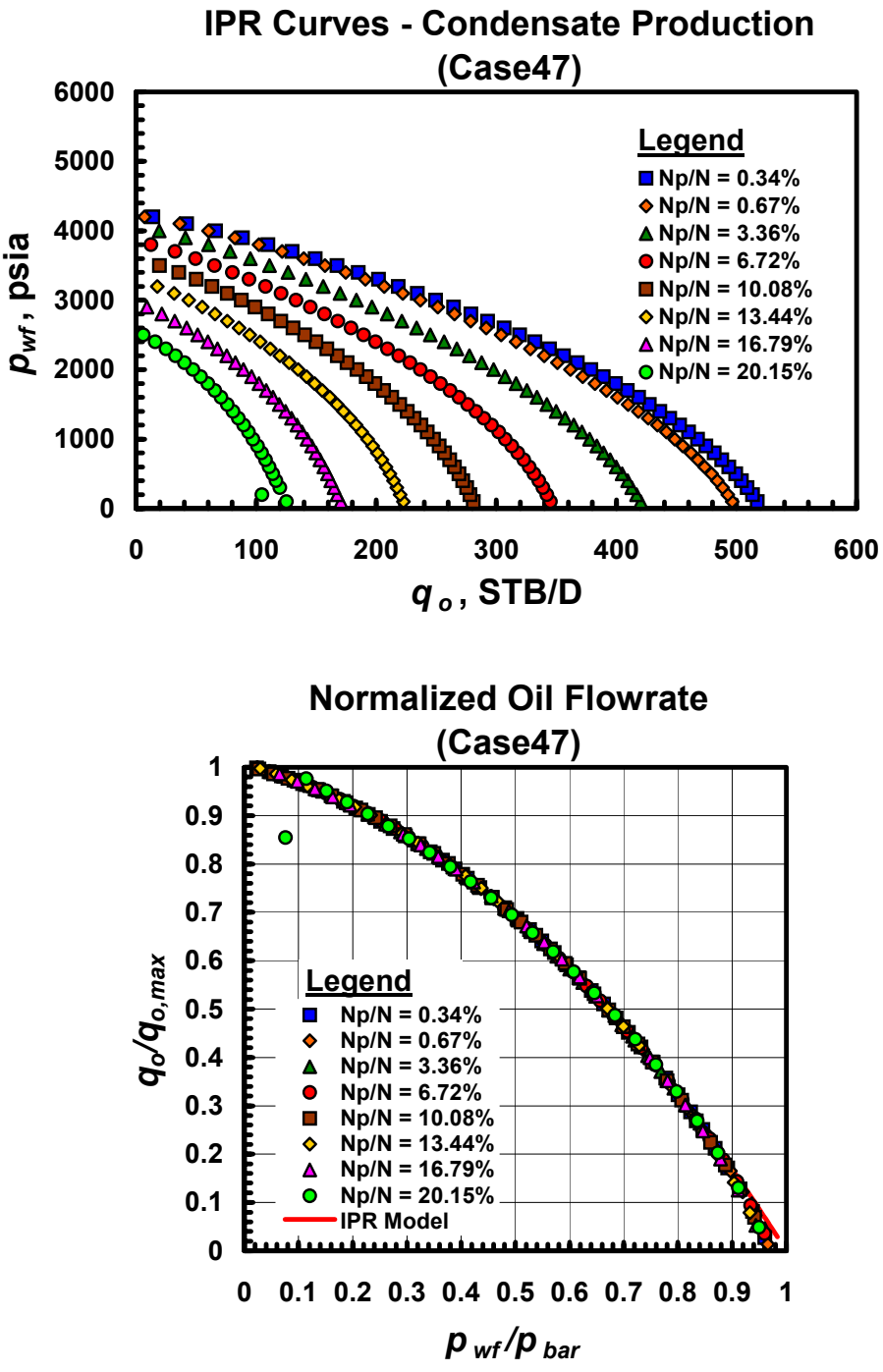

Fig. A.47.a — Dimensional and dimensionless IPR trends for Case 47 — gas condensate performance trends.

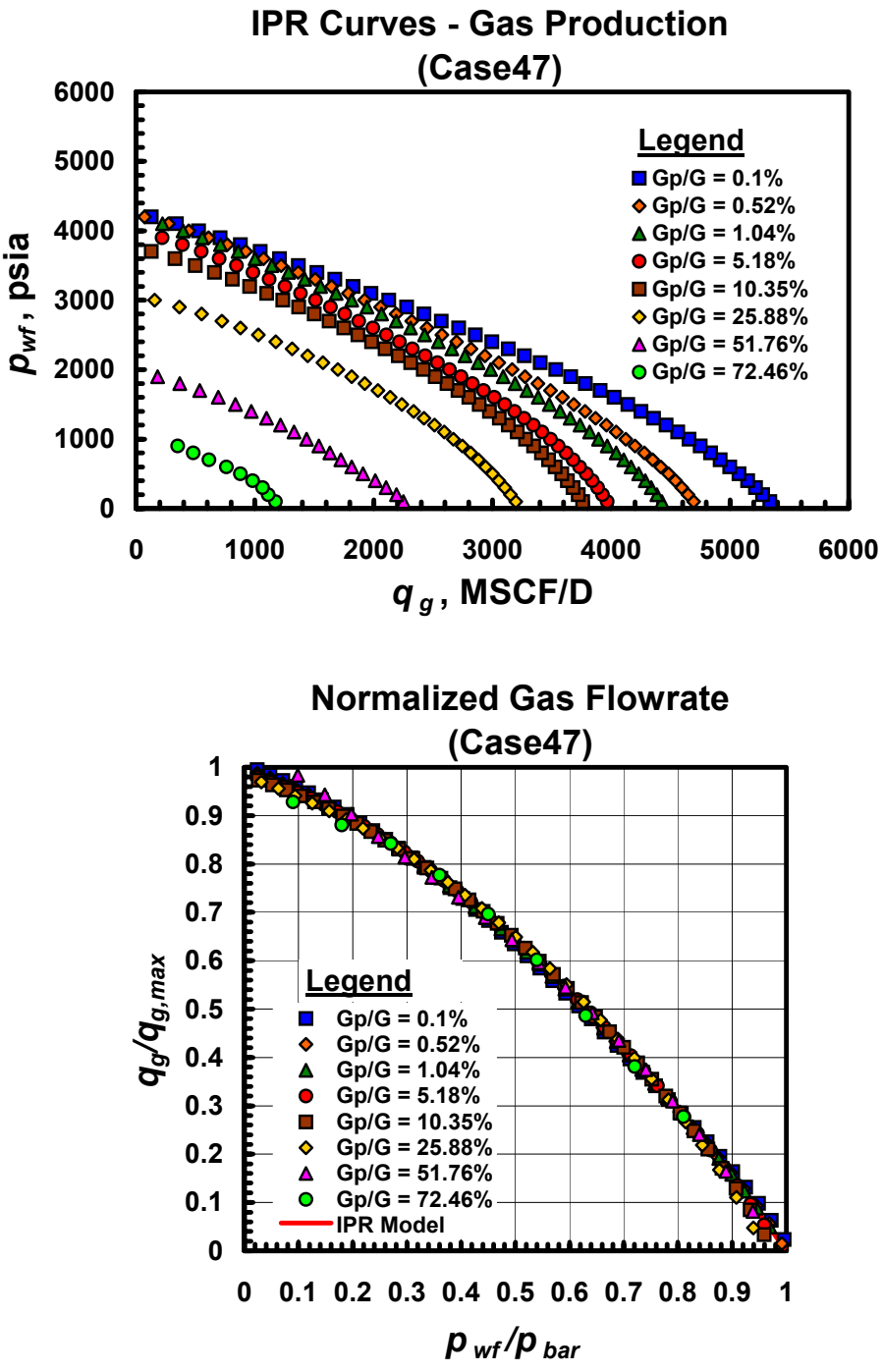

Fig. A.47.b — Dimensional and dimensionless IPR trends for Case 47 — gas performance trends.

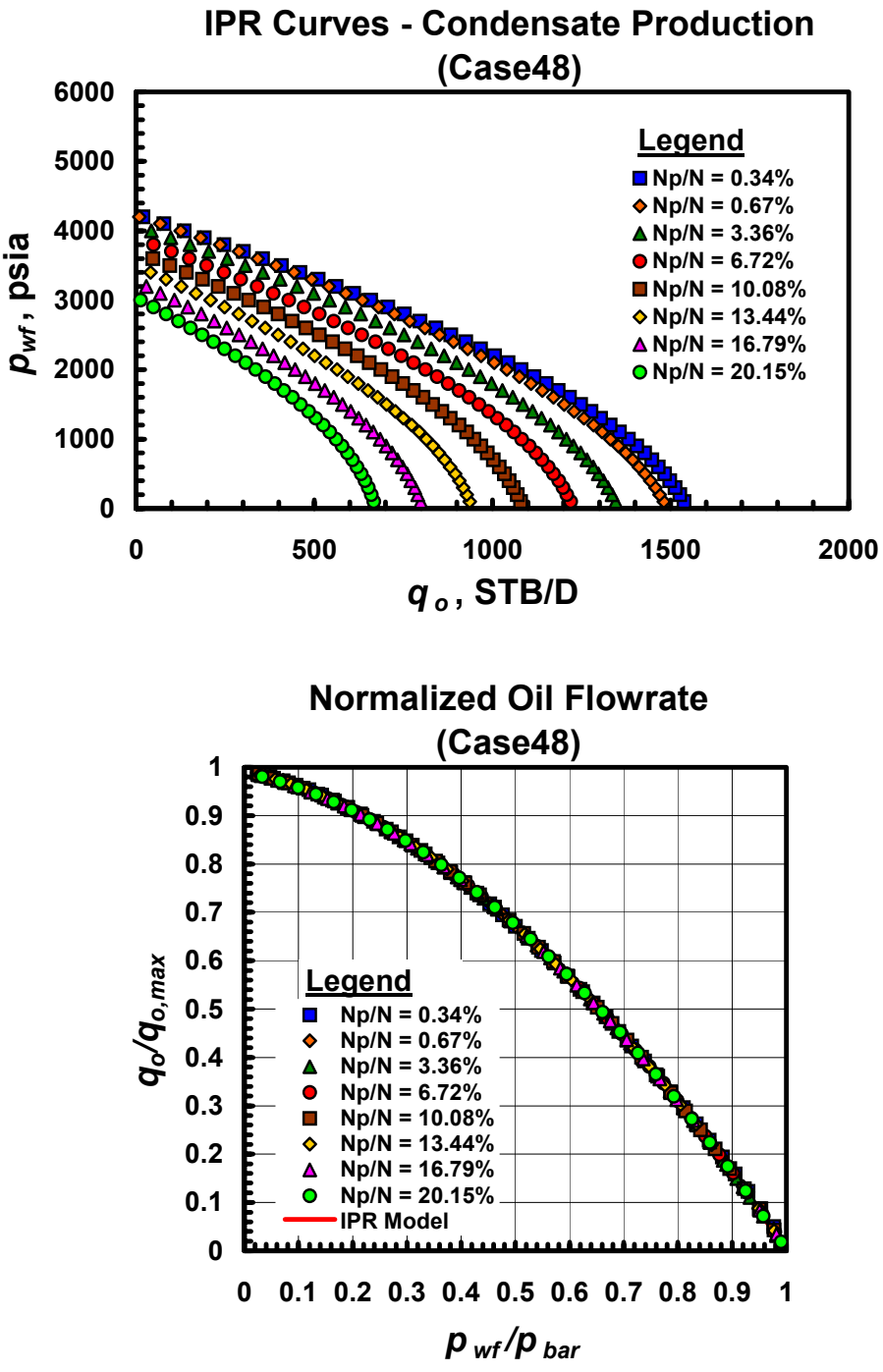

Fig. A.48.a — Dimensional and dimensionless IPR trends for Case 48 — gas condensate performance trends.

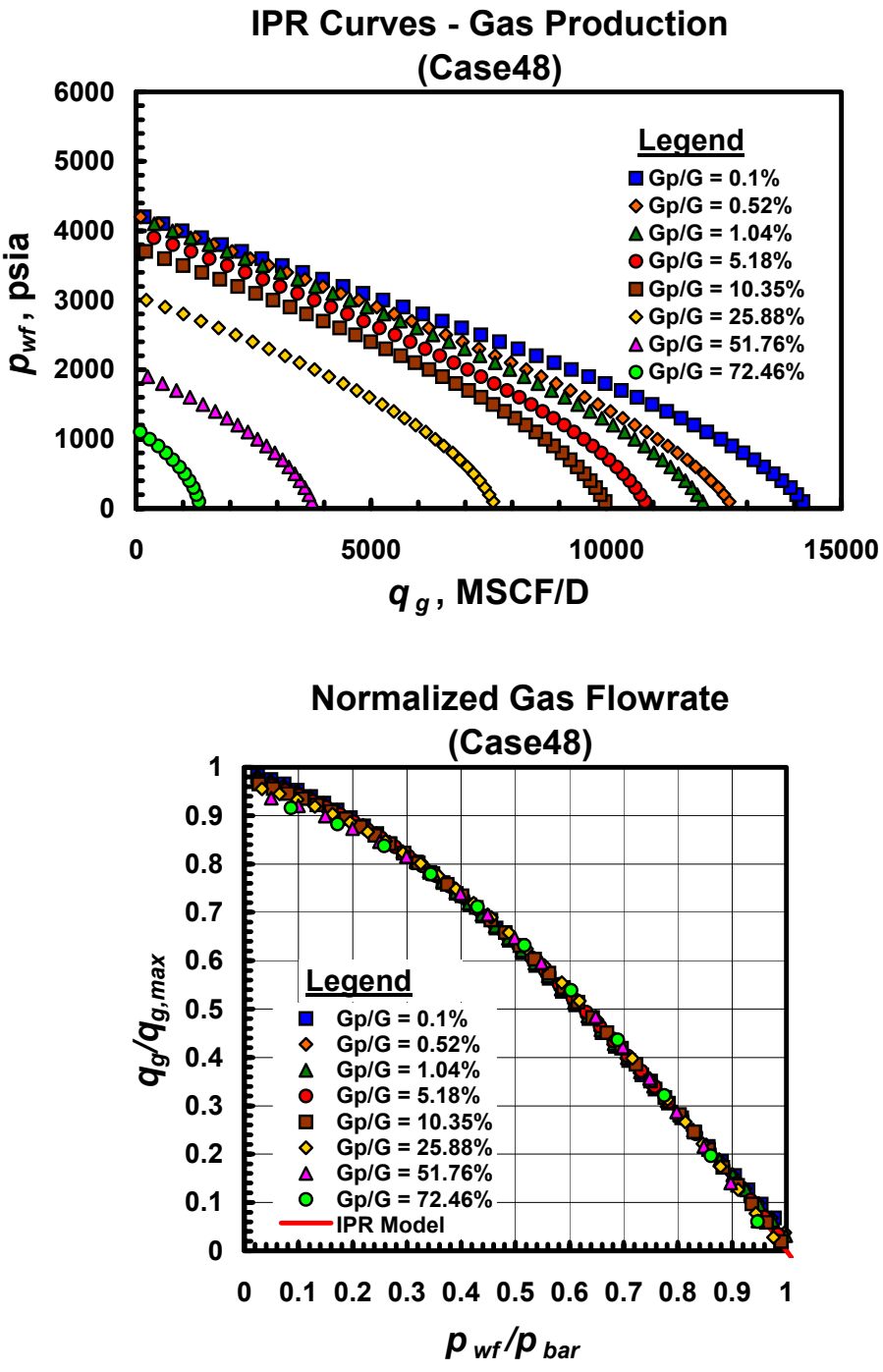

Fig. A.48.b — Dimensional and dimensionless IPR trends for Case 48 — gas performance trends.

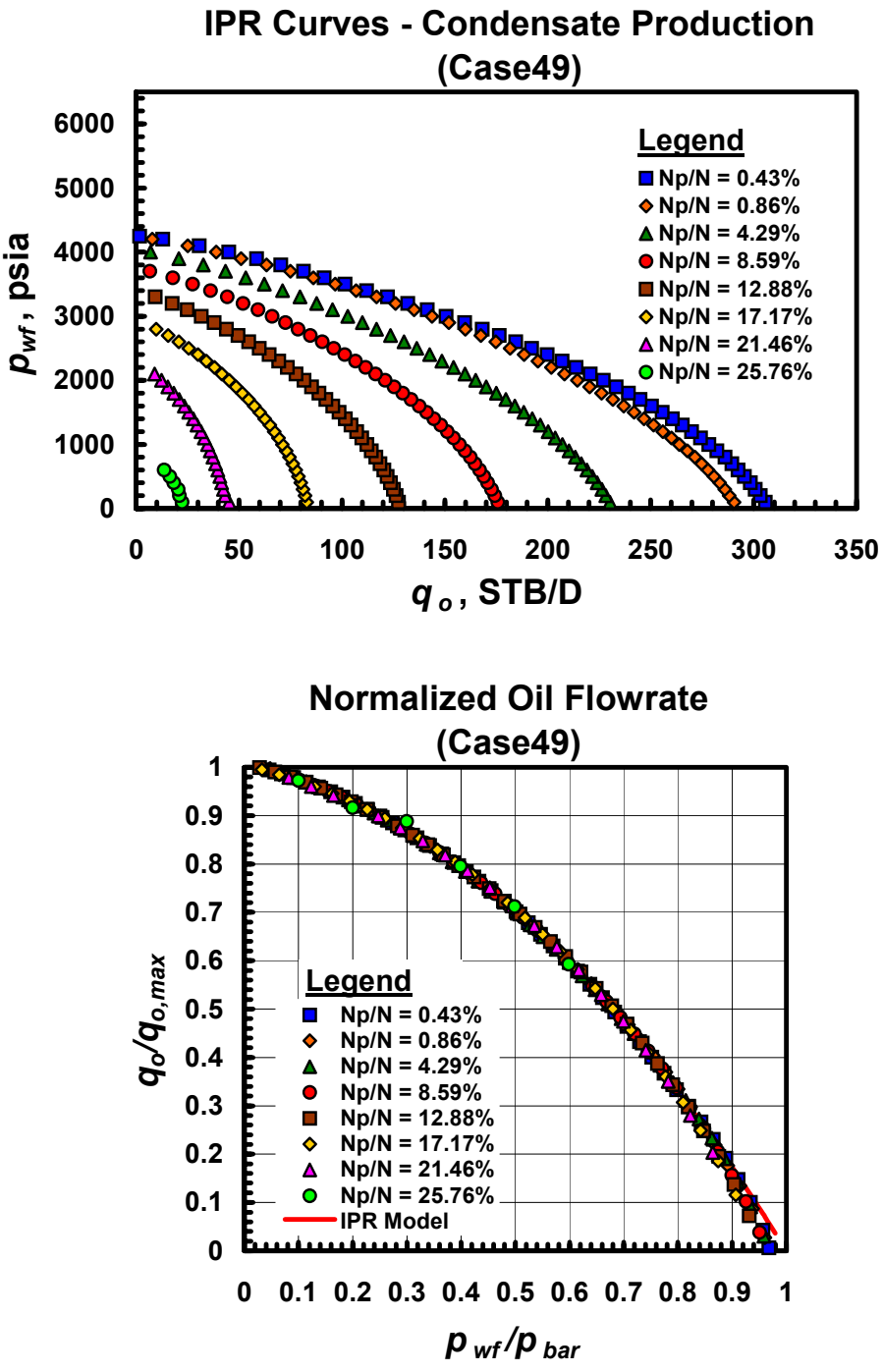

Fig. A.49.a — Dimensional and dimensionless IPR trends for Case 49 — gas condensate performance trends.

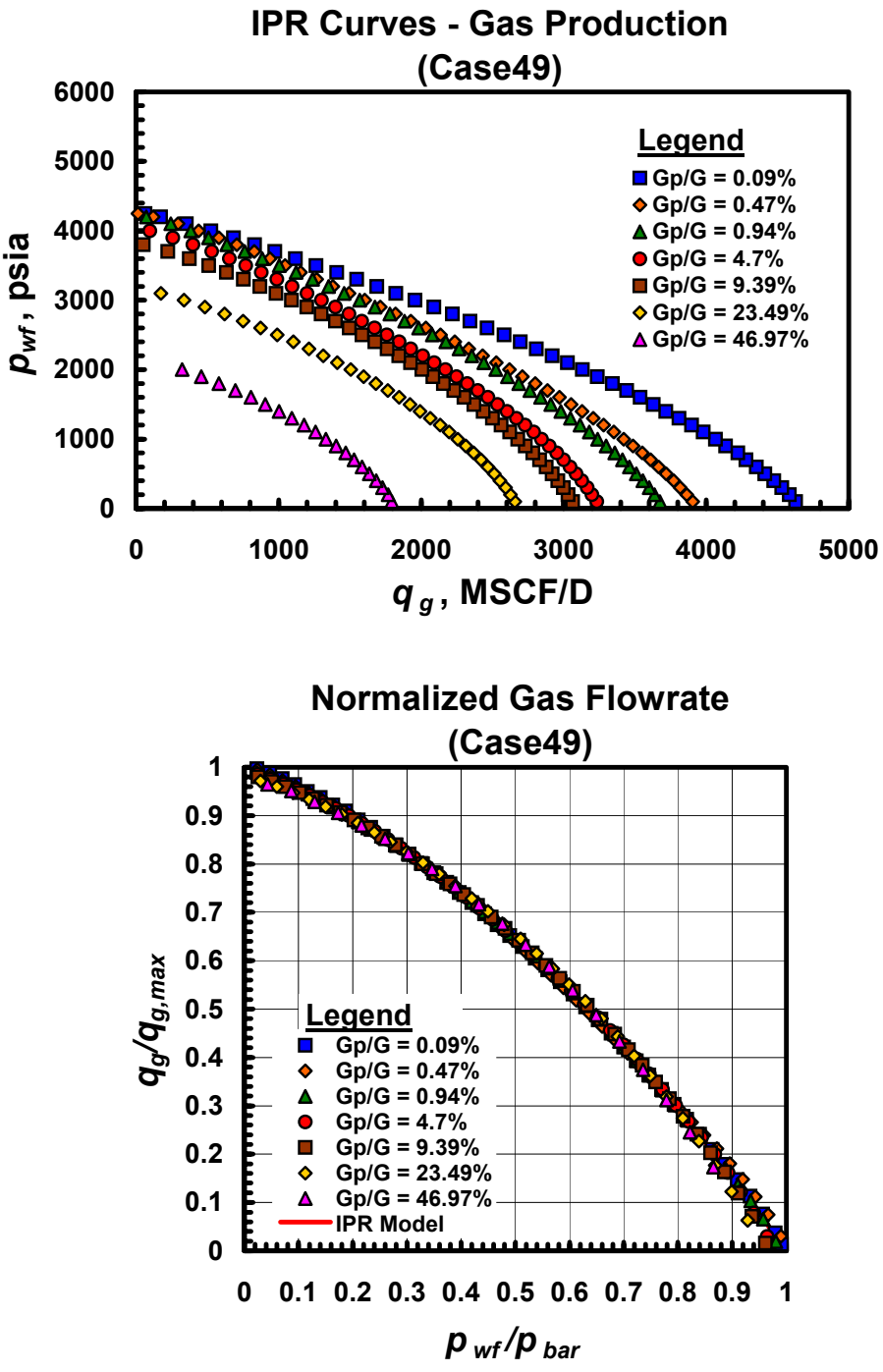

Fig. A.49.b — Dimensional and dimensionless IPR trends for Case 49 — gas performance trends.

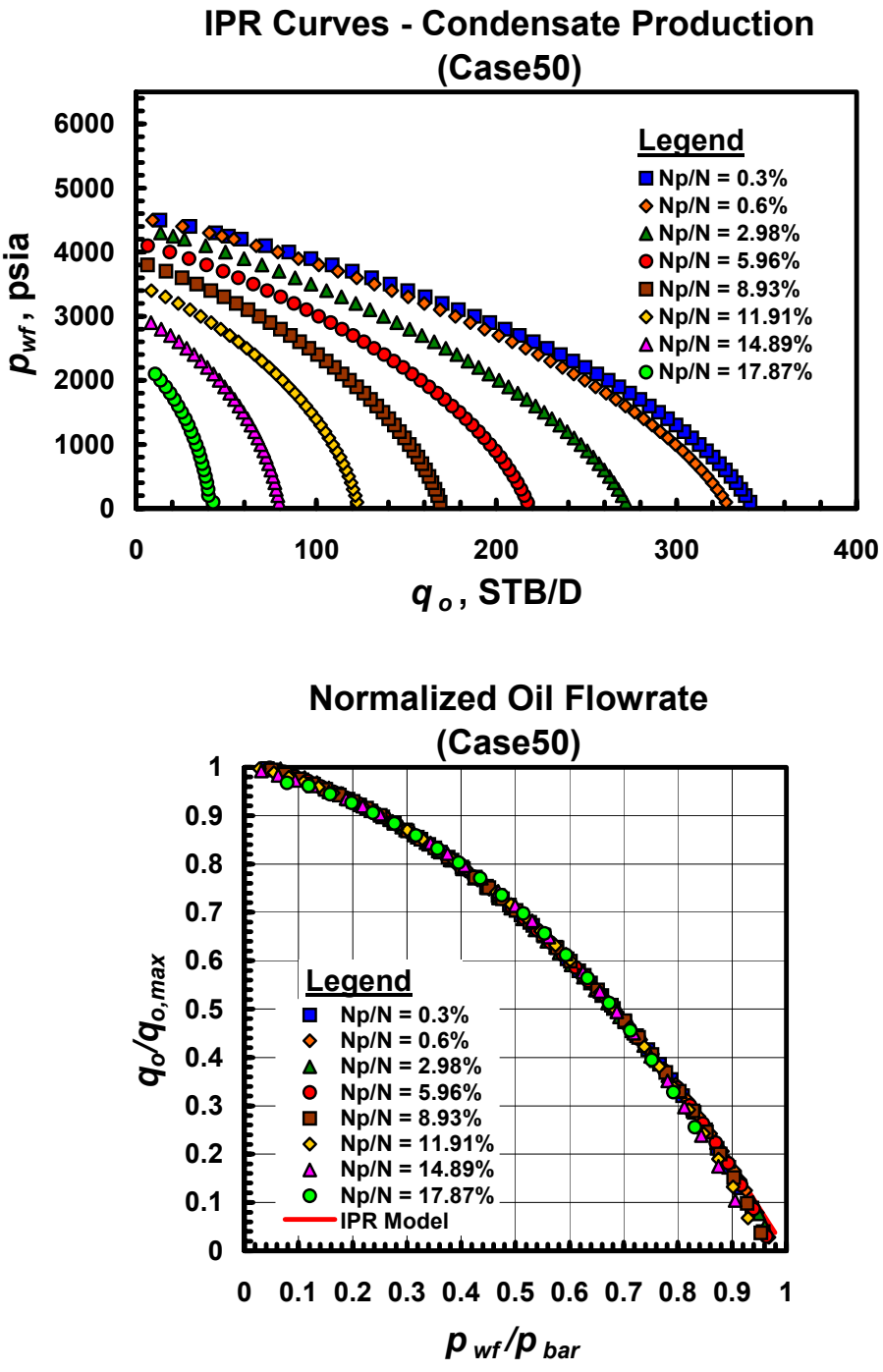

Fig. A.50.a — Dimensional and dimensionless IPR trends for Case 50 — gas condensate performance trends.

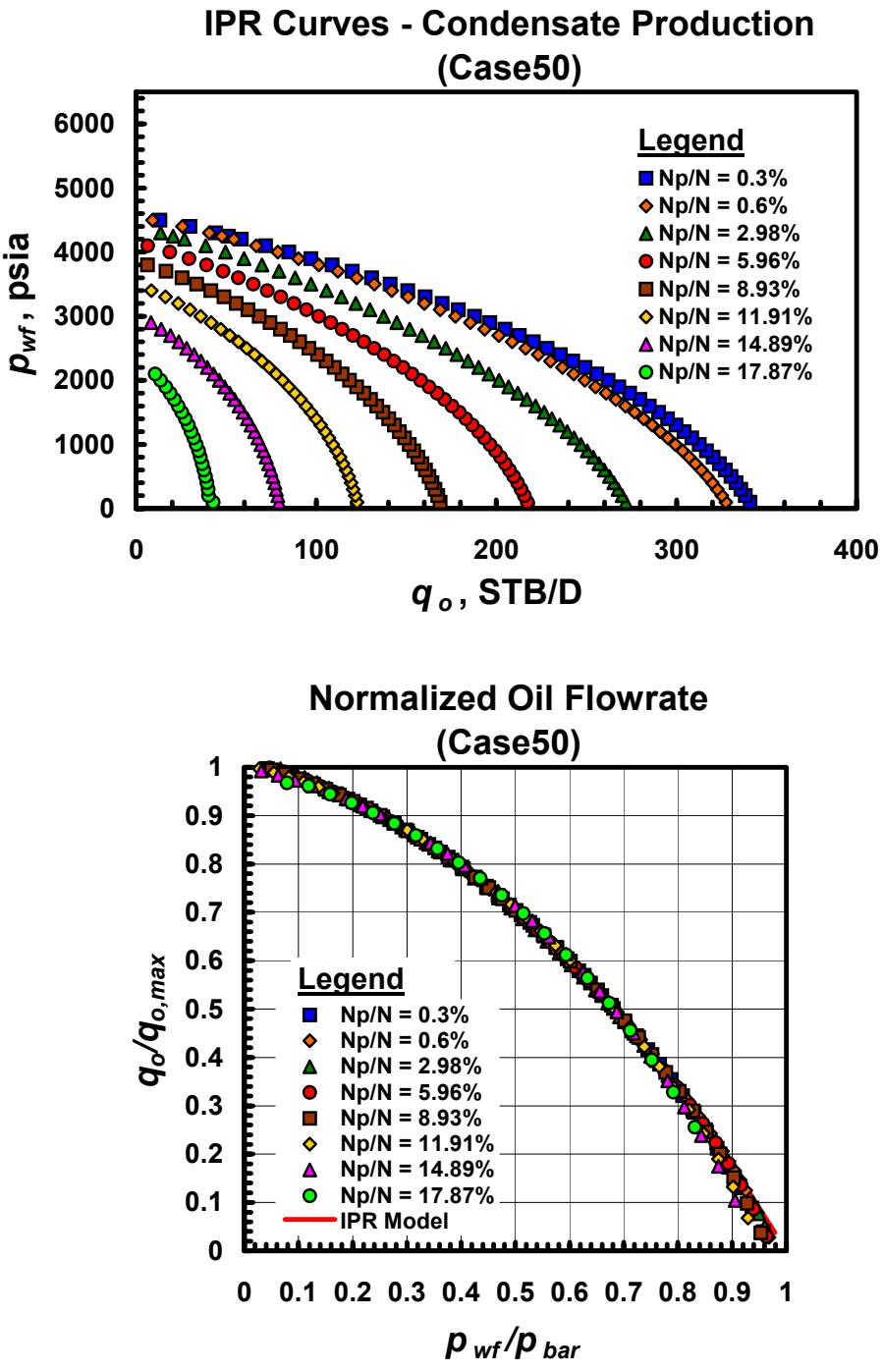

Fig. A.50.b — Dimensional and dimensionless IPR trends for Case 50 — gas performance trends.

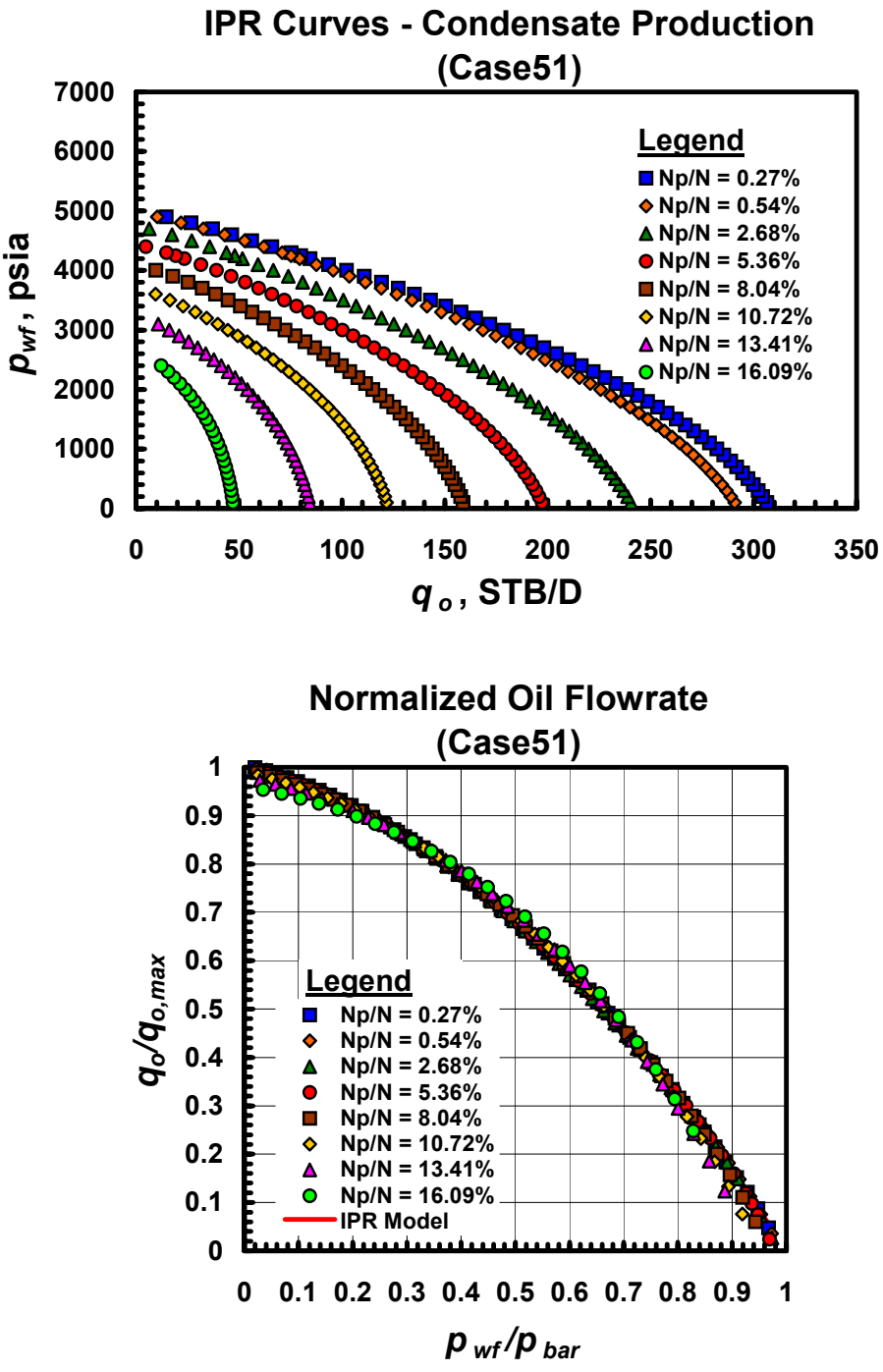

Fig. A.51.a — Dimensional and dimensionless IPR trends for Case 51 — gas condensate performance trends.

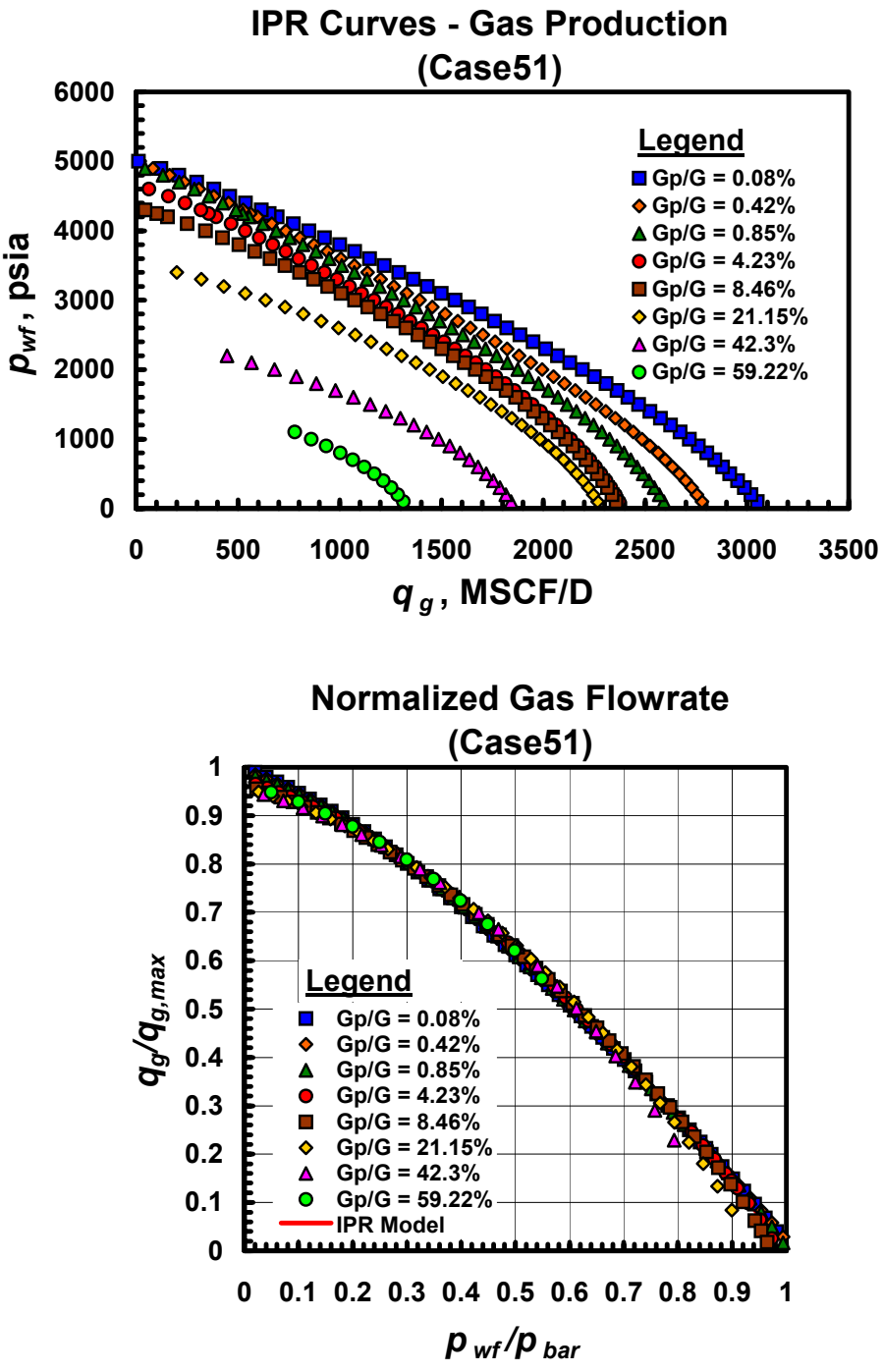

Fig. A.51.b — Dimensional and dimensionless IPR trends for Case 51 — gas performance trends.

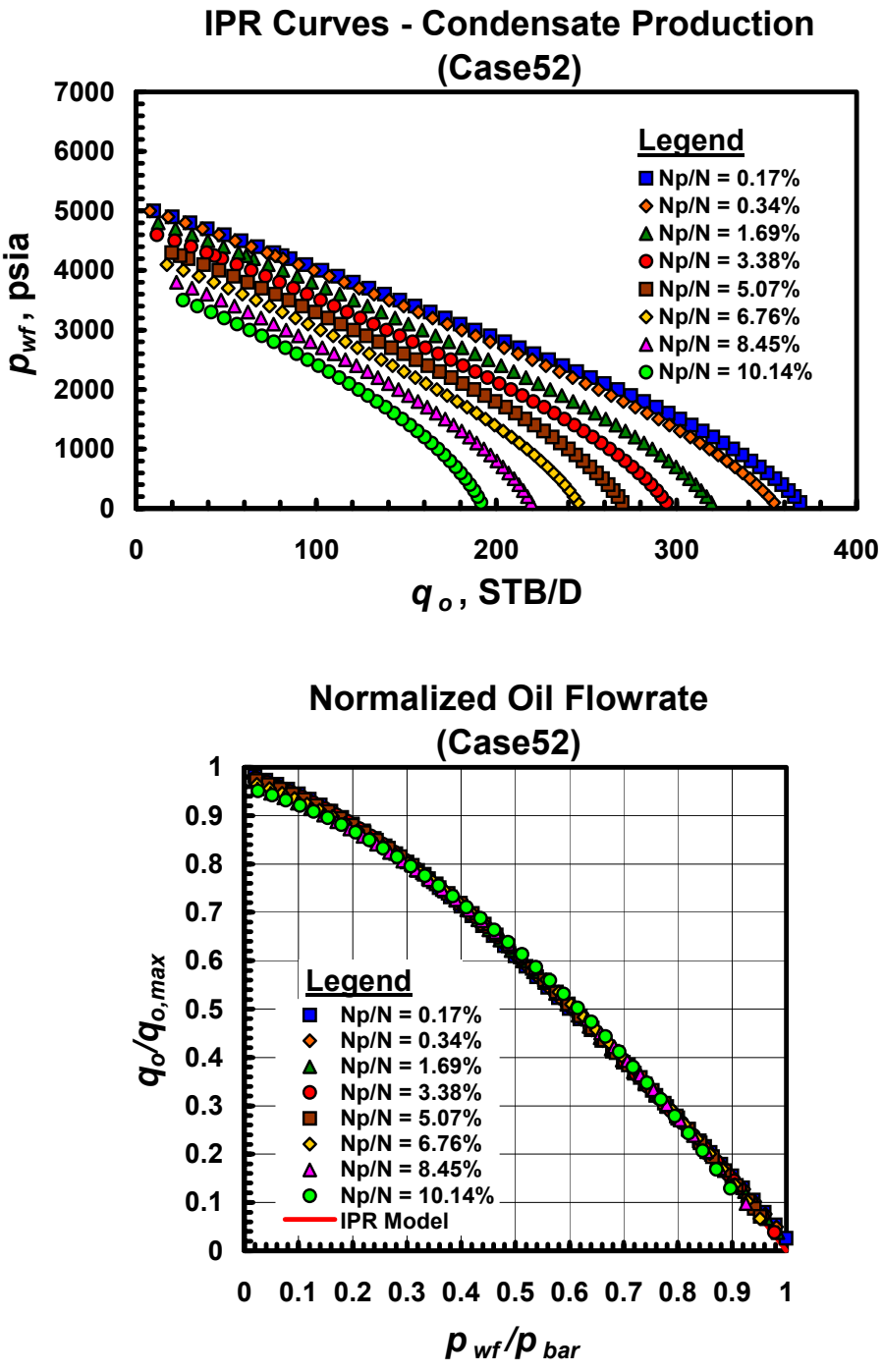

Fig. A.52.a — Dimensional and dimensionless IPR trends for Case 52 — gas condensate performance trends.

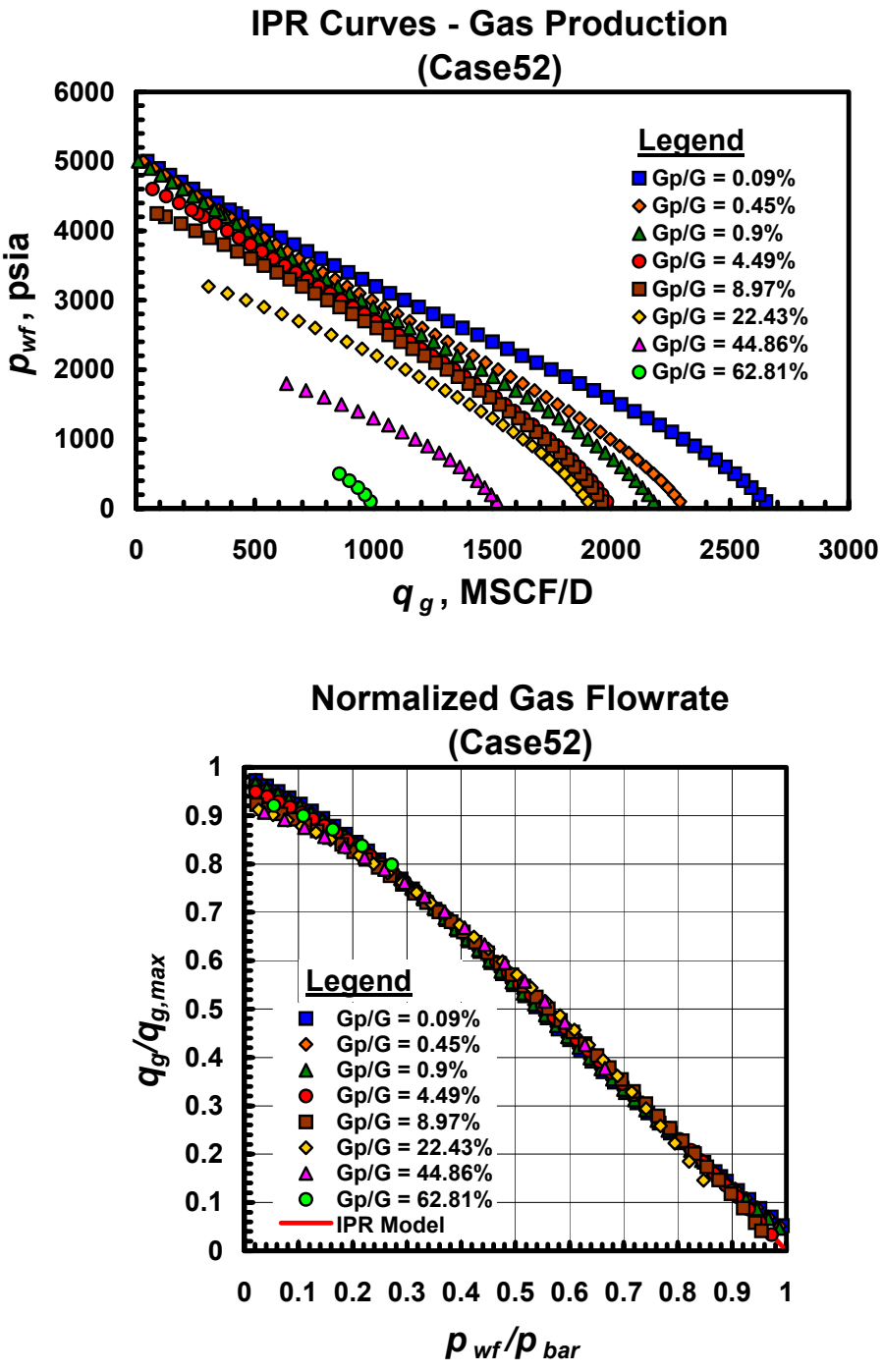

Fig. A.52.b — Dimensional and dimensionless IPR trends for Case 52 — gas performance trends.

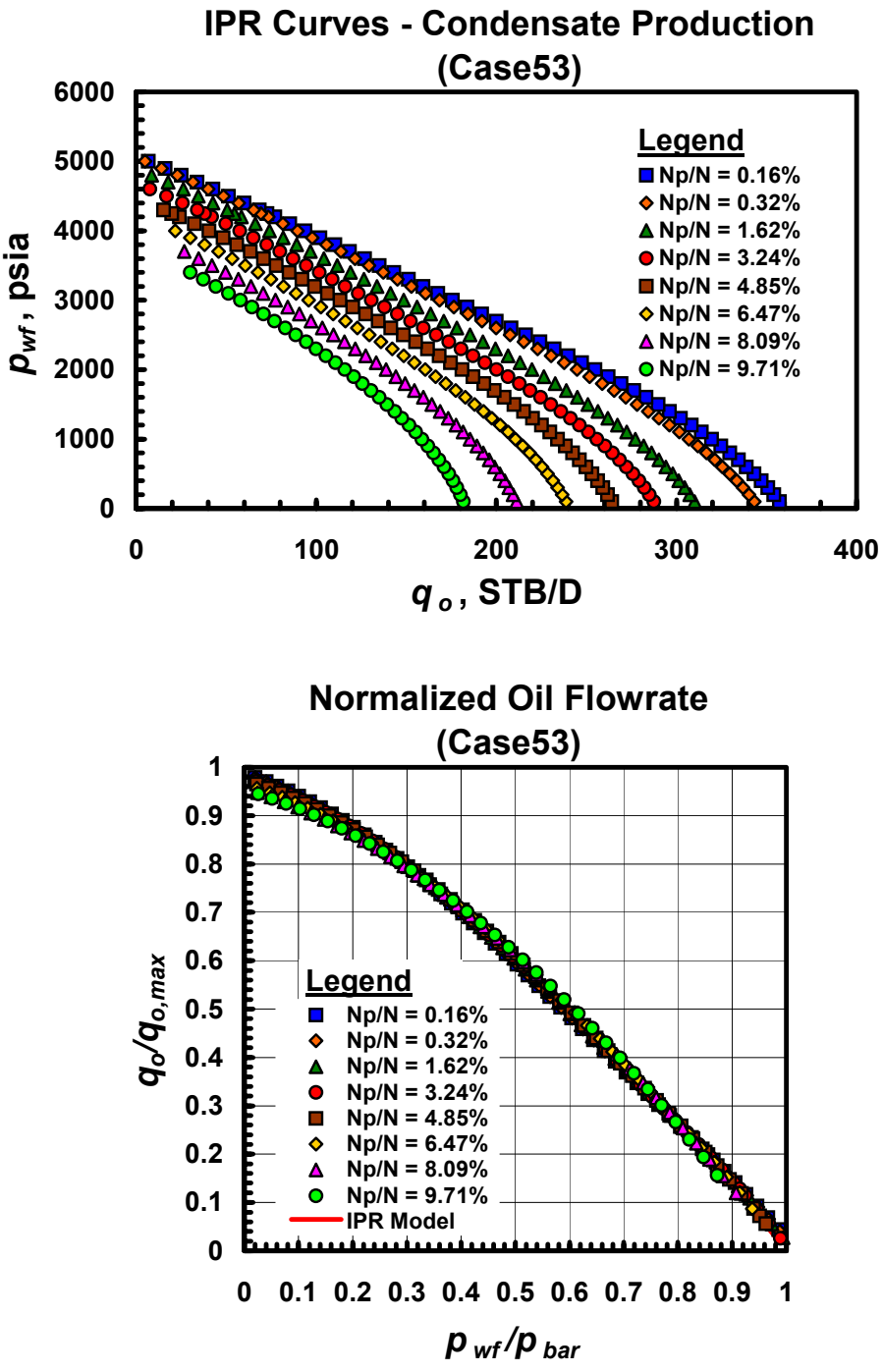

Fig. A.53.a — Dimensional and dimensionless IPR trends for Case 53 — gas condensate performance trends.

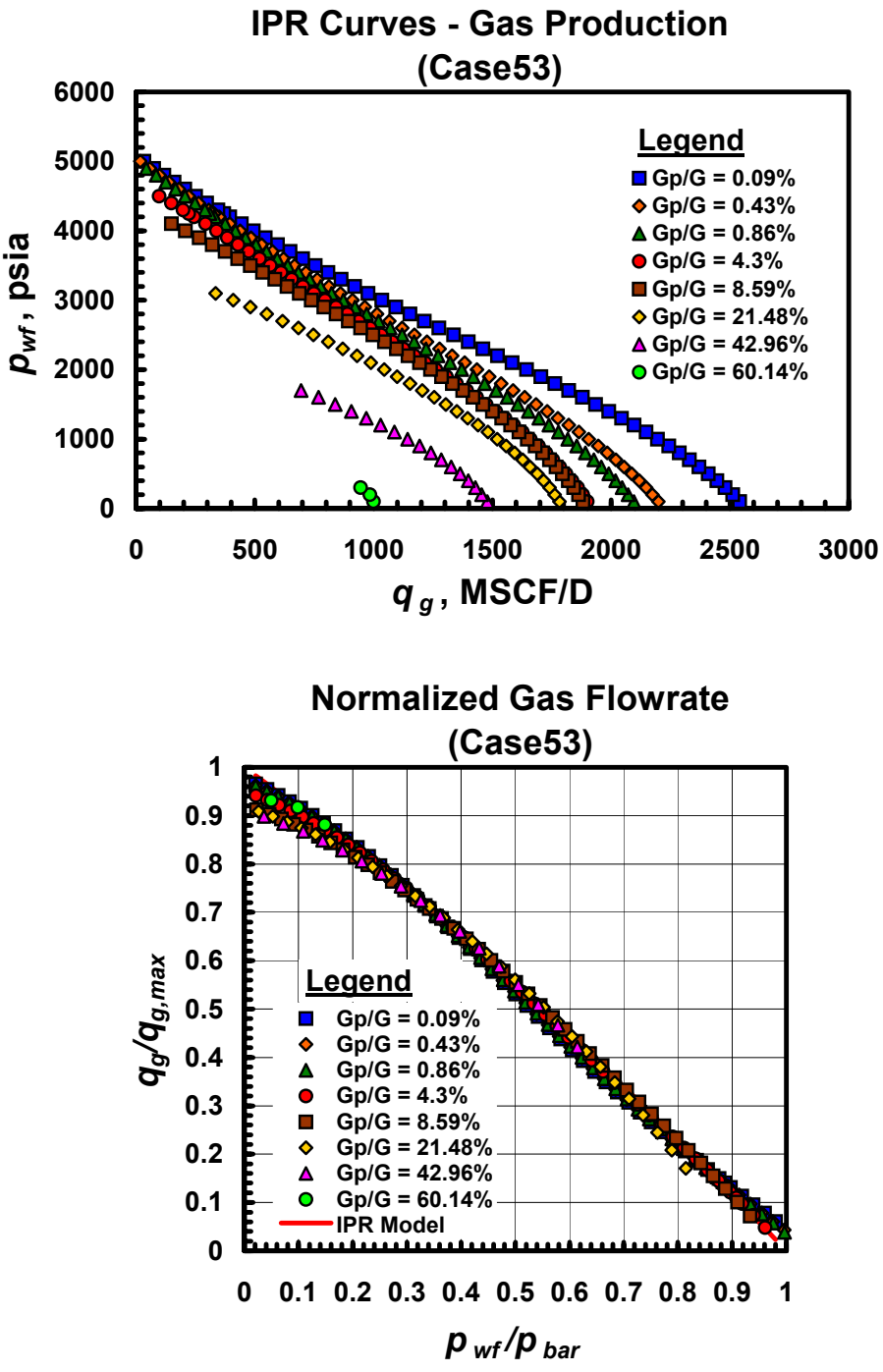

Fig. A.53.b — Dimensional and dimensionless IPR trends for Case 53 — gas performance trends.

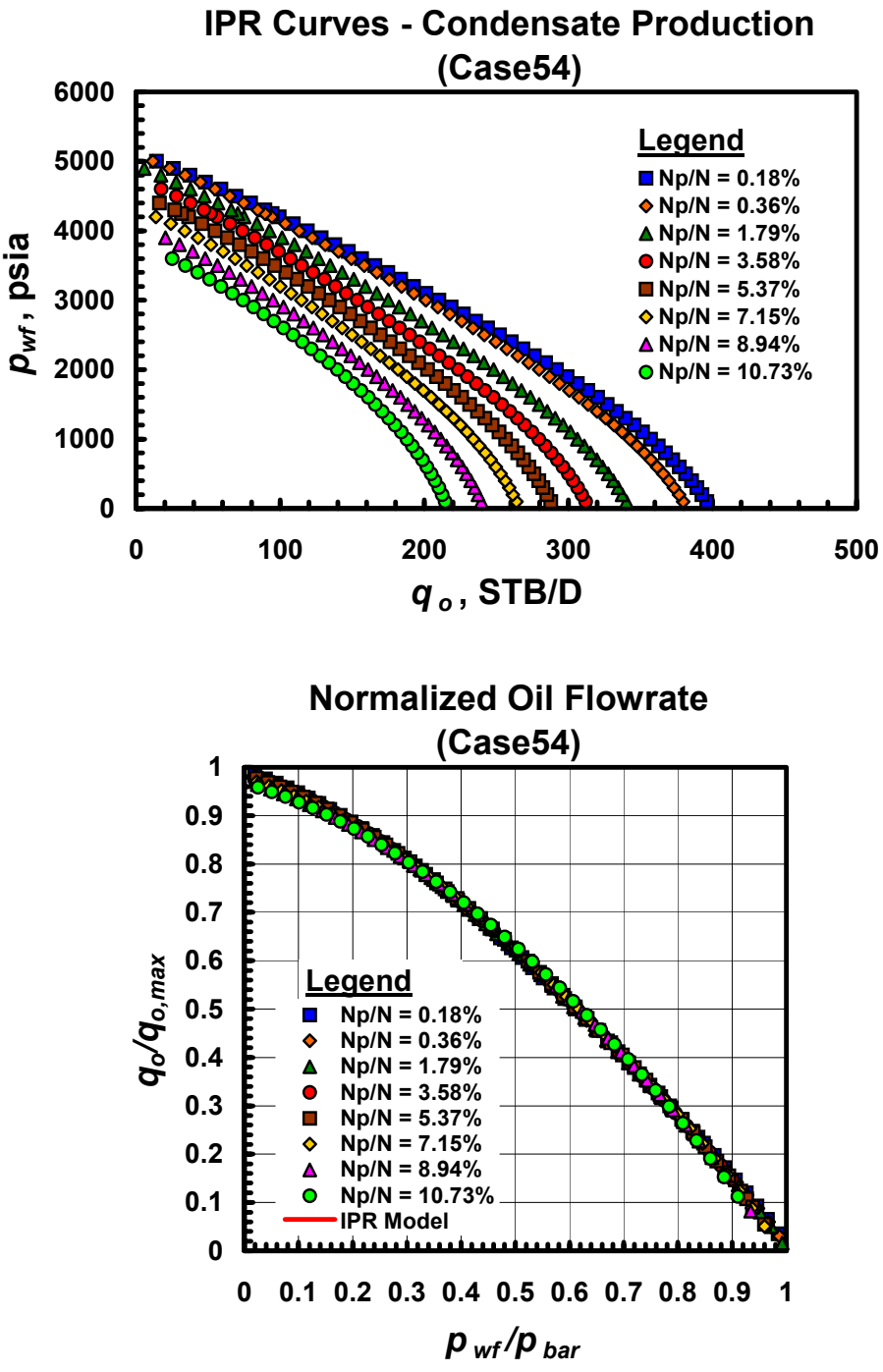

Fig. A.54.a — Dimensional and dimensionless IPR trends for Case 54 — gas condensate performance trends.

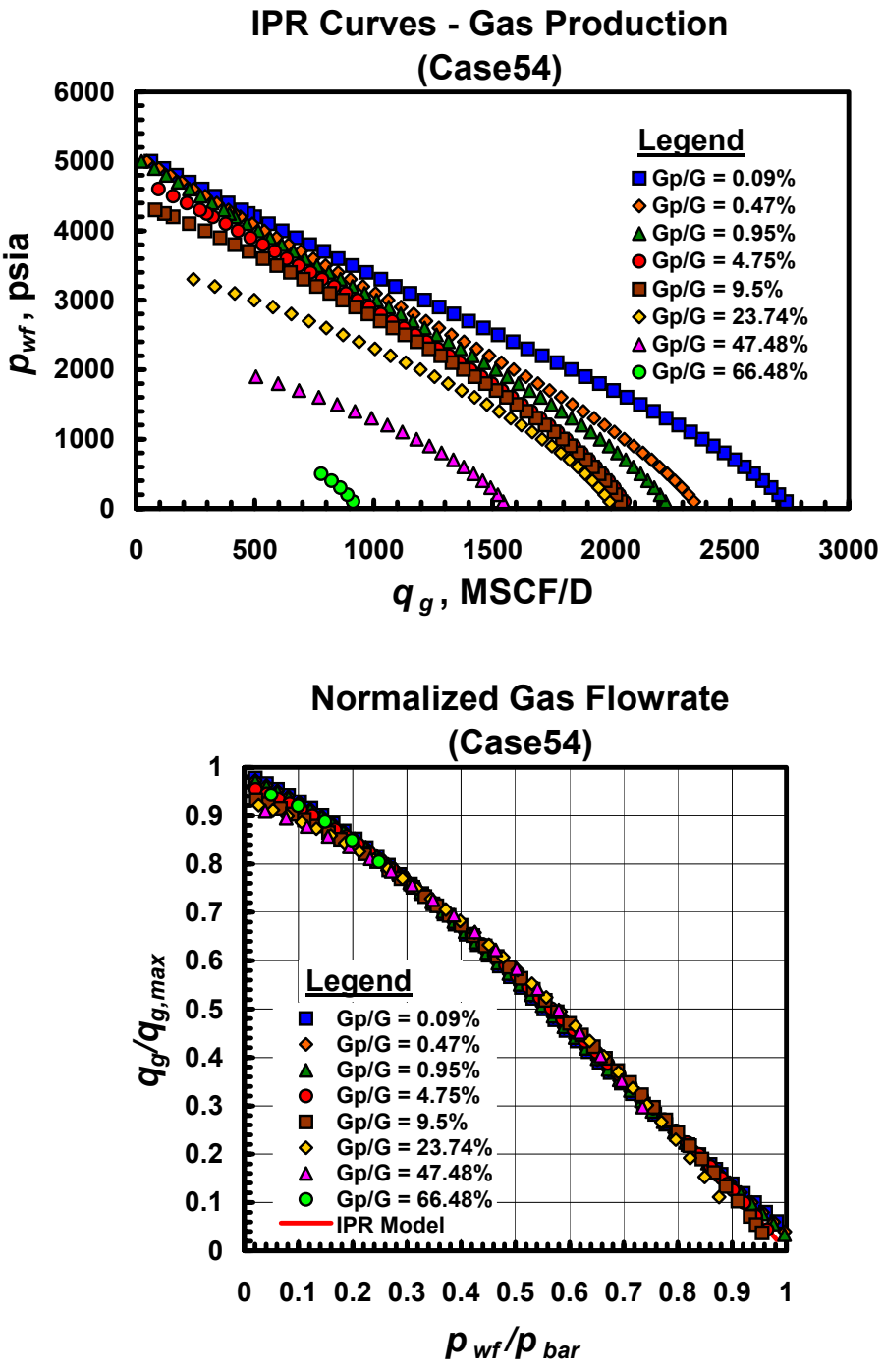

Fig. A.54.b — Dimensional and dimensionless IPR trends for Case 54 — gas performance trends.

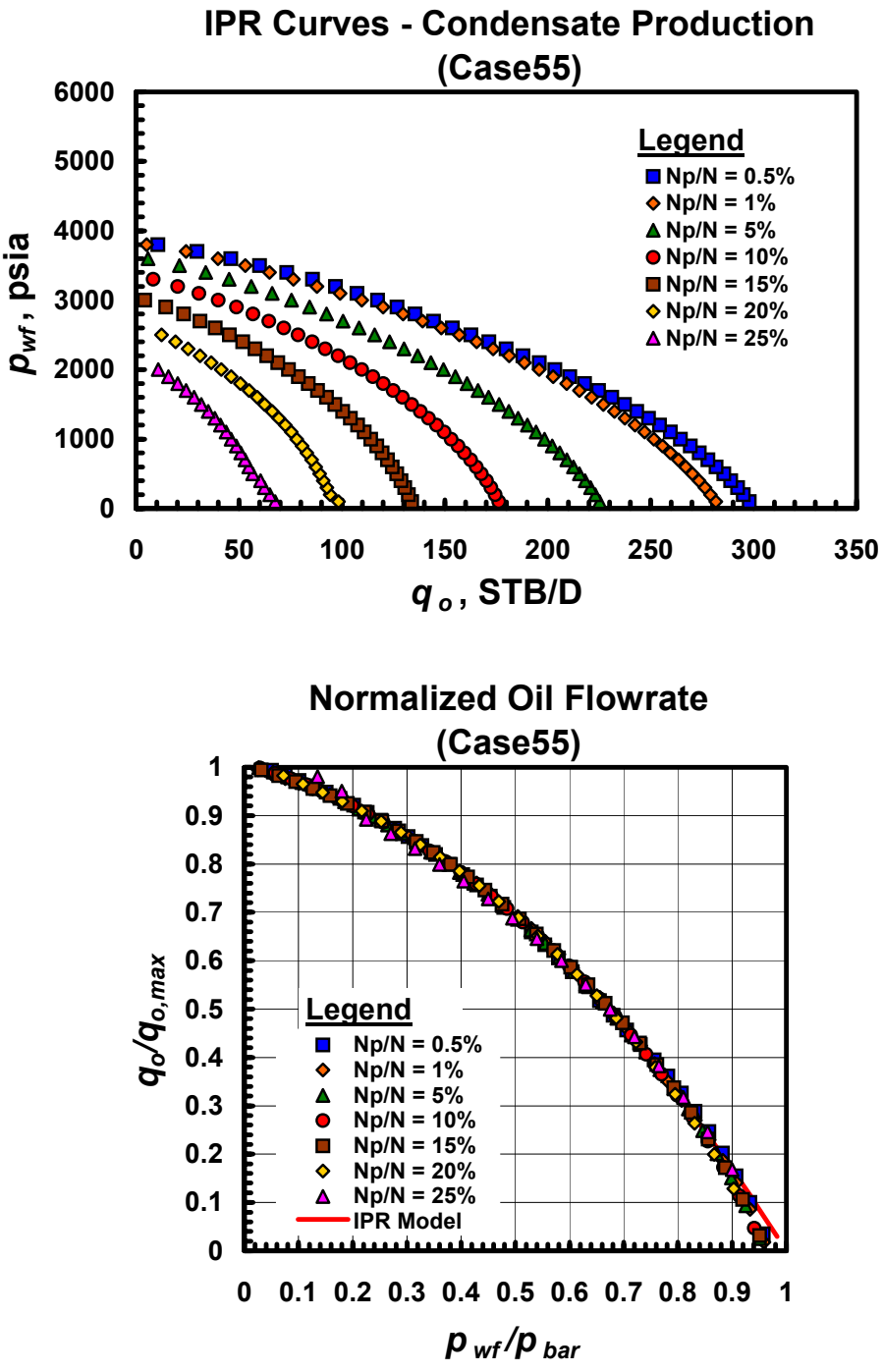

Fig. A.55.a — Dimensional and dimensionless IPR trends for Case 55 — gas condensate performance trends.

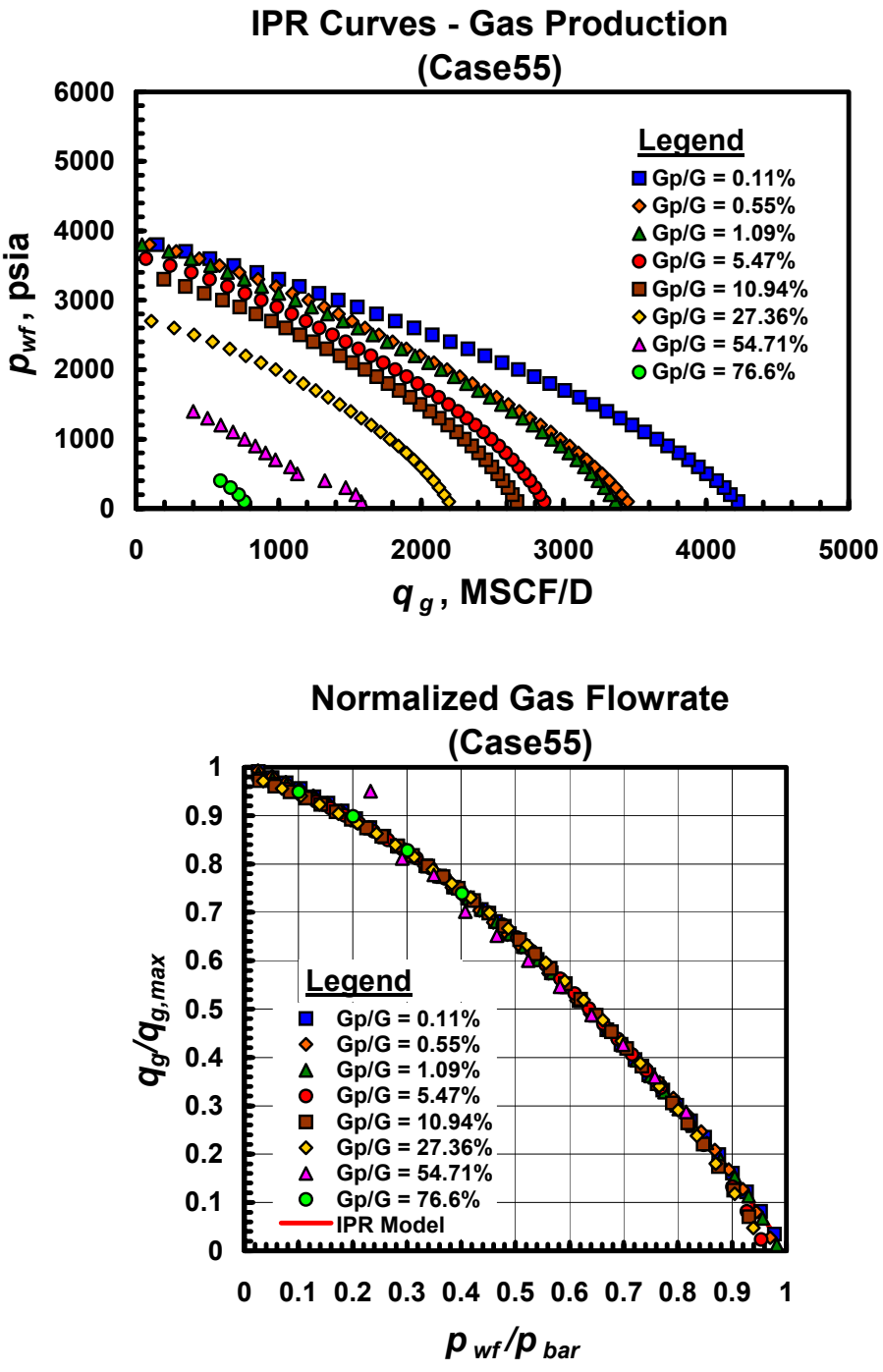

Fig. A.55.b — Dimensional and dimensionless IPR trends for Case 55 — gas performance trends.

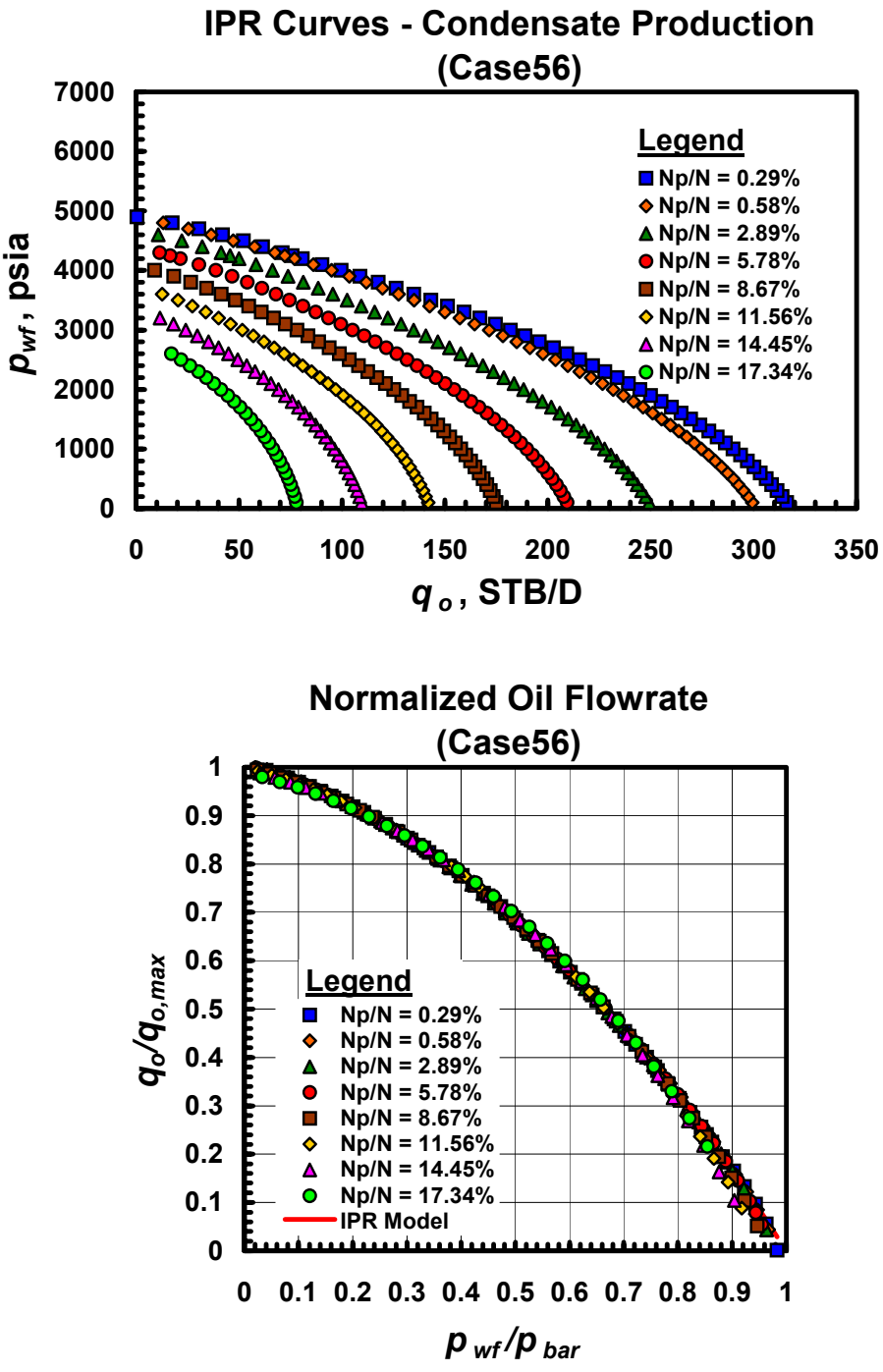

Fig. A.56.a — Dimensional and dimensionless IPR trends for Case 56 — gas condensate performance trends.

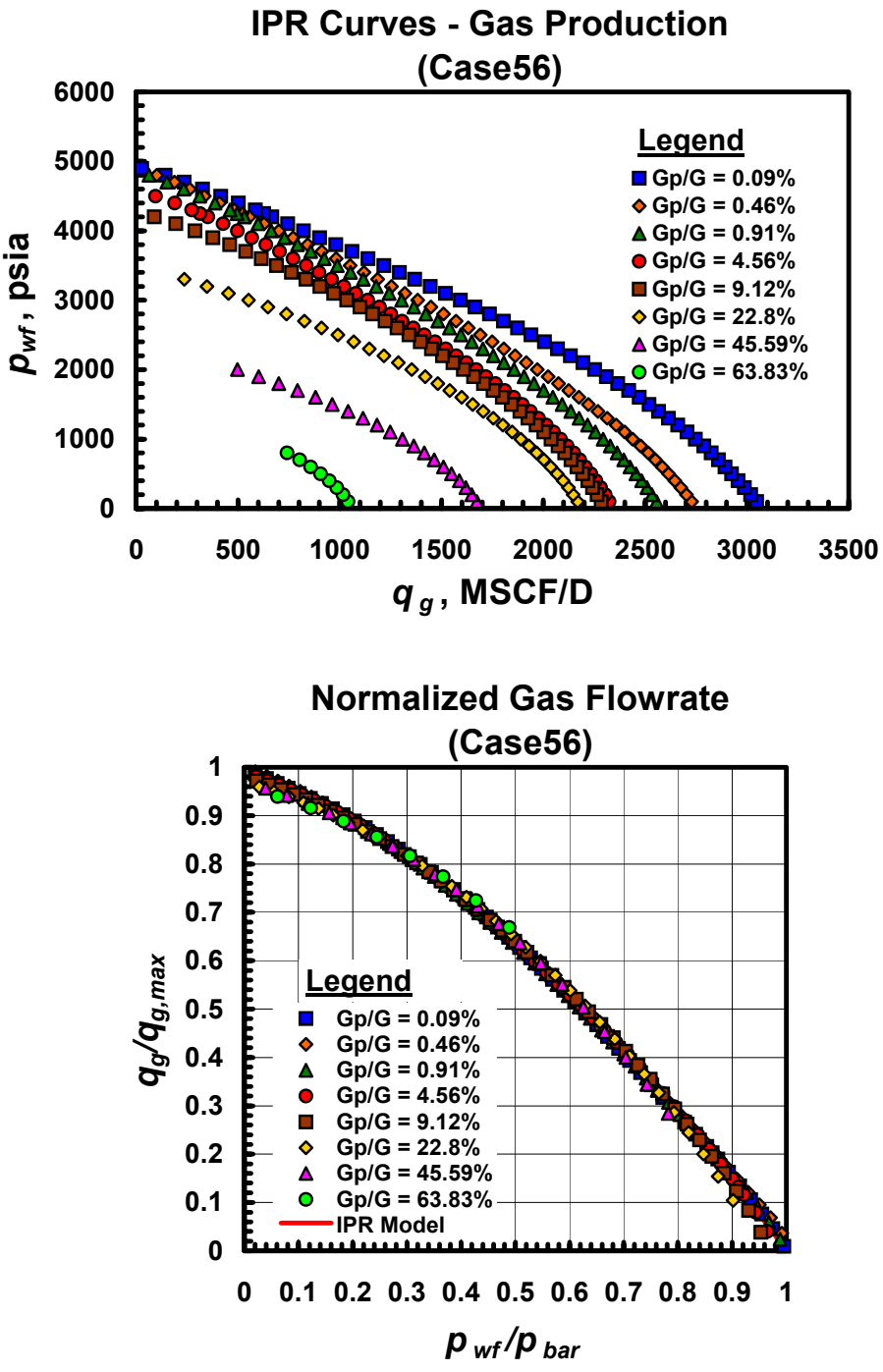

Fig. A.56.b — Dimensional and dimensionless IPR trends for Case 56 — gas performance trends.

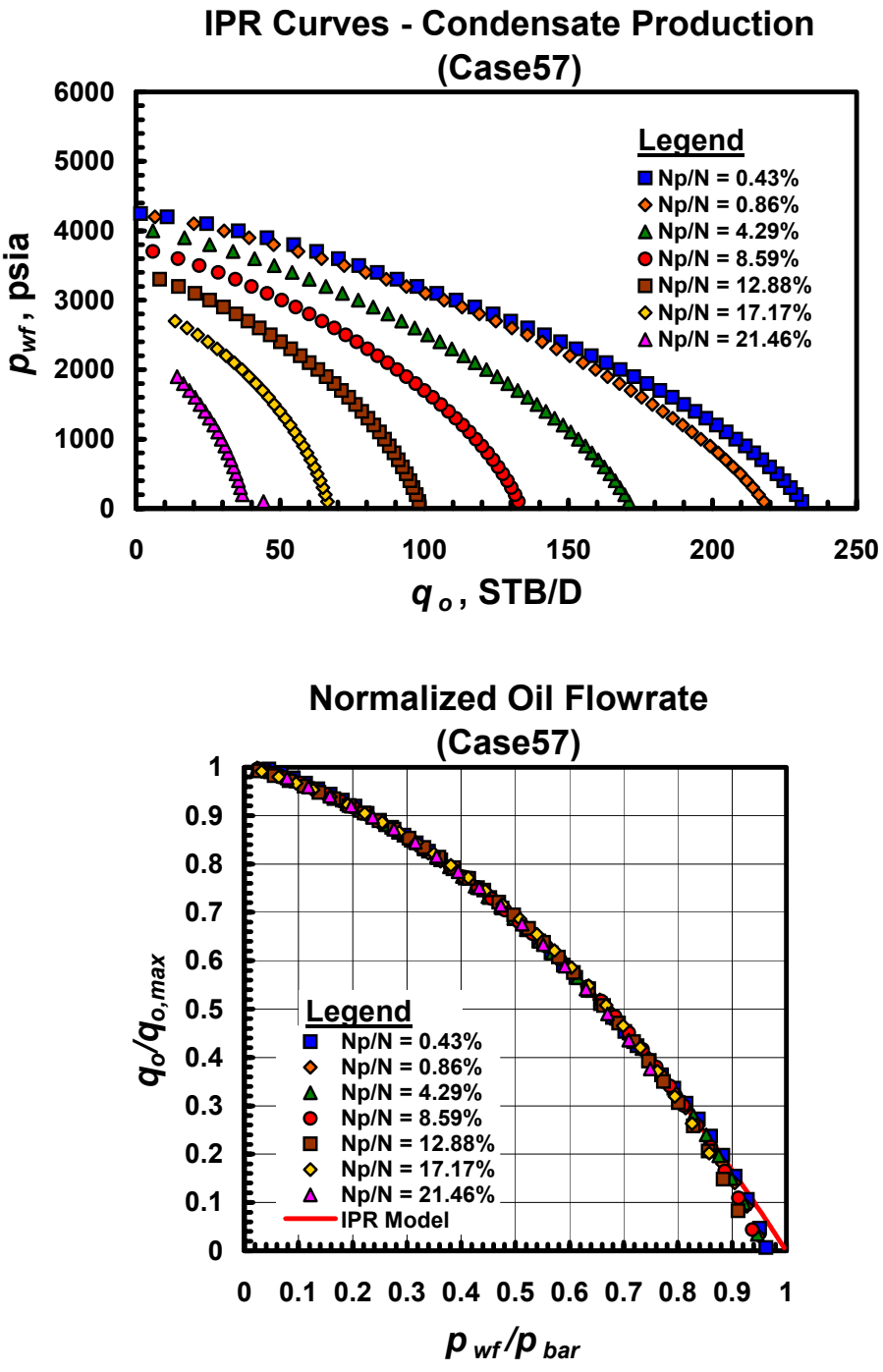

Fig. A.57.a — Dimensional and dimensionless IPR trends for Case 57 — gas condensate performance trends.

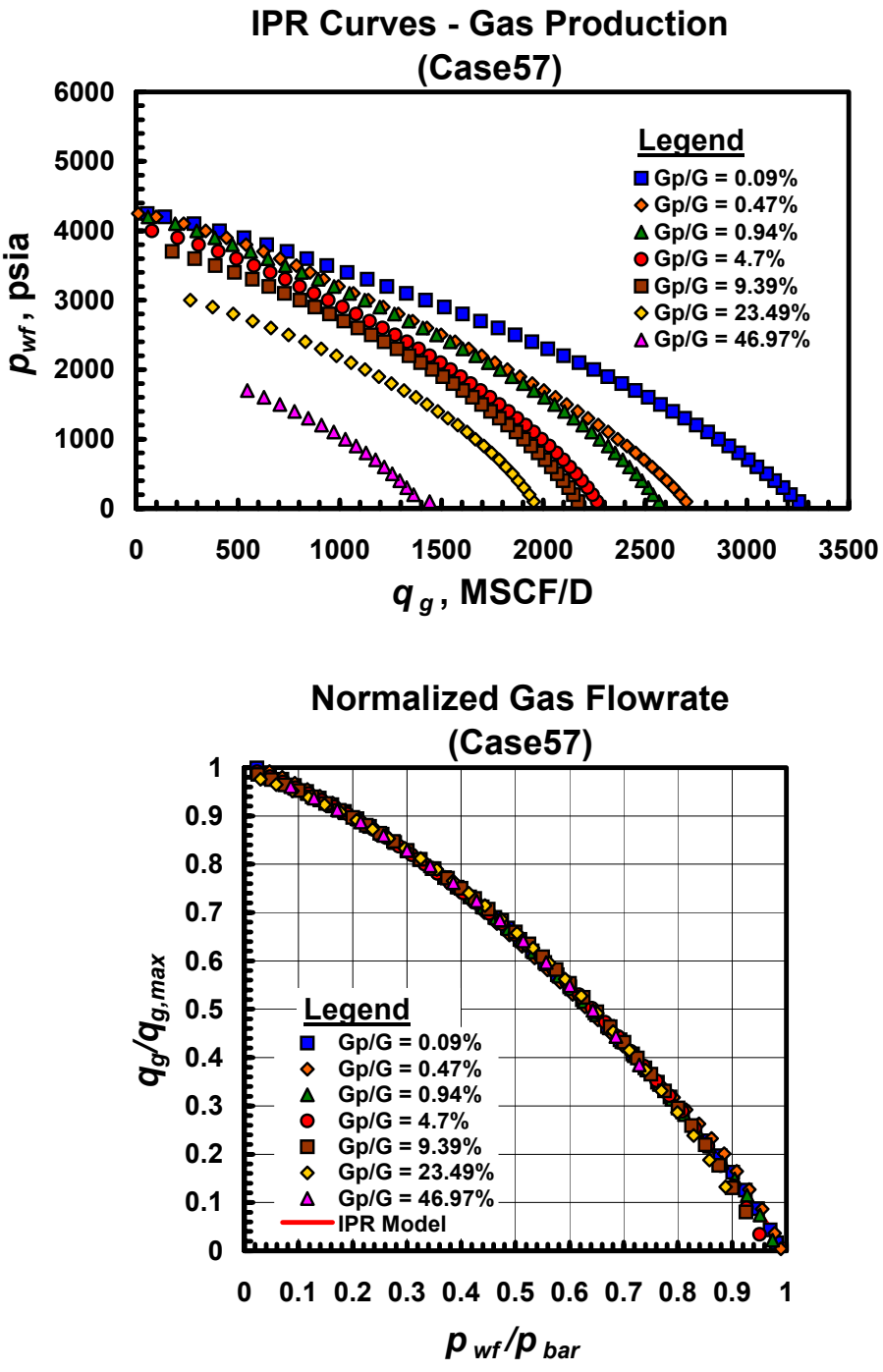

Fig. A.57.b — Dimensional and dimensionless IPR trends for Case 57 — gas performance trends.

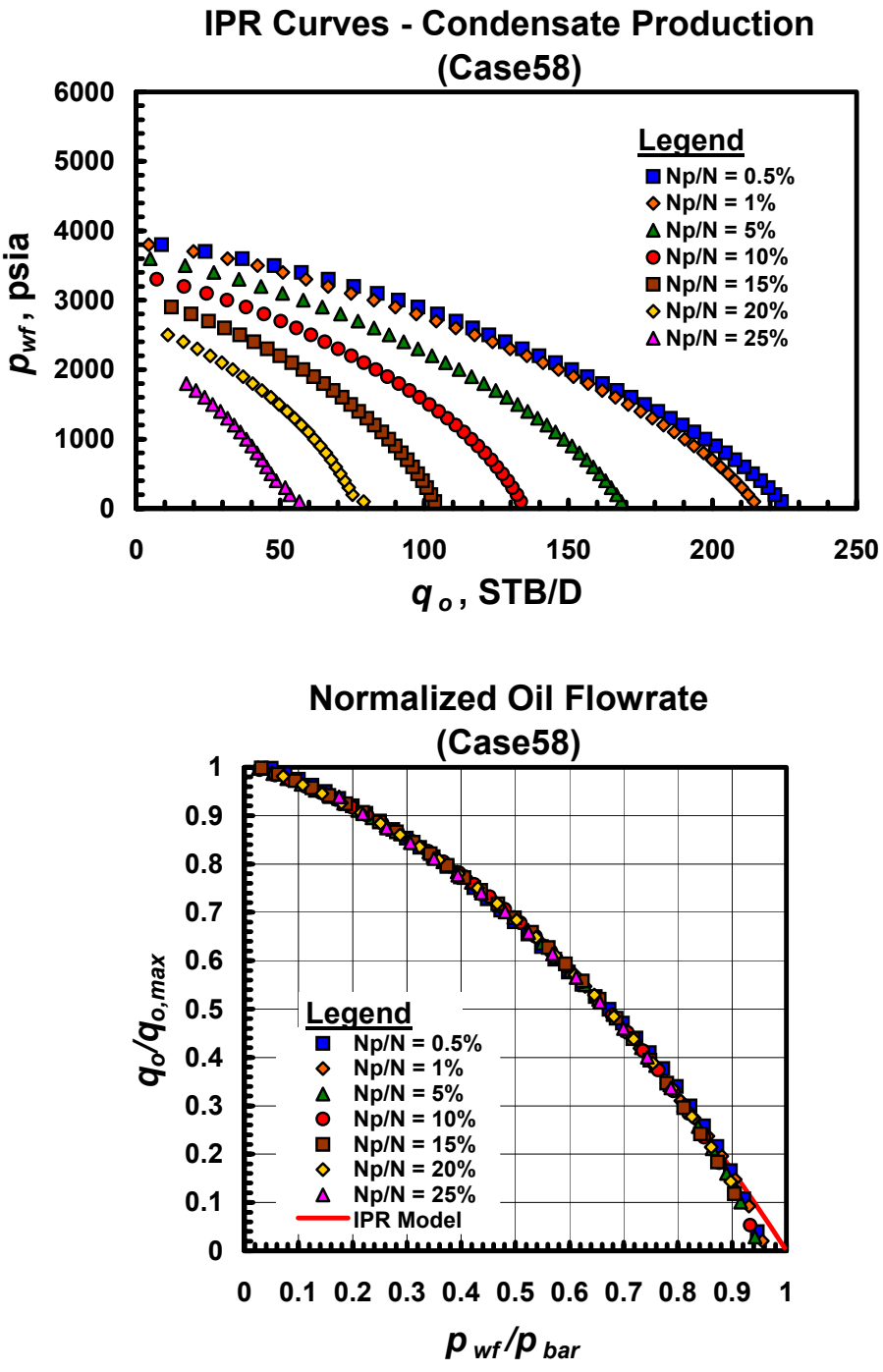

Fig. A.58.a — Dimensional and dimensionless IPR trends for Case 58 — gas condensate performance trends.

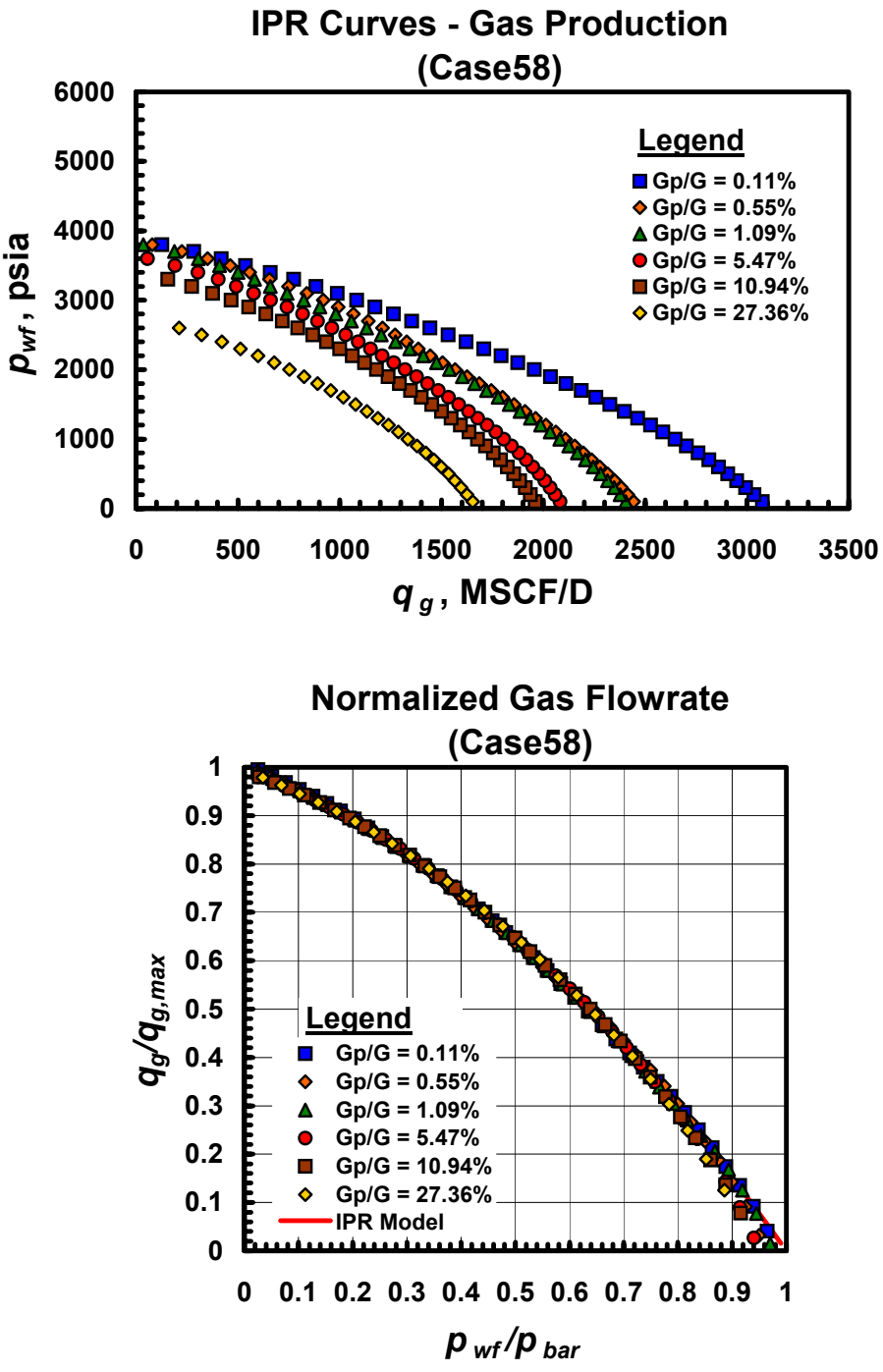

Fig. A.58.b — Dimensional and dimensionless IPR trends for Case 58 — gas performance trends.

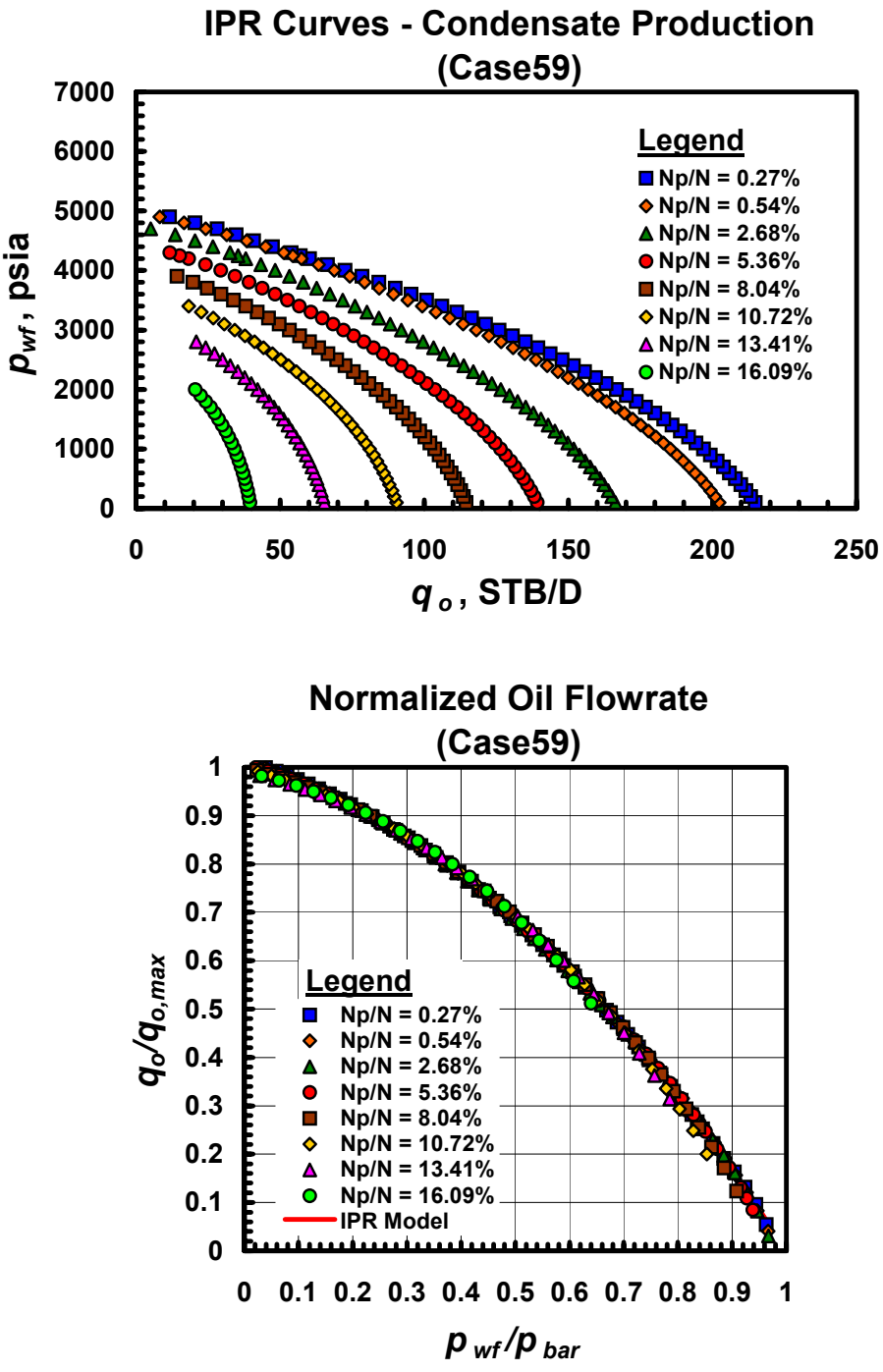

Fig. A.59.a — Dimensional and dimensionless IPR trends for Case 59 — gas condensate performance trends.

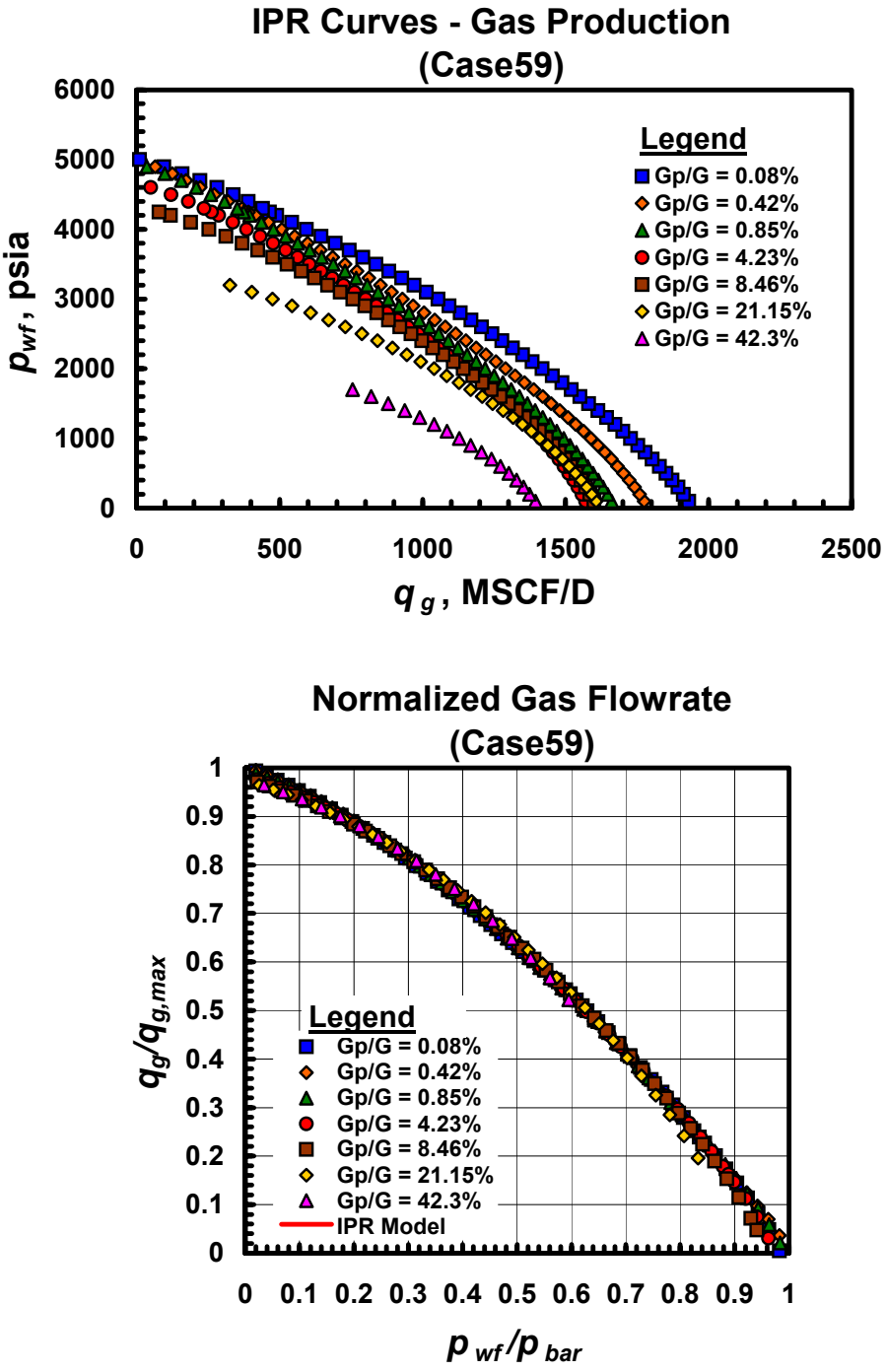

Fig. A.59.b — Dimensional and dimensionless IPR trends for Case 59 — gas performance trends.

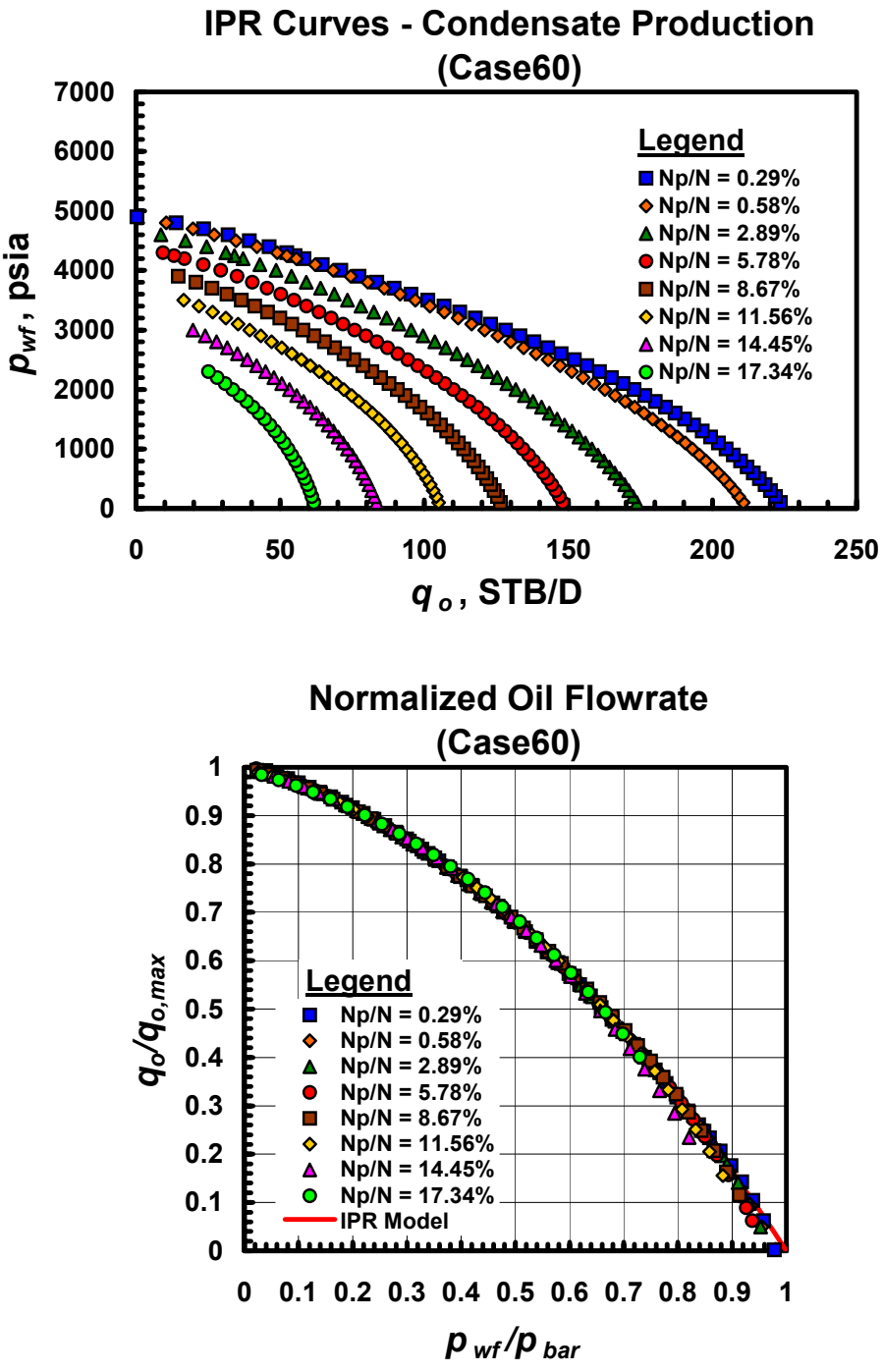

Fig. A.60.a — Dimensional and dimensionless IPR trends for Case 60 — gas condensate performance trends.

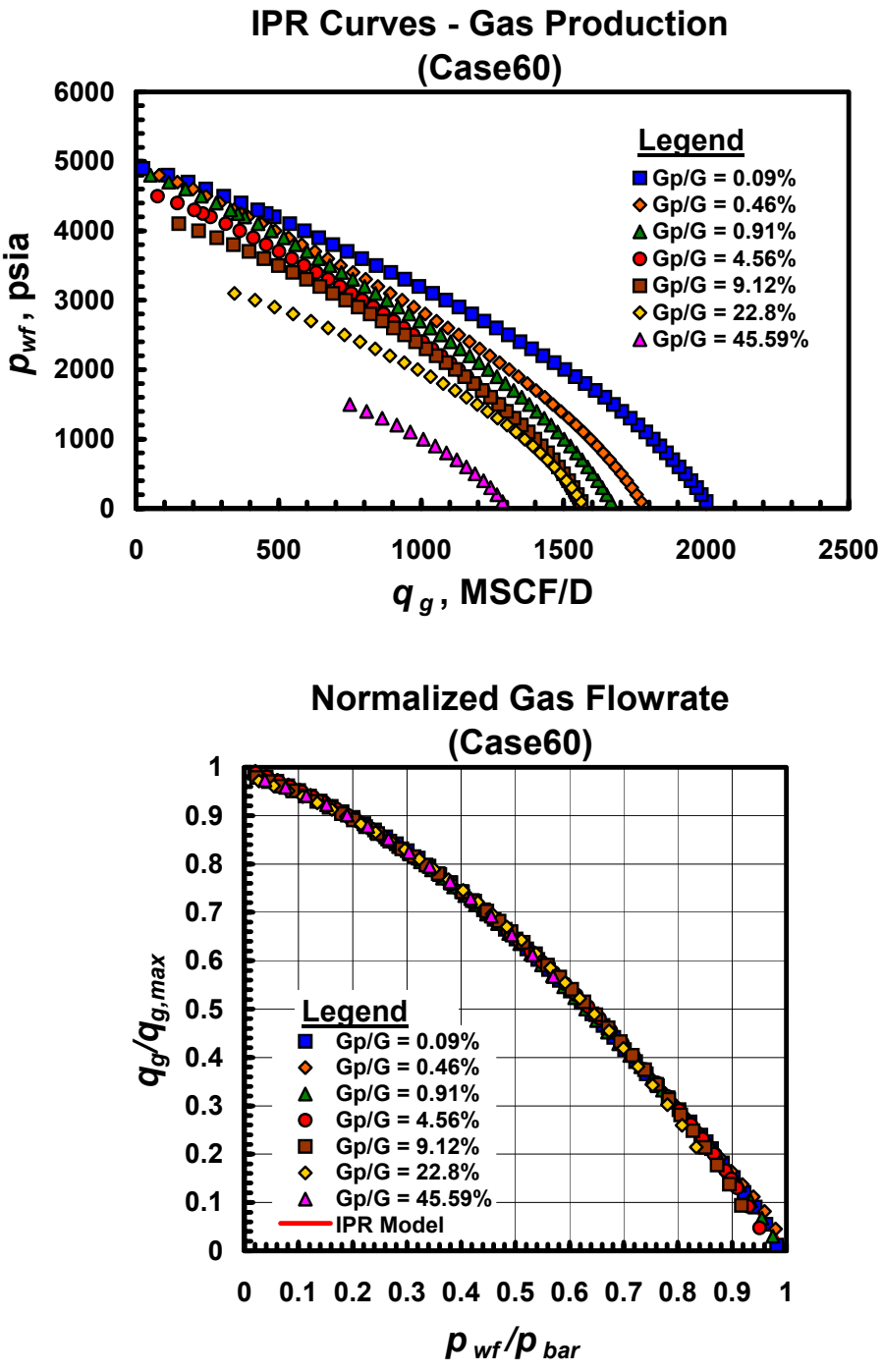

Fig. A.60.b — Dimensional and dimensionless IPR trends for Case 60 — gas performance trends.

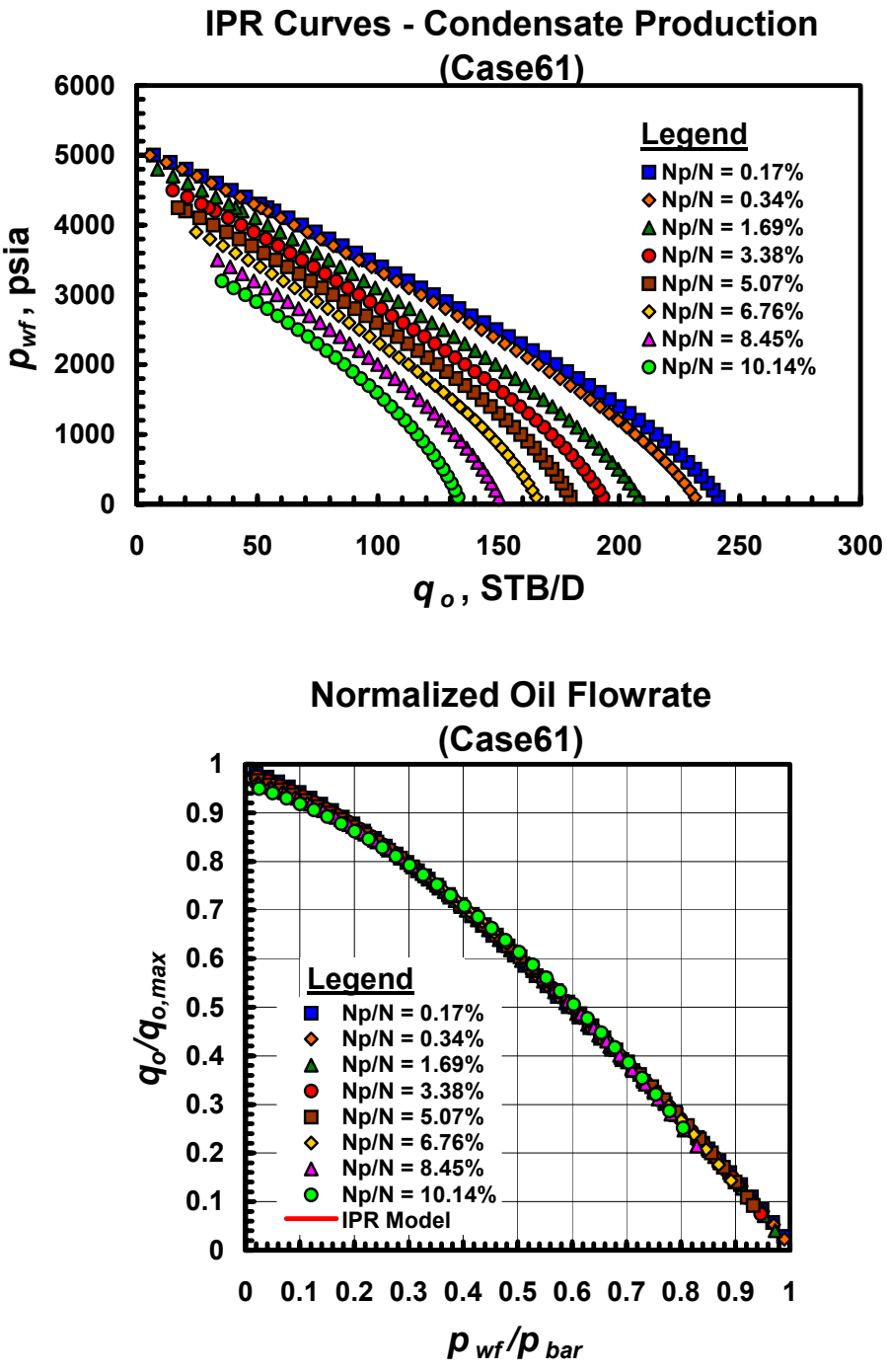

Fig. A.61.a — Dimensional and dimensionless IPR trends for Case 61 — gas condensate performance trends.

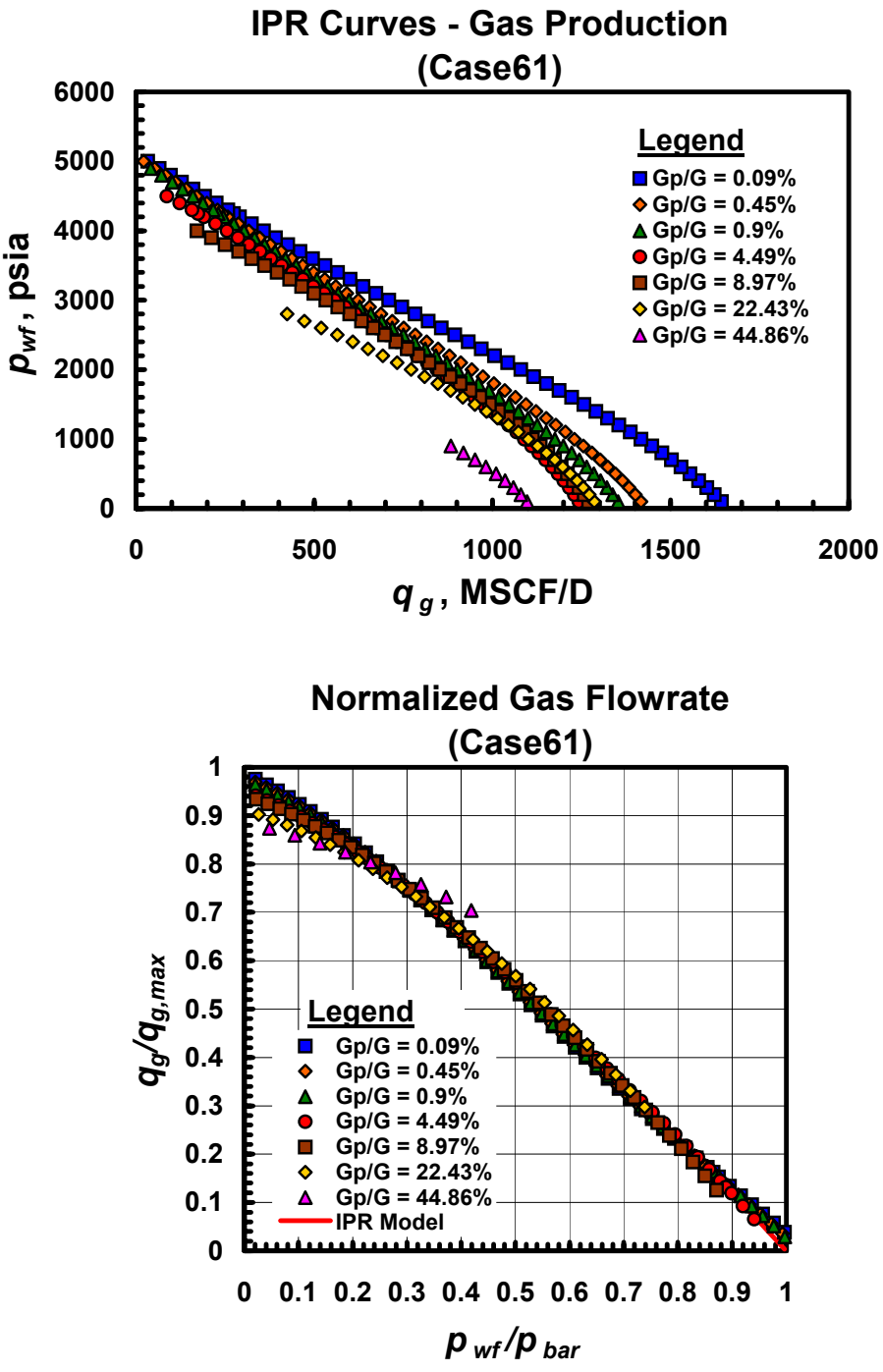

Fig. A.61.b — Dimensional and dimensionless IPR trends for Case 61 — gas performance trends.

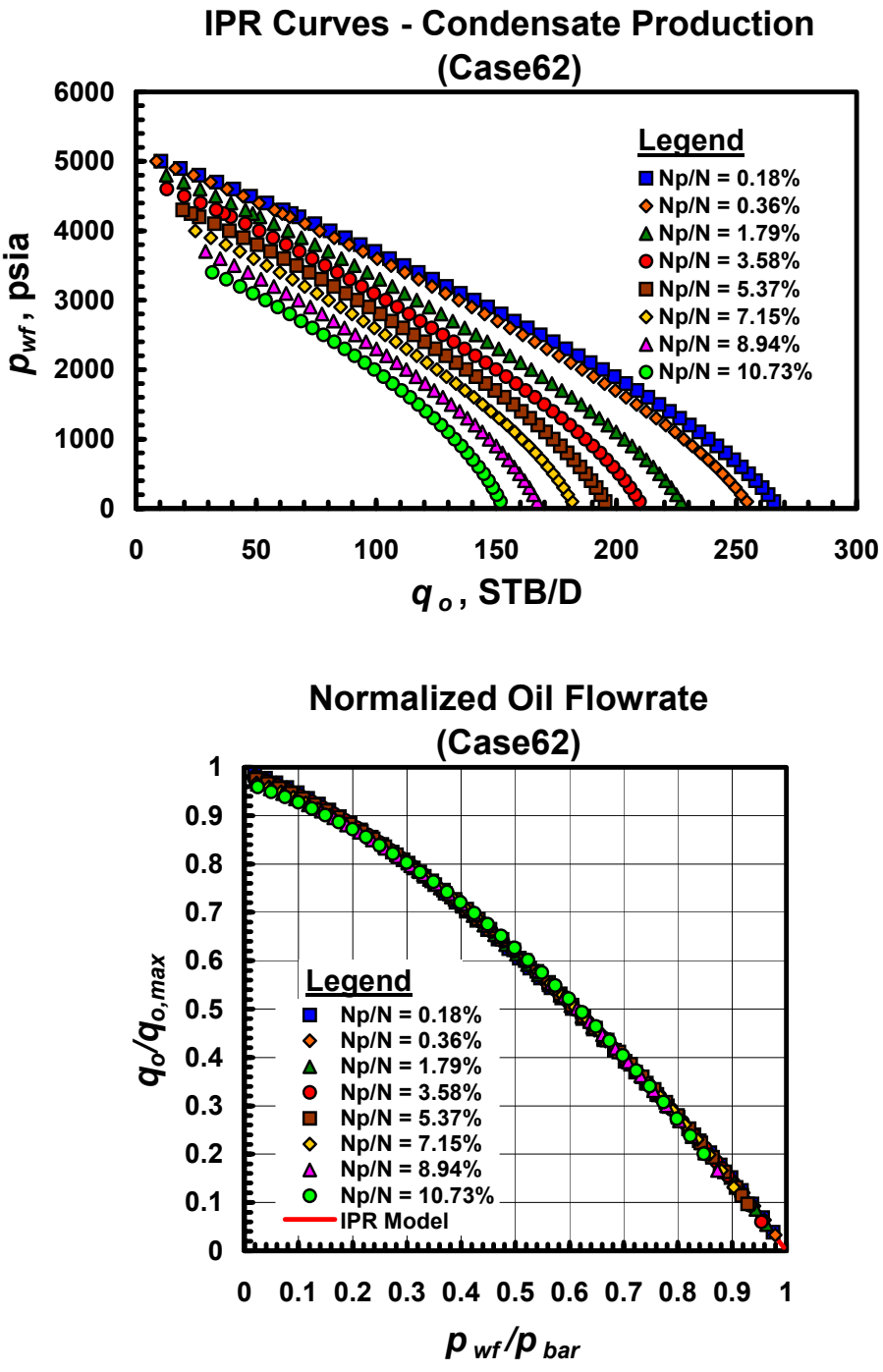

Fig. A.62.a — Dimensional and dimensionless IPR trends for Case 62 — gas condensate performance trends.

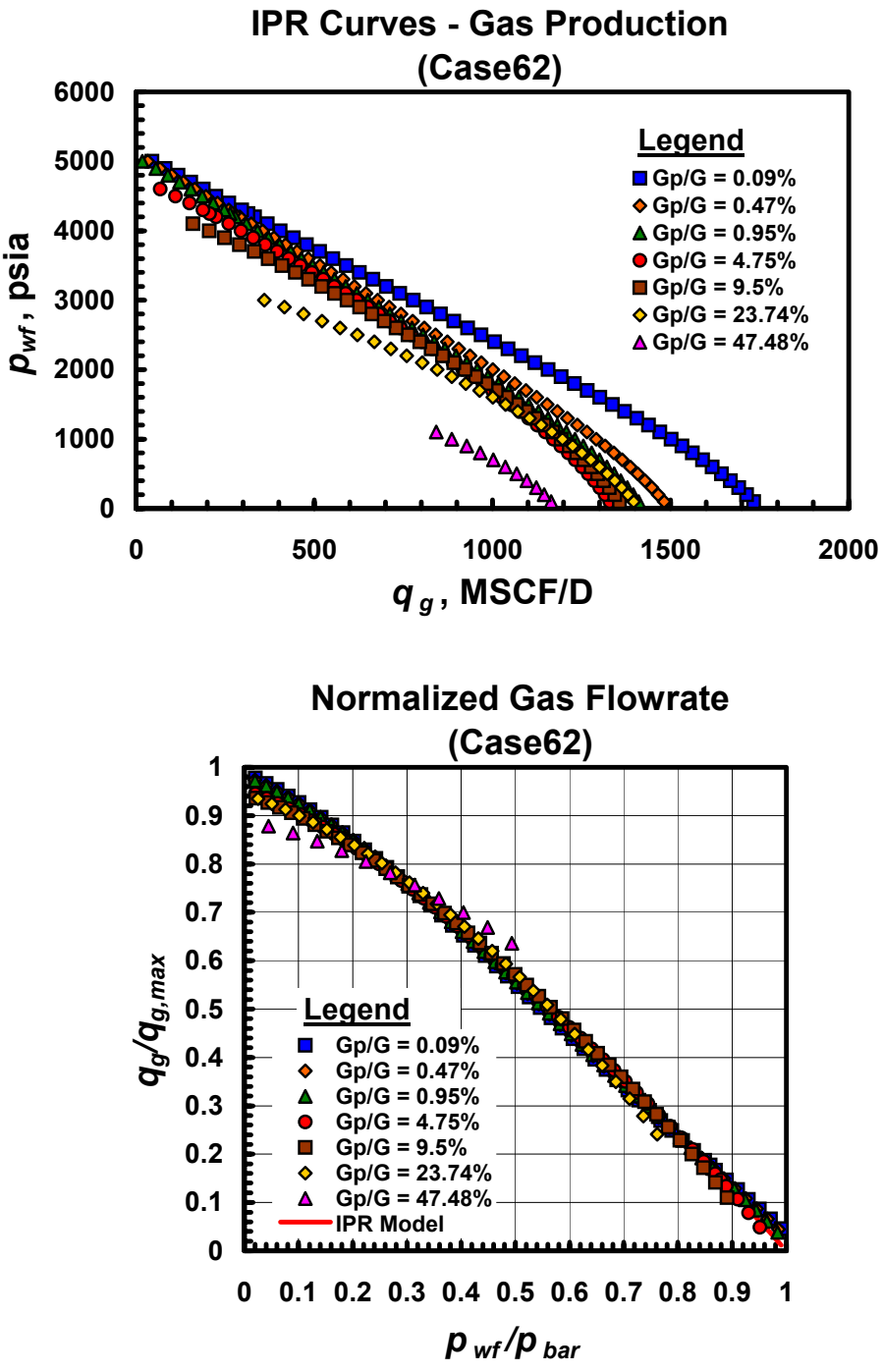

Fig. A.62.b — Dimensional and dimensionless IPR trends for Case 62 — gas performance trends.

APPENDIX B

EXAMPLE 5 — SIMULATED PERFORMANCE CASE

B.1 Data – Example 5 (Eclipse 300 Case)

Table B.1 shows the compositional data as well as the reservoir and fluid properties for Example 5 (a case generated using Eclipse 300)

Table B.1 — Example 5 — Compositional data.

Components	Mole fraction	Molecular weight	Critical pressure (psia)	Critical temperature (deg R)	Critical volume (MSCF/lb_m)	Critical compressibility factor
CO2	0.0121	44.0100	1071.33	548.46	1.51	0.27
N2	0.0194	28.0130	492.31	227.16	1.44	0.29
C1	0.6599	16.0430	667.78	343.08	1.57	0.28
C2	0.0869	30.0700	708.34	549.77	2.37	0.28
C3	0.0591	44.0970	618.70	665.64	3.20	0.28
IC4	0.0239	58.1240	529.05	734.58	4.21	0.28
NC4	0.0278	58.1240	550.66	765.36	4.08	0.27
IC5	0.0157	72.1510	483.50	828.72	4.93	0.27
NC5	0.0112	72.1510	489.52	845.28	4.98	0.27
C6	0.0181	84.0000	484.38	921.60	5.62	0.28
C7+	0.0659	140.0000	335.09	1129.51	8.90	0.25
$M_{mixture}$ (lb_m/lb-mole)	32.5742					

Reservoir temperature = 200 deg F
Initial reservoir pressure = 4365 psia
Dew point pressure = 4365 psia

For this simulation case, "Set 7" was used for the relative permeability curves, the water saturation were set to zero, and the porosity and absolute permeability values were 0.25 and 50 md respectively. In addition, the Zudkevitch-Joffe-Redlick-Kwong EOS was used to model the fluid behavior. The initial pressure for our simulation (*i.e.*, the dewpoint pressure of the fluid) was established using the PBSAT function in Eclipse 300.

B.1.1 Results for Gas Condensate Performance

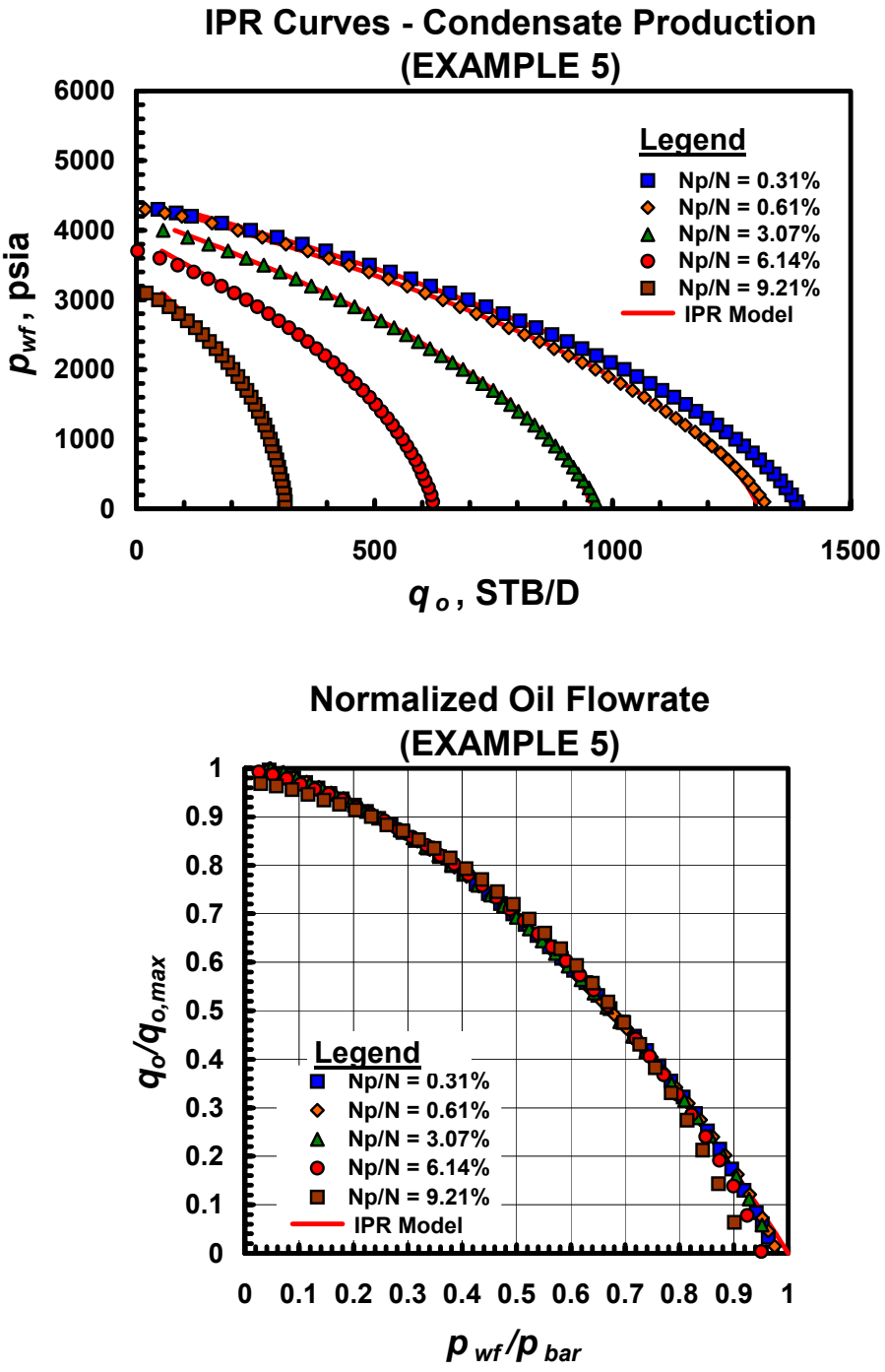

Fig. B.1 — Comparison between measured (simulation) and calculated (IPR model) values ($\nu_o = 0.22$).

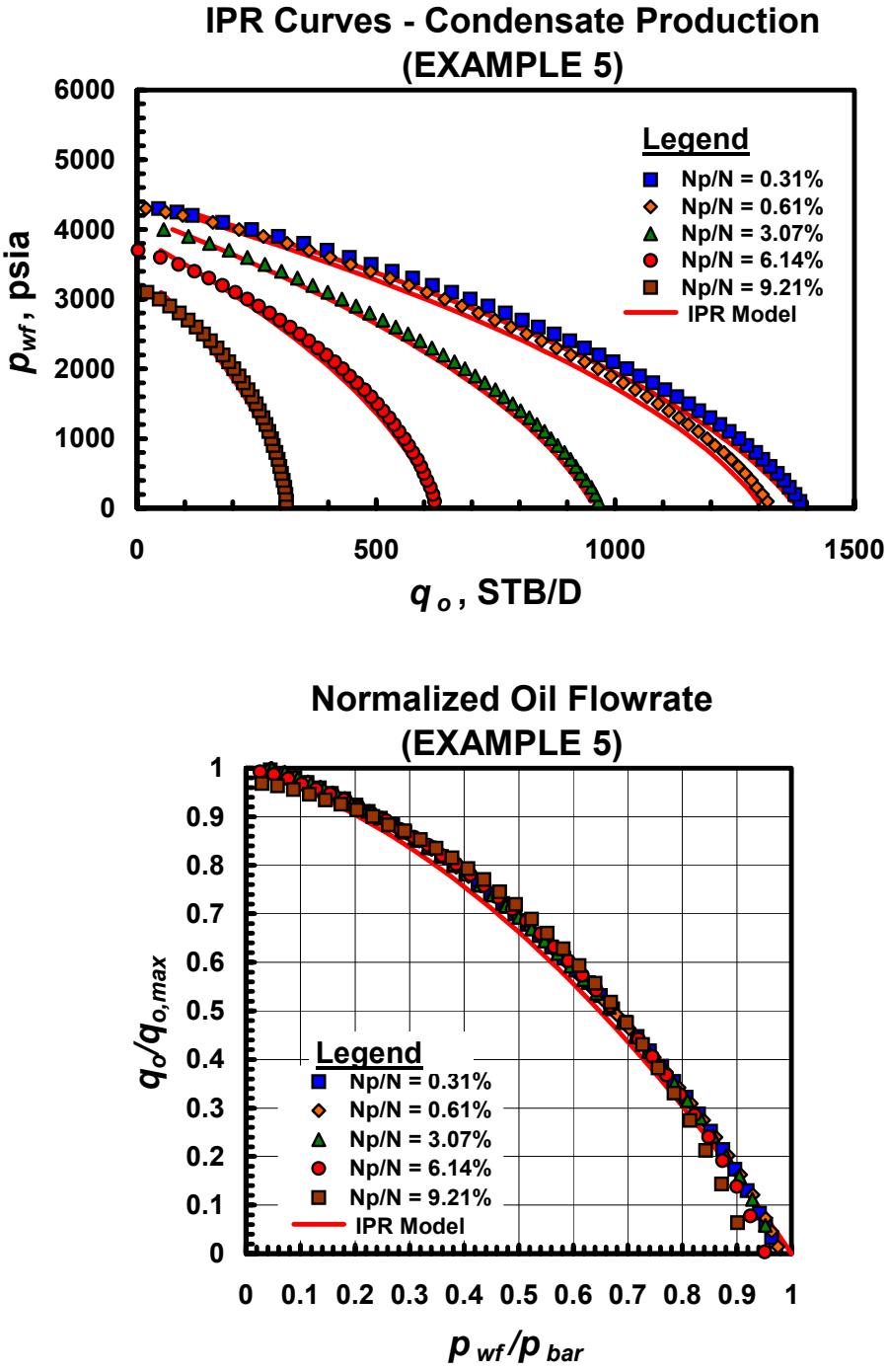

Fig. B.2 — Comparison between measured (simulation) and calculated (IPR model) values ($\nu_o = 0.35$).

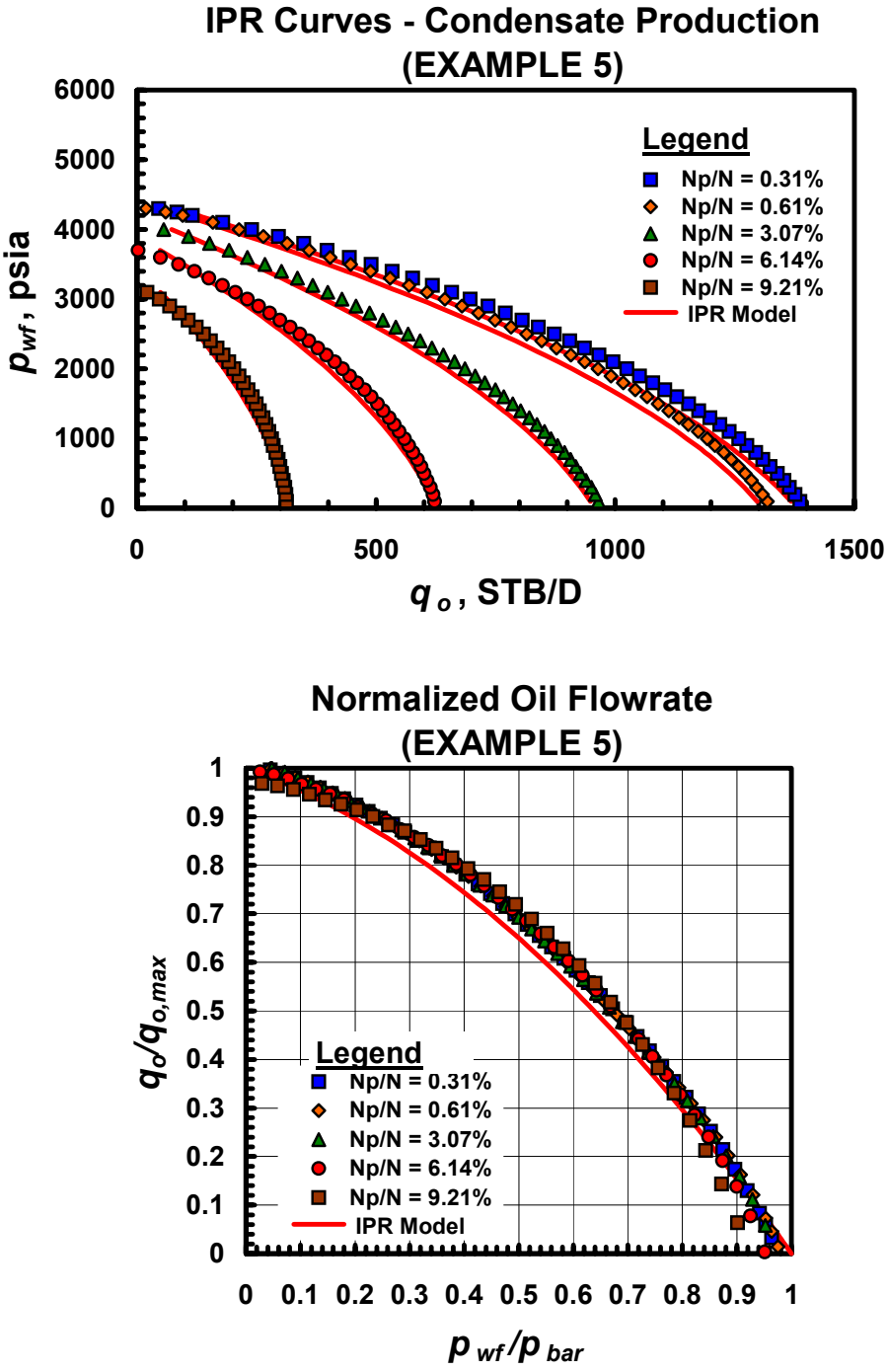

Fig. B.3 — Comparison between measured (simulation) and calculated (IPR model) values ($\nu_o = 0.40$).

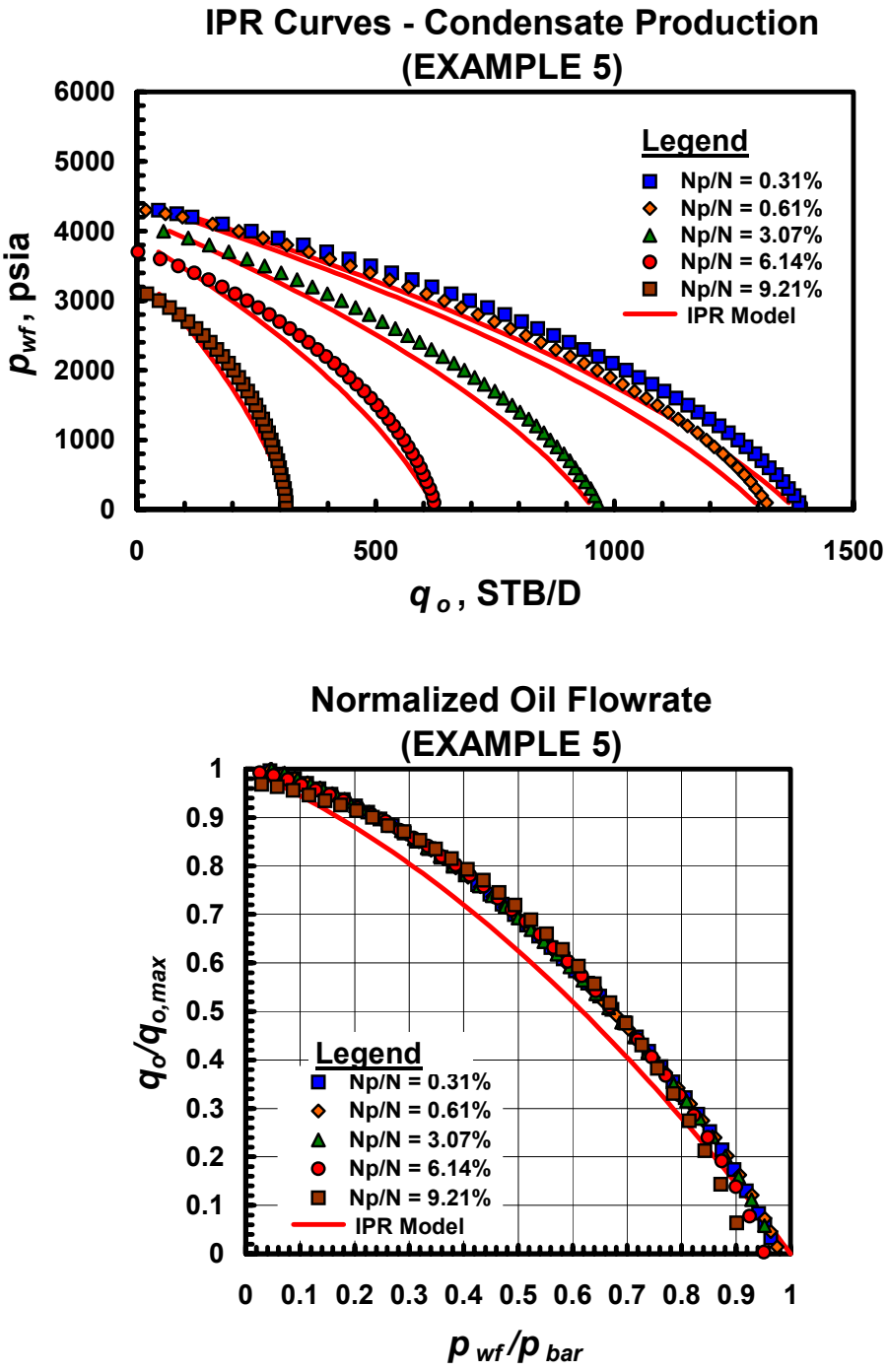

Fig. B.4 — Comparison between measured (simulation) and calculated (IPR model) values ($\nu_o = 0.50$).

B.1.2 Results for Dry Gas Performance

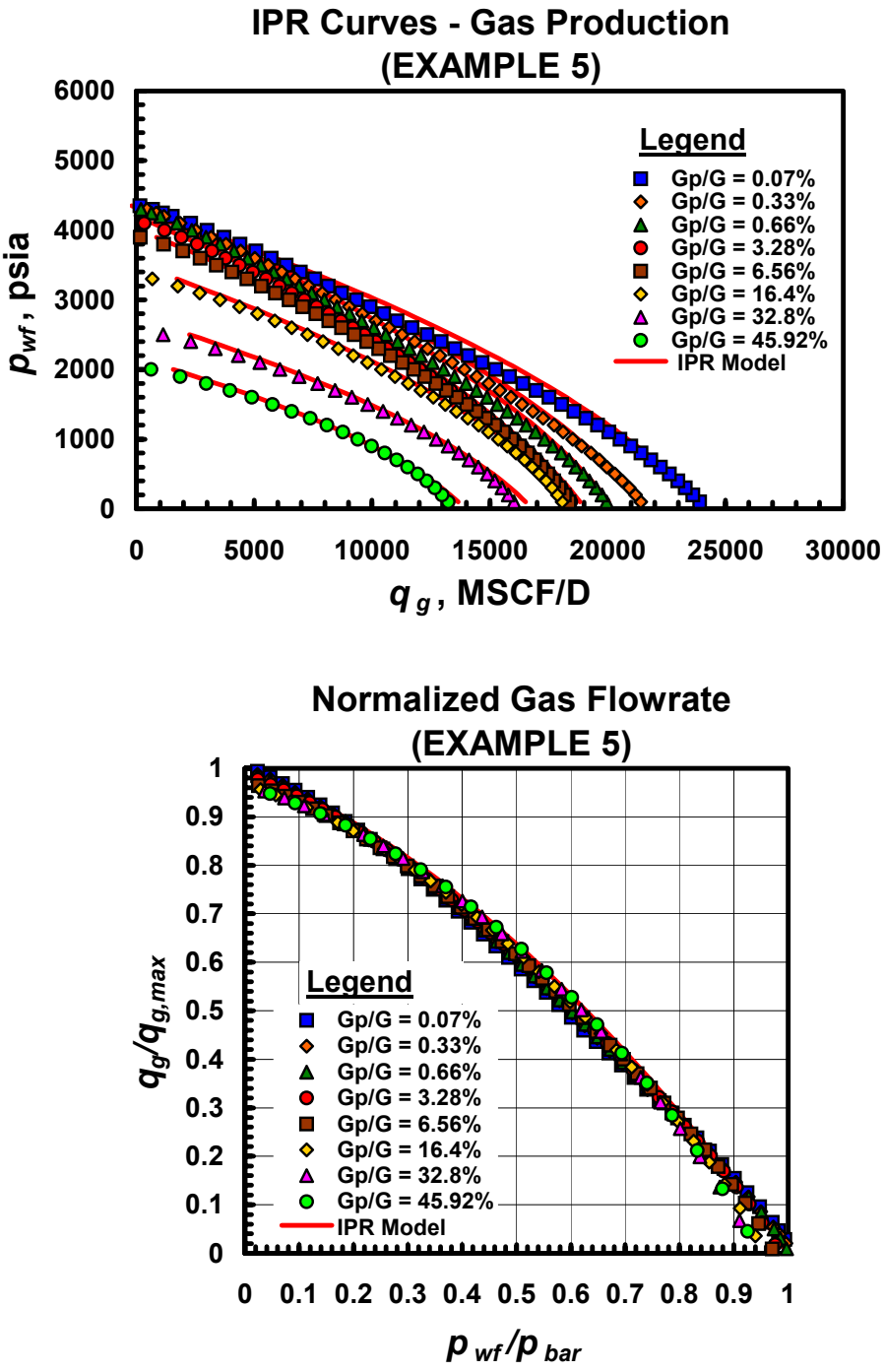

Fig. B.5 — Comparison between measured (simulation) and calculated (IPR model) values ($\nu_g = 0.45$).

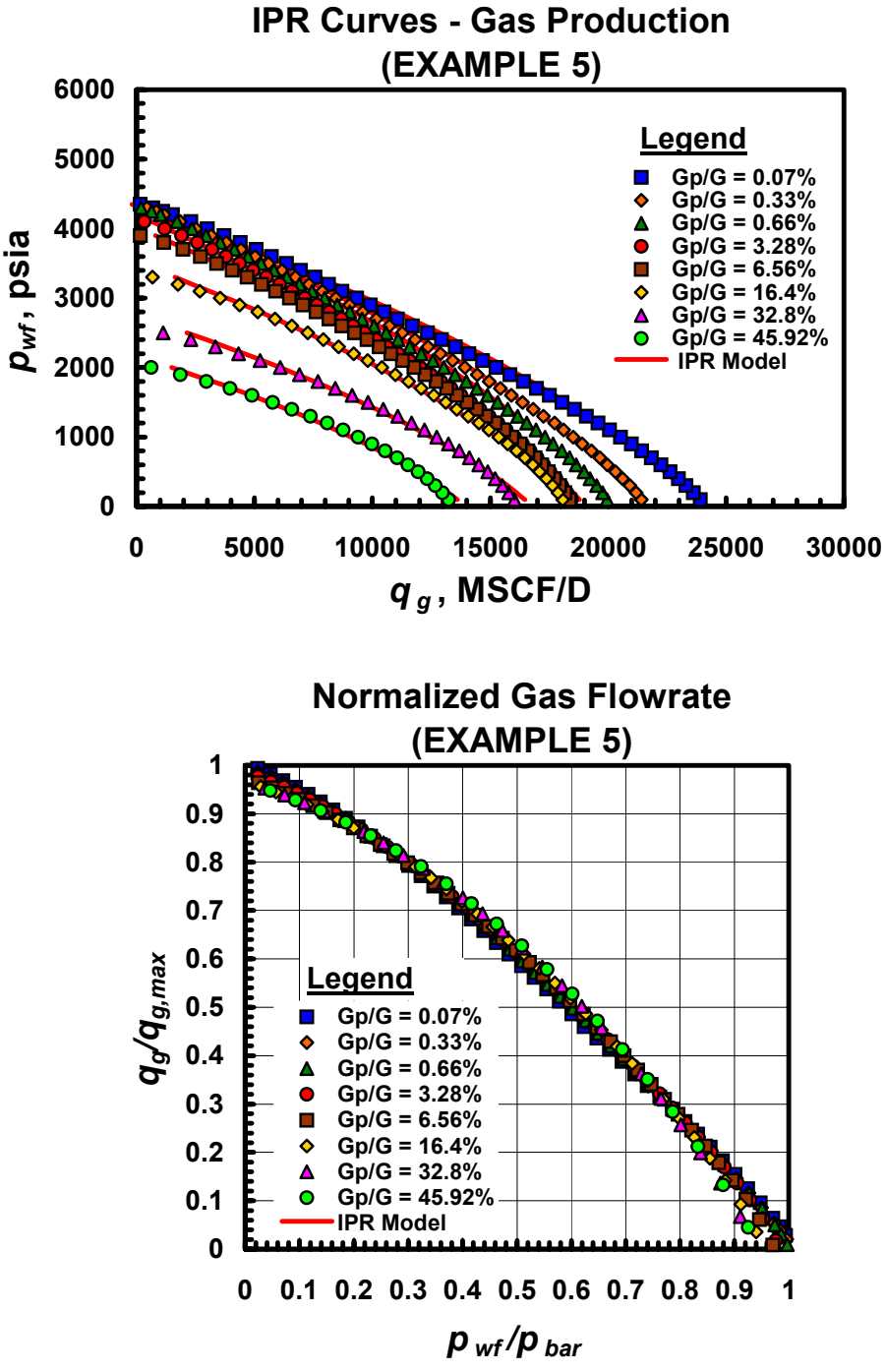

Fig. B.6 — Comparison between measured (simulation) and calculated (IPR model) values ($\nu_g = 0.54$).

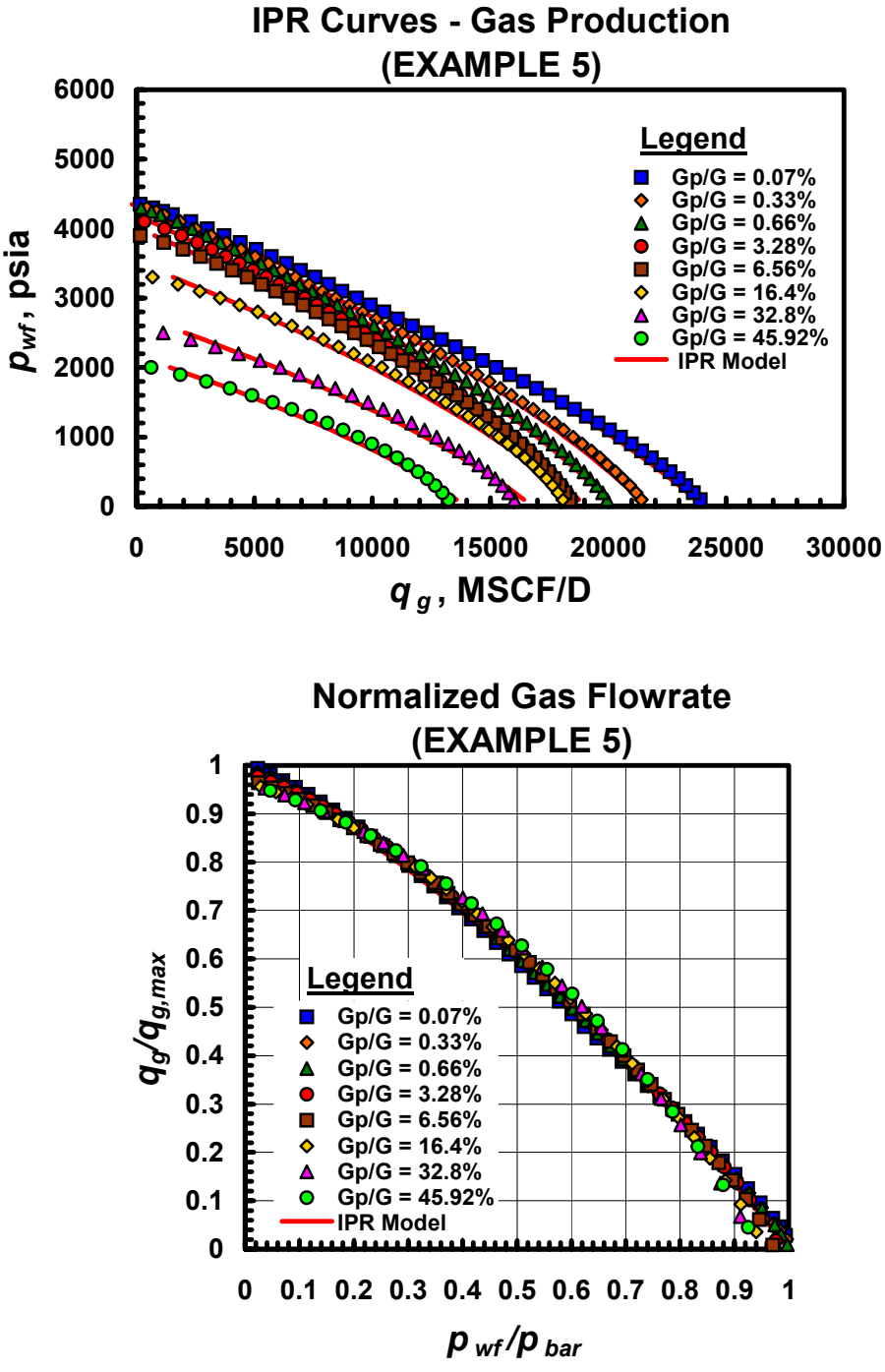

Fig. B.7 — Comparison between measured (simulation) and calculated (IPR model) values ($\nu_g = 0.60$).

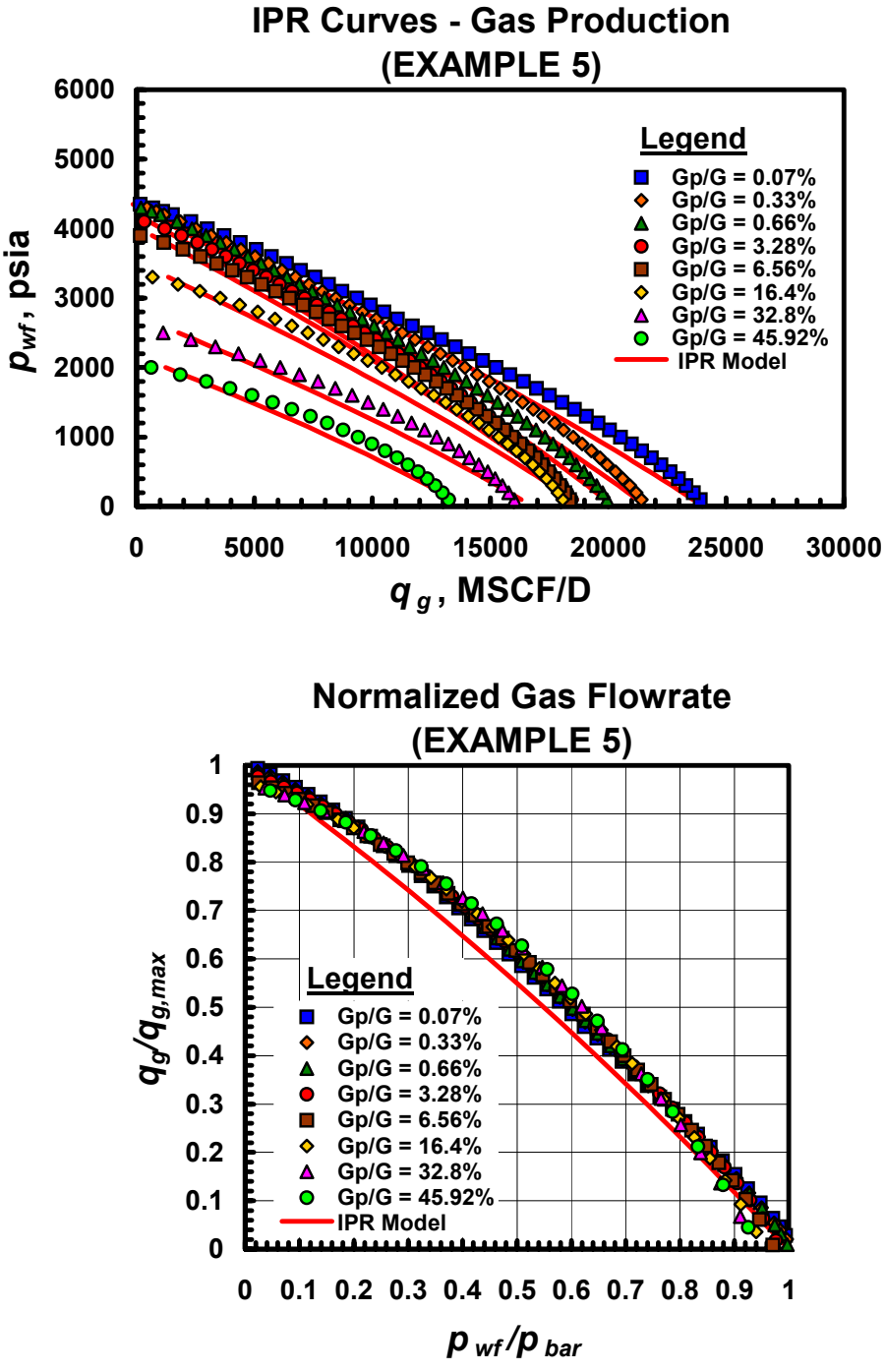

Fig. B.8 — Comparison between measured (simulation) and calculated (IPR model) values ($\nu_g = 0.80$).

B.2 Data – SPE 35649 (ref. 22)

Table B.2 shows the compositional data as well as the reservoir and fluid properties for SPE paper 35649.

Table B.2 — SPE 35649 — Compositional data.

Components	Mole Fraction	Molecular Weight
CO2	0.0023	44.0100
N2	0.0051	28.0130
C1	0.8407	16.0430
C2	0.0705	30.0700
C3	0.0269	44.0970
IC4	0.0093	58.1240
NC4	0.0078	58.1240
IC5	0.0038	72.1510
NC5	0.0028	72.1510
C6	0.0042	86.1780
C7+	0.0266	--

Reservoir temperature = 209.75 deg F
Initial reservoir pressure = 31.48 (MPa) = 4565.78 psia
Dew point pressure = 31.26 (MPa) = 4548.38 psia

$C7^+$ additional data:
Critical pressure = 2.98 (MPa) = 432.21 psia
Critical temperature = 1074.96 deg R = 615.29 deg F

Relative permeability end points:
S_{oc} = 0.2015
S_{gr} = 0.2915

Since the molecular weight of the $C7^+$ fraction was not part of the data provided. We estimated this value using the Matthews, *et al.*[25] correlation and the Stewart, *et al.*[26] method by adjusting the $C7^+$ pseudocritical properties (**Table B.3**). **Table B.4** shows the molecular weight of the $C7^+$ fraction obtained using these methods.

Table B.3 — Adjustment of Pseudocritical Properties of the $C7^+$ Fraction.

		Value	
		Calculated	Actual
Matthews, et. al correlation			
$p_{pc}\_C7^+$ (psia)		436.53	432.21
$T_{pc}\_C7^+$ (deg R)		1075.73	1074.96
Stewart, et .al method			
Specific gravity ($C7^+$)	0.7902		
$T_b\_C7^+$	734.44		
$p_{pc}\_C7^+$ (psia)		441.73	432.21
$T_{pc}\_C7^+$ (deg R)		1074.96	1074.96

Table B.4 — Results of the $C7^+$ Fraction Adjustment.

Component	Mole fraction ($\check{z}_i$)	Molecular weight (M_i)	$M_i\check{z}_i$	Critical pressure p_{ci} (psia)	Critical temperature T_{ci} (deg R)	$\check{z}_i T_{ci}$	$\check{z}_i p_{ci}$
N2	0.0051	28.0130	0.1429	492.31	227.16	1.1585	2.5108
C1	0.8407	16.0430	13.4874	667.78	343.08	288.4274	561.4026
CO2	0.0023	44.0100	0.1012	1071.30	548.46	1.2615	2.4640
C2	0.0705	30.0700	2.1199	708.34	549.77	38.7588	49.9380
C3	0.0269	44.0970	1.1862	615.76	665.64	17.9057	16.5639
IC4	0.0093	58.1240	0.5406	529.05	734.58	6.8316	4.9202
NC4	0.0078	58.1240	0.4534	550.66	765.36	5.9698	4.2951
IC5	0.0038	72.1510	0.2742	491.58	828.72	3.1491	1.8680
NC5	0.0028	72.1510	0.2020	488.79	845.28	2.3668	1.3686
C6	0.0042	86.1780	0.3619	436.62	913.50	3.8367	1.8338
C7+	0.0266	**114.2310**	3.0385	432.21	1074.96	28.5939	11.4969
		$M_{mixture}$ (lb_m/lb-mole)	21.9082				
		Gas specific gravity (SC)	0.756				

Once the molecular weight of the $C7^+$ fraction was calculated, we then determined the molecular weight of the gas mixture as well as the specific gravity of the gas at standard conditions. To determine the gas density at the dewpoint pressure and at reservoir temperature it was necessary to calculate the pseudo-critical properties of the mixture using Kay's[21] mixing rule as well as Sutton's[26] correlation. Once the required pseudocritical values were obtained, the compressibility factor (z) was calculated for both approaches as shown in **Table B.5** using the Standing-Katz[25] (graphical) correlation. Finally, the density values for the gas mixture were very similar: 14.45 lb_m/ft^3 (Kay's rule) and 14.30 lb_m/ft^3 (Sutton approach).

Table B.5 — Gas density calculation.

Kay's Mixing Rule	
Pseudocritical temperature (deg R)	398.2598
Pseudocritical pressure (psia)	658.6619
Pseudoreduced temperature	1.68
Pseudoreduced pressure	6.9055
z	0.96
Gas density (lb_m/ft^3)	14.4461
Sutton's Correlation	
Pseudocritical temperature (deg R)	391.2312
Pseudocritical pressure (psia)	655.6474
Pseudoreduced temperature	1.71
Pseudoreduced pressure	6.9372
z	0.97
Gas density (lb_m/ft^3)	14.3033

B.2.1 Results for Dry Gas

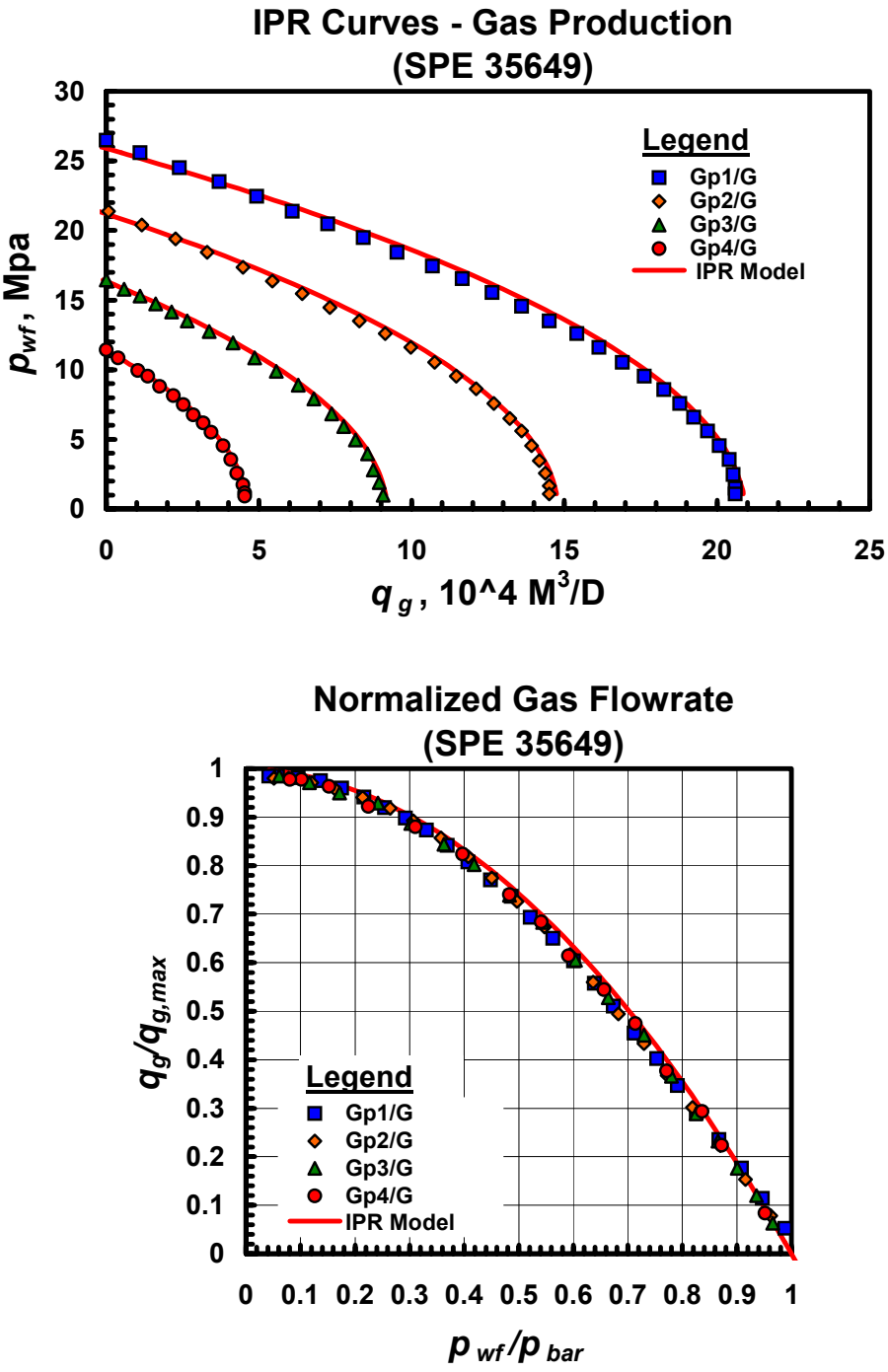

Fig. B.9 — Comparison between measured (simulation) and calculated (IPR model) values ($\nu_g = 0.03$).

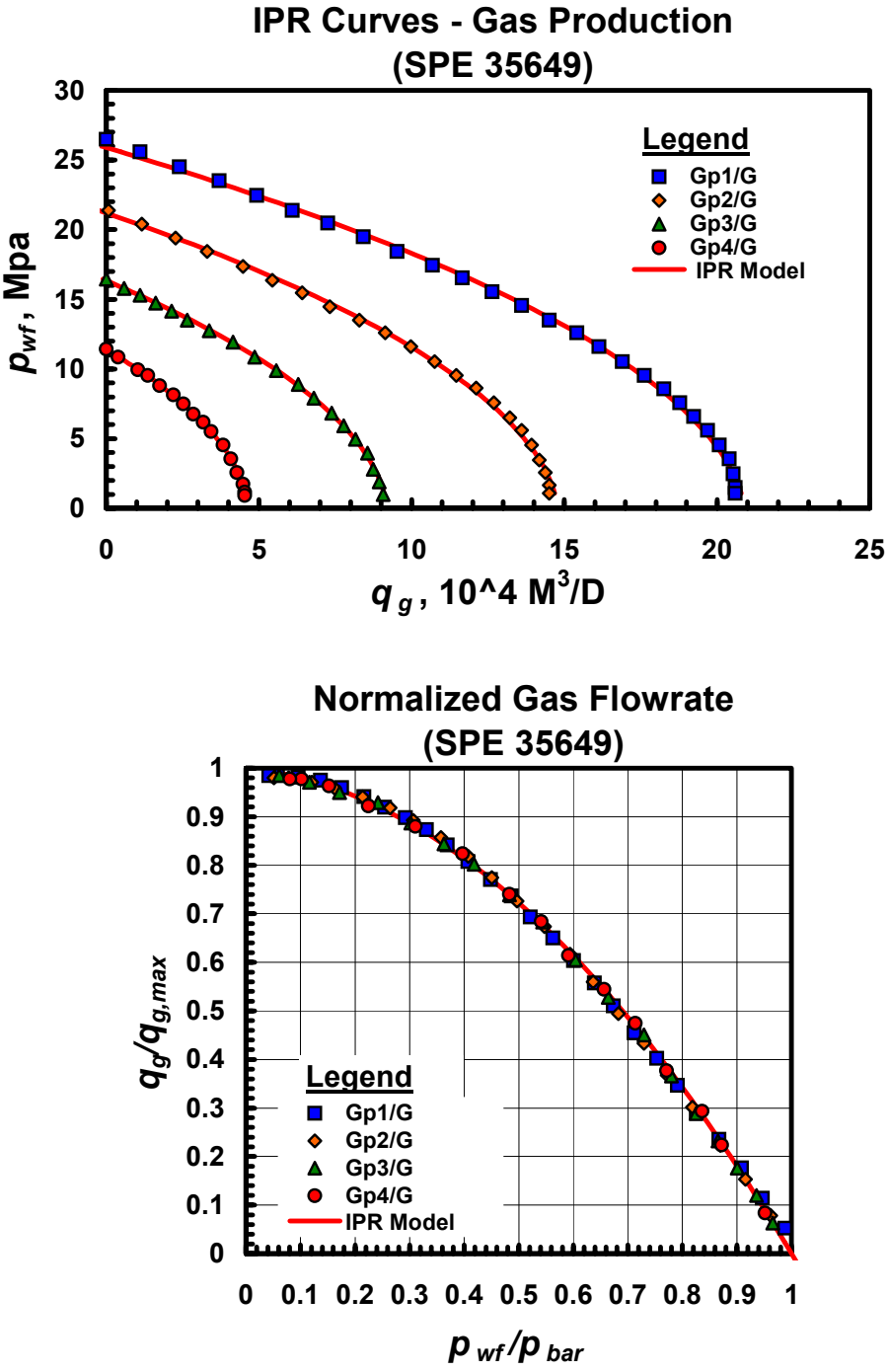

Fig. B.10 — Comparison between measured (simulation) and calculated (IPR model) values ($\nu_g = 0.11$).

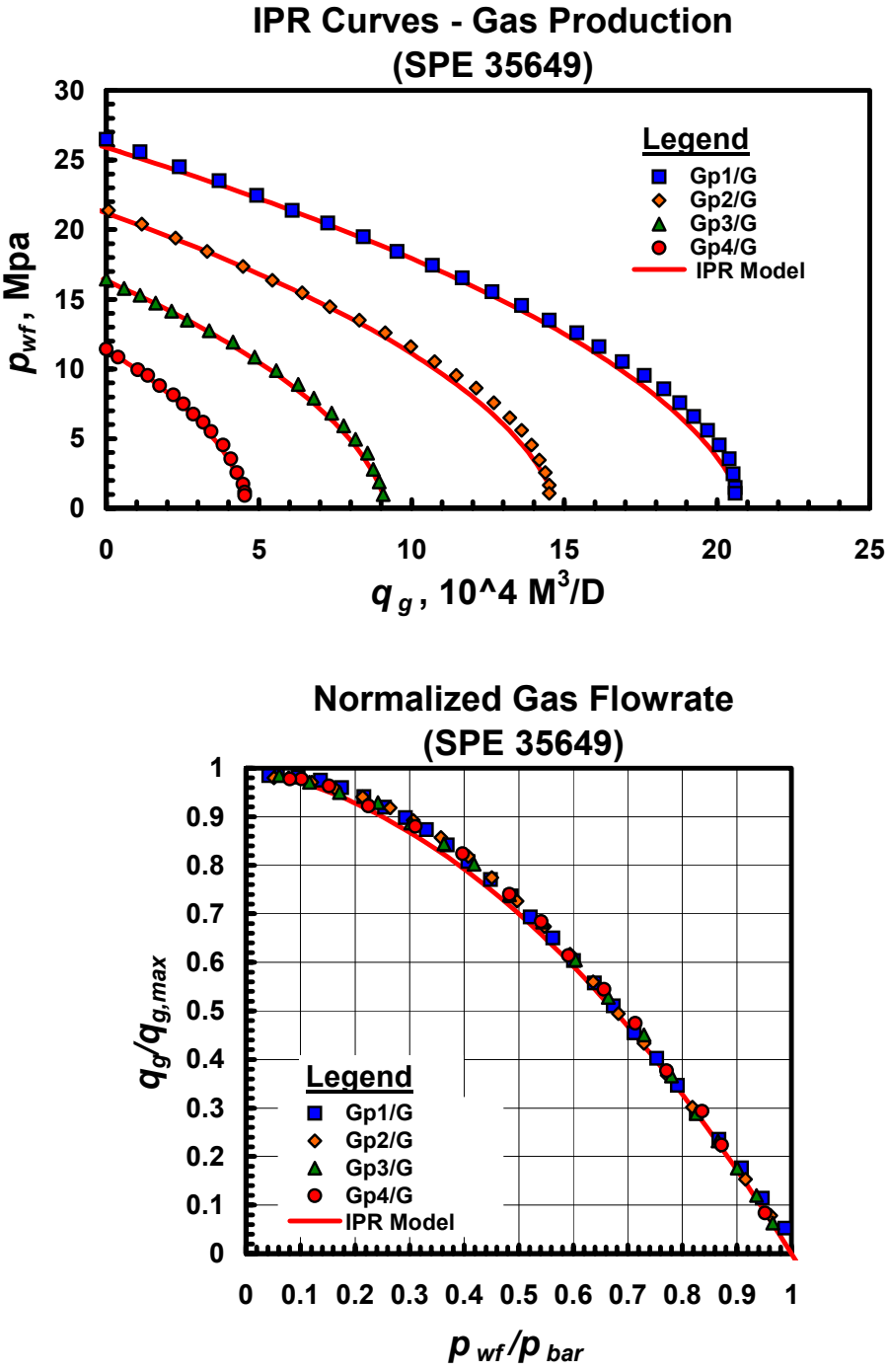

Fig. B.11 — Comparison between measured (simulation) and calculated (IPR model) values ($\nu_g = 0.20$).

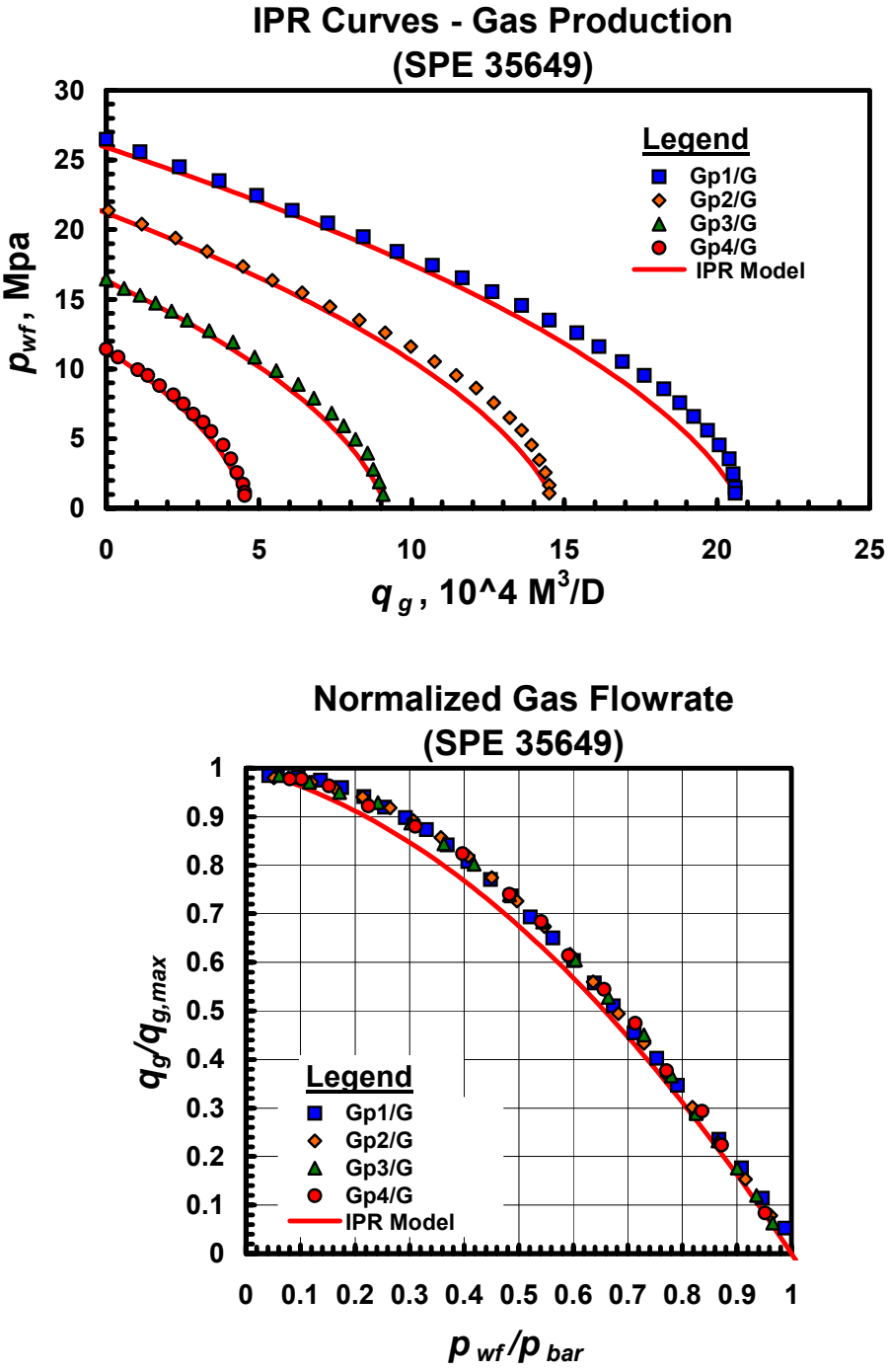

Fig. B.12 — Comparison between measured (simulation) and calculated (IPR model) values ($\nu_g = 0.30$).

APPENDIX C

WIGGINS THEORETICAL APPROACH —VOGEL *IPR* CONCEPT

C.1 Concept

Wiggins[9] presented a theoretical approach as an attempt to establish the validity of the Vogel *IPR* model where this approach is based on a multiphase flow concept that uses Taylor series (*i.e.*, polynomial expansions to represent the mobility-pressure profile). The derivation of this approach for a "solution gas-drive" reservoir system is given below:

For the oil-phase we have:

$$\nabla.\left\{\frac{kk_{ro}}{\mu_o B_o}\nabla p\right\}=\frac{\partial}{\partial t}\left(\frac{\phi S_o}{B_o}\right) \quad \text{.....(C-1)}$$

And for the gas-phase:

$$\nabla.\left\{\frac{kk_{rg}}{\mu_g B_g}+\frac{kk_{ro}R_s}{\mu_o B_o}\right\}\nabla p=\frac{\partial}{\partial t}\left(\frac{\phi S_g}{B_g}+\frac{\phi S_o R_s}{B_o}\right) \quad \text{.....(C-2)}$$

Ignoring capillary effects, gravity effects, and the solubility of gas in the water (recall that we neglect the water phase completely) — the solution of Eq. C-1 (*i.e.*, the partial differential equation for the oil case) for an isotropic and homogeneous reservoir during boundary-dominated flow is given by:

$$q_o=\frac{kh}{141.2\left[\ln(re/rw)-3/4+s\right]}\int_{p_{wf}}^{\bar{p}}\left[\frac{k_{ro}}{\mu_o B_o}\right]dp \quad \text{.....(C-3)}$$

Or, more compactly, we have:

$$q_o=C\int_{p_{wf}}^{\bar{p}}\left[\frac{k_{ro}}{\mu_o B_o}\right]dp \quad \text{.....(C-4)}$$

where the "C" coefficient is given by:

$$C=\frac{kh}{141.2\left[\ln(re/rw)-3/4+s\right]} \quad \text{.....(C-5)}$$

Defining the pressure drop term, we have:

$$\Delta p=\bar{p}-p \quad \text{.....(C-6)}$$

Using Eq. C-6 as the basis of a variable of substitution, Eq. C-4 can be normalized (or transformed) to yield the following form:

$$q_o = C.\overline{p}\int_0^{\frac{\Delta P}{\overline{p}}}\left[\frac{k_{ro}}{\mu_o B_o}\right]d\left(\frac{\Delta p}{\overline{p}}\right) \quad \text{.....(C-7)}$$

During boundary-dominated flow (*i.e.*, pseudosteady-state), the oil production rate is a function of pressure drop only, thus Eq. C-7 can be rewritten as:

$$q_o\left(\hat{p}_D\right) = C.\overline{p}\int_0^{\hat{p}_D}\left[\frac{k_{ro}}{\mu_o B_o}\right]d\left(\hat{p}_D\right) \quad \text{.....(C-8)}$$

where:

$$\hat{p}_D = \frac{\overline{p}-p}{\overline{p}} = \frac{\Delta p}{\overline{p}} \quad \text{.....(C-9)}$$

$\hat{p}_D$ is normalized (or dimensionless) pressure function. Eq. C-8 can be expanded about zero using a Taylor series as (note that *n* is the order of the derivative for a particular term):

$$q_o(\hat{p}_D) = q_o(0) + \sum_{n=1}^{n=\infty}\frac{q_o^n(0)}{n!}(\hat{p}_D)^n \quad \text{.....(C-10)}$$

Inspecting various components of Eq. C-10, we obtain:

$$q_o(0) = 0 \quad \text{.....(C-11)}$$

$$q_o^1(0) = C.\overline{p}\left[\frac{k_{ro}}{\mu_o B_o}\right]_{\hat{p}_D=0} \quad \text{.....(C-12)}$$

For $n \geq 2$ we obtain the following general result:

$$q_o^n(0) = C.\overline{p}\left[\frac{k_{ro}}{\mu_o B_o}\right]_{\hat{p}_D=0}^{n-1} \quad \text{.....(C-13)}$$

Using only the first five terms of the Taylor approximation (*i.e.*, Eq. C-10), we have:

$$q_o(\hat{p}_D) = C.\overline{p}\left\{\left[\frac{k_{ro}}{\mu_o B_o}\right]_{\hat{p}_D=0}\left(\hat{p}_D\right) + \frac{1}{2}\left[\frac{k_{ro}}{\mu_o B_o}\right]'_{\hat{p}_D=0}\left(\hat{p}_D\right)^2 + \frac{1}{6}\left[\frac{k_{ro}}{\mu_o B_o}\right]''_{\hat{p}_D=0}\left(\hat{p}_D\right)^3 \cdots\cdots\right.$$

$$\left. + \frac{1}{24}\left[\frac{k_{ro}}{\mu_o B_o}\right]'''_{\hat{p}_D=0}\left(\hat{p}_D\right)^4\right\} + \xi \quad \text{.....(C-14)}$$

Eq. C-14 allows flow rate estimation for any bottomhole flowing pressure for a specific reservoir pressure. Then, the maximum flow rate at zero bottomhole pressure $\left(p_{\hat{D}} = 1 \right)$ can be calculated as:

$$q_{o,\max}(1) = C.\overline{p}\left\{ \left[\frac{k_{ro}}{\mu_o B_o} \right]_{\hat{p}_D=0} + \frac{1}{2}\left[\frac{k_{ro}}{\mu_o B_o} \right]'_{\hat{p}_D=0} + \frac{1}{6}\left[\frac{k_{ro}}{\mu_o B_o} \right]''_{\hat{p}_D=0} + \frac{1}{24}\left[\frac{k_{ro}}{\mu_o B_o} \right]'''_{\hat{p}_D=0} + \xi_1 \right\} \quad \text{.....(C-15)}$$

Note that ξ and ξ_1 are the errors resulting from truncating the Taylor series. Finally using only five terms in the Taylor series, an analytical inflow performance relationship (Eq. C-16) based on the physical nature of the system was presented.

$$\frac{q_o}{q_{o,\max}} = 1 + \frac{C_1}{D}\left[\frac{p_{wf}}{\overline{p}} \right] + \frac{C_2}{D}\left[\frac{p_{wf}}{\overline{p}} \right]^2 + \frac{C_3}{D}\left[\frac{p_{wf}}{\overline{p}} \right]^3 + \frac{C_4}{D}\left[\frac{p_{wf}}{\overline{p}} \right]^4 \quad \text{.....(C-16)}$$

where:

$$C_1 = -\left\{ \left[\frac{k_{ro}}{\mu_o B_o} \right]_{\hat{p}_D=0} + \left[\frac{k_{ro}}{\mu_o B_o} \right]'_{\hat{p}_D=0} + \frac{1}{2}\left[\frac{k_{ro}}{\mu_o B_o} \right]''_{\hat{p}_D=0} + \frac{1}{6}\left[\frac{k_{ro}}{\mu_o B_o} \right]'''_{\hat{p}_D=0} \right\} \quad \text{.....(C-17)}$$

$$C_2 = -\frac{1}{2}\left[\frac{k_{ro}}{\mu_o B_o} \right]'_{\hat{p}_D=0} + \frac{1}{2}\left[\frac{k_{ro}}{\mu_o B_o} \right]''_{\hat{p}_D=0} + \frac{1}{4}\left[\frac{k_{ro}}{\mu_o B_o} \right]'''_{\hat{p}_D=0} \quad \text{.....(C-18)}$$

$$C_3 = -\left\{ \frac{1}{6}\left[\frac{k_{ro}}{\mu_o B_o} \right]''_{\hat{p}_D=0} + \frac{1}{6}\left[\frac{k_{ro}}{\mu_o B_o} \right]_{\hat{p}_D=0} \right\} \quad \text{.....(C-19)}$$

$$C_4 = \frac{1}{24}\left[\frac{k_{ro}}{\mu_o B_o} \right]'''_{\hat{p}_D=0} \quad \text{.....(C-20)}$$

$$D = \left[\frac{k_{ro}}{\mu_o B_o} \right]_{\hat{p}_D=0} + \frac{1}{2}\left[\frac{k_{ro}}{\mu_o B_o} \right]'_{\hat{p}_D=0} + \frac{1}{6}\left[\frac{k_{ro}}{\mu_o B_o} \right]''_{\hat{p}_D=0} + \frac{1}{24}\left[\frac{k_{ro}}{\mu_o B_o} \right]'''_{\hat{p}_D=0} \quad \text{.....(C-21)}$$

We note that the C_1, C_2, C_3, C_4 and D are functions of mobility (*i.e.*, $k_{ro}/(\mu_o B_o)$) and the respective derivatives of the mobility with respect to pressure. The analytical relationship presented in Eq. C-16 implies there is no explicit dependence of flow geometry, reservoir porosity, absolute permeability, formation thickness, flow regime (radial, linear, etc.) or skin effect on the *IPR* behavior since the "C" coefficient (Eq. C-5) is cancelled in this $q_o/q_{o,max}$ formulation. Moreover, Eq. C-16 has the same form of the Vogel *IPR* (although the Vogel formulation is only quadratic). This result suggests that the coefficients of the Vogel *IPR* model are not arbitrary parameters, but rather, that these parameters have a physical basis.

To illustrate this comparison we present the generalized Vogel *IPR* model:

$$\frac{q_o}{q_{o,max}} = 1 - \nu\left[\frac{p_{wf}}{\bar{p}}\right] - (1-\nu)\left[\frac{p_{wf}}{\bar{p}}\right]^2 \quad \text{.....(C-22)}$$

In Eq. C-22 we observe that the "ν-coefficient" can be obtained by comparison to the Wiggins, *et al.* relation (Eq. C-16), where this comparison leads to the conclusion that:

$$\nu = \frac{C_1}{D} \quad \text{.....(C-23)}$$

Similarly, the $(1-\nu)$ term is:

$$(1-\nu) = \frac{C_2}{D} \quad \text{.....(C-24)}$$

We prefer not to speculate on the specifics of the definitions given by Eqs. C-23 and 24, but rather, we would like to comment that the Wiggins, *et al.* result appears both logical and consistent. Wiggins, *et al.* present a number of validation cases generated using numerical simulation to support their model — and we concur that the approach appears to be valid. Our only concern is that the mobility function ($k_{ro}/(\mu_o B_o)$ *and its derivatives* must be known explicitly. Since the mobility term is a function of *both* pressure and saturation, the effects of production rate, reservoir depletion, and skin factor must be considered. As noted, Wiggins, *et al.*[9] performed such a study and showed that different analytical *IPR* cases are evident for different stages of depletion. Wiggins, *et al.* also established that skin effects do not significantly affect the application of the "analytical *IPR*" model. We noted earlier that, intuitively, skin effects should not affect the *IPR* model in general.

The main contribution of the Wiggins, *et al.*[9] approach was that this work provides some "semi-analytical" validation of the (otherwise) empirical definition of the Vogel *IPR* model for solution gas-drive reservoir systems. We note that the weakness of this approach is that it requires the determination of the variation of relative permeability as well as the fluid properties with respect to pressure *and the corresponding derivatives of these functions* — which would be very difficult to achieve in practice. A further complication is that the saturation-pressure profile would also have to be known (for the k_{ro} term).

APPENDIX D

DERIVATION OF AN INFLOW PERFORMANCE RELATIONSHIP (*IPR*) FOR SOLUTION GAS-DRIVE RESERVOIRS

D.1 Concept

In this Appendix we show that an inflow performance relationship (*IPR*) can be developed based on the pseudosteady state flow equation for a single well in a solution gas-drive reservoir (pseudopressure formulation) and using an approximate relation for the mobility of the oil phase. The definition of the oil-phase pseudopressure for a single well in a solution gas-drive reservoir is given as:

$$p_{po}(p) = \left[\frac{\mu_o B_o}{k_o}\right]_{p_n} \int_{p_{base}}^{p} \left[\frac{k_o}{\mu_o B_o}\right] dp \quad \text{.....(D-1)}$$

The pseudosteady-state flow equation for the oil-phase in a solution gas-drive reservoir is given by:

$$p_{po}(\bar{p}) = p_{po}(p_{wf}) + q_o b_{pss} \quad \text{.....(D-2)}$$

where:

$$b_{pss} = 141.2\left[\frac{\mu_o B_o}{k_o}\right]_{p_n} \frac{1}{h}\left[\ln(r_e/r_w) - 3/4 + s\right] \quad \text{.....(D-3)}$$

For the solution gas-drive case, we propose the following model for the oil mobility function, $\left[\frac{k_o}{\mu_o B_o}\right]_p$:

$$\left[\frac{k_o}{\mu_o B_o}\right]_p = f(p) = a + 2bp \quad \text{.....(D-4)}$$

We note that the model for the oil mobility function given in Eq. D-4 is very similar to the relation proposed by Fetkivoch[5] for the case of a solution gas-drive reservoir system. We also note that Fetkovich utilized a "zero intercept" (*i.e.*, the mobility at zero pressure is zero (see **Fig. D.1**)).

In our proposal (Eq. D-4), we do not presume a zero intercept of the mobility function — from **Fig. D.1** we conclude that the zero mobility at zero pressure was based on the assumption (by Fetkovich) that at zero pressure the k_{ro} term would be zero (*i.e.*, no oil would flow). Using **Fig. D.1** as a guide, we note that our concept (*i.e.*, Eq. D-4) is plausible.

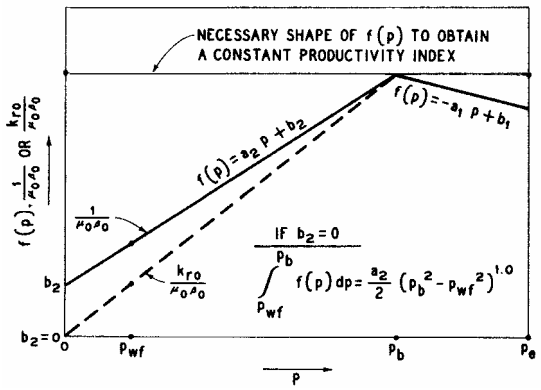

Fig. D.1 — Mobility-pressure behavior for a solution gas-drive reservoir (after Fetkovich (ref. 5)).

We will first establish the *IPR* formulation for the pseudopressure form of the oil flow equation for a solution gas-drive system. Solving Eq. D-2 for the oil rate, q_o, we have:

$$q_o = \frac{1}{b_{pss}}[p_{po}(\bar{p}) - p_{po}(p_{wf})] \quad \text{.....(D-5)}$$

Solving Eq. D-5 for the case of the "maximum oil rate," $q_{o,max}$, (*i.e.*, p_{wf}=0 (or $p_{po}(p_{wf})$ =0)), we have:

$$q_{o,max} = \frac{1}{b_{pss}}[p_{po}(\bar{p}) - p_{po}(p_{wf} = 0)] \quad \text{.....(D-6)}$$

Dividing Eq. D-5 by Eq. D-6 gives us the "*IPR*" form (*i.e.*, $q_o/q_{o,max}$) — which yields:

$$\frac{q_o}{q_{o,max}} = \frac{p_{po}(\bar{p}) - p_{po}(p_{wf})}{p_{po}(\bar{p}) - p_{po}(p_{wf} = 0)} \quad \text{.....(D-7)}$$

At this point we will note that *it is not our goal* to proceed with the development of an *IPR* model in terms of the pseudopressure function, $p_{po}(p)$ — rather, our goal is to develop a simplified *IPR* model using Eqs. D.4 and D.7 as base relations. Given that Eq. D.4 is given in terms of pressure (p), we can presume that some type of pressure-squared formulation will result (as was the case in the Fetkovich work (ref. 5)).

Substituting Eq. D.4 into Eq. D.1, we have:

$$p_{po}(p) = \left[\frac{\mu_o B_o}{k_o}\right]_{p_n} \int_{p_{base}}^{p} (a + 2bp)\, dp$$

Or,

$$p_{po}(p) = \left[\frac{\mu_o B_o}{k_o}\right]_{p_n} \left[(ap + bp^2) - (ap_{base} + bp_{base}^2)\right] \quad \text{.....(D-8)}$$

Substituting Eq. D.8 into Eq. D.7, gives us:

$$\frac{q_o}{q_{o,max}} = \frac{\left[[(a\bar{p} + b\bar{p}^2) - (ap_{base} + bp_{base}^2)] - [(ap_{wf} + bp_{wf}^2) - (ap_{base} + bp_{base}^2)]\right]}{\left[[(a\bar{p} + b\bar{p}^2) - (ap_{base} + bp_{base}^2)] - [(a(0) + b(0)^2) - (ap_{base} + bp_{base}^2)]\right]}$$

Cancelling like terms, we obtain:

$$\frac{q_o}{q_{o,max}} = \frac{(a\bar{p} + b\bar{p}^2) - (ap_{wf} + bp_{wf}^2)}{(a\bar{p} + b\bar{p}^2)} \quad \text{.....(D-9)}$$

Dividing through Eq. D-9 by $(a\bar{p} + b\bar{p}^2)$ gives us the following forms:

$$\frac{q_o}{q_{o,max}} = 1 - \frac{(ap_{wf} + bp_{wf}^2)}{(a\bar{p} + b\bar{p}^2)} \quad \text{.....(D-10a)}$$

$$\frac{q_o}{q_{o,max}} = 1 - \frac{ap_{wf}}{(a\bar{p} + b\bar{p}^2)} - \frac{bp_{wf}^2}{(a\bar{p} + b\bar{p}^2)} \quad \text{.....(D-10b)}$$

$$\frac{q_o}{q_{o,max}} = 1 - \frac{a}{(a + b\bar{p})}\left[\frac{p_{wf}}{\bar{p}}\right] - \frac{b}{(a\frac{1}{\bar{p}} + b)}\left[\frac{p_{wf}}{\bar{p}}\right]^2 \quad \text{.....(D-10c)}$$

$$\frac{q_o}{q_{o,max}} = 1 - \frac{1}{(1 + \frac{b}{a}\bar{p})}\left[\frac{p_{wf}}{\bar{p}}\right] - \frac{1}{(1 + \frac{a}{b}\frac{1}{\bar{p}})}\left[\frac{p_{wf}}{\bar{p}}\right]^2 \quad \text{.....(D-10d)}$$

Defining $\alpha = a/b$ and substituting this definition into Eq. D-10d, we have:

$$\frac{q_o}{q_{o,max}} = 1 - \frac{1}{(1 + \alpha\bar{p})}\frac{p_{wf}}{\bar{p}} - \frac{1}{(1 + \frac{1}{\alpha\bar{p}})}\frac{p_{wf}^2}{\bar{p}^2} \quad \text{.....(D-11)}$$

Defining a "lumped parameter," ν:

$$\nu = \frac{1}{(1 + \alpha\bar{p})} \quad \text{.....(D-12)}$$

Therefore:

$$(1 - \nu) = 1 - \frac{1}{(1 + \alpha\bar{p})} = \frac{(1 + \alpha\bar{p})}{(1 + \alpha\bar{p})} - \frac{1}{(1 + \alpha\bar{p})} = \frac{\alpha\bar{p}}{(1 + \alpha\bar{p})}$$

Or,

$$(1 - \nu) = \frac{1}{(1 + \frac{1}{\alpha\bar{p}})} \quad \text{.....(D-13)}$$

Substituting Eqs. D-12 and D-13 into Eq. D-11, we have:

$$\frac{q_o}{q_{o,max}} = 1 - \nu\left[\frac{p_{wf}}{\overline{p}}\right] - (1-\nu)\left[\frac{p_{wf}}{\overline{p}}\right]^2 \quad \text{.....(D-14)}$$

Where we note that Eq. D-14 is of exactly the same form as the empirical result proposed by Vogel.[6] We suggest that Eq. D-14 serves as a semi-analytical validation of the Vogel result — and while we recognize that the ν-parameter is not "constant," this parameter can be established directly from the proposed model for mobility (*i.e.*, Eq. D-4). As the ν-parameter is given as a function of the average reservoir pressure, $\overline{p}$, we recall Eq. D-4 and express this result in terms of $\overline{p}$.

$$\left[\frac{k_o}{\mu_o B_o}\right]_{\overline{p}} = a + 2b\overline{p} \quad \text{.....(D-15)}$$

At $\overline{p} = 0$ Eq. D-15 becomes:

$$\left[\frac{k_o}{\mu_o B_o}\right]_{\overline{p}=0} = a$$

Or,

$$a = \left[\frac{k_o}{\mu_o B_o}\right]_{\overline{p}=0} \quad \text{.....(D-16)}$$

Dividing through Eq. D-15 by the a-parameter, we define a new parameter, β:

$$\beta = \frac{\left[\frac{k_o}{\mu_o B_o}\right]_{\overline{p}}}{\left[\frac{k_o}{\mu_o B_o}\right]_{\overline{p}=0}} = 1 + 2\frac{b}{a}\overline{p} \quad \text{.....(D-17a)}$$

Or, using the definition $\alpha = a/b$, we have:

$$\beta = 1 + 2\alpha\overline{p} \quad \text{.....(D-17b)}$$

Recalling Eq. D-12 (*i.e.*, the definition of the n-parameter), we have:

$$\nu = \frac{1}{(1+\alpha\overline{p})} \quad \text{.....(D-12)}$$

Solving the "β" definition (Eq. D-17b) for the $\alpha\overline{p}$ term gives us:

$$\alpha\overline{p} = \frac{\beta - 1}{2}$$

Therefore, the $(1+\alpha\bar{p})$ term is given by $\alpha\bar{p}$ term gives us:

$$(1+\alpha\bar{p}) = \frac{2}{2} + \frac{\beta-1}{2} = \frac{\beta+1}{2}$$

And,

$$\frac{1}{(1+\alpha\bar{p})} = \frac{2}{\beta+1} \quad \text{..... (D-18)}$$

We note that Eq. D-12 (i.e., the definition for the ν-parameter) and Eq. D-18 (an equality based on the β-parameter) are equivalent — which leads to the following definition:

$$\nu = \frac{2}{\beta+1} \quad \text{..... (D-19)}$$

A similar relation can be derived for the (1-ν) group directly from Eq. D-19. This derivation is given as:

$$(1-\nu) = \frac{\beta+1}{\beta+1} - \frac{2}{\beta+1}$$

Or,

$$(1-\nu) = \frac{\beta-1}{\beta+1} \quad \text{.....(D-20)}$$

Substitution of Eqs. D-19 and D-20 into the *IPR* model (Eq. D-14) gives the following result in terms of the β-parameter:

$$\frac{q_o}{q_{o,max}} = 1 - \frac{2}{\beta+1}\left[\frac{p_{wf}}{\bar{p}}\right] - \frac{\beta-1}{\beta+1}\left[\frac{p_{wf}}{\bar{p}}\right]^2 \quad \text{.....(D-21)}$$

We note that Eq. D-21 (*i.e.*, the *IPR* model given in terms of the β-parameter) is presented for completeness — we continue to advocate the "conventional form" of the *IPR* model (*i.e.*, Eq. 14, which is given in terms of the ν-parameter).

For compactness, we will continue to use the β-parameter as the preferred variable for expressing the mobility function. Recalling the definition of the β-parameter (Eq. D-17a), we have:

$$\beta = \frac{\left[\frac{k_o}{\mu_o B_o}\right]_{\bar{p}}}{\left[\frac{k_o}{\mu_o B_o}\right]_{\bar{p}=0}} \quad \text{.....(D-17a)}$$

We state explicitly that the β-parameter is not constant — however, we propose that concept of using a single parameter to represent a particular segment of performance is well-established. We believe that the modified "Vogel" model (Eq. D-14) is directionally correct and does have theoretical justifications (as shown in this Appendix). But we also recognize that this concept requires further proof — particularly

from the standpoint of proving that the β-parameter can be estimated using conventional PVT and relative permeability data. Such a proof is beyond the scope of this work, which has laid the foundation for the concept, and we encourage other investigators to make such efforts in the future.

As a final effort, we propose to define the ν and (1-ν) groups in terms of the mobility parameters. We achieve these definitions using the results from Eq. D-17a (*i.e.*, the base definition) and Eqs. D-19 and D-20 (the ν and (1-ν) definitions, respectively). Substituting Eq. D-17a into Eq. D-20 gives:

$$(1-\nu)=\frac{\dfrac{\left[\dfrac{k_o}{\mu_o B_o}\right]_{\overline{p}}}{\left[\dfrac{k_o}{\mu_o B_o}\right]_{\overline{p}=0}}-1}{\dfrac{\left[\dfrac{k_o}{\mu_o B_o}\right]_{\overline{p}}}{\left[\dfrac{k_o}{\mu_o B_o}\right]_{\overline{p}=0}}+1}$$

Or,

$$(1-\nu)=\frac{\left[\dfrac{k_o}{\mu_o B_o}\right]_{\overline{p}}-\left[\dfrac{k_o}{\mu_o B_o}\right]_{\overline{p}=0}}{\left[\dfrac{k_o}{\mu_o B_o}\right]_{\overline{p}}+\left[\dfrac{k_o}{\mu_o B_o}\right]_{\overline{p}=0}} \quad \text{.....(D-22)}$$

Solving Eq. 22 for the ν-parameter, we have

$$\nu=1-\frac{\left[\dfrac{k_o}{\mu_o B_o}\right]_{\overline{p}}-\left[\dfrac{k_o}{\mu_o B_o}\right]_{\overline{p}=0}}{\left[\dfrac{k_o}{\mu_o B_o}\right]_{\overline{p}}+\left[\dfrac{k_o}{\mu_o B_o}\right]_{\overline{p}=0}}=\frac{\left[\dfrac{k_o}{\mu_o B_o}\right]_{\overline{p}}+\left[\dfrac{k_o}{\mu_o B_o}\right]_{\overline{p}=0}}{\left[\dfrac{k_o}{\mu_o B_o}\right]_{\overline{p}}+\left[\dfrac{k_o}{\mu_o B_o}\right]_{\overline{p}=0}}-\frac{\left[\dfrac{k_o}{\mu_o B_o}\right]_{\overline{p}}-\left[\dfrac{k_o}{\mu_o B_o}\right]_{\overline{p}=0}}{\left[\dfrac{k_o}{\mu_o B_o}\right]_{\overline{p}}+\left[\dfrac{k_o}{\mu_o B_o}\right]_{\overline{p}=0}}$$

Or,

$$\nu=\frac{2\left[\dfrac{k_o}{\mu_o B_o}\right]_{\overline{p}=0}}{\left[\dfrac{k_o}{\mu_o B_o}\right]_{\overline{p}}+\left[\dfrac{k_o}{\mu_o B_o}\right]_{\overline{p}=0}} \quad \text{.....(D-23)}$$

It is worth comment to not that if the mobility function is constant, then Eq. D-23 reduces to unity, and Eq. D-22 reduces to zero — which is the result for the single-phase, slightly compressible liquid case.

As an attempt to validate the linear mobility profile (*i.e.*, Eq. D-4) we present data from Camacho and Raghavan (ref. 28) in **Figs. D.2 and D.3** — where we note that the oil relative permeability function (k_{ro}) was not provided, and, as such, has been assumed to be unity. We believe that the trends in **Figs. D.2 and D.3** do provide validation of Eq. D-4 as a mobility model — at least in a directional sense.

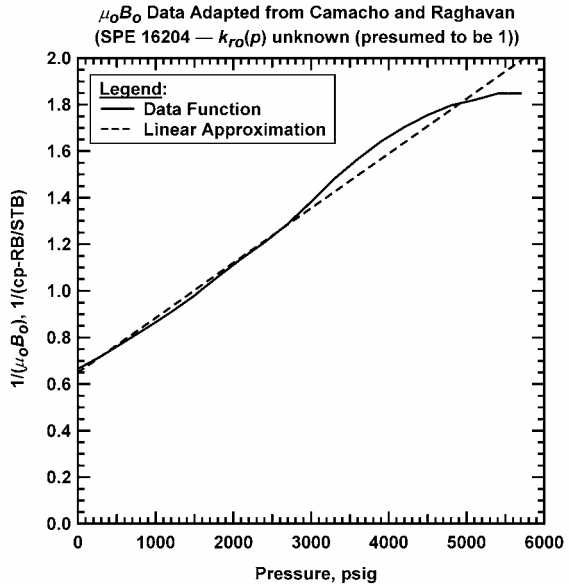

Fig. D.2 — Example of the $1/\mu_o B_o$ profile for a solution gas-drive system (adapted from Camacho and Raghavan[28]).

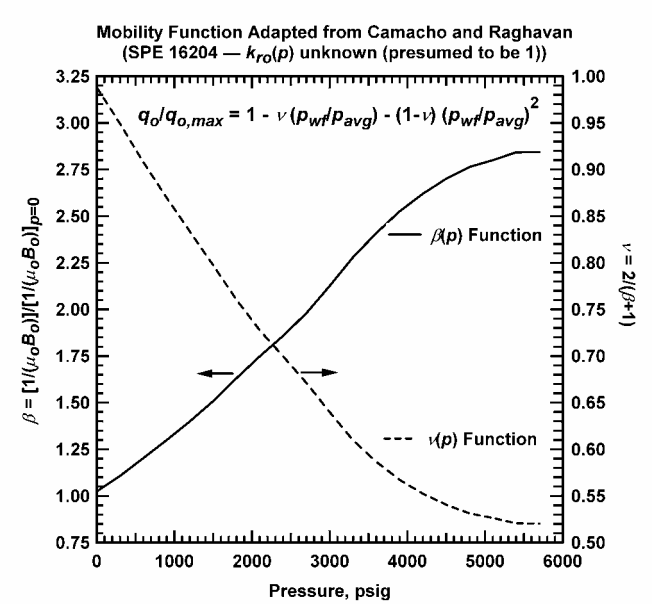

Fig. D.3 — Example of the "β" profile for a solution gas-drive system (adapted from Camacho and Raghavan[28]).

APPENDIX E

ECLIPSE DATA FILE (EXAMPLE)

E.1 Eclipse data set

```
==========================================================================
-- Study                : Gas Condensate IPR
-- Author               : Yanil Del Castillo
-- Simulator            : Eclipse 300
-- Date                 : February 2003
==========================================================================
-- Gas condensate case - Fluid 5 Cusiana
-- Real 7 pseudocomponents
-- Peng-Robinson EOS with correction
-- AIM - Adaptive Implicit solution method
-- Radial grid 30*1*1
-- Field units
-- Natural
==========================================================================

==========================================================================
-- RUNSPEC section
==========================================================================

MEMORY
1000 20 /

FIELD

RADIAL

AIM

COMPS
7 /

EOS
PR3 /

DIMENS
-- NR NTHETA NZ
   30  1    1 /

WELLDIMS
    1    1    1    1/

-- Single phase fluid is gas
ISGAS

MULTSAVE
1 /
FMTOUT
UNIFOUT
```

```
================================================================
-- GRID section
================================================================
INIT

INRAD
.25 /
DR
0.2500   0.50    0.6539   0.9655   1.4255   2.1046   3.1072 4.5876
6.7732    10    10    10    10    35    40    47    68   100   150
200   200   300   500   500   500   500   500   500   500   500
/

EQUALS
DTHETA
360 /
DZ
30 /
TOPS
7000/
PORO
 0.20 /
/

PERMR
3*5 27*5 /
PERMTHT
30*0 /

================================================================
-- PROPS section
================================================================

-- Include file with detailed fluid description
INCLUDE
FLUID.INC
/

-- Temperature in deg F
RTEMP
260.33/

-- Include KR tables
INCLUDE
KR.INC
/

--Rock and water pressure data
ROCK
5015 0.000004 /

PVTW
5015 1.0 0.000003 0.31 0.0 /

--Surface density of water
 DENSITY
1* 63.0 1* /
```

```
========================================================================
-- SOLUTION section
========================================================================
EQUALS
PRESSURE
5015 /
SWAT
0 /
SGAS
1 /
/
-Initial composition
ZMF
30*.0457
30*.6949
30*.1307
30*.0469
30*.04
30*.025
30*.0168
/
OUTSOL
PRES SOIL XMF YMF VMF VOIL VGAS BOIL BGAS DENO DENG KRG KRO ZMF /
RPTPRINT
13*0/
========================================================================
-- SUMMARY section
========================================================================
RUNSUM
RPTONLY
-- Bottom hole pressure
WBHP
P/
-- Average reservoir pressure (pore volume weighted)
FPR
-- Average field oil saturation
FOSAT
--Oil Production rate
FOPR
--Gas production rate
FGPR
--Oil production total
FOPT
--Gas production total
FGPT
```

```
================================================================
-- SCHEDULE section
================================================================

SEPCOND
SEP FIELD 1 60 14.7 /
/

--Define the production well
WELLSPEC
P FIELD 1 1 1*  SEP/
/

COMPDAT
--name i j k1 k2 flag sat.tab trans id kh skin D dir
   P   1 1 1  1 'OPEN' 1*     1*   .5 1*  0   1* 'Z'/
/

-- Production constraint Pwf = constant
-- Pwf = 500 psi

WELLPROD
P BHP 4* 500 /
/

TUNING
--1.1574E-6  1.1574E-1  1.1574E-7  1*  1.1  0.5   /
1.0E-6 30.0 1.0E-7  1*  1.1  0.5   /
 /
 /
TSTEP
3*3.8581E-6      4.0205610e-06   5.4171651e-06   7.2989013e-06
9.8342877e-06/

TSTEP
1.3250380e-05   1.7853104e-05   2.4054656e-05   3.2410414e-05
4.3668673e-05   5.8837662e-05   7.9275835e-05   1.0681352e-04
1.4391685e-04   1.9390860e-04   2.6126576e-04/

TSTEP
30.0 30.0 30.0 30.0 30.0 30.0 30.0 30.0 30.0 30.0
30.0 30.0 30.0 30.0 30.0 30.0 30.0 30.0 30.0 30.0
30.0 30.0 30.0 30.0 30.0 30.0 30.0 30.0 30.0 30.0
30.0 30.0 30.0 30.0 30.0 30.0 30.0 30.0 30.0 30.0
30.0 30.0 30.0 30.0 30.0 30.0 30.0 30.0 30.0 30.0 /

END
```

E.2 KR.INC (file)

```
-- Set 4  of relative permeability
```

```
SGFN
-- Sg    krg    Pcg
0.00000 0.00000 0.00000
0.05000 0.00024 0.00000
0.10000 0.00190 0.00000
0.15000 0.00624 0.00000
0.20000 0.01440 0.00000
0.25000 0.02734 0.00000
0.30000 0.04590 0.00000
0.35000 0.07074 0.00000
0.40000 0.10240 0.00000
0.41000 0.10958 0.00000
0.42000 0.11706 0.00000
0.43000 0.12483 0.00000
0.44000 0.13289 0.00000
0.45000 0.14124 0.00000
0.46000 0.14990 0.00000
0.47000 0.15885 0.00000
0.48000 0.16810 0.00000
0.49000 0.17765 0.00000
0.50000 0.18750 0.00000
0.51000 0.19765 0.00000
0.52000 0.20810 0.00000
0.53000 0.21885 0.00000
0.54000 0.22990 0.00000
0.55000 0.24124 0.00000
0.56000 0.25289 0.00000
0.57000 0.26483 0.00000
0.58000 0.27706 0.00000
0.59000 0.28958 0.00000
0.60000 0.30240 0.00000
0.61000 0.31550 0.00000
0.62000 0.32889 0.00000
0.63000 0.34256 0.00000
0.64000 0.35652 0.00000
0.65000 0.37074 0.00000
0.66000 0.38524 0.00000
0.67000 0.40001 0.00000
0.68000 0.41505 0.00000
0.69000 0.43035 0.00000
0.70000 0.44590 0.00000
0.71000 0.46171 0.00000
0.72000 0.47776 0.00000
0.73000 0.49405 0.00000
0.74000 0.51058 0.00000
0.75000 0.52734 0.00000
0.76000 0.54433 0.00000
0.77000 0.56154 0.00000
0.78000 0.57895 0.00000
0.79000 0.59658 0.00000
0.80000 0.61440 0.00000
```

```
0.81000 0.63241 0.00000
0.82000 0.65061 0.00000
0.83000 0.66899 0.00000
0.84000 0.68754 0.00000
0.85000 0.70624 0.00000
0.86000 0.72510 0.00000
0.87000 0.74411 0.00000
0.88000 0.76325 0.00000
0.89000 0.78252 0.00000
0.90000 0.80190 0.00000
0.91000 0.82139 0.00000
0.92000 0.84098 0.00000
0.93000 0.86066 0.00000
0.94000 0.88042 0.00000
0.95000 0.90024 0.00000
0.96000 0.92013 0.00000
0.97000 0.94005 0.00000
0.98000 0.96002 0.00000
0.99000 0.98000 0.00000
1.00000 1.00000 0.00000
/
SOF2
-- So    krog
0.00000 0.00000
0.11000 0.00000
0.12000 0.00001
0.13000 0.00002
0.14000 0.00004
0.15000 0.00007
0.16000 0.00011
0.17000 0.00017
0.18000 0.00026
0.19000 0.00036
0.20000 0.00049
0.21000 0.00066
0.22000 0.00086
0.23000 0.00110
0.24000 0.00139
0.25000 0.00174
0.26000 0.00214
0.27000 0.00260
0.28000 0.00314
0.29000 0.00375
0.30000 0.00444
0.31000 0.00523
0.32000 0.00612
0.33000 0.00711
0.34000 0.00822
0.35000 0.00945
0.36000 0.01082
0.37000 0.01232
```

```
0.38000 0.01398
0.39000 0.01579
0.40000 0.01778
0.41000 0.01994
0.42000 0.02230
0.43000 0.02486
0.44000 0.02763
0.45000 0.03062
0.46000 0.03386
0.47000 0.03733
0.48000 0.04107
0.49000 0.04509
0.50000 0.04938
0.51000 0.05398
0.52000 0.05889
0.53000 0.06412
0.54000 0.06970
0.55000 0.07562
0.56000 0.08192
0.57000 0.08861
0.58000 0.09569
0.59000 0.10318
0.60000 0.11111
0.65000 0.15779
0.70000 0.21778
0.75000 0.29340
0.80000 0.38716
0.85000 0.50174
0.90000 0.64000
0.95000 0.80501
1.00000 1.00000
/
```

E.3 FLUID.INC (file)

```
EOS
--
-- Equation of State (Peng- Robinson)
--
   PR3
/
NCOMPS
--
-- Number of Components
--
       7
/
```

```
CNAMES
--
-- Component Names
--
   'CO2'
   'GRP1'
   'GRP2'
   'GRP3'
   'GRP4'
   'GRP5'
   'GRP6'
/
MW
--
-- Molecular Weights (Reservoir EoS)
--
         44.01
    16.1325726
   34.55606427
   67.96383608
      112.5175
       178.788
   303.6435714
/
ZMFVD
  1.0000E+00   0.0457  0.6949  0.1307  0.0469  0.04   0.025  0.0168
  1.0000E+04   0.0457  0.6949  0.1307  0.0469  0.04   0.025  0.0168/
OMEGAA
--
-- EoS Omega-A Coefficient (Reservoir EoS)
--
      0.477635
      0.477635
      0.477635
      0.457236
      0.457236
      0.380486
      0.380486
/
OMEGAB
--
-- EoS Omega-B Coefficient (Reservoir EoS)
--
      0.070049
      0.070049
      0.070049
      0.077796
      0.077796
      0.07256
      0.07256
/
```

```
TCRIT
--
-- Critical Temperatures (Reservoir EoS)
--
   548.4599855
    342.212551
   586.8298284
   809.9493175
   1051.582472
   1241.582367
   1460.809749
/
PCRIT
--
-- Critical Pressures (Reservoir EoS)
--
   1056.6352099669
   651.772745079581
   664.036546479197
   490.468298884635
   384.191974487964
   269.516340491557
   180.198300994355
/
VCRIT
--
-- Critical Volumes (Reservoir EoS)
--
   1.50573518513559
   1.56885008183587
   2.63712620491114
   4.67964434648799
   7.26188848439886
   11.0953460957193
   17.6736680960253
/
ZCRIT
--
-- Critical Z-Factors (Reservoir EoS)
--
   0.2740777974
   0.2847159002
   0.2842260192
   0.2719781757
   0.256686814
   0.2366761979
   0.2197244778
/
```

```
SSHIFT
--
-- EoS Volume Shift (Reservoir EoS)
--
   -0.04579201311
   -0.1441688522
   -0.0950276543
   -0.04100635693
    0.003672142675
    0.008934047066
    0.01156164308
/
ACF
--
-- Acentric Factors (Reservoir EoS)
--
   0.327911086
   0.01320204346
   0.1158061209
   0.2285995736
   0.3309925
   0.490667998
   1.124565237
/
PARACHOR
--
-- Component Parachors
--
            78
   76.73060872
   121.5282336
   215.8816613
   358.2117489
   490.0019888
   781.5087913
/
PEDERSEN
--
-- Use Pedersen et al. for Viscosity Calculation
--
BIC
0.06571622708
0.06571622708  0.0
0.06571622708  0.0657162261   0.0
0.06571622708  0.02477685516  0.006571622463  0.0
0.06571622708  0.1051586553   0.02264839242   0.0  0.0
0.06571622708  0.12313464     0.02264839242   0.0  0.0  0.0
/
```

VITA

Name:	Yanil Del Castillo Maravi
Born:	14 June 1972 Lima, Peru
Permanent Address:	Av. Tahuantinsuyo 399 – El Tambo Huancayo – Junin PERU (yani_delcastillo@hotmail.com)
Education:	Universidad Nacional de Ingenieria, Lima, Peru. Bachelor of Science Degree in Petroleum Engineering December 1994
	Texas A&M University, College Station, Texas, USA Master of Science Degree in Petroleum Engineering August 2003